



NEUTRONS  
FOR SCIENCE



ANNUAL REPORT **2014**  
Institut Laue-Langevin

---

The world's leading facility in neutron science and technology.

---

ANNUAL **20**  
REPORT **14**  
Institut Laue-Langevin





## PUBLISHING INFORMATION

**Editors:**  
Helmut Schober and Giovanna Cicognani

**Production team:**  
Giovanna Cicognani, Virginie Guérard, Robert Corner, Susan Tinniswood and Alison Mader

**Design:**  
Morton Ward Limited

**Photography:**  
ILL (unless otherwise specified)

Further copies can be obtained from:  
Institut Laue-Langevin  
Communication Unit  
CS 20156, F-38042 Grenoble Cedex 9  
communication@ill.eu  
www.ill.eu

## CONTENTS

DIRECTOR'S FOREWORD	4
WHAT IS THE ILL	
About the ILL	6
Why neutron scattering is useful	7
SCIENTIFIC HIGHLIGHTS	
Introduction	8
College introductions	10
ILL in the press	14
Materials science	16
Chemistry and Crystallography	30
Magnetism	36
Soft matter	52
Biology and Health	58
Nuclear and Particle Physics	68
Theory	72
MILLENNIUM PROGRAMME AND TECHNICAL DEVELOPMENTS	
Introduction	78
Millennium Programme	80
New experimental techniques	82
Technical developments	86
EXPERIMENTAL AND USER PROGRAMME	
Introduction	90
User programme	92
User and beamtime statistics	94
Instrument list	98
REACTOR OPERATION	
Introduction	100
Reactor operation in 2014	102
The Fukushima reinforcement work	104
MORE THAN SIMPLY NEUTRONS	
Introduction	106
The EPN-Campus	108
Scientific Support Laboratories	110
WORKSHOPS AND EVENTS	
ILL workshops and schools in 2014	112
ILL chronicle 2014	113
A year in photos	114
FACTS AND FIGURES	
Facts and figures	119
Publications in 2014	121
Organisation chart	122

# DIRECTOR'S FOREWORD



It is an honour and a responsibility to introduce this report on the activities of the ILL, the unique multi-national flagship of neutron scattering, a wonderful laboratory dedicated to scientific progress. After a full year at the ILL I feel more at ease than I did in January 2014 in writing this introduction. The *raison d'être* of the ILL is to provide neutrons and state of the art instrumentation to the European and international scientific community. It was with this fundamental goal in mind that the extensive work programme of the long shutdown from August 2013 continued during the first half of 2014. This exceptionally long shutdown was necessary to carry out a number of major projects. Some are part of the Millennium upgrade programme while others are the result of the safety assessment performed by the ILL following the accident at Fukushima.

The ILL's principal, and essential, research tool is our unique high-flux reactor. A major step towards the fulfillment of our commitment to the scientific community was achieved with the restart of the reactor on 8 July for a short (18-day) cycle at a reduced power of 30 MW; this preparatory cycle proved to be an invaluable period of tests and preparation for our staff working on the reactor and its ancillary equipment, as well as the instrument suite, a large part of which had been replaced or refurbished over the previous year. Full reactor power was re-established during the following full cycle starting on 28 August, after a brief "hiccup" due to problems with the vertical cold source refrigeration system. This cycle, and the final cycle of 2014, was exploited to its full potential with external users carrying out their scheduled experiments on all operational instruments.

I feel that it is important to comment on the financial difficulties that became apparent in February of 2014. The first half of the year was dominated by the need to make major adjustments to the 2014 budget and that of future years to account for the very large over-spend on the post-Fukushima budget. For the first time a long-term financial plan (LTFP) has been developed (for the years 2015 to 2024), with the advice and assistance of the ILL's Associates, to provide a global view of forthcoming scientific and technical programmes along with the associated financial implications. With the LTFP the ILL has now a very useful financial planning tool, based on a number of critical assumptions (contributions to the ILL's budget from the Associates and Scientific Members, the Endurance upgrade programme, fuel cycle costs, key reactor component programme costs ...) which will be reassessed as they evolve. In parallel with financial "repair" measures, an in-depth analysis has been carried out to investigate the reasons for the ILL's post-Fukushima

financial mismanagement. Measures to improve inter-divisional communication, financial reporting and a strict adherence to in-house procedures have been implemented, while relevant modifications to internal structures have been initiated. The ILL has a proud record over more than forty years of successful source and instrument development programmes. I believe that these changes to our internal procedures will improve further our project management and prevent future problems of this nature.

Despite the severe financial pressure, implementation of the demanding post-Fukushima reinforcements and new safety circuits continued over the year. As well as physical reinforcement of the double-walled reactor building and the ILL4 office and laboratory building, the new emergency control room PCS3 became operational in November. This bunkertype building is designed to allow control of the principal reactor functions after a highly improbable sequence of catastrophic events – an exceptionally severe earthquake and subsequent flood of the Grenoble valley. The PCS3 is a key element in the ILL's response to the requirements of the French safety authorities. It is important to stress the pioneering role played by the ILL's engineering teams in the development of the post-Fukushima projects – no other French nuclear installation has been reinforced yet to respond to the simultaneous risk of major earthquake and flood.

Over the last decade, the Scientific Member countries have become increasingly important contributors to the ILL's scientific life and to the institute's budget; their contribution to the annual budget is now at about the same level as that of one of the ILL's three Associates. Consequently the recent negotiations with the 12 partner countries of this "fourth Associate" were a crucial part of future scientific and financial planning. The good news is that almost all of the discussions are complete, with new contracts signed for the period 2014 to 2018. The renewal of the contract with India is due this year; these negotiations are underway.

A noteworthy event early in 2014 was the official inauguration of the Science Building, a ceremony attended by a large number of VIPs including the (then) French Minister of Higher education and Research, Mme Geneviève Fioraso. The Science Building, a joint ILL-ESRF project exemplifying the strong interactions between the European Photon and Neutron (EPN) Science Campus's two principal partners, is a custom-designed building housing chemistry laboratories, the joint library, the Industrial Liaison offices and the Theory Groups of the two

partners. This new building is also the home of the ILL's Large Scale Structures Group and the Soft Matter Support Service; space has been reserved for future industrial-related activities.

During 2014 significant progress was made towards the realisation of Europe's next major international scientific project, the European Spallation Source (ESS); first neutrons are scheduled for 2019 or 2020. Many of the ILL's partner countries participate in this "next generation" pulsed neutron source; their representatives gathered on 9 October at the construction site in Lund (Sweden) for a "foundation stone" ceremony. As the world's leading neutron-scattering laboratory the ILL will play an increasingly important role in the preparation phase of the ESS over the next decade, working in partnership on technical projects, such as detector development, and offering the help and advice of the ILL's expert staff.

At the start of 2015 we are all looking forward to a year dedicated to the scientific programmes of our users, a year in which the Millennium upgrade programme gives way to Endurance. The final instrument of Millennium, the WASP spin-echo spectrometer (co-financed by the ILL's German Associate, the Forschungszentrum Jülich) is under construction on-site while ThALES (financed by Charles University our Czech Scientific Member) reaches full productivity with the other Millennium instruments. We plan now to move ahead rapidly with detailed planning for the Endurance instruments and infrastructure projects. This year is also special since the 6<sup>th</sup> European Conference on Neutron Scattering, ECNS2015, will be hosted by our partner country Spain in Zaragoza at the end of August. ILL staff will participate in this important conference; we will take this opportunity to show that, after the major construction period of 2013–2014, the ILL is back in business and intends to play a leading role in neutron-scattering research over the next decades.

In the following pages my colleagues of the ILL's management team will describe in more detail the highlights of 2014 as seen from their different viewpoints – science, Millennium and Endurance Programmes, technical developments, the User Programme, reactor operation and a summary of relevant facts and figures. Taken together these reports provide an in-depth picture of the ILL's activities. I hope that you find this report interesting and useful – we all look forward to a busy and creative 2015, the first of many more productive years for the ILL.

**W.G. Stirling**  
Director of the ILL

## About the Institut Laue-Langevin

The Institut Laue-Langevin (ILL) is an international research centre at the leading edge of neutron science and technology, where neutrons are used to probe the microscopic structure and dynamics of a broad range of materials at molecular, atomic and nuclear level.

The ILL is owned by the three founding countries – France, Germany and the United Kingdom. These three Associate countries contributed a total of about 62 M€ to the institute in 2014, a sum enhanced by significant contributions from the ILL's Scientific Member countries of Austria, Belgium, the Czech Republic, Denmark, Hungary, India, Italy, Poland, Spain, Slovakia, Sweden and Switzerland. The ILL's overall budget in 2014 amounted to approximately 91 M€.

The Institut Laue-Langevin operates the most intense neutron source in the world, based on a single-element, 58.3 MW nuclear reactor designed for high brightness. The reactor normally functions round-the-clock during four 50-day cycles per year, feeding neutrons to a suite of 40 high-performance instruments that are constantly upgraded.

As a service institute, the ILL makes its facilities and expertise available to visiting scientists. Our user community is world-wide: every year, about 2 000 researchers from close to 40 countries visit the ILL to perform over 800 experiments selected by a scientific review committee. The ILL monitors the papers published as a result of the use of our facilities, of which there are about 600 per year. We pay particular attention to papers published in high-impact journals. About 140 such papers are published per year from data taken on ILL instruments. This is a factor of two higher than the second most productive neutron source in the world.

The ILL has a Director and two Associate Directors who represent each of the Associate countries and are appointed on short-term contracts, normally for five years. The scientific council, comprising external scientists from the member countries, advises the Directors on scientific priorities for the

institute and how to develop the instrument suite and technical infrastructure in order to best meet the needs of the user research programme. It also assesses the scientific output of the institute. Our governing body is the Steering Committee, which meets twice yearly and is made up of representatives of the Associates and the Scientific Members together with the Directors and staff representatives. Within the framework of the Intergovernmental Convention between our Associate countries, the Steering Committee has ultimate responsibility for determining operational and investment strategies for the institute.

### NEUTRONS AND SOCIETY

The scope of the research carried out at the ILL is very broad, embracing condensed matter physics, chemistry, biology, materials and earth sciences, engineering, and nuclear and particle physics. Much of it impacts on many of the challenges facing society today, from sustainable sources of energy, better healthcare and a cleaner environment to new materials for information and computer technology. For example, neutron-scattering experiments have given us new insights into the structure and behaviour of biological and soft condensed matter, important in designing better drug delivery systems and for improving polymer processing. They also provide a unique probe into the phenomena that underpin high-temperature superconductivity as well as the molecular magnetism that may provide the technology on which the computers of the future are based.

### PREPARING FOR THE FUTURE

In 2001, the ILL launched an ambitious programme to modernise its instruments and infrastructure. Called the ILL Millennium Programme, its aim was to optimise the ILL's instrument suite (Phase M0: 2001-2008; Phase M1: 2008-2014). We are now looking forward to and setting the scene – in the framework of our ENDURANCE programme – for developments still further into the future, in order to maintain the institute's world-leading position for another 20 years.

## Why neutron scattering is useful

When used as a probe for small samples of materials, neutron beams have the power to reveal what is invisible using other radiations. Neutrons can appear to behave as particles, waves or microscopic magnetic dipoles, and it is these specific properties which enable them to uncover information that is often impossible to access using other techniques.

### WAVELENGTHS OF TENTHS OF NANOMETERS

Neutrons have wavelengths varying from 0.01 to 100 nanometers. This makes them an ideal probe of atomic and molecular structures ranging from those consisting of single atomic species to complex biopolymers.

### ENERGIES OF MILLI-ELECTRONVOLTS

The associated energies of milli-electronvolts are of the same magnitude as the diffusive motions of atoms and molecules in solids and liquids, the coherent waves in single crystals (phonons and magnons) and the vibrational modes in molecules. An energy exchange between the incoming neutron and the sample of between 1  $\mu$ eV (even 1 neV with spin-echo) and 1eV can easily be detected.

### MICROSCOPICALLY MAGNETIC

Neutrons possess a magnetic dipole moment which makes them sensitive to magnetic fields generated by unpaired electrons in materials. Precise details of the magnetic behaviour of materials at the atomic level can be investigated. In addition, the scattering power of a neutron by an atomic nucleus depends on the orientation of the spin of both the neutron and the atomic nuclei in a sample, thereby providing a powerful tool for detecting the nuclear spin order.

### ELECTRICALLY NEUTRAL

Neutrons are electrically neutral and so can penetrate deep into matter while remaining non-destructive. This makes them an ideal probe for studying, for example, biological samples or engineering components under extreme conditions of pressure, temperature or magnetic field, or within chemical-reaction vessels.

### HIGH SENSITIVITY AND SELECTIVITY

The scattering power from nucleus to nucleus in a sample varies in a quasi-random manner, even in different isotopes of the same atom. This means that light atoms are visible in the presence of heavy atoms and atoms that are close to one another in the periodic table may be distinguished from each other. This introduces the possibility of using **isotopic substitution** (for example deuterium for hydrogen or one nickel isotope for another) to allow contrast to be varied in certain samples, thereby highlighting specific structural features.

In addition, neutrons are particularly sensitive to hydrogen atoms and therefore they are a powerful probe of hydrogen storage materials, organic molecular materials, and biomolecular samples or polymers.



# SCIENTIFIC HIGHLIGHTS



The scientific highlights presented in this year's annual report demonstrate how research with neutrons continues to push back the frontiers of science

MATERIALS SCIENCE	16
CHEMISTRY AND CRYSTALLOGRAPHY	30
MAGNETISM	36
SOFT MATTER	52
BIOLOGY AND HEALTH	58
NUCLEAR AND PARTICLE PHYSICS	68
THEORY	72

**2014** was another outstandingly successful year for science at the ILL. Since the ILL was founded over forty years ago, many new neutron sources have been built around the world. Despite this, the ILL remains the reference in terms of scientific output, whatever performance indicators you may wish to use. This success is the fruit of safe and reliable reactor operations, an outstanding instrument suite under permanent modernisation, a dynamic and broad user community, a vibrant scientific environment, excellence in instrumentation, and highly motivated, service-oriented staff.

Like most other scientific institutions, the ILL is facing the challenge of maintaining the quality of its services despite the fallout of the global financial crisis, a crisis which has been affecting most European science budgets since 2008. Unlike other scientific institutions, however, the ILL is also having to deal with the impact of the 2011 Fukushima disaster, by satisfying ever more demanding safety requirements.

The very high number of complex operations successfully performed on all fronts during the recent long reactor shutdown has confirmed the ILL's ability to respond positively to these challenges. During the shutdown, in addition to completing the bulk of the reactor reinforcement work, the ILL has pursued its commitment to maintaining an ultra-modern set of experimental facilities. Preliminary measurements on the new or renovated instruments confirm the performance gains expected. These not only make for faster measurements; in many cases they open up completely new avenues of investigation. Our services to users have also been enhanced by the installation of new laboratories in the recently inaugurated Science Building.

Whenever an analytical method develops to the point where it is finally capable of answering long-standing scientific questions, breakthroughs can be expected. The neutron studies performed at the ILL into biological systems are just one illustration of the impressive array of excellent science being performed here. It has to be said that biologists have been particularly well served by the modernisation of our instrumentation and user services. In this introduction I would like to dwell on a few cases in point – research using neutrons in biology for health.

Living organisms depend on a multitude of finely-tuned and strongly interconnected biochemical regulation mechanisms. Even slight variations in the functioning of a single process may have drastic consequences for the entire body. To determine why biological processes go wrong, we need analytical probes allowing us to monitor these processes at the right length scale and under a variety of conditions. The significant role played here by X-ray crystallography is widely acknowledged. There are, however, a number of cases where additional information from neutron scattering can provide the missing key.

This is true, for example, whenever we need to identify the position of hydrogen atoms to understand a specific chemical transformation, or if the process under study is photosensitive. And both conditions hold when studying the oxidation states of enzymes, the macromolecules (proteins essentially, with a cofactor) that catalyse biochemical

processes. Some of these processes involve changes in the oxidation state of the cofactor accompanied by proton transfer. They are of paramount importance in living organisms and are always involved when energy has to be transferred for storage or activation.

If we use X-rays to obtain high-resolution structures of the compounds, there is a risk that the very high exposure levels required produce photo-chemical changes in the oxidation state. We can circumvent the problem using neutrons, as has recently been very successfully demonstrated by the ILL's Casadei and Blakeley (p.60). Using state-of-the-art instrumentation at both the ILL and FRM-II (Forschungsreaktor München-II), a team of scientists from the University of Leicester and the ILL has come up with answers to a long-standing question concerning the oxidation state of the iron ion in enzymes containing heme-groups.

***The ILL remains the reference in terms of scientific output, whatever performance indicators you may wish to use.***

There is even more to "neutrons for health" than high-resolution diffraction studies, however. Many of the processes to be investigated actually require information on intermediate length scales, where both neutron- and X-ray small-angle scattering come into their own. The article by Gabel, Hennig and Sattler (p.64) shows how several macromolecules form a complex with the messenger RNA, thus regulating the synthesis of proteins. The specific case dealt with is the regulation of proteins expressed by the sex chromosome in female and male *Drosophila melanogaster* flies (see picture on the left). At even larger length scales, the articles by Demé and Schneck (p.58) show how neutron reflectometry casts light on the organisation and binding affinities of membranes, and how these affect the membranes' biological mechanisms. In some cases structural information is not sufficient; dynamical studies are required to complete the picture of the biochemical processes under study. This is demonstrated by the work of Schreiber *et al.* (p.66) on protein diffusion in crowded environments. If you would like to know more about health-related science with neutrons, you might enjoy our recently published "Neutrons and Health" brochure (<http://www.ill.eu/quick-links/publications/topical-brochures/>).

So much for biology and health... but I invite you to read on. You will see that the ILL has been producing remarkable results across the full range of its portfolio, from innovative electrode materials for lithium ion batteries to the intriguing mysteries of quantum mechanics. I hope that as you turn these pages you will understand my enthusiasm, for they show how scientists have been benefitting from our continuous efforts to develop new instrumentation, constantly review our options, and above all, produce the science our society needs.

*Helmut Schober*

**Helmut Schober**  
Associate Director

??

QUERY - this person is not mentioned as an author at p.58

# COLLEGE INTRODUCTIONS

## COLLEGE 1 – APPLIED METALLURGY, INSTRUMENTATION AND TECHNIQUES

A. Stunault (College 1 Secretary)

College 1 has a strong applied orientation, receiving proposals from engineers and scientists to investigate the real-world problems they wish to solve. About one half of the proposals submitted concern problems in engineering and metallurgy involving the microscopic analysis of strains and stresses using the ILL's strain scanner SALSA. Other proposals correspond to fields also covered by other Colleges, but with an emphasis on applications and technical developments. Finally, a small number of research proposals deal with neutron methods and instrumentation. The experiments performed on SALSA are largely related to processes, such as casting and rolling, and to the basic materials sciences at the heart of a wide range of industries, such as the automotive industry (turbochargers), the aerospace industry (large-scale aluminium alloy components and engines) and furnace manufacturing. An increasing number of studies also concern ALM (additive layer manufacturing), highlighting current interest in additive methods.

The non-SALSA-related studies span a large number of fields and are spread across most of the ILL instrument suite: time-of-flight, small-angle scattering, three-axis spectroscopy and, predominantly, diffraction. Of particular interest are studies in geology, battery cell development, cultural heritage and neutron instrumentation.

## COLLEGE 2 – THEORY

M.B. Lepetit (College 2 Secretary)

The reorganisation of the ILL Theory College two years ago broadened the scope of the scientific areas covered by our College but did not change its tradition of hosting visitors for several months. In 2014 our visitors worked on such varied subjects as competing nesting instabilities (PG), absorption of ultracold neutrons (PG), tunnelling in ferromagnetic-superconductor junctions (KK), and interface effects on composite layered magnetic structures (STC).

One piece of work in the field of chemical physics exemplifies particularly well the dynamism of our regular visitors. In the course of this work (p.76), proton transfer by quantum tunnelling in short hydrogen bonds was shown to occur in all such bonds, even at low temperatures. This is an important result, for example in enzyme catalysis under physiological conditions, since short hydrogen bonds with low barriers are known to be essential in enhancing catalytic rates through proton transfers.

The Theory College also remained particularly active in the area of condensed matter. This is illustrated by the highlight on p.72, where the inhomogeneous nature of the mechanical response at the nanoscale was studied in disordered solids, such as glasses. In such systems, the elastic heterogeneities strongly affect the nature of the sound waves, which, in contrast to perfect crystals, cannot be completely rationalised in terms of phonons.

The soft matter activity was strengthened by the arrival of Felix Roosen Runge, who has launched a number of new projects in close collaboration with different ILL experimental groups. In condensed matter, electronic structure calculations are a very useful tool for unravelling the origin of properties such as ferroelectricity and magneto-electric coupling in multiferroic compounds. In the highlight on p.74, we see not only that the  $\text{GeV}_4\text{S}_8$  compound is a multiferroic system but also how first principle calculations demonstrate that the polarisation originates from an orbital ordering and is then further amplified.

Finally, it is important to emphasise the active involvement of the members of the Theory College in the scientific life of the ILL. The College was responsible for the organisation of a number of events, including a workshop on spin currents and related materials, which was part of a programme involving the Japanese Atomic Energy Authority and Delft University, and a school on Materials and Competing Interactions, which was part of a French national programme dedicated to the training of young researchers.

## COLLEGE 3 – NUCLEAR AND PARTICLE PHYSICS

A. Blanc (College 3 Secretary)

The activities of College 3 focus on the fields of nuclear and particle physics and cover an extremely broad scope, ranging from fission yield measurements for nuclear reactor applications to the study of very fundamental quantum mechanics effects, such as the Quantum Cheshire Cat effect, whose idea was proposed for the first time in 2013 and was named after the well-known cat in Alice in Wonderland. It refers to an object (the cat) whose properties (the cat's grin) can be separated from its physical location and detected at a different location. This effect was measured for the first time at the instrument S18 using neutron interferometry (p.68). The polarised neutron beam was split into two paths with different spin directions. Small magnetic fields were applied to the paths to test the location of the neutron's spin component. At the end of this experiment, it was clearly shown that, statistically, the neutron (the cat) and the neutron's spin component (the cat's grin) took different paths. As a pure quantum mechanics effect, this astonishing effect can be applied to any quantum system, a fact which may open the way to new applications in the field of quantum information technology.

The qBounce collaboration recently published the results of an experiment performed using the ultra-cold neutrons delivered by the PF2 instrument (p.70). The kinetic energy of these neutrons is so low ( $\sim 300$  neV) that the gravitational effects are no longer negligible and some neutrons actually form bound quantum states in the gravity potential of the earth. The Gravity Resonance Spectroscopy method developed by the qBounce collaboration makes it possible to measure the energy of the eigenvalues via Rabi spectroscopy, which translates them into a simple frequency measurement. The measured frequency was compared to predictions of non-Newtonian gravity effects which may

explain the existence of Dark Matter and/or Dark Energy. This comparison provided new experimental limits which are five orders of magnitude more restrictive than previous measurements. This method is extremely sensitive to new physics and may in the future become a very powerful tool for research beyond the standard model of particle physics.

## COLLEGE 4 – MAGNETIC EXCITATIONS

G. Nilsen (College 4 Secretary)

The continuing success story of inelastic neutron scattering and magnetism has grown by several chapters over the past year, with many interesting twists and turns along the way. The word 'turn' is particularly appropriate to the material  $\text{ErMnO}_3$ , where the manganese magnetic moments turn from site to site in the crystal lattice. The coupling of this complex magnetic order to the structure produces a fascinating phenomenon known as multiferroicity, whereby the electrical properties of the material can be controlled via its magnetism and vice versa. An inelastic neutron-scattering study carried out on the IN5 and IN22 spectrometers elegantly illustrates how the excitations in  $\text{ErMnO}_3$  manifest this coupling (p.40).

The highlight on p.46 deals with another fundamental excitation. As the dimensionality of a magnetic material is reduced, quantum fluctuations become more and more important to its properties. A perfect example of this is  $\text{BaCo}_2\text{V}_2\text{O}_8$ , which contains one-dimensional chains of magnetic moments. Data from the three-axis spectrometer IN12 show that the coupling between these chains generates a remarkable ladder of magnetic excitations, including a never-before-seen quantum mode.

The quantum nature of magnetism is also key to the story of  $\text{TlCuCl}_3$  (p.36). Using state-of-the-art ILL high-pressure equipment in conjunction with the IN14 three-axis spectrometer, it was possible to clarify the differing roles of classical and quantum fluctuations on passing through the quantum critical point separating the low-temperature ordered and disordered phases. The viability of the experiment on IN14 promises a bright future for similar experiments on the ThALES triple-axis spectrometer, which will enter the user programme as of the third cycle of 2015.

The most surprising plot twist of the year was supplied by  $\text{CeB}_6$ , a material which displays a so-called hidden order, i.e. a magnetic order which is not dipolar. For years, it has been assumed that the dominant magnetic interactions in the system are antiferromagnetic. This view is now being challenged by the study described in the highlight on p.38, whose authors found a strong excitation emanating from a ferromagnetic position in reciprocal space using the IN5 chopper spectrometer. As well as forcing a re-evaluation of  $\text{CeB}_6$ , this work also has wide-reaching implications for other hidden order systems.

Now that 2014 has come to a satisfactory conclusion, it is time to look forward to what the world-class partnership between neutrons and magnetism has to offer in the coming year.

## COLLEGE 5A – CRYSTALLOGRAPHY

T.C. Hansen (College 5A Secretary)

College 5A deals with the study of the nuclear atomic-scale structure of crystalline solid matter, either in single-crystal or polycrystalline ("powder") form, and evaluates applications for beamtime primarily on the ILL's diffractometers. Neutron diffraction is a vital tool for studying the structure of many minerals and functional materials. While most inorganic materials can be studied by powder diffraction, more complex materials, in particular biologically relevant materials, require the high precision and resolution which only single-crystal diffractometers, such as D19, can deliver (p.32).

In contrast to X-ray diffraction, neutrons make it possible to locate light elements accurately in the presence of heavier ones, as well as to distinguish (most) neighbouring elements in the periodic table. Furthermore, as a weak probe, neutrons are scattered by the bulk of a sample and not just by the surface and thus provide a better picture of the sample as a whole. Similarly, neutrons penetrate most shielding materials without substantial losses and allow the use of complex sample environments. In this way, for example, it was possible to study the structure of nickel cyanide at very high pressure and low temperatures in order to understand its peculiar negative thermal expansion and linear compressibility behaviour (p.18).

Not only does neutron diffraction provide access to instantaneous structures, it also allows us to study their evolution with thermodynamic conditions, such as temperature and pressure, as well as with time. At the ILL, neutron diffraction is increasingly used to study the activity and behaviour of materials under non-ambient and chemically active conditions. Studies of even the simplest materials, such as oxygen in confined geometry or at high pressure or water ice at certain temperatures and preparation conditions, lead to new, fundamental insights. Last year saw the *in situ* formation of a new phase low-density form of ice, ice XVI, or, rather, of an empty gas hydrate/clathrate [Falenty *et al.*, Nature 516 (2014) 231].

Neutron diffraction is a vital tool for the characterisation of economically important "energy materials". The number of beamtime proposals relating to the most promising rechargeable battery materials, which are based on the light element lithium, has risen tremendously. Lithium ion batteries are already widely used, but their outreach into other application domains, such as transportation, needs to be improved. The position of lithium ions in an oxide host can be determined by neutron powder diffraction, and the pathway of these ions during charge and discharge cycles can be traced *in operando*. Rapid data acquisition, combining detector technology and high neutron flux, makes time-resolved powder neutron diffraction possible in specially adapted batteries (p.16).

# COLLEGE INTRODUCTIONS

## COLLEGE 5B – MAGNETIC STRUCTURES

C. Ritter (College 5B Secretary) and C. Dewhurst (vice-Secretary)

For the proposal round in autumn 2014, a significant change was made to the College 5B subcommittee. As a consequence of the ongoing high number of proposals submitted, it was decided to set up a so-called “FOCUS” group within the College. All proposals using small-angle scattering or reflectometry methods to study elastic magnetic scattering are now discussed and assessed within this FOCUS group by subcommittee members specialised in these topics.

Although it is difficult to establish clear scientific trends from just two proposal rounds (there were no proposal rounds in 2013), it is possible to identify a continuing interest in flux line lattices and an increasing number of proposals relating to magnetic systems with unusual ground-states (quantum, frustrated, multiferroics). An example is given in one of our highlights (p.48), which shows how magnetic frustration and a strong magnetic anisotropy lead to an incommensurate antiferromagnetic order in  $\text{SrTb}_2\text{O}_4$ . This very complete study combines results from D7 using polarisation analysis, from the single crystal diffractometer D23 and from the three-axis spectrometer IN12. While the interest in iron pnictide and chalcogenide superconductors seems to be slowly waning, work on high-temperature cuprate superconductors continues. Taking advantage of its very low background, IN14 was used for a study (p.42) on the electronic phase separation in the system  $\text{La}_{2-x}\text{Sr}_x\text{CuO}_{4+\delta}$  where it was shown that co-doping by Sr/O leads to a surprising stabilisation of superconducting and magnetic phases.

Multi-parameter studies of magnetism using neutron powder diffraction are gaining in importance. One example is the work described on p.50, where the effect of pressure on the magnetic transition temperature in the spin-crossover compound  $\text{Fe}^{\text{II}}(\text{1-methyltetrazole})_2(\text{Fe}^{\text{II}}\text{Br}_4)_2$  as determined on the high intensity powder diffractometer D1B was studied. While these pressure studies were performed using conventional clamp cells, the use of the Paris-Edinburgh pressure cell has become routine for pressures up to 9 GPa and temperatures down to 5 K, especially on the high intensity powder diffractometer D20. This instrument also allows a 10 T cryomagnet to be installed; the highlight on p.44 presents the example of the quantum spin system  $\text{CuBrSr}_2\text{Nb}_3\text{O}_{10}$  where neutron diffraction under a magnetic field showed that a magnetisation plateau found in this layered square lattice  $S = 1/2$  system is only coincidentally centred at a value of  $1/3$  of the saturation magnetisation.

## COLLEGE 6 – LIQUIDS AND GLASSES

V. Cristiglio (College 6 Secretary)

College 6 receives proposals for probing the structure and dynamics of a wide range of substances, from monomolecular to high molecular weight polymers. What this wide range of apparently unrelated substances have in common is that the properties of interest, whether it be structure or dynamics, must be found when the substance is in either the glassy or the liquid state. Proposals range from investigating fundamental physics to determining the structure of future energy storage materials. A noticeable trend over the past year has been a significant increase in the number of proposals to probe the properties of molecular liquids

and glasses. A growing number of proposals are based on experiments at the technical limits of the instruments, which is very encouraging as it shows that the community is embracing high-risk, high-reward proposals. From a structural perspective, the D4 diffractometer remains the most in-demand instrument, whilst inelastic studies are spread across both quasi-elastic and spin-echo instruments.

There has also been an increase in the number of proposals seeking to exploit non-standard sample environments, particularly novel pressure cells. This trend is illustrated perfectly by a study on D4 of network-forming tetrahedra (p.26), which play a key role in governing the physical and chemical properties of disordered oxide materials. Such studies are vital if we are to understand the behaviour of materials ranging from photonic glasses to the fluids in planetary interiors. The authors used the Paris-Edinburgh pressure cell to measure structure up to pressures of 8.5 GPa to show that the co-ordination number of these motifs can be rationalised in terms of the oxygen-packing fraction.

Another highlight (p.28) illustrates the role of interdisciplinarity in the science of liquids and glasses, which is often underpinned by the development of new chemical methodologies to generate ever more exotic materials. The authors used a variety of inelastic spectrometers to access a wide range of energy transfers to probe the dynamics of endofullerenes. Innovative developments in synthetic organic chemistry have enabled small molecules, such as water and dihydrogen, to be permanently encased inside the cage of a  $\text{C}_{60}$  fullerene molecule. The strongly quantum mechanical properties of the isolated, entrapped molecule can be probed by inelastic neutron scattering. In doing so the authors of this highlight made the surprising discovery of a new form of selection rule.

## COLLEGE 7 – SPECTROSCOPY AND MODELLING

M. Zbiri (College 7 Secretary)

The activities of College 7 continue to reflect the increased interest in scientific topics dealing with the dynamics of advanced functionalised materials, including energy. These basically represent 50 % of the research proposals evaluated by the College 7 subcommittee, as has been systematically observed over the last few proposal rounds. Therefore, this tends to shape a scientific core business for the College. Due to practical considerations and societal requirements, functionalised materials play a vital role in our everyday lives. Nowadays, such materials are indispensable for industrial engineering, energy supply and sustainability, the environment, healthcare, as well as life sciences. However, in order to develop tailored macroscopic functions with optimised performances, the time evolution of the complex structure-dynamics-property relationships, in the solid-state phase, must first be carefully studied at the microscopic level. In this context, neutron spectroscopy is a robust master technique for probing dynamics at the meV and nanometer scales. This can be clearly seen from the four highlights presented in this report.

The neutron backscattering technique was used on (the now decommissioned) IN16, as well as the newly commissioned IN16B, to study the dynamics of a relaxor ferroelectric (p.22). The authors observed a clear inelastic component. This feature and its temperature dependence highlight for the first time a direct link between the characteristic relaxation behaviour and the lattice dynamics of the relaxor materials as “sensed” by neutrons.

Where surface dynamics and friction are concerned, the ILL time-of-flight spectrometer IN6 and spin-echo spectrometer IN11 were used, together with OSIRIS at ISIS, to trace the motion of benzene molecules on graphite (p.20). The team identified this system as showing an almost perfect two-dimensional Brownian diffusion of nano-cogwheels with negligible surface friction. The third highlight presents a combined high-pressure study by neutron diffraction, using D20, and inelastic neutron scattering (INS), using IN6, to probe in a synergistic way the structure and dynamics of the two-dimensional layered negative thermal expansion material  $\text{Ni}(\text{CN})_2$  (p.18). The authors showed for the first time the occurrence of pressure-driven phase transitions and isomerisation. The fourth highlight in this section deals with the dynamics of quantum rotors entrapped within fullerenes (p.28). The authors employed INS techniques, using IN4, IN5 and IN1-Lagrange, to probe quantum mechanical properties of permanently encased  $\text{H}_2$  and  $\text{H}_2\text{O}$  molecules inside  $\text{C}_{60}$  leading to the discovery of a new form of selection rule.

## COLLEGE 8 – BIOLOGY

B. Demé (College 8 Secretary)

Experiments performed in the field of biology and health cover a wide range of techniques for studying structures and dynamics, including inelastic scattering, single crystal diffraction, SANS on macromolecular solutions, and reflectivity studies on monolayer, single- and multi-layer membrane systems. This year’s highlights illustrate again this diversity and they confirm the current trend towards increasingly complex model and biological systems.

The new backscattering spectrometer IN16B has opened up unprecedented opportunities to study the relation between protein function and dynamics under physiological conditions, as can be seen in the study of the effect of macromolecular crowding on  $\gamma$ -globulin’s global and internal protein dynamics (p.66).

Thylakoid membranes inherited from ancestral cyanobacteria were investigated on D16 in the form of reconstituted multilayers (p.58). Their organisation, as regular lamellar stacks of bilayers or as hexagonal domains, is regulated by hydration and by a subtle tuning of the lipid composition. In developmental contexts or in response to environmental variations, the results contribute to explaining the highly dynamic flexibility of these structures.

Moving to atomic resolution, neutron cryo-crystallography on LADI provides a way to determine the structure of enzyme intermediates – including the positions of hydrogen atoms – while also avoiding radiation damage issues that can occur using X-rays. Studying the structure of a transient intermediate using neutrons has made it possible to propose a new catalytic mechanism for the heme enzyme cytochrome c peroxidase (p.60).

In the field of orthopaedic implants, results obtained on D17 with different types of proteins highlight both the importance of hydrophilic polymer brushes used to prevent undesired protein adsorption to biomedical devices and the implications of PEG’s often neglected antigenicity (p.62).

Finally, neutrons helped to reveal the structural basis of a gene regulation mechanism in *Drosophila* flies (p.64). For the evolved diversity of life, it is not only the number of genes that is important. Differences during the regulation of gene

translation also play a critical role. In order to obtain a model of the three-dimensional structure of a ternary protein-RNA complex, a combination of complementary techniques was used: NMR, crystallography, SAXS and SANS on D22.

As a result of the extension of the ILL22 guide hall, instrument resiting and the installation of the new H5 guides during the long shutdown, several instruments (D22, D16 and IN15) involved in experiments in biology have benefited from upgrades. We are looking forward to conducting challenging experiments in 2015 on these upgraded instruments.

## COLLEGE 9 – SOFT CONDENSED MATTER

O. Czakkel (College 9 Secretary) and L. Porcar (vice-Secretary)

Following the long reactor shutdown, Soft Condensed Matter science has maintained its prominent position in the ILL’s user programme. With 19 % of the submitted proposals, College 9 had the second highest number of requests for beamtime in 2014. Similarly to earlier years, both fundamental and applied science are represented in the studies undertaken, which very often lie on the interface of physics, chemistry and biology. Thanks to the contrast variation technique, neutron studies offer a unique insight into soft matter systems. Bio-related studies are still at the forefront of soft-matter science. A systematic small-angle neutron-scattering (SANS) study on D22 involving Cowpea Chlorotic Mottle virus (CCMV) has revealed a method that makes it possible to determine the weight of polymers packaged in viral capsids. The results may help to reveal the nonspecific origin of genome selectivity for a number of viral systems (p.54).

Studying soft matter systems under deformation is a current challenge. A new state-of-the-art flow-SANS sample environment has been developed and implemented on D22, which made it possible to perform a detailed study on stress and structure evolution in sheared micellar solutions. The successful combination of rheometry and time-resolved flow-SANS will certainly provide new opportunities to investigate a broad range of nonlinear flow phenomena in complex fluids (p.52).

Environmental protection-related subjects are also current hot topics. A neutron reflection study on FIGARO addressed the question of the modification effect of pollutants on the atmospheric composition. Thanks to the high stability and flux of the ILL reactor, an outstanding time resolution of 3-5 seconds was achieved during kinetic measurements to explore the efficiency of different gases for oxidising organic films at the air/water interface. The results demonstrated that these kinds of surface studies can provide important missing data for the development of atmospheric models of climate change (p.30).

A new and comprehensive study has been performed on the microscopic dynamics of ring polymers by neutron spin-echo spectroscopy on IN15. The experiments provided the first experimental verification of theoretical models that invoke lattice animals or crumpled globules, where the loop size would be an intrinsic ring property (p.56).

One final important development over the last year is that soft matter scientists coming to the ILL (and ESRF) are now able to fully exploit the new laboratories of the Partnership for Soft Condensed Matter (PSCM) located in the new Science Building. The official scientific programme of the PSCM can be expected to grow significantly from 2015 onwards, as the affiliation process for the first partners is due to be completed at the beginning of the year.

# ILL in the press

1. Published in *eEconomista* on 30 May 2014
2. Published in *The Huffington Post* on June 2014
3. Published in *BBC NEWS* on 29 July 2014
4. Published in *Financial Times* on 8 August 2014

1. **elEconomista.es** | Ciencia  
Viernes, 30 de Mayo de 2014 Actualizado a las 16:04

Portada Mercados y Cotizaciones Empresas Economía Tecnología Vivienda Opinión/BI  
Actualidad | EcoDiario GLOBAL ESPAÑA DEPORTES MEDIO AMBIENTE CULTURA Pr

## Las emisiones del biodiésel reducen las precipitaciones

Europa Press | 30/05/2014 - 16:04

0 comentarios

Puntúa la noticia: Nota de los usuarios: 5.0 (1 votos)

Un estudio sobre cómo las moléculas orgánicas en la atmósfera afectan a la formación de nubes ha descubierto que un componente principal del biodiésel, el oleato de metilo, reacciona con el ozono sorprendentemente rápido.

Así contrarresta el crecimiento de las gotas de agua provenientes de emisiones, lo que a su vez inhibe la formación de nubes y, por lo tanto, afecta al ciclo del agua de una manera muy compleja.



2. **HUFF POST SCIENCE**  
Edition: U.S. | Like (113k) | Follow | Newsletters

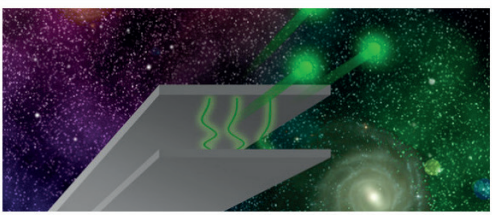
FRONT PAGE POLITICS BUSINESS ENTERTAINMENT ARTS TECH GREEN TASTE EDUCATION

Science • Asteroids • Brain • Dinosaurs • Girls In STEM • Human Origins • ISS • Mars Rover • Physics • Search

Astronauts Put A Camera Inside An Orb Of Water, And This Happened  
Yes, This Is North America On Jupiter

## Bouncing Neutrons Aid Search For Dark Matter, Dark Energy

Space.com | By Charles Q. Choi  
Posted: 05/06/2014 8:46 am EDT | Updated: 05/06/2014 8:59 am EDT



395 142 31 22 5 16

Neutrons bouncing in Earth's gravity are helping to shed light on two of the greatest mysteries in the universe, dark matter and dark energy, researchers say.

3. **BBC NEWS SCIENCE & ENVIRONMENT**  
Home UK Africa Asia Australia Europe Latin America Mid-East US & Canada Business Video

29 July 2014 Last updated at 17:36 GMT

## 'Quantum Cheshire Cat' becomes reality

By James Morgan  
Science reporter, BBC News



The Cheshire Cat mysteriously disappeared leaving only his mischievous grin

Scientists have for the first time separated a particle from one of its physical properties - creating a "quantum Cheshire Cat".

The phenomenon is named after the curious feline in Alice in Wonderland, who vanishes leaving only its grin.

Researchers took a beam of neutrons and separated them from their magnetic moment, like passengers and their baggage at airport security.

They describe their feat in *Nature Communications*.

Related Stories  
Quantum 'world record' smashed  
Is Alice in Wonderland really about drugs?  
Are birds hijacking quantum physics?

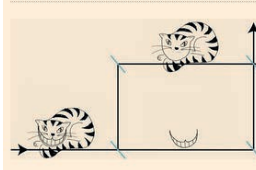
4. **FT Magazine**  
Home UK World Companies Markets Global Economy Lex Comments  
Arts Magazine Food & Drink House & Home Lunch with the FT Style Books Pursuits

August 8, 2014 4:52 pm

## Quantum physics: the curious case of a neutron and its spin

By Clive Cookson

Scientists succeed in separating a particle from its physical properties, a phenomenon they called the 'quantum Cheshire cat'



The weird world of quantum physics has thrown up another strange and paradoxical phenomenon, which scientists call the "quantum Cheshire cat". It involves separating a particle from one of its physical properties, just as the cat in *Alice's Adventures in Wonderland* was separated from its grin.

Researchers from Vienna University of Technology report in the journal *Nature Communications* that they have achieved this feat for the first time, separating neutrons from their magnetic moment, a fundamental property of subatomic particles. They carried out the experiment – which, like most quantum research, is impossible to explain in simple language – at the Institut Laue-Langevin (ILL), a powerful neutron source near Grenoble in France.

5. **Le Point.fr**  
SPECIAL GRENOBLE

## La médecine en mutation



endroits du cœur pour traiter certaines insuffisances cardiaques. A Grenoble, STMicroelectronics, le CEA Leti et le laboratoire de génie des procédés y ont participé à la recherche préclinique. « Nous sommes parvenus à un rapport puissance-volume intéressant, se réjouit Philippe Cingolati. Avec un diamètre de 100 micromètres, nous produisons 500 microwatts, alors qu'il en faut entre 10 et 20 pour un pacemaker. Au terme de tests vivants à démontrer son innocuité à long terme, la biopile devrait être commercialisée dans les cinq ans.

**Précurseurs.** Comment les chercheurs grenoblois en biotechnologie sont en train d'inventer les remèdes de demain.

d'une dizaine de brevets, permettra d'éviter les opérations chirurgicales chez des patients à qui on a implanté des dispositifs dont les batteries réclament d'être rechargées tous les sept à huit ans. Ainsi, stimulateurs cardiaques mais aussi cérébraux, pompes à insuline ou encore optiques virtuelles artificielles (en développement chez Uromems, une start-up grenobloise).

**Fiables.** Grâce à la trousse du professeur Philippe Cingolati, les implants deviendront autonomes en énergie.

**Inédites.** Traiter un cancer sans effets secondaires, tel est le défi de Laurence.

6. **nature** International weekly journal of science  
Home News & Comment Research Careers & Jobs Current Issue Archive Audio & Video For Authors

NATURE | NEWS

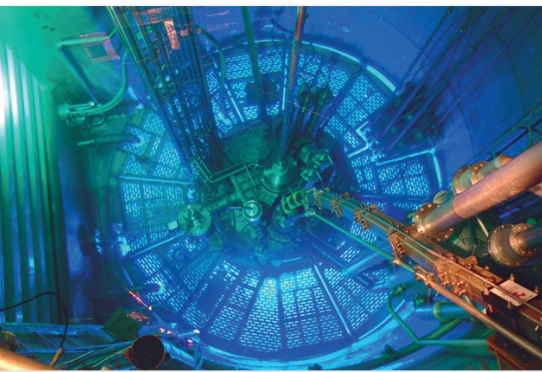
## Bouncing neutrons probe dark energy on a table-top

An experiment measuring gravity's effects at the quantum scale finds no deviations from Newton's laws.

Elizabeth Gibney

18 April 2014

Rights & Permissions



The High-Flux Reactor at the Laue-Langevin Institute in Grenoble, France, produced the neutrons used in an experiment that tested for possible deviation from the known laws of gravity.

5. Published in *Le Point* on 9 August 2014
6. Published in *Nature* on 18 April 2014
7. Published in *The Hindu* on 15 May 2014
8. Published in *Welt der Physik* on 30 July 2014

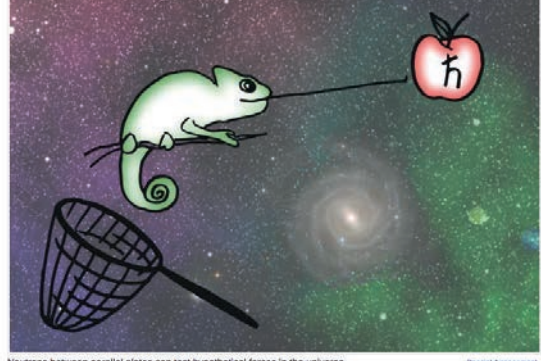
7. **THE HINDU**  
Home News Opinion Business Sport S&T Features Entertainment Books

S&T • SCIENCE Updated: May 15, 2014 00:02 IST

## No chameleons in dark energy?

Euro Exchange Rates - Excellent Euro Exchange Rates Free Transfers, No Fees. Get Quote!  
www.torfx.com/France

SHUBASHREE DESIKAN



Neutrons between parallel plates can test hypothetical forces in the universe.

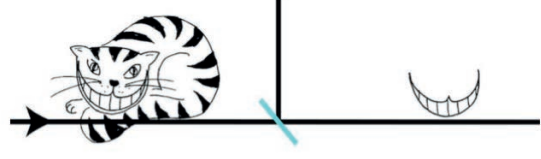
These measurements, in fact, disprove the existence of the hypothetical "quintessence" particles which form one explanation for dark energy, at this level of accuracy.

Particle physics always conjures up images of very high-energy experiments, particle accelerators etc. A recent study – a table-top experiment with low-energy neutrons – shatters this image and introduces a low-energy technique to probe gravity, dark energy and dark matter.

8. **welt der physik** ...heute schon geforscht?

Gebiete Themen vor Ort Mediathek Navigator Über uns

Kräfte, Teilchen, Kerne Nachrichten über Kräfte, Teilchen und Kerne 2014



## Quanten-Paradoxon experimentell bestätigt

Schrödingers Katze gehört zu den bekanntesten Phänomenen der Quantenphysik. Das Gedankenexperiment beschreibt eine Katze, die in einer Box eingeschlossen ist, in dem ein Gift freigesetzt wird, sobald ein radioaktives Teilchen zerfällt. Solange die Box nicht geöffnet wird, besagen die Gesetze der Quantenmechanik, dass sich dieses Teilchen in einem überlagerten Zustand aus „zerfallen“ und „nicht zerfallen“ befindet. Ergebnis: Die Katze ist gleichzeitig tot und lebendig.

Forscher um Yvonne Hassler von der TU Wien ließen es nun nur noch ein weiteres Quantenphänomen

# MATERIALS SCIENCE

## Real-time neutron diffraction studies of electrode materials for Li-ion batteries

### High-intensity two-axis diffractometer D20

In the last 30 years Li-ion (lithium-ion) batteries have become the leading technology for powering portable electronics and are, more recently, spreading to the automotive market. The key to improving their performance is understanding lithium's extraction and insertion reaction from/into the electrode materials. Diffraction is a great technique for determining crystal structure changes in such materials but, while X-rays provide useful information, they are poorly sensitive to light elements like lithium. Luckily, neutrons have a different scattering mechanism and can therefore "see" lithium ions moving through the electrodes.

#### AUTHORS

M. Bianchini and E. Suard (ILL)

#### REFERENCES

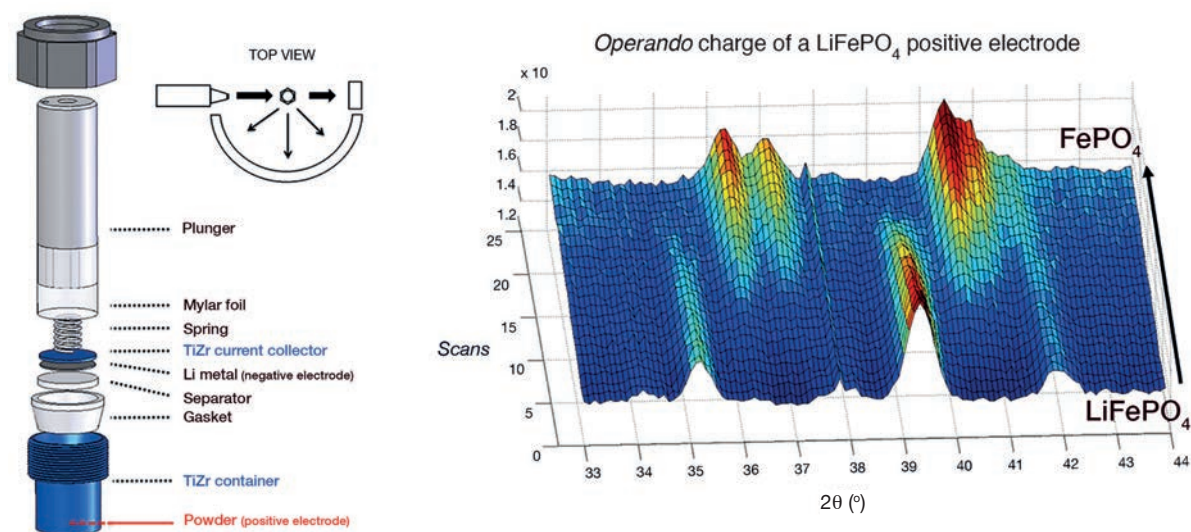
- [1] M. Armand *et al.*, *Nature* 451, 7179 (2008) 652
- [2] M. Morcrette *et al.*, *Electrochimica Acta* 47 (2002) 3137
- [3] M. Roberts *et al.*, *Journal of Power Sources* 226 (2013) 249
- [4] M.M. Thackeray, *Progress in Solid State Chemistry* 25(1-2), (1997) 1

For this reason we developed a sample environment to study electrode materials for Li-ion batteries using neutron diffraction, *in real time*, while a battery is charged and discharged. This is crucial because, like in any time-dependent experiment, a better understanding is achieved when the time resolution is improved. In our case we did this by moving away from standard *ex situ* experiments providing only a few snapshots of the charge/discharge of a material, to a movie of its entire evolution.

The sample environment we developed is essentially an electrochemical cell able to function using massive electrodes (200 mg or more – massive on the electrochemistry scale but a small sample for neutrons) with good performance, and to produce neutron diffraction patterns of high quality for data analysis. The most important feature of such cells is the use in the manufacturing process of a (Ti,Zr) alloy, known for being neutron-transparent. This way only the signal from the electrode of interest can be collected, thus avoiding other unwanted contributions from the cell. Moreover, the use of a deuterated version of the electrolyte present in the battery further reduces incoherent scattering and improves the signal obtained.

**Figure 1**

**Left:** Scheme of the developed *in situ* cell.  
**Right:** 3D view of the *operando* charge of a  $\text{LiFePO}_4$  electrode measured on the D20 diffractometer. The  $\text{LiFePO}_4$  phase can be observed to disappear, while the  $\text{FePO}_4$  charged phase appears.



Our studies are conducted on the D20 high-flux diffractometer, the high flux being an extremely important feature given the small (on the neutrons scale) samples.

A first phase of testing with relatively well-known electrode materials such as  $\text{LiFePO}_4$  was undertaken, where we verified the proper functioning of the cell in terms of electrochemistry, the quality of the neutron diffraction patterns and the feasibility of performing such measurements in real-time. This means doing them *in situ* AND *operando* – Latin terms meaning that the measurements are done while the battery is charging and discharging (**figure 1**).

Studies of electrode materials with such a cell started with the manganese spinel  $\text{LiMn}_2\text{O}_4$ . This is a very interesting positive electrode material, given its good capacity and high-rate capabilities. However, its capacity quickly fades upon cycling, making its industrial application impossible. The issue is solved in the synthesis process thanks to the use of more lithium, giving rise to compositions written as  $\text{Li}_{1+x}\text{Mn}_{2-x}\text{O}_4$ , where x is the amount of extra lithium in the structure, added at the expense of manganese. This reduces the usable capacity but, more importantly, eliminates the problem of capacity fading. We thus synthesised  $\text{LiMn}_2\text{O}_4$ ,  $\text{Li}_{1.05}\text{Mn}_{1.95}\text{O}_4$  and  $\text{Li}_{1.10}\text{Mn}_{1.90}\text{O}_4$  and performed neutron diffraction experiments in real time upon lithium's extraction from the three materials (i.e. looking at the charge of the batteries, **figure 2**).

Our study showed not only that the volume change induced by the delithiation is reduced while going from  $\text{LiMn}_2\text{O}_4$  to  $\text{Li}_{1.10}\text{Mn}_{1.90}\text{O}_4$ , but also that the mechanism by which this

happens is modified. In fact, while  $\text{Li}_{1.10}\text{Mn}_{1.90}\text{O}_4$  reacts through a simple monophasic reaction (a solid solution where only one crystallographic phase is involved),  $\text{Li}_{1.05}\text{Mn}_{1.95}\text{O}_4$  shows the existence of a solid solution process followed by a biphasic reaction, while  $\text{LiMn}_2\text{O}_4$  even shows a sequence of two biphasic reactions.

Both the above mentioned features contribute to make over-lithiated  $\text{Li}_{1.10}\text{Mn}_{1.90}\text{O}_4$  a much better candidate for use in Li-ion batteries than the standard stoichiometric  $\text{LiMn}_2\text{O}_4$ .

All this can be studied thanks to neutrons; what's more, the data analysis procedure is richer with neutrons than with X-rays because we can actually understand what lithium is doing in the material. In more detail, this means that we can use the Rietveld method to increase the accuracy of our time-dependent structural model. In the specific case of spinels  $\text{Li}_{1+x}\text{Mn}_{2-x}\text{O}_4$  this raises the possibility of correlating, for the first time, the evolution of lithium's concentration with the electrochemical features of the materials, which is of key importance for understanding and therefore improving Li-ion battery materials.

Given these promising results, the study of spinel materials is expanding to different compositions (i.e.  $\text{LiMn}_{1.6}\text{Ni}_{0.4}\text{O}_4$ ) operating at higher voltages and thus having more energy. The cell will be also used for several further studies on new positive and negative electrode materials during the current and future reactor cycles at ILL, finally transforming neutron diffraction from a promising technique into a reality for understanding lithium's behaviour and structural modifications occurring in Li-ion batteries.

[This work is part of the ILL thesis work of Matteo Bianchini].

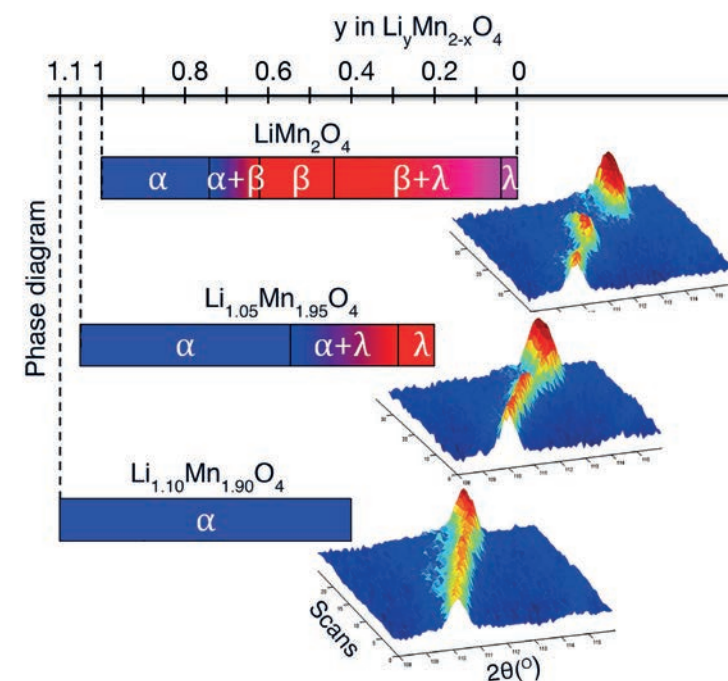


**Figure 2**

**Left:** Phase diagram observed *operando* upon charge ( $\text{Li}^+$  extraction) for  $\text{LiMn}_2\text{O}_4$  (top),  $\text{Li}_{1.05}\text{Mn}_{1.95}\text{O}_4$  (middle) and  $\text{Li}_{1.10}\text{Mn}_{1.90}\text{O}_4$  (bottom).  
**Right:** Focus on a narrow  $2\theta$  angular range of the respective neutron diffraction patterns, showing the peaks' evolution.

# MATERIALS SCIENCE

## A high-pressure neutron-scattering study sheds light on the stability, compressibility and phase transitions in Ni(CN)<sub>2</sub>

High intensity diffractometer D20 and time-of-flight spectrometer IN6

Negative thermal expansion (NTE) and negative linear compressibility (NLC) properties are attracting much attention. This is because their tailoring paves the way for the design of zero expansion and compressibility composites in view of potential applications in the fields of civil engineering, aerospace industry and biomedicine. However, this depends on the prior understanding of these intriguing behaviours at the microscopic level. By combining high-pressure elastic (diffraction) and inelastic neutron scattering (INS), we explored structure and dynamics of 2-D Ni(CN)<sub>2</sub> by studying its compressibility, stability and phase transitions.

### AUTHORS

M. Zbiri, T. Hansen and H. Schober (ILL)  
S.K. Mishra, R. Mittal, R. Rao, P. Goel and S.L. Chaplot (BARC, Mumbai, India)  
A.M. Chippindale and S.J. Hibble (University of Reading, UK)

### REFERENCES

- [1] C. Lind, *Materials*, 5(6) [2012] 1125
- [2] A. Cairns, A. Thompson, M. Tucker, J. Haines and A. Goodwin, *J. Am. Chem. Soc.*, 134 [2012] 4454
- [3] Y. Mo and E. Kaxiras, *Small*, 3 [2007] 1253
- [4] R. Mittal, M. Zbiri, H. Schober, E. Marelli, S. Hibble, A. Chippindale and S. Chaplot, *Phys Rev B*, 83 [2011] 024301
- [5] S. Mishra, R. Mittal, M. Zbiri, R. Rao, P. Goel, S. Hibble, A. Chippindale, T. Hansen, H. Schober and S. Chaplot, *Phys Rev B* (under review)
- [6] J. Lefebvre, R. Batchelor and D. Leznoff, *J. Am. Chem. Soc.*, 126(49) [2004] 16117
- [7] C. Bayse, J. Ming, K. Miller, S. McCollough and R. Pike, *Inorg. Chim. Acta* 375 [2011] 47
- [8] A. Chippindale, S. Hibble, E. Bilbé, E. Marelli, A. Hannon, C. Allain, R. Pansu and F. Harli, *J. Am. Chem. Soc.*, 134 [2012] 16387
- [9] S. Hibble, A. Chippindale, E. Bilbé, E. Marelli, P. Harris and A. Hannon, *Inorg. Chem.*, 50 [2011] 104

Metal cyanides, formed by linking together M(C≡N)<sub>x</sub> building units, can exhibit a range of structural dimensionalities, including layered structures. Atomistic disorder within the C≡N groups is common, as both the atoms can occupy the same crystallographic positions due to their similar size and co-ordination preferences.

NTE (shrinkage upon heating) is of a larger magnitude in these materials than is found in other compounds, e.g. transition-metal oxides and zeolites [1]. Further, the rare phenomenon of NLC (expansion under pressure) has also been recently observed in cyanide materials under applied pressure [2]. Moreover, the study of Ni(CN)<sub>2</sub>-related materials is particularly topical. Ni(CN)<sub>2</sub> has indeed been proposed as a novel semiconductor material when doped, either in sheet form, by analogy with graphene, or when rolled into nanotubes [3].

Ni(CN)<sub>2</sub> has a two-dimensional layered structure which is formed from linked, square-planar Ni(CN)<sub>4</sub>/Ni(NC)<sub>4</sub> units, with long-range order only within the *a-b* plane and no true periodicity along *c*-axis. The phonon spectra of Ni(CN)<sub>2</sub> do not show any significant temperature dependence [4]. The absence of any soft modes revealed that the inter-planar coupling is certainly not negligible. Therefore, the contraction of the plane should certainly influence the physics along the stacking axis. This could be investigated by application of pressure. We considered the layered structure and lack of periodicity in Ni(CN)<sub>2</sub> to study the effect of pressure on its structure and dynamics, by performing high-pressure neutron diffraction and INS measurements on the diffractometer D20 and the time-of-flight spectrometer IN6, respectively [5]. It should be noted that neutron scattering continues to play a master role in this field by correctly probing the positions and motions of the light C and N atoms, critical for the understanding of NTE and NLC, besides the scattering from the (heavier) metal atoms.

Diffraction data (figure 1) show a change in the slope of the “*c*” lattice parameter as well as in the volume at about 1 kbar, signature of a phase transition, which we ascribe to a change in CN order within the nickel-cyanide layers. This is well corroborated by the results of our pressure-dependent INS measurements (figure 2). The mode Grüneisen parameters  $\Gamma(E)/B$ , where *B* is the bulk modulus and *E* is a phonon energy, were extracted from the INS data considering two different pressure ranges (figure 2). The low-energy peaks shift significantly towards higher energies with increasing pressure, while the others are not affected. This is consistent with previous assignment of these low-energy modes [4] to dynamics, involving out-of-plane atomic motions, becoming more difficult under pressure as the layers are squeezed together. Interestingly, from the two different pressure regimes the values of

$\Gamma(E)/B$  are found to differ significantly, evidencing for the first time a pressure-induced phase transition in Ni(CN)<sub>2</sub> in accordance with our diffraction results. It should be noted that these findings are also well supported by our high-pressure Raman measurements (not shown here) [5]. Associated with the change in CN order within the layers and consequent softening of the C≡N stretching modes at about 1 kbar, there appears to be a change in interlayer interactions and a sudden relaxation in the *c* direction. This reflects an isomerisation induced by a change in the symmetry of individual layers occurring from D<sub>4h</sub> to C<sub>2v</sub>, i.e. a change from layers containing Ni(CN)<sub>4</sub> and Ni(NC)<sub>4</sub> units to ones containing only units of the type *cis*-Ni(CN)<sub>2</sub>(NC)<sub>2</sub>.

At higher pressures (figure 1) the “*c*” lattice parameter decreases but at different rates. The compressibility values were inferred from the neutron diffraction data [5]. Overall, the response of the lattice parameters of Ni(CN)<sub>2</sub> to applied pressure is strongly anisotropic as a function of the interlayer spacing, with a significantly larger axial contraction than in the *a-b* plane. Last but not least, our high-pressure Raman data point towards a second (also newly observed) phase transition taking place at 70 kbar, as suggested by the increase in the number of the C≡N stretching modes [5].

The curious NTE and NLC properties of metal cyanides are not the only reason for studying these materials. A number of them exhibit interesting photophysical properties e.g. vapochromism and photoluminescent behaviour [6,7]. The successful synthesis of new metal cyanides with 1-, 2- and 3-D frameworks possessing novel properties [8,9] calls for a continuous probe of the temperature and pressure dependences of their structure and dynamics to explore and understand their fascinating behaviours and make them practically relevant.

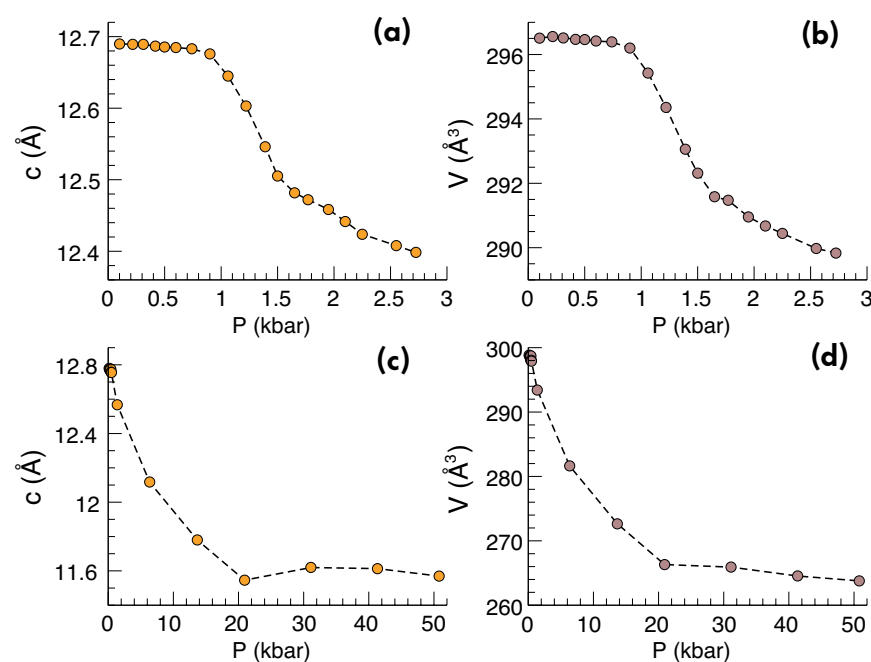


Figure 1

Pressure dependence of the lattice parameter “*c*” and volume “*V*” of Ni(CN)<sub>2</sub> from room temperature diffraction measurements on D20, up to 2.7 kbar using the argon gas pressure cell – **a)** and **b)**, and up to 50 kbar using the Paris-Edinburgh device – **c)** and **d)**.

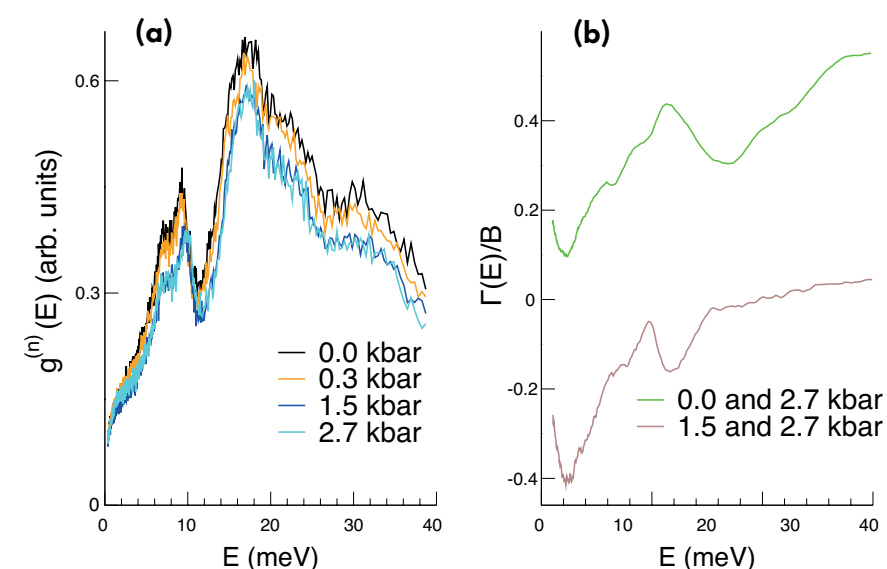


Figure 2

**a)** Pressure dependence of the phonon spectra of Ni(CN)<sub>2</sub> from INS measurements on IN6, at 300 K. **b)** The related experimental mode Grüneisen parameters,  $\Gamma(E)/B$ , as a function of phonon energy *E* (averaged over the whole Brillouin zone). The pressure shifts were obtained from the measurements carried out within the two pressure ranges 0 - 2.7 kbar, and 1.5 - 2.7 kbar.

# MATERIALS SCIENCE

## An (almost) perfect two-dimensional Brownian gas

*Time-of-flight spectrometer IN6 and spin-echo spectrometer IN11*  
*Time-of-flight spectrometer OSIRIS at ISIS*

Nanometer-size mechanical systems are expected to play a major technological role in the next decades [1]. If we want to understand these systems, however, we have to measure real time motion with nanometer spatial resolution at technically relevant temperatures and pressures, a highly non-trivial task. Hence, comparatively little experimental data are available and the existing models of friction and diffusion on surfaces are often highly hypothetical. Using a range of high-resolution neutron spectrometers we have identified a sample that shows almost perfect two-dimensional Brownian diffusion of nano-cogwheels with negligible surface friction [2].

### AUTHORS

I. Calvo-Almazan (ILL and University of Zaragoza, Spain)  
E. Bahn, M.M. Koza, M. Zbiri and P. Fouquet (ILL)  
M. Maccarini (ILL and University Grenoble Alpes TIMC-IMAG, France)  
M.T.F. Telling (ISIS, Chilton and Oxford University, UK)  
S. Miret-Artés (CSIC, Madrid, Spain)

### REFERENCES

- [1] W.R. Browne and B.L. Feringa, Nat. Nanotechnol. 1 (2006) 25
- [2] I. Calvo-Almazan, E. Bahn, M.M. Koza, M. Zbiri, M. Maccarini, M.T.F. Telling, S. Miret-Artés and P. Fouquet, Carbon 79 (2014) 183
- [3] A. Einstein, Ann. Phys. 17 (1905) 549
- [4] D. Chandler, J. Chem. Phys. 62 (1975) 1358

Brownian diffusion is a key concept in the study of diffusion and was generically explained 110 years ago by Einstein in a seminal paper [3]. We find three-dimensional Brownian diffusion every day, as it describes the motion of gas molecules in the air around us. Brownian particles move without resistance until they hit another particle, upon which they exchange momentum and energy. The diffusivity of molecules in Brownian diffusion is determined by the particle-particle interaction, which finds its macroscopic expression in the viscosity,  $\eta$ . Great progress was made in the 1970s in deriving the viscosity and other macroscopic transport coefficients from the microscopic properties of gas or liquid molecules [4].

When molecules are bound to a surface, however, we find in most cases that the mutual interactions between the adsorbed molecules are negligible and that the diffusion is dominated by the substrate-molecule interaction potential. Thus, adsorbed molecules either stick at a fixed site without being able to diffuse at all, or they perform a *jump diffusion*, where the molecules stay at their adsorption site for extended periods until they finally receive a thermal "kick" and jump to a neighbour site. Benzene

molecules adsorbed on a graphite surface (**figure 1**) are an exception to this rule: although the attractive potential between benzene and graphite is strong enough to keep benzene adsorbed in a flat geometry, the lateral variation of the potential energy surface is so small that the molecules can diffuse with almost negligible resistance.

To prove this, we used a range of high-resolution spectrometers at ILL and at ISIS, namely, the time-of-flight spectrometers IN6 and OSIRIS as well as the neutron spin-echo spectrometer IN11. Taken together, these spectrometers allowed us to trace nanometer motion of benzene molecules in a time window from picoseconds to nanoseconds. It turned out that the diffusive motion of benzene on graphite depends strongly on the density of the adsorbed molecules, the so-called coverage. As we increased the coverage from 0.1 ML first to 0.2 ML and then to 0.5 ML (1 monolayer, ML, refers to a single, dense layer of adsorbed molecules) we observed that the friction coefficient,  $\eta_T$  (the 2D equivalent of the viscosity) increased almost linearly with the coverage (**figure 2**). The strong coverage dependence of the benzene

diffusion clearly demonstrates that the diffusivity is mainly determined by the molecule-molecule interactions. An extrapolation of the measured friction to zero coverage actually shows that the surface friction is close to zero.

This finding prompted us to re-examine the 3D hydrodynamic framework from the 1970s that successfully derived the transport coefficients of liquids from a model of rough hard spheres [4], and to develop its two-dimensional counterpart. The derived model assumes collisions of hard disks with infinitely steep potential wells, where linear as well as rotational momentum and energy are exchanged. This rough hard disk model allowed us to calculate the friction coefficient from the dimensions and the mass of the molecule. The model gives  $\eta_T$  as a function of coverage and temperature and contains only one free parameter, the rotational coupling between molecules. As can be seen in **figure 2**, we find an excellent agreement between the rough hard disk model and our experimental data at low coverage when we assume maximum rotational coupling, i.e. we find that the benzene molecules behave like tiny cog-wheels.

[This work was part of the ILL thesis work of Irene Calvo-Almazan and Emmanuel Bahn].

**Figure 1**

The benzene molecules were adsorbed on chemically exfoliated graphite samples. These samples consist of graphite tablets that have been exploded and re-compressed, such that they offer a very large surface area per weight while keeping a preferential orientation of the graphite crystallites in one plane.

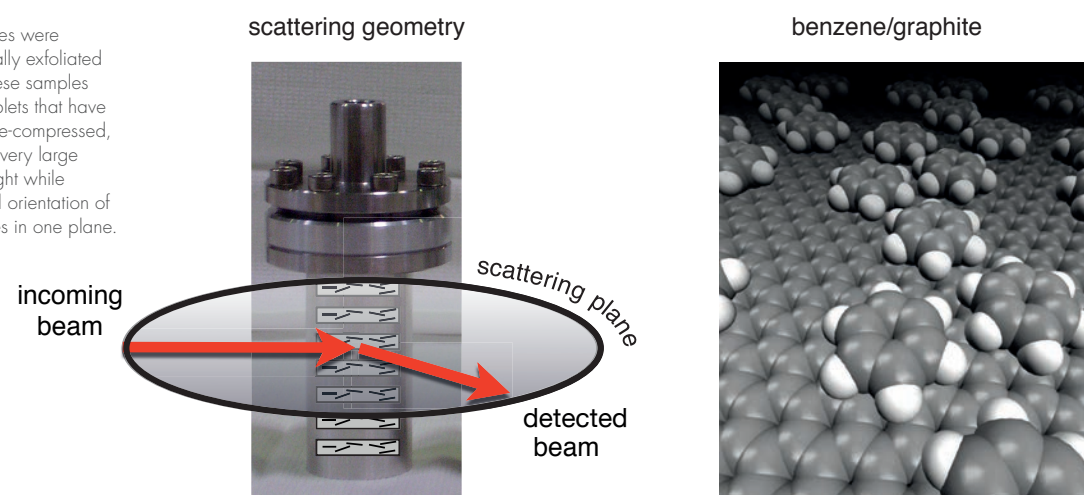
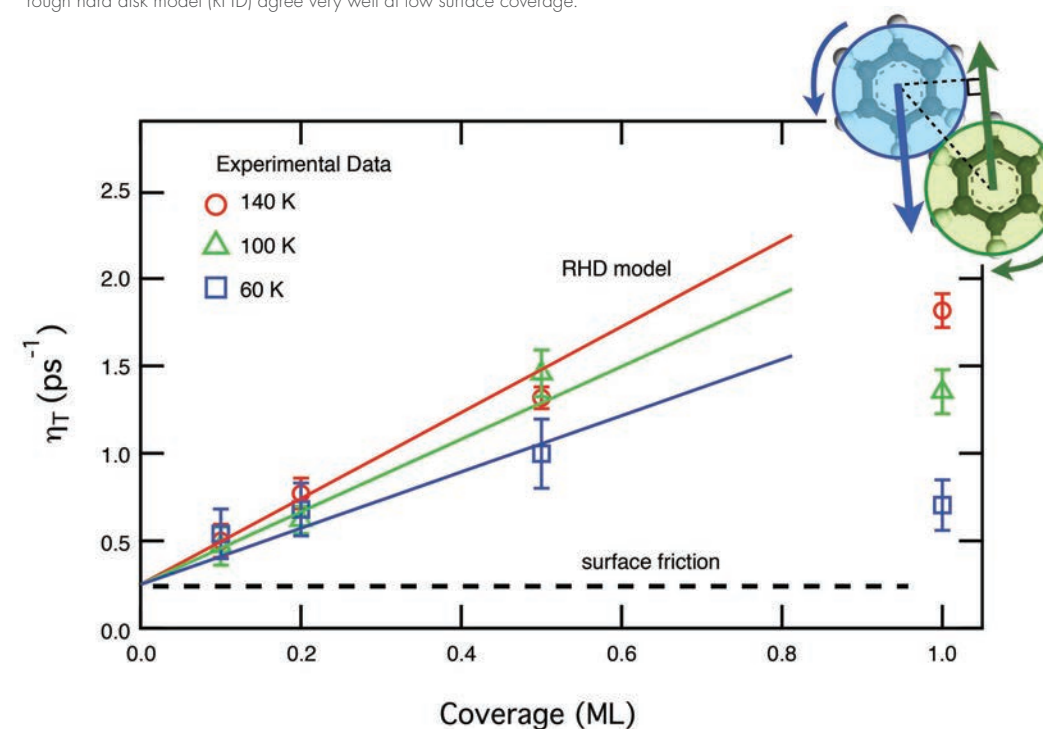


**Figure 2**

The friction,  $\eta_T$ , measured in this study and the friction predicted by a rough hard disk model (RHD) agree very well at low surface coverage.



# MATERIALS SCIENCE

## Dynamics of nanoscale polarisation fluctuations in a uniaxial relaxor

Backscattering spectrometer IN16B

Relaxor ferroelectrics are known for their extraordinary dielectric and electromechanical properties widely used in industrial applications ranging from micro-capacitors to transducers and actuators. At the same time the fundamental understanding of their behaviour at a microscopic level, involving disorder effects and nanoscale structural correlations, remains one of the challenges of contemporary solid state physics.

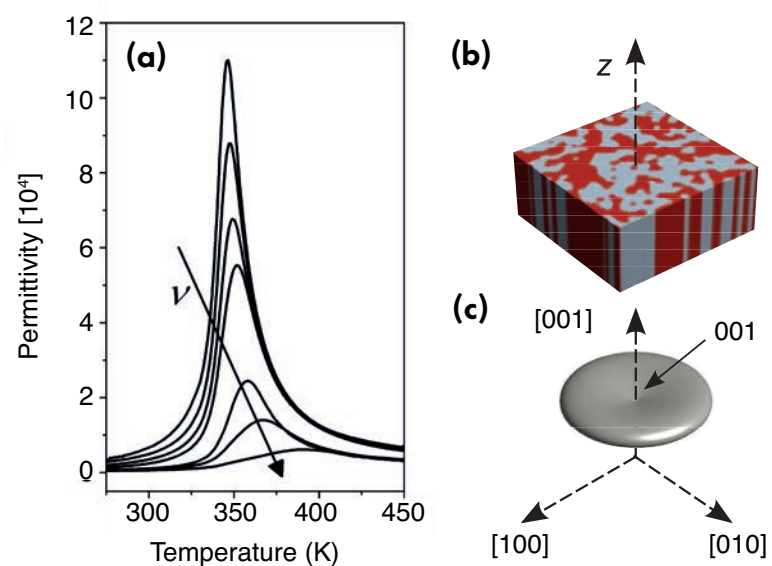


**Figure 1**  
**a)** Temperature dependence of the real c-axis dielectric permittivity of  $\text{Sr}_{0.61}\text{Ba}_{0.39}\text{Nb}_2\text{O}_6$  at probing frequencies from 0.01 Hz to 100 MHz [1,4].  
**b)** and **c)** indicate a typical nanodomain structure of a uniaxial relaxor and the equi-intensity surface of the associated diffuse scattering, respectively.

### AUTHORS

P. Ondrejčkov, M. Kempa and J. Hlinka (Academy of Sciences of the Czech Republic)  
 J. Kulda, B. Frick and M. Appel (ILL)  
 J. Combet (CNRS-UdS, Strasbourg, France)  
 J. Dec (University of Silesia, Katowice, Poland)  
 T. Lukasiwicz (Institute of Electronic Materials Technology, Warsaw, Poland)

### REFERENCES

- [1] E. Buixaderas, M. Savinov, M. Kempa, S. Veljko, S. Kamba, J. Petzelt, R. Pankrath and S. Kapphan, *J. Phys. Condens. Matter* 17 (2005) 653
- [2] F. Prokert and R. Schalge, *Phys. Status Solidi B* 87 (1978) 179
- [3] S.N. Gvasaliya, R.A. Cowley, L.I. Ivleva, S.G. Lushnikov, B. Roessli, and A. Zheludev, *J. Phys. Condens. Matter* 26 (2014) 185901
- [4] P. Ondrejčkov, M. Kempa, J. Kulda, B. Frick, M. Appel, J. Combet, J. Dec, T. Lukasiwicz, and J. Hlinka, *Phys. Rev. Lett.* 113 (2014) 167601

One of the most remarkable properties of relaxor materials is their extraordinarily large dielectric permittivity appearing over a broad temperature interval and attaining its maximum at a temperature  $T_{\text{max}}$ , which varies linearly with the logarithm of the probing frequency ( $\log \nu$ , see **figure 1a**). Contrary to the usual Arrhenius relationship (direct proportionality between the  $\log \nu$  and the absolute temperature, describing the slowing down of thermally activated processes in nature), here, at low frequencies,  $T_{\text{max}}$  tends towards a finite characteristic temperature  $T_{\text{VF}}$ , which is typically hundreds of Kelvins. This type of dependence is known in dynamics of glass-forming liquids as the Vogel-Fulcher (VF) law. In general it represents an exponentially broad spectrum of relaxation times and correlation lengths. This aspect brings relaxor ferroelectrics into a wide family of disordered materials of current interest, including fragile glass-forming liquids, structural glasses, diluted or frustrated spin glasses, superconducting vortex lattices, confined water and others.

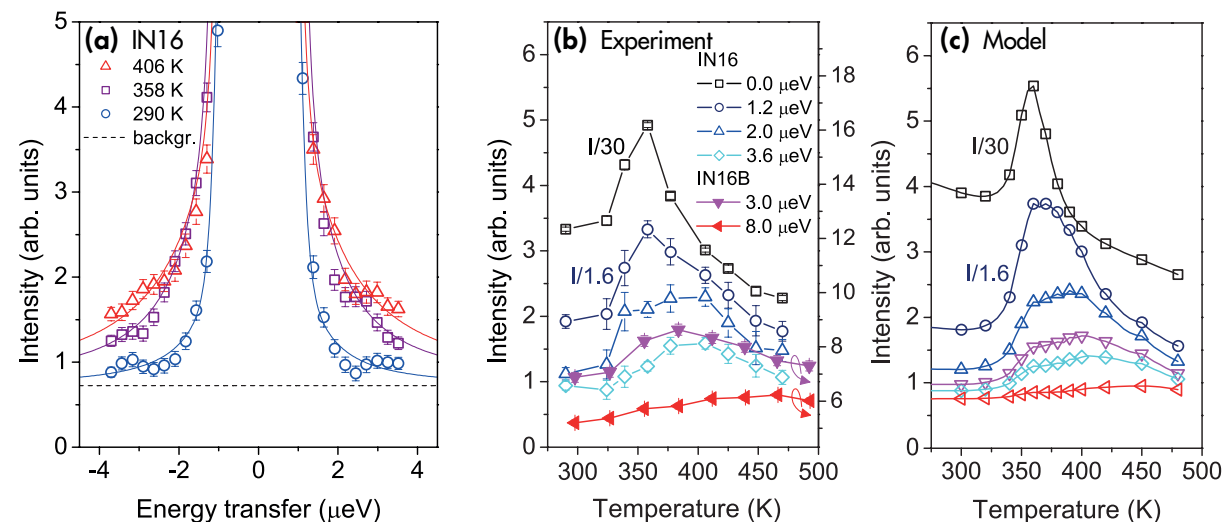


**Figure 2**

Neutron-scattering intensity at  $\mathbf{Q} \sim [0.15, 0, 1]$  as a function of  
**a)** energy transfer and  
**b)** temperature compared with  
**c)** a model based on an analysis of dielectric spectra [1,4].

Although the relaxor-glass analogy has to be treated with care, it has been widely accepted that the VF behaviour in relaxor ferroelectrics is related to a temperature-dependent length scale of nano-range polar inhomogeneities. While there is clear experimental evidence for nanoscale polar entities in the low-temperature relaxor state from neutron and X-ray scattering investigations and from piezoresponse scanning force microscopy, the exact topology of the spatial polarisation distribution is still debated. As a consequence, the microscopic origins of the Vogel-Fulcher-type dynamics continue to represent the most enigmatic aspect of relaxor physics and, as in the case of a glass transition, it calls for further investigations at multiple time and length scales.

A pronounced VF-type dielectric relaxation, considered a hallmark of relaxor behaviour, has also been found in tetragonal tungsten bronze crystals such as  $\text{Sr}_{0.61}\text{Ba}_{0.39}\text{Nb}_2\text{O}_6$  (SBN61) [1], which can be considered almost ideal uniaxial relaxors. In their case both the local polarisation and the nanodomain (or polar cluster) boundaries can be expected to lie parallel to the easy axis of the material (z-axis in the following). A schematic representation of the nanodomain structure in tetragonal tungsten bronze-type crystals, as deduced from piezoresponse force scanning microscopy measurements, is sketched in **figure 1b**. Nanoscale domains with opposite polarisation orientations are extended along the z-axis and exhibit irregular boundaries within the xy plane. This highly anisotropic picture is confirmed in diffraction experiments by disk-shaped, transverse, diffuse scattering intensity distributions located close to the Brillouin zone centres with non-zero L index (see **figure 1c**) [2,3].

Having taken a lesson from former, less fruitful attempts by neutron three-axis spectroscopy and by the neutron spin-echo technique, which produced results dominated by a

strong elastic central peak accompanied by the response from a fast (0.1-1 THz) Arrhenius-like relaxation mode, we have opted for the neutron backscattering technique. Its great advantage is the capability to detect weak quasi-elastic scattering signals at the foot of an elastic line having several orders of magnitude higher intensity. Our experiments were performed using the ILL instruments IN16 and IN16B, offering an energy resolution of 0.8 - 1  $\mu\text{eV}$  (about 200 MHz) [4]. The data were collected in the vicinity of the 001 Brillouin zone centre of a cylindrical SBN61 single crystal with a volume of about 3  $\text{cm}^3$ .

Typical data are displayed in **figure 2a**, showing a clear inelastic component which broadens with increasing temperature and which can be well described by a simple model based on an analysis of dielectric spectra [1,4]. The agreement between the experiment and model data can be more greatly appreciated when the scattering intensity at a fixed energy transfer is traced as a function of temperature (**figure 2b** and **figure 2c**). This comparison demonstrates that with increasing energy transfers the peak positions shift towards higher temperatures, closely following the Vogel-Fulcher law determined from the dielectric measurements.

The results show for the first time a direct link between the Vogel-Fulcher-type relaxation dominating the dielectric permittivity and the lattice dynamics of the relaxor materials as revealed by neutrons. The apparent disparity between the huge effect in dielectric permittivity and the weak component of the neutron response is explained by the different interaction mechanisms: while the external electric field couples exclusively to the electric dipole moments arising from charge redistribution within the polar nanodomains, the corresponding tiny displacements of atomic nuclei contribute just a little to the neutron response, which is dominated by the general crystal structure and lattice vibrations.

# MATERIALS SCIENCE

## Graphene oxide hydration and solvation: an *in situ* neutron reflectivity study

Reflectometer SuperADAM

Simple and inexpensive methods of purification could lead to the wider use of ethanol, for example as a biofuel. Recent studies have demonstrated that while water vapours penetrate graphene oxide (GO) membranes unimpeded, the same membranes serve as an efficient barrier for ethanol vapours. It has therefore been suggested that GO membranes could be used to separate water-ethanol binary mixtures using vapour permeation and pervaporation [1]. The difference between the permeation of water and ethanol is presumably due to the selective absorption properties of the GO membranes for water. However, to date there has been no quantitative evaluation of water and ethanol absorption into the interlayers of GO membranes and this evaluation has proved impossible using, for example, diffraction methods.

In our study we demonstrate that neutron reflectivity (NR) can be used for the time-dependent quantification of the amounts of solvent intercalated into the GO structure, and thus to predict and quantify selectivity in the permeation of solvent vapours through layered membranes.

### AUTHORS

A. Vorobiev and A. Dennison (Uppsala University, Sweden and ILL)  
D. Chernyshov (SNBL and ESRF, France)  
V. Skrypnichuk, D. Barbero and A.V. Talyzin (Umeå University, Sweden)

### REFERENCES

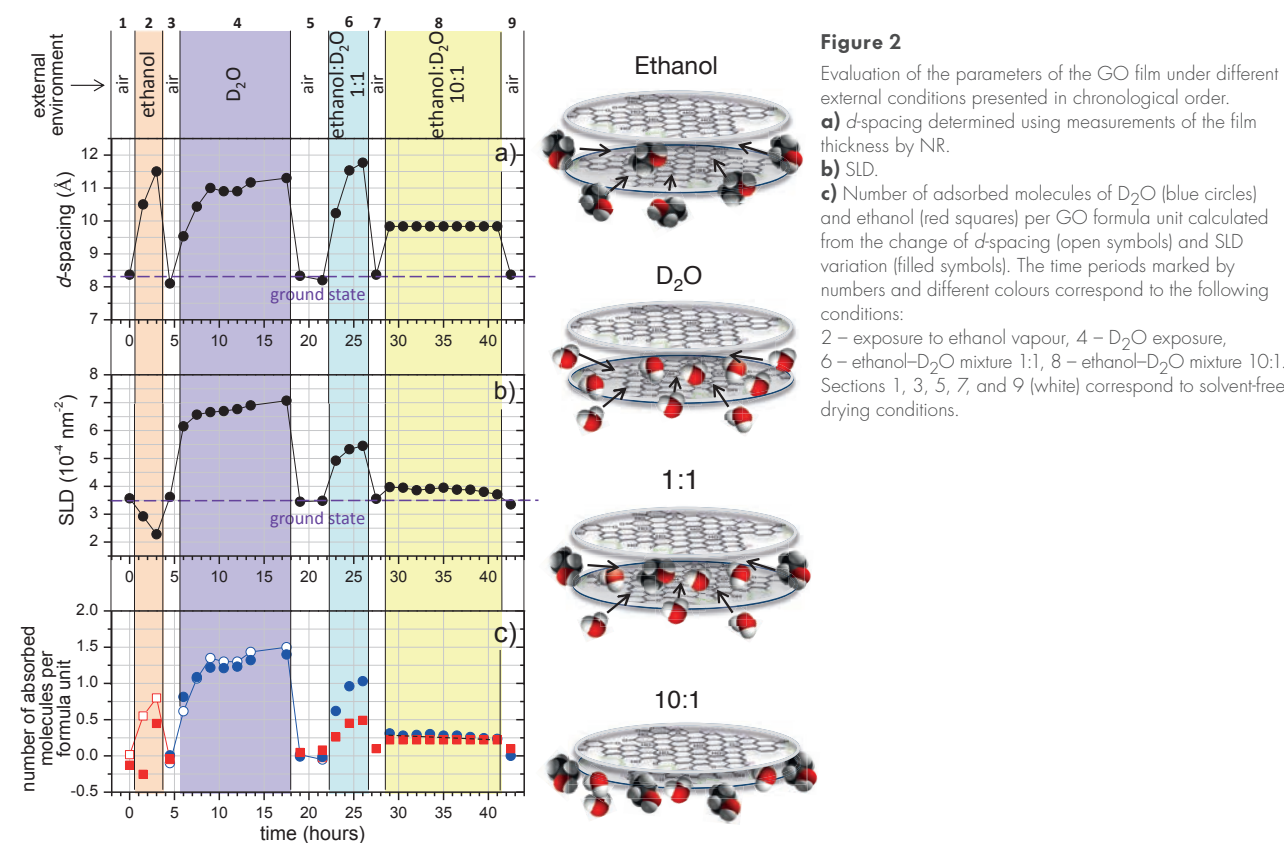
- [1] R.R. Nair *et al.*, *Science*, 335 (2012) 442  
[2] V.F. Sears, *Neutron News*, 3 (1992) 26

We report here on the first NR study of GO thin films deposited on an Si (silicon) wafer and exposed to D<sub>2</sub>O, ethanol and D<sub>2</sub>O-ethanol vapours. By using one of the solvents in the deuterated state, it is possible to quantify the absorption of each of the solvents due to the significant difference in scattering length density (SLD) between D<sub>2</sub>O and ethanol. This parameter can then be used to calculate the precise amounts of water and ethanol intercalated into the GO film.

Examples of the NR data collected from the pristine film and for the same film when exposed to ethanol and D<sub>2</sub>O vapours are shown in **figure 1**, together with the fitting results. NR methods provide structural information about thin films (up to a few hundred nm), including film thickness, roughness and SLD. The neutron SLD is calculated as  $B/V$ , where  $V$  is the volume of the unit cell and  $B = \sum b_i$  is the total neutron-scattering length (NSL) of all the elements in the cell. Individual NSL  $b_i$  is a unique quantity for every chemical element and its isotopes [2]. **Figure 1** clearly highlights the substantial differences in the experimental data associated with the intercalation of solvent molecules of different types, i.e. which have different SLD values.

The results of the experiment are summarised in **figure 2**, which shows the  $d$ -spacing (**a**) and SLD (**b**) of the GO films as a function of time and vapour composition. The total film thickness was used to extract the  $d$ -spacing of the GO film, which consisted of 32 monolayers.

Variations of  $d$ -spacing provide important insight into the kinetics of intercalation but allow only a very rough estimation of the amount of intercalated solvent, even for pure solvents. For example, insertion of the diluted solvent layer may result in the same lattice change as that for a close-packed solvent layer. In the case of binary solvents, the same lattice expansion can also be explained by the intercalation of two solvents but in different amounts/proportions. In contrast, the analysis of neutron SLD variation makes it possible to determine exactly which solvents intercalate GO and in what proportion. The numbers of solvent



molecules intercalated into the GO structure per formula unit (taken as C<sub>2</sub>O<sub>0.76</sub>H<sub>0.24</sub>), calculated using  $d$ -spacing (open symbols) and SLD values (filled symbols), are shown and, where possible, compared in **figure 2c**.

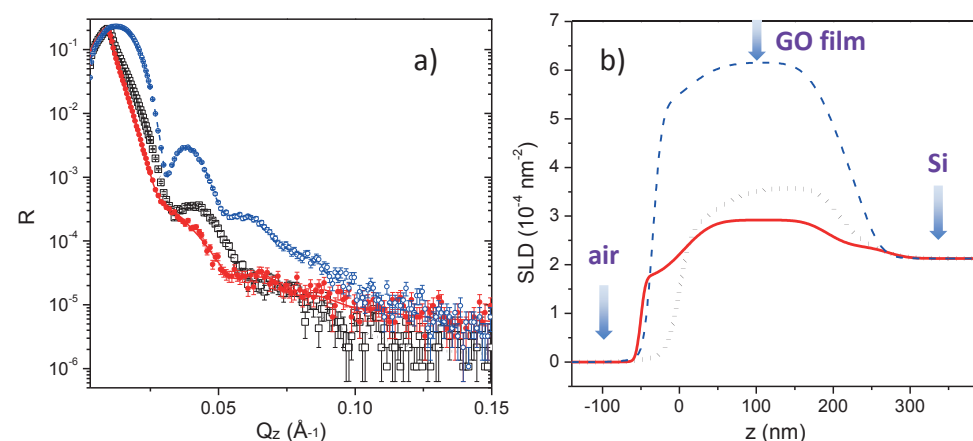
The results of our quantitative analysis can be summarised as follows:

- Intercalation (**figure 2**, section 2) shows that the expansion of the GO lattice starts before any significant change of SLD. This can be explained if a very small amount of ethanol intercalated into the GO structure results in a large increase in interlayer distance. Most likely, a few ethanol molecules insert into the edge regions of the GO interlayer during the initial stages of solvation and serve as “pillars” which separate the GO layers from each other.
- Exposure of the GO film to D<sub>2</sub>O vapour results in the insertion of 1.4 molecules per formula unit. This amount correlates well with lattice expansion (3 Å), assuming the thickness of the D<sub>2</sub>O monolayer is 2 Å (**figure 2**, section 4). Thus we can assume that the lateral density of the intercalated D<sub>2</sub>O monolayer is equal to 1 water molecule per 1 GO formula unit, i.e. per two C atoms.
- Exposure of the GO film to 1:1 D<sub>2</sub>O-ethanol vapour clearly results in the intercalation of both solvents (**figure 2c**, section 6) according to SLD data. However, the interlayer distance remains almost the same as that in pure ethanol. This could be explained by assuming that ethanol forms a diluted monolayer with less than 0.45 molecules per unit cell and that the spaces between the ethanol molecules are sufficient to accommodate 1 additional molecule of water per GO unit cell. Alternatively, water and ethanol could form nm-size clusters of pure solvent, with the ethanol clusters serving as “pillars”.
- Exposure of the GO film to the 10:1 ethanol-D<sub>2</sub>O mixture results in smaller  $d$ -spacing compared with that for pure ethanol (**figure 2c**, section 8). The same result was observed previously in liquid solvents. An increase in  $d$ -spacing compared with the ground state corresponds to 0.75 D<sub>2</sub>O molecules per GO formula unit, while an increase in SLD corresponds to a much smaller value, namely 0.25 D<sub>2</sub>O molecules per GO formula unit. We are therefore forced to conclude that both water and ethanol are intercalated into the GO structure from the binary D<sub>2</sub>O-ethanol mixture vapours, but the proportion of water intercalated is greater than that of ethanol, thus proving a certain degree of selectivity. The selective insertion of water into the GO structure would explain the faster permeation of water through the GO membrane compared with ethanol. This water-ethanol selectivity reaches a factor of two in 1:1 vapour mixtures, while it increases to a factor of fifteen in 10:1 vapour mixtures. Although the phenomenon is quite evident, it is far from the absolute selectivity reported in [1]. GO membranes are therefore not suitable for water/ethanol separation in the pristine state. Further structural modification is required to improve the selectivity of water/ethanol separation.

With our study, we have demonstrated that the NR method can be a very efficient tool for the quantitative estimation of membrane permeation properties.

**Figure 1**

**a**) Examples of the neutron reflectivity data (circles) and corresponding fit lines obtained from the original dry film (black), film in ethanol vapour (red) and in heavy water vapour (blue).  
**b**) Model scattering length density profiles used to fit experimental curves. The thickness of the dry film 26.7 nm and the  $d$ -spacing 8.3 Å show that the sample consists of 32 GO monolayers. The zero of the x-axis corresponds to the level of the top surface of the pristine GO film.



# MATERIALS SCIENCE

## Packing and the structural transformations in liquid and amorphous oxides from ambient to extreme conditions

Liquids and glasses diffractometer D4

Network-forming structural motifs such as  $\text{SiO}_4$  tetrahedra play a key role in governing the physical and chemical properties of disordered oxide materials, which range from photonic glasses to the fluids in planetary interiors. Here we show that the co-ordination number of these motifs, which has a profound effect on the connectivity of an atomic network [1], can be rationalised in terms of the oxygen-packing fraction over an extensive pressure and temperature range.

### AUTHORS

A. Zeidler and P.S. Salmon (University of Bath, UK)  
L.B. Skinner (State University of New York, USA)  
H.E. Fischer (ILL)

### REFERENCES

- [1] J.C. Phillips, *J. Non-Cryst. Solids* 34 (1979) 153
- [2] ILL News, December 2012, p.6 (<http://www.ill.eu/quicklinks/publications/ill-news/>)
- [3] A. Zeidler, P.S. Salmon and L.B. Skinner, *Proc. Natl. Acad. Sci. USA* 111 (2014) 10045
- [4] J.D. Bernal and J. Mason, *Nature* 188 (1960) 910
- [5] M.M. Smedskjaer, J.C. Mauro, S. Sen and Y. Yue, *Chem. Mater.* 22 (2010) 5358

At ambient conditions in a material such as silica glass (the main component of optical fibres), an open network is formed from corner-linked  $\text{SiO}_4$  tetrahedra. When the glass is compressed the network collapses, and a point is reached where the Si-O co-ordination number (meaning the average number of oxygen O atoms around an Si atom) increases:  $\text{SiO}_4$  tetrahedra transform into corner- and edge-linked  $\text{SiO}_6$  octahedra. These changes affect the network connectivity and hence the physico-chemical properties of the material. But is there a way of predicting when such changes must occur, and can this be generalised to other oxide materials under extreme conditions (figure 1)?

To help answer these questions, information is required on the A-O co-ordination number  $\bar{n}_A^O$  for network-forming structural motifs such as  $\text{AO}_3$  triangular units and  $\text{AO}_4$  tetrahedra, where A denotes a chemical species such as B, Si or Ge. These co-ordination numbers can be measured under extreme conditions by using neutron or X-ray diffraction. After consulting the available literature, we performed complementary diffraction experiments. For instance, the neutron diffractometer D4 at the ILL was used to measure the structure of glassy  $\text{B}_2\text{O}_3$ ,  $\text{SiO}_2$  and  $\text{GeO}_2$  using a Paris-Edinburgh press at pressures up to 8.5 GPa (figure 2). These experiments took advantage of

Figure 1

An illustration of liquid oxides under extreme conditions.



Figure 2

A Paris-Edinburgh high-pressure press mounted on the diffractometer D4 at the ILL.

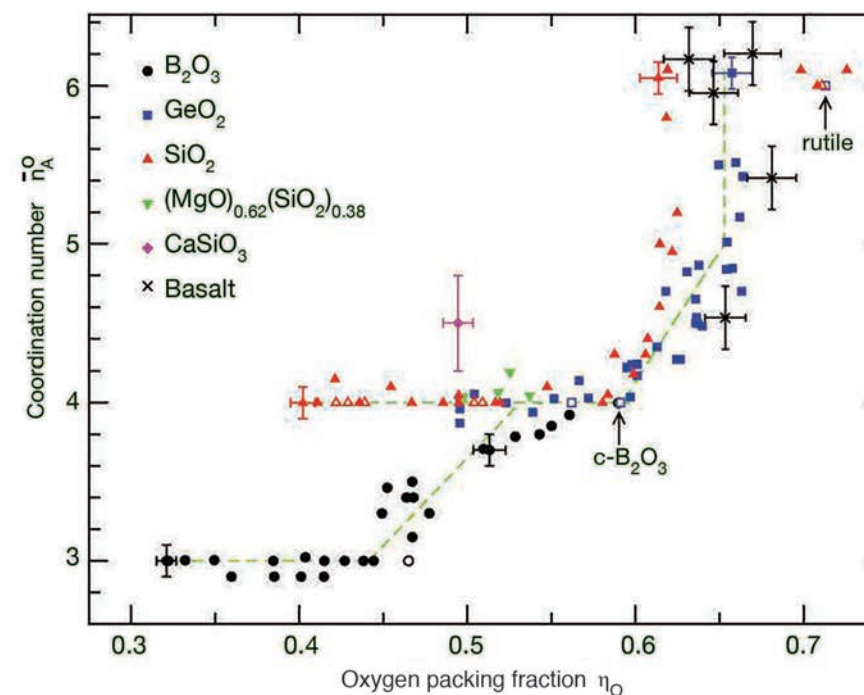
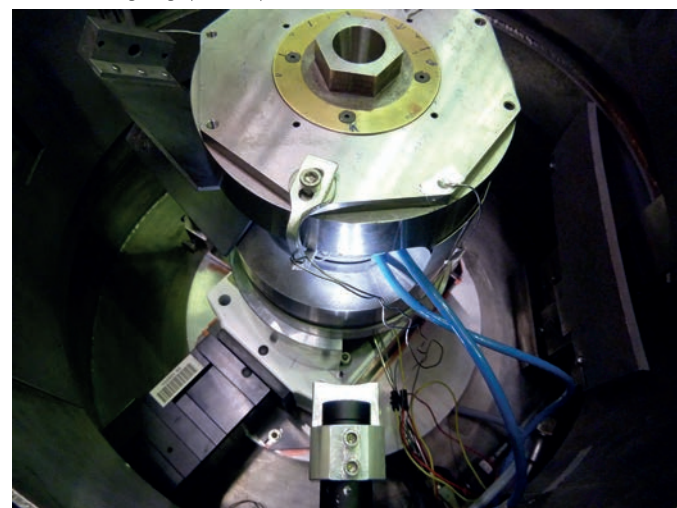


Figure 3

The dependence of the A-O co-ordination number  $\bar{n}_A^O$  for A-centred (A = B, Ge or Si) network-forming structural motifs on the oxygen-packing fraction  $\eta_0$  for a variety of glassy and liquid oxide materials under extreme conditions [3]. Results are given for glassy  $\text{B}_2\text{O}_3$ ,  $\text{SiO}_2$ ,  $\text{GeO}_2$  and  $(\text{MgO})_{0.62}(\text{SiO}_2)_{0.38}$  under pressure; liquid  $\text{CaSiO}_3$  at high pressure and high temperature; and molten basalt under deep mantle conditions. The open symbols correspond to the room-temperature polymorphs of crystalline  $\text{B}_2\text{O}_3$ ,  $\text{SiO}_2$  and  $\text{GeO}_2$ .

developments made under the aegis of an ILL long-term proposal (LTP-6-1, [2]). For example, the combination of a short incident neutron wavelength of 0.5 Å and excellent counting statistics, coupled with a low and stable background, ensured the measurement of reliable A-O co-ordination numbers.

If the  $\bar{n}_A^O$  values measured at different pressures and temperatures are plotted against the oxygen-packing fraction  $\eta_0$ , namely the fraction of volume in a glass or liquid that is occupied by oxygen atoms, then a structural map emerges (figure 3) [3]. This map gives a means for predicting the likely regimes of topological change. For example, the  $\text{SiO}_4$  tetrahedra that are present in silica glass under ambient conditions start to become unstable as the density increases and the oxygen-packing fraction approaches the range  $\eta_0 = 0.55-0.60$  expected for a random loose packing of hard spheres. With further increase of density, the Si-O co-ordination number continues to grow so that  $\text{SiO}_6$  octahedra predominate as the oxygen-packing fraction approaches the limit  $\eta_0 = 0.64$  expected for a random close packing of hard spheres [4].

The structural map will prove useful in helping to predict the network connectivity of a given material under high-pressure and high-temperature conditions, and when this connectivity is likely to change. Such information is important for understanding the properties of magma-related melts because the topology of a network will affect its compressibility and transport properties such as the viscosity. Information on the network connectivity is also pertinent for understanding the properties of high-density liquids to aid in the design of new glasses with the desired structural and functional properties (figure 4) [5].



Figure 4

The structure and properties of liquid and amorphous oxide materials can be manipulated by modifying the network connectivity via control of the packing fraction of spherical oxide ions.

# MATERIALS SCIENCE

## An endofullerene nanolaboratory: quantum rotors entrapped within C<sub>60</sub>

Time-of-flight spectrometers IN4, IN5 and three-axis spectrometer INI-LAGRANGE

In recent years, innovative developments in synthetic organic chemistry have enabled small molecules such as water (H<sub>2</sub>O) and dihydrogen (H<sub>2</sub>) to be permanently encased inside the cage of a C<sub>60</sub> fullerene molecule. This provides a highly symmetrical 'nanolaboratory' environment in which the strongly quantum mechanical properties of the isolated, entrapped molecule may be probed by inelastic neutron scattering (INS). Among the new insights gained from experiments at the ILL is the surprising discovery of a new form of selection rule.

### AUTHORS

A.J. Horsewill and S. Mamone (University of Nottingham, UK)  
S. Rols, J. Ollivier, M. Jiménez-Ruiz and M.R. Johnson (ILL)

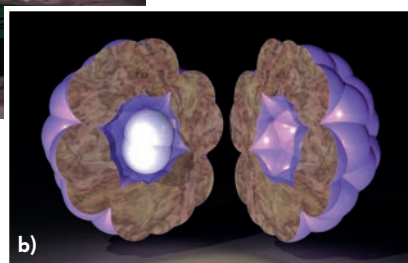
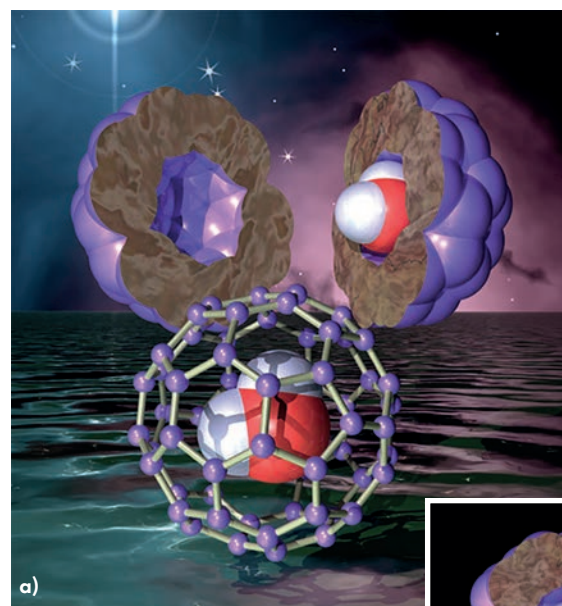
### REFERENCES

- [1] K. Kuratobi and Y. Murata, *Science* 333 (2011) 613 & K. Komatsu *et al.*, *Science* 307 (2005) 238  
[2] K.S. Goh *et al.*, *Phys. Chem. Chem. Phys.* 16 (2014) 21330  
[3] M. Xu *et al.*, *Phys. Rev. Lett.* 113 (2014) 123001

That matter has wave-like properties is one of the founding principles of quantum mechanics. This concept was encapsulated in Louis de Broglie's proposal that a particle's wavelength is inversely proportional to its momentum,  $p$ . This applies to all matter including fundamental particles, atoms and molecules alike. When a small molecule is confined inside the nearly spherical cavity of a fullerene cage, the matter waves resemble standing-waves and we observe quantisation of the translational energy relating to centre-of-mass displacements of the molecule. In an analogous way the rotational energy of the molecule is also quantised. The confinement therefore has many desirable consequences, enabling the wave-like and quantum features to be revealed in addition to providing a closed environment in which the isolated molecule can be studied, largely free from interactions with neighbouring atoms and molecules.

To encapsulate a molecule inside C<sub>60</sub> requires a procedure known as 'molecular surgery' [1]. Starting with pure C<sub>60</sub>, multiple chemical reactions are used to open an orifice in the cage and squeeze the molecule through the opening before finally resealing the cage to produce the endofullerene H<sub>2</sub>@C<sub>60</sub> or H<sub>2</sub>O@C<sub>60</sub>. Here the small molecule is permanently trapped inside the C<sub>60</sub> molecule.

A further significant quantum effect arises for H<sub>2</sub> and H<sub>2</sub>O that has no analogue in classical mechanics. This has its origin in the Pauli Exclusion Principle and gives rise to the property of nuclear spin-isomerism. As a result they are often classified as 'Quantum Rotors'. The molecular wave function must be antisymmetric with respect to exchange of identical fermions, in this case the two nuclei of the hydrogen atoms in H<sub>2</sub> and H<sub>2</sub>O. As a result, the space and spin degrees of freedom become entangled and we identify the ortho-spin isomers of H<sub>2</sub> and H<sub>2</sub>O which have total nuclear spin  $I=1$ , and the para-spin isomers of H<sub>2</sub> and H<sub>2</sub>O which have total nuclear spin  $I=0$ . Given in an INS experiment, the interaction between the neutron and the nucleus is mediated by spin, the neutron-scattering process can induce transitions between *ortho*- and *para*-states, providing INS with a unique advantage over other forms of spectroscopy for which such transitions are totally forbidden.



Artistic view of

a) H<sub>2</sub>O and  
b) H<sub>2</sub> in C<sub>60</sub>

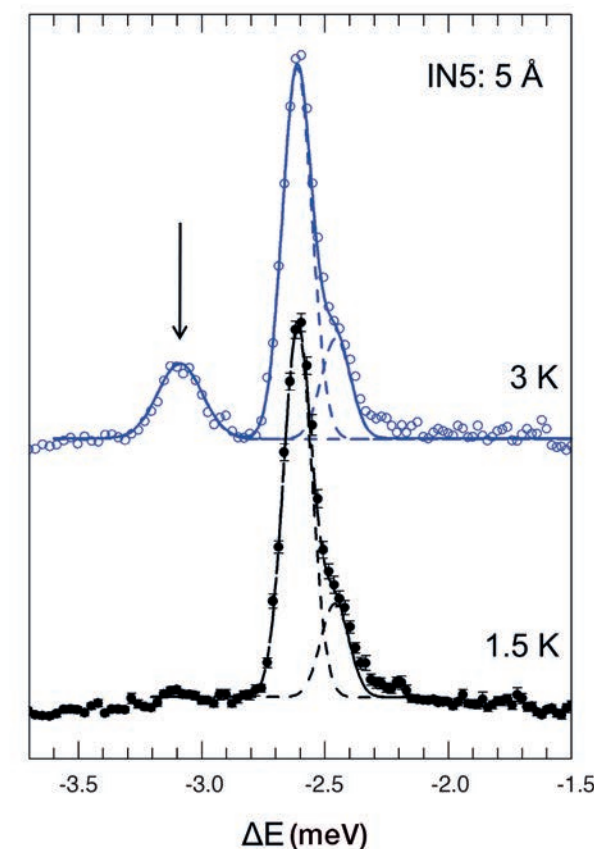
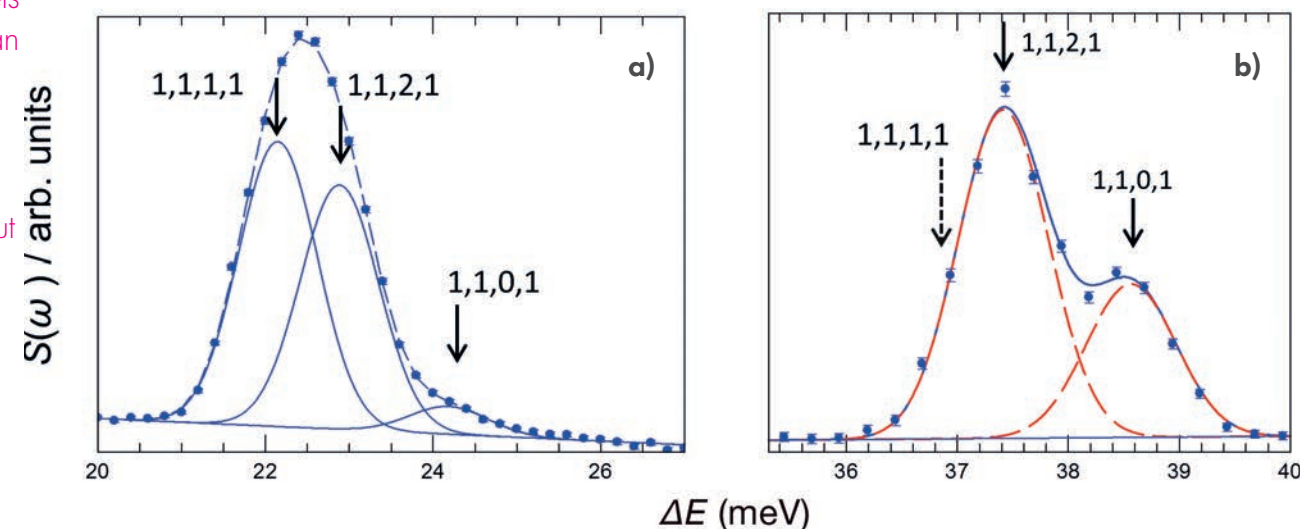


Figure 1

The INS spectrum of H<sub>2</sub>O@C<sub>60</sub> recorded at 1.5 K and 3 K on IN5 ( $\lambda_{\text{ini}} = 5 \text{ \AA}$ ). The appearance of the peak at -3.09 meV (arrowed) confirms the symmetry-breaking interaction that splits the *ortho*-H<sub>2</sub>O ground state.

Figure 2

In these spectra of H<sub>2</sub>@C<sub>60</sub> recorded on INI-LAGRANGE, the final state is a translational multiplet observed in transitions originating in a) the ground *ortho*-H<sub>2</sub> state;  $(0,1,1,0) \rightarrow (1,1,\lambda,1)$ ; and b) the ground *para*-H<sub>2</sub> state;  $(0,0,0,0) \rightarrow (1,1,\lambda,1)$ . A forbidden transition is indicated with a dashed arrow.



??  
bottom axis legend on fig 1 & 2 match but fig 2 is italics fig 1 isn't - should they be the same?

??  
arb. units in brackets rather than after /  
to match style throughout

For H<sub>2</sub>O@C<sub>60</sub>, the spectrum recorded on the IN5 spectrometer has led to the discovery of a symmetry-breaking arising from the interactions of the water molecule with the C<sub>60</sub> cage. This is analogous to a Jahn-Teller effect in which there is a spontaneous distortion of the complex, resulting in a splitting of the ground *ortho*-H<sub>2</sub>O state. This discovery was evident in a highly characteristic and unmistakable change in the INS spectrum with temperature, see figure 1 [2]. At 1.5 K a single INS peak centred on -2.61 meV is observed: this is a transition from meta-stable *ortho*-H<sub>2</sub>O to the ground state of *para*-H<sub>2</sub>O, hence the neutron gains energy from the water molecule. Increasing the temperature to just 3 K leads to the appearance of a second peak at -3.09 meV. Studying the intensities of these two peaks over the full temperature range confirms the symmetry-breaking induced splitting of the *ortho*-H<sub>2</sub>O state.

For H<sub>2</sub>@C<sub>60</sub>, the analysis of the INS spectra recorded on IN4, IN5 and INI-LAGRANGE has enabled a complete and detailed determination of the translation-rotation energy levels of H<sub>2</sub> inside its cage [3]. Of particular interest is the observation of a coupling between rotational and translational angular momenta. This leads to splittings of particular multiplet states, observed as fine-structure of the INS excitations, enabling the strength of the angular momentum coupling to be determined. In figure 2 two extracts from the INS spectra are shown, where the intrinsically narrow peaks of H<sub>2</sub>@C<sub>60</sub> and the high resolution of the LAGRANGE spectrometer enable such translation-rotation splittings to be resolved. In figure 2b it was observed that one of the expected components was completely absent (identified by a dashed arrow). This signalled the surprising discovery of a new type of selection rule in neutron scattering, running counter to the widely held view that INS spectroscopy of molecular compounds is not subject to any selection rules [3].

In conclusion, as well as providing aesthetically appealing chemical structures, the small molecule endofullerenes provide a fascinating nanolaboratory environment for studying the fundamental physics of quantum rotor dynamics. Unforeseen discoveries have emanated from the highly detailed INS spectra which continue to provide new physical insights.

# CHEMISTRY AND CRYSTALLOGRAPHY

## Atmospheric implications of the ozonolysis of methyl oleate monolayers at the air/water interface

### Horizontal reflectometer FIGARO

It has been proven beyond reasonable doubt that the emission of pollutants by heavy industry is changing the behaviour of our climate. The mechanisms by which different pollutants modify the atmospheric composition, however, are extremely complex. One such mechanism is when pollutants oxidise organic coatings of cloud droplets resulting in faster evaporation rates [1]. Accelerated droplet evaporation can lead to lower cloud cover and then the sun may heat up the Earth more efficiently [2]. This process is directly linked to global warming.

#### AUTHORS

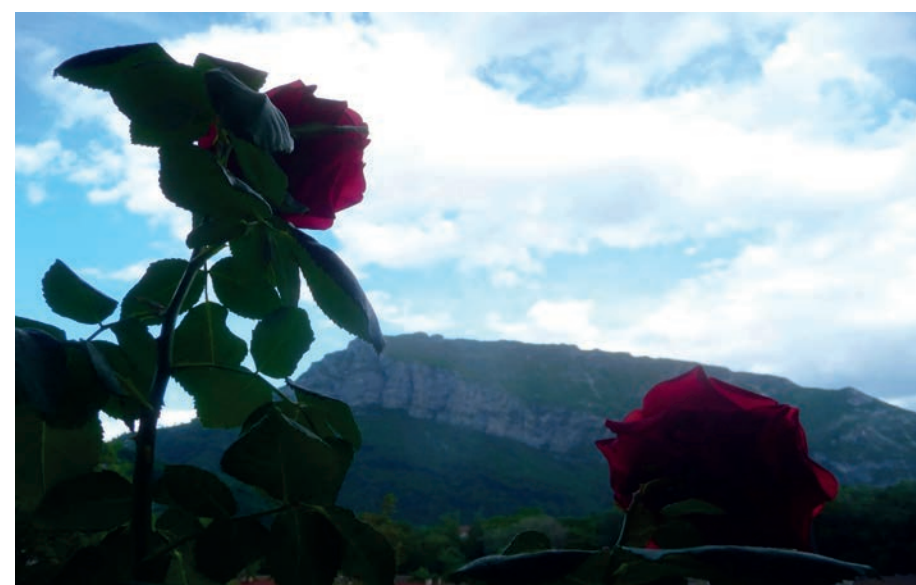
C. Pfrang and I.D. Hoare (University of Reading, UK)  
F. Sebastiani (University of Reading, UK and ILL)  
C.O.M. Lucas and M.D. King (Royal Holloway University of London, Egham, UK)  
D. Chang (Lund University, Sweden)  
R.A. Campbell (ILL)

#### REFERENCES

- [1] U. Lohmann and J. Feichter. *Atmos. Chem. Phys.* 5 (2005) 715
- [2] U. Pöschl. *Angew. Chem., Int. Ed.* 44 (2005) 7520
- [3] C. Pfrang, F. Sebastiani, C.O.M. Lucas, M.D. King, I.D. Hoare, D. Chang and R.A. Campbell. *Phys. Chem. Chem. Phys.* 16 (2014) 13220
- [4] M.D. King, A.R. Rennie, K.C. Thompson, F.N. Fisher, C.C. Dong, R.K. Thomas, C. Pfrang and A.V. Hughes. *Phys. Chem. Chem. Phys.* 11 (2009) 7699

The efficiency of different gases to oxidize organic films at the air/water interface has been the topic of our recent investigations using neutrons on the FIGARO reflectometer. Here the macroscopic planar surface of a Langmuir trough is used as a model for the surface of cloud droplets. This approximation is rationalised by the fact that the surface of even a tiny cloud droplet is effectively flat on molecular length scales. We have studied a range of organic monolayers with different gaseous pollutants to date. We started with a study of the oxidation by ozone of the organic compound methyl oleate [3]. Methyl oleate is an interesting compound to study because it is likely to be produced in larger amounts in the future due to increasingly popular fatty acid methyl ester biodiesels.

In our neutron reflectivity experiments, a large Langmuir trough was housed in a custom-built reaction chamber, a monolayer of deuterated methyl oleate was spread on the free liquid surface and the internal atmosphere was exposed to ozone at different concentrations. The ozone reacts with a double bond close to the centre of the organic molecules and effectively snaps it in half. The small reaction products are sufficiently soluble or volatile that they do not remain at the surface. The neutrons are used to measure the amount of organic material at the interface as a function of time, and the rate of loss of material is measured



Clouds above the Neron mountain in Grenoble: a climate worth understanding.

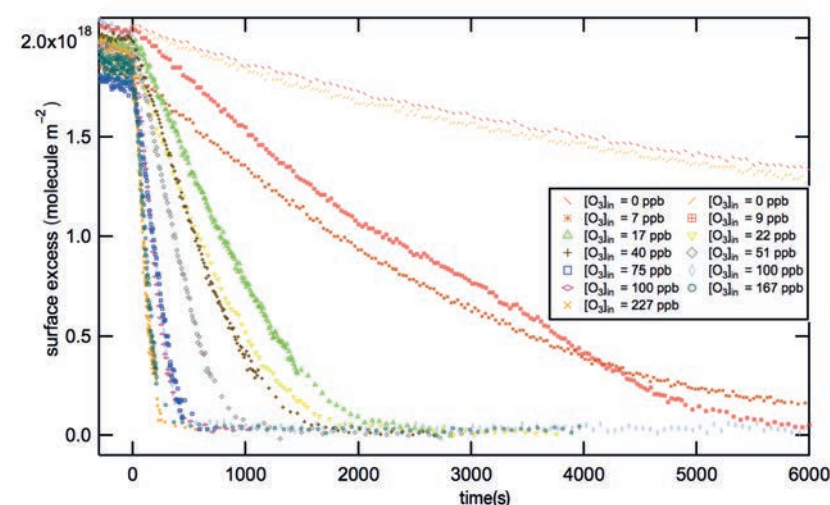


Figure 1

Surface excess of monolayers of deuterated methyl oleate on an aqueous sub-phase during oxidation by ozone with respect to the reaction time and ozone concentration. *In situ* ozone generation was initiated at  $t = 0$ .

with respect to the ozone concentration. FIGARO is extremely well-suited to these kinetic surface excess studies due to its high flux settings and of course the stable reactor source. We performed measurements typically with scans of three or five seconds in contrast to previous studies which had a time resolution of five minutes.

Figure 1 shows different surface excess decays with time as a function of the ozone concentration. A kinetic model is applied to these decays to calculate a first-order rate coefficient for each reaction. For a typical concentration of ozone in the atmosphere of 50 ppb this corresponds to a lifetime of about 10 minutes, which is surprisingly short. Interestingly, the organic material was eliminated extremely efficiently from the interface during the oxidation reaction as < 2 % of the material remained after the reaction had finished. Such efficient elimination of the organic material would not have been predicted from previous studies on other related compounds. In the atmosphere the rapid and complete loss of surface activity of organic material upon oxidation would result in cloud droplets growing more slowly, making it more difficult to form clouds. This behaviour is different to what was determined recently for the compound oleic acid [4]. We may conclude that small changes in the nature of the reaction products can lead to fundamentally different atmospheric behaviour.

Figure 2 shows a second-order rate plot for the reactions, which is a plot of the first-order rate decay coefficients with respect to the ozone concentration. A linear fit to these data revealed the bimolecular rate coefficient of  $(5.7 \pm 0.9) \times 10^{-10} \text{ cm}^2 \text{ molecule}^{-1} \text{ s}^{-1}$ , which corresponds to an uptake coefficient of about  $3 \times 10^{-5}$ .

These results show that the reduction in ozone reactivity at the droplet surface compared with that in the bulk is about an order of magnitude less pronounced for methyl oleate than oleic acid, a compound which differs only in its type of head group [4]. The surface reactions on aqueous droplets encountered in the atmosphere should therefore be considerably more important for methyl oleate than for oleic acid, in particular if transport of gas-phase oxidants into the aerosol particle is hindered. This finding illustrates that a small modification in the molecular structure (methyl

ester vs. parent acid) strongly affects the reactivity of the organic film. Thus we succeeded in demonstrating the key importance of studies of the reactivity of surface layers, which can provide important missing data for the development of atmospheric models of climate change.

It remains a key challenge to understand both the oxidation rate and the phase behaviour of more realistic organic monolayers on cloud droplets. The increasing complexity of laboratory studies, e.g. multi-component systems as well as variations in temperature and dynamic surface conditions, in conjunction with the development of realistic models, will be essential steps towards an improved understanding of oxidation effects in real atmospheric aerosols.

[This work was part of the ILL thesis work of Federica Sebastiani].

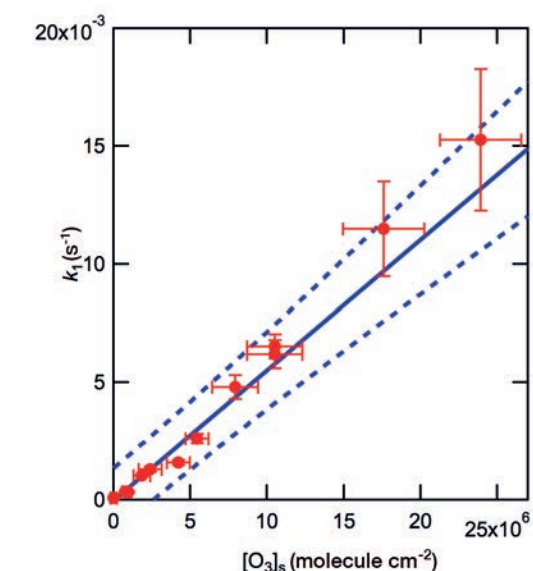


Figure 2

Pseudo first-order decay rate coefficients for methyl oleate at the air/water interface,  $k_1$ , as a function of the ozone surface concentration,  $[O_3]_s$ . The data points and error bars represent experimental data and associated uncertainties at one standard deviation. The solid line corresponds to an orthogonal distance regression fit weighted by the uncertainties both in  $k_1$  and  $[O_3]_s$ . The dashed lines represent the 95 % prediction bands.

# CHEMISTRY AND CRYSTALLOGRAPHY

## Neutrons, X-rays and high-performance computing help unlock enzymatic synthesis of rare sugars

Single crystal diffractometer D19  
Protein Crystallography Station at  
Los Alamos National Laboratory

A comprehensive X-ray/neutron crystallographic study in combination with molecular calculations and simulations has been performed to locate H and D atoms during isomerisation of L-arabinose sugar into L-ribulose and its subsequent epimerisation to L-ribose catalysed by enzyme D-xylose isomerase. L-ribose, a rare sugar not present in nature, is an essential starting material for the synthesis of antiviral and anti-cancer drugs. Crystallographic evidence and quantum-mechanical/molecular mechanics (QM/MM) calculations unlock the mode of substrate binding and draw a new mechanistic picture for the sugar epimerisation. Molecular dynamics (MD) simulations establish possible mutations that can enhance the sugar binding to improve the production of rare sugars.

### AUTHORS

P. Langan, A. Kovalevsky, A.K. Sangha, T. Wymore, J.M. Parks, Z. Koo Yang and D.E. Graham (Oak Ridge National Laboratory, USA)  
L. Hanson (University of Toledo, USA)  
Z. Fisher (Los Alamos National Laboratory, USA)  
S.A. Mason and M.P. Blakeley (ILL)  
V.T. Forsyth (ILL and Keele University, UK)  
J.P. Glusker and H.L. Carrell (Fox Chase Cancer Center, Philadelphia, USA)  
J.C. Smith (Oak Ridge National Laboratory and University of Tennessee, Knoxville, USA)  
D.A. Keen (ISIS, UK)

### REFERENCES

- [1] K. Okano, *Tetrahedron* 65 (2009) 1937
- [2] Y.-J. Jeon, M.B. Park and I.-H. Kim, *Bioprocess Biosyst. Eng.* 33 (2010) 87
- [3] M. Leisola, J. Jokela, J. Finell and O. Pastinen, *Biotechnol. Bioeng.* 72 (2001) 501
- [4] P. Langan, A.K. Sangha, T. Wymore, J.M. Parks, Z.K. Yang, B.L. Hanson, Z. Fisher, S.A. Mason, M.P. Blakeley, V.T. Forsyth, J.P. Glusker, H.L. Carrell, J.C. Smith, D.A. Keen, D.E. Graham, A. Kovalevsky, *Structure* 22 (2014) 1287

Rare sugars have attracted considerable attention from the pharmaceutical industry because drugs based on rare sugars do not interfere with cellular processes and have fewer side effects, unlike drugs based on natural saccharides [1]. As a result, rare sugars like L-ribose, a cousin and a mirror image of the ubiquitous D-ribose found in our DNA and RNA, are utilised for the synthesis of different antiviral and anti-cancer drugs. The problem, however, is that rare sugars are generally synthesised using hazardous chemicals, such as transition metals and solvents, and the chemical synthesis requires purified starting material [2]. Conversely, biotechnological production of rare sugars using enzymes such as D-xylose isomerase is advantageous because enzymes can work effectively on crude biomass pulps or hydrolysates. Yet, the bottleneck is that epimerisation of L-arabinose to L-ribose catalysed by D-xylose isomerase is very slow and inefficient [3].

One approach to improving the suitability of D-xylose isomerase for commercial production of L-ribose is protein engineering. Informed rational engineering requires an understanding of the catalytic mechanism involved in the multi-step conversion of L-arabinose into L-ribose; however, the substrate binding mode and the exact manner in which

the enzyme accomplishes the epimerisation reaction have remained unknown. The enzymatic reaction is proposed to follow a double isomerisation route: first, L-arabinose is isomerised into L-ribulose, and then the latter is isomerised into L-ribose (**figure 1**). Each stage involves several steps, including opening the ring of the sugar to obtain the linear form of a substrate, the sugar isomerisation between aldose and ketose forms, and closure of the product sugar ring.

Hydrogen atoms are transferred at each step and the knowledge of their exact locations is critical for correctly mapping the mechanism. Neutron crystallography provides a direct means of locating hydrogen atoms in macromolecules and visualising at unprecedented detail the binding of substrates to enzyme active sites. Hydrogens are observed even better when the light isotope H is exchanged with the heavy isotope D (deuterium).

Neutron crystallographic data for two D-xylose isomerase complexes with L-arabinose were collected using the ILL instrument D19 and the neutron Protein Crystallography Station at Lujan Center at Los Alamos National Laboratory. The neutron data were supplemented with room-temperature X-ray diffraction data on several complexes with L-ribulose and L-ribose. We augmented the crystallographic approach with QM/MM calculations and MD simulations. This is the first time that the combination of neutron crystallography with theoretical calculations has been applied to a study of substrate binding and enzymatic mechanism [4].

By using transition metal ions  $\text{Cd}^{2+}$  and  $\text{Ni}^{2+}$  the enzyme-substrate complexes with cyclic and linear forms of L-arabinose, respectively, have been trapped in crystals. Surprisingly, L-arabinose adopted a high-energy skew-boat conformation ( ${}^5S_1$ ) in the complex with cadmium instead of a low-energy chair conformation ( ${}^4C_1$ ) observed with substrates D-xylose or D-glucose (**figure 2**). QM/MM calculations based on the neutron structure provided evidence that the enzyme complex containing  ${}^5S_1$  L-arabinose is more stable by 10 kcal/mol than the one with  ${}^4C_1$  sugar. Crystallographic evidence in combination with the theoretical calculations explained the apparent low affinity of D-xylose isomerase to L-arabinose: with  ${}^4C_1$  sugar conformer being abundant in solution at room temperature and the unstable skew-boat conformer being very scarce, there would be a limited amount of the substrate available to bind to the enzyme. The distribution of the hydrogen atoms before and after the ring opening step suggested that the isomerisation of L-arabinose to L-ribulose follows the same mechanism as with the physiological substrate D-xylose. In addition, MD simulations revealed that L-arabinose binding can be improved by specific amino acid substitutions in the D-xylose isomerase active site, which will enhance the enzyme's performance.

Remarkably, in all X-ray structures with L-ribulose or L-ribose sugars were found in their five-member furanose ring forms regardless of whether the inhibitory ( $\text{Cd}^{2+}$  or  $\text{Ni}^{2+}$ ) or activating ( $\text{Mg}^{2+}$ ) ions were bound to D-xylose isomerase. These complexes are likely to be inhibitory because no

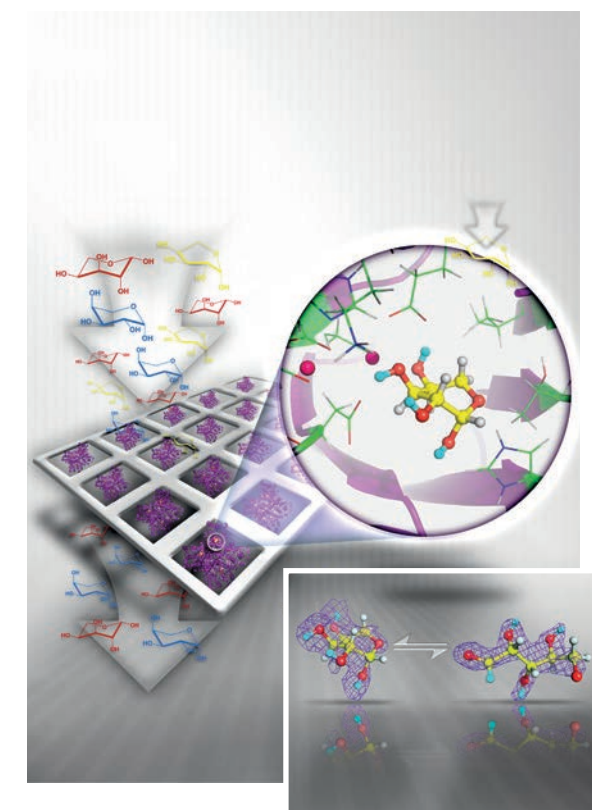


**Figure 2**

An artist's rendering of the enzyme D-xylose isomerase as it isomerises L-arabinose into rare sugars not found in nature. The enzyme acts as a filter by capturing and performing catalysis only on the high-energy  ${}^5S_1$  conformation of L-arabinose, while remaining inactive on other more abundant sugar conformations. Neutron macromolecular crystallography has unequivocally demonstrated how this high-energy conformer of L-arabinose binds in the enzyme active site and is converted to the linear intermediate form. Simulations provide evidence for the experimental results  
**Inset bottom right:** Neutron-scattering length density map contoured at  $1.4\sigma$  level for the cyclic substrate, and at  $1.0\sigma$  level for the linear substrate (Image credit: Genevieve Martin/ORNL).

reaction was observed. However, complexes with  $\text{Ni}^{2+}$  and L-ribulose or L-ribose may represent reactive binding of the sugars, and the isomerisation between these two sugars may proceed through a cis-enediol mechanism instead of the generally accepted hydride shift mechanism at play for converting D-xylose into D-xylulose and L-arabinose into L-ribose.

In conclusion, neutron and X-ray crystallographic results have been combined with QM/MM molecular calculations and MD simulations for the first time to address the mechanism of enzymatic synthesis of rare sugars from the biomass-derived natural sugar. The results demonstrate the power of this approach to inform theoretical calculations that may otherwise fail if the hydrogen atom positions have to be inferred from basic chemical knowledge. Therefore, combining neutrons, X-rays, molecular calculations and simulations provides an unparalleled means to study protein structure-function, perform rational enzyme engineering and, perhaps, take drug design to a new level.

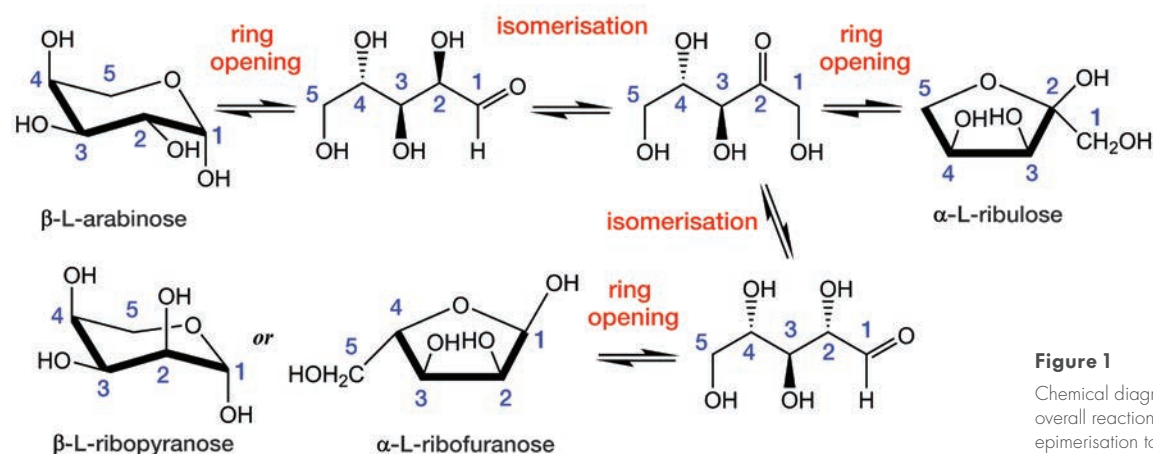


**Figure 1**

Chemical diagram for the overall reaction of L-arabinose epimerisation to L-ribose.

# CHEMISTRY AND CRYSTALLOGRAPHY

## Formation of nano-MOF-5 in the presence of a modulator: does the modulator wrap around the nanoparticle?

Small-angle scattering diffractometer D11

Metal organic frameworks (MOF) are hybrid materials made up of organic and inorganic components. Their large internal surface renders these materials promising candidates for gas storage, gas separation, and catalysis. MOFs have generally been produced by solvothermal synthesis, resulting in micro and macro crystalline materials. However, precipitation from supersaturated solutions by mixing the component solutions has evolved as an interesting alternative to solvothermal synthesis [1]. This alternative route constitutes a powerful bottom-up approach, as it is based on nucleation and growth. The technique generates nanocrystals, thus providing new routes to the development of hierarchical mesopore structures with even larger surfaces. To exploit this potential we need detailed knowledge of the underlying mechanisms. One of the ways to achieve this is to investigate the formation of MOF-5 nanoparticles [2], [3].

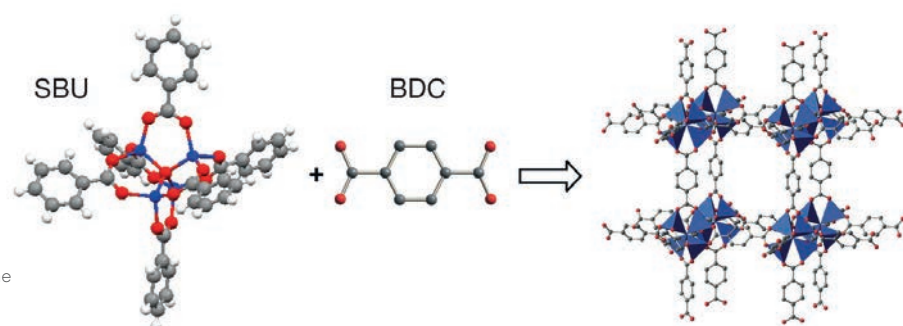


Figure 1

Synthesis of MOF-5, achieved by mixing the preformed pre-SBU dissolved in DMF with the linker BDC dissolved in DMF.

### AUTHORS

D. Zacher and R.A. Fischer (Ruhr-University, Bochum, Germany)  
R. Nayuk and K. Huber (Paderborn University, Germany)  
R. Schweins (ILL)

### REFERENCES

- [1] L. Huang, H. Wang, J. Chen, Z. Wang, J. Sun and D. Zhao, Y. Yan, *Microporous Mesoporous Mater.* 58 (2003) 105
- [2] S. Hermes, T. Witte, T. Hikov, D. Zacher, S. Bahn Müller, G. Langstein, K. Huber, and R.A. Fischer, *J. Am. Chem. Soc.*, 129 (2007) 5324
- [3] S. Hausdorf, F. Baitalow, T. Böhle, D. Rafaja and F. Mertens, *J. Am. Chem. Soc.*, 132 (2010) 10978
- [4] K.M. Choi, H. J. Jeon, J.K. Kang and O.M. Yaghi, *J. Am. Chem. Soc.*, 133 (2011) 11920
- [5] P. Mittelbach and G. Porod, *Acta Phys. Austriaca* 14 (1961) 185

In a relatively sophisticated small-angle neutron scattering (SANS) experiment, set up to elaborate an alternative to solvothermal synthesis for the production of metal organic frameworks, we hand-mixed two dimethylformamide (DMF) solutions: one with the secondary building unit  $Zn_4O(C_6H_5COO)_6$  (pre-SBU), and one with terephthalic acid (BDC) as a linker (**figure 1**). Five minutes after generation of the mixture, we added monodentate 4-n-decylbenzoic acid as a modulator agent. The concentration of pre-SBU was 0.83 mmol/l, applied at molar ratios pre-SBU:BDC:modulator = 1 : 1 : X, with X = 0 (without modulator) or 5 (with modulator). The samples obtained enabled us to study the formation of particles at different concentrations of the two principal constituents and to investigate the impact of the modulator agent on the process.

The experiment – using time-resolved small-angle scattering on the ILL's D11 instrument – demonstrated that the size dispersity of the growing nanoparticles narrows as nanoparticles are formed. The addition of the modulator accelerates the focusing of the width of the size distribution. One crucial question to be solved in this context is the modulator's location whilst it participates in nanoparticle formation.

During the experiment we observed the formation of a layer of modulator molecules wrapped around the growing particles. We could prove that the modulator forms a shell around the nano-MOFs by an elegant contrast variation experiment. This is only possible using

Figure 2

Design of the SANS experiment, based on contrast variation making it possible to address either the modulator agent alone (Case 1) or the MOF-5 (Case 2). If the modulator envelops the MOF-5 particles, appropriate matching (centre) reveals a shell.

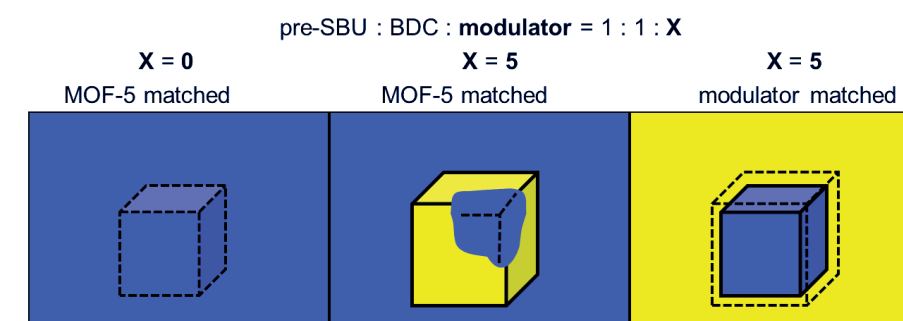


Figure 3

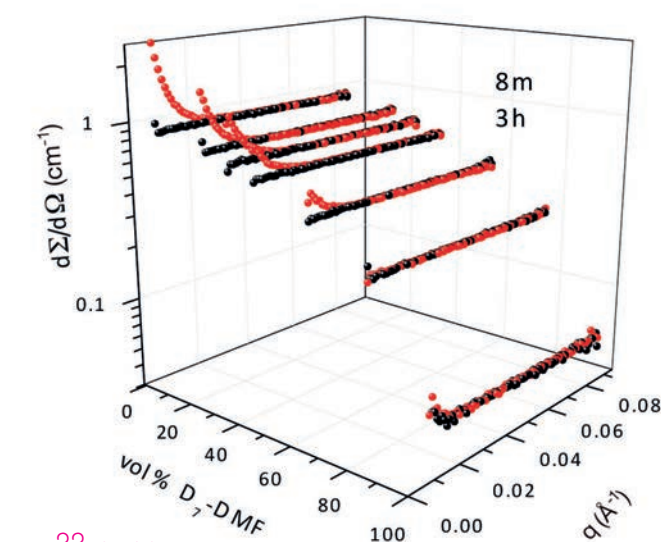
Scattering curves of MOF-5 dissolved in DMF, as recorded on D11 at a detector distance of 8 m. The curves demonstrate the variation of the scattering contrast of MOF-5 in mixtures of h-DMF/d-DMF at different ratios of h-DMF to d-DMF. The symbols indicate pure solvent (●) and MOF-5 solutions (●). At a ratio of h-DMF/d-DMF = 20%/80%, the scattering of the solution is indistinguishable from the scattering of the pure solvent. This suggests that this mixture is an ideal solvent mixture for the analysis of the modulator.

neutron-scattering techniques, as the contrast of the solvent medium varies if the deuterated solvent (d-DMF) is mixed with the hydrogenated solvent (h-DMF) (**figure 2**). It is this contrast variation that allows us to identify h-DMF/d-DMF solution mixtures, which will match either the contrast of the nano-MOF-5 alone (case 1) or the contrast of the fully hydrogenated modulator (case 2). Case 1 reveals the isolated scattering of the modulator and its morphology, and case 2 the scattering of the nano-MOF-5 particles.

As is shown in **figure 3**, we identified a solution mixture which verified full contrast matching of the nano-MOF-5 at h-DMF/d-DMF = 20%/80%. We practically achieved case 2 in h-DMF. There is indirect evidence in the literature [4] for shell formation of this type, but this experiment provides direct proof.

The main results are summarised in **figure 4**. The scattering curve corresponding to the situation where only the modulator is matched shows a trend which can be reconciled nicely with the model of a polydisperse cube. If the solvent ratio of h-DMF/d-DMF = 20%/80% is used, which matches the contrast of nano-MOF-5, the scattering is significantly lower although still detectable. The trend shows decay with a power of  $q^2$ , which agrees with the scattering of thin layers. We therefore consider this to be proof of the existence of a shell forming on growing particles.

In conclusion, a highly sophisticated SANS experiment has provided information on the formation mechanism of MOF-5, and the impact of a modulator on this process which forms an enveloping shell in the present system. The experiment also demonstrates the feasibility of placing cargo on the outer surface of the nano-MOF. Above all, the experiment represents the first attempt to achieve such an ambitious proof, providing an unprecedented case study for demonstrating the presence of structural features such as thin shells around nanoparticle cores.



?? query

should D on left x-axis be cap or lower case

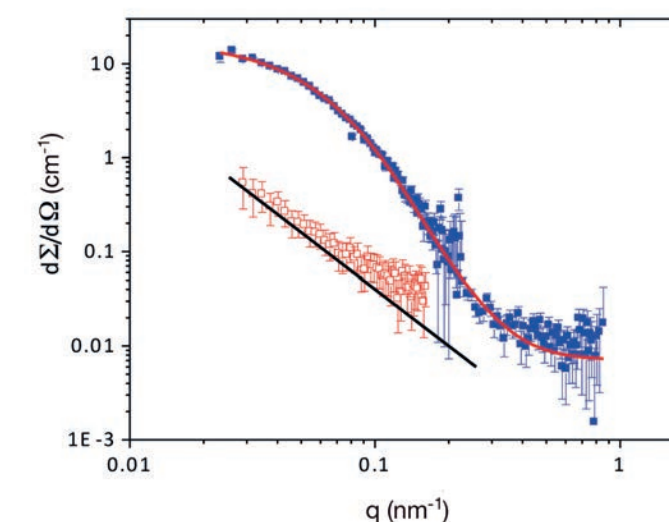


Figure 4

SANS curves on the formation of MOF-5 nanoparticles in DMF, assisted by a modulator. The experiment in which the modulator has been matched (■) corresponds to case 2 (right-hand image in figure 2); the experiment in which the MOF-5 nanoparticles have been matched (□) corresponds to case 1 (centre image in figure 2). The straight line in black denotes the decay typical for thin layers and the red curve is a model fit based on polydisperse cubes [5].

# MAGNETISM

## Quantum and thermal melting in magnets

### Three-axis spectrometer IN14

The behaviour of a broad class of magnetic materials is governed by the rules of quantum mechanics, which makes the underlying physical principles notoriously difficult to understand. Fresh insight comes now from high-precision experiments performed on IN14 on the model quantum dimer material  $\text{TlCuCl}_3$ . The ability to precisely tune quantum fluctuations in magnets *in situ* and to measure fully quantitatively their complex spin dynamics and scaling behaviours at quantum phase transitions is unique to neutron scattering.

#### AUTHORS

Ch. Rüegg (Paul Scherrer Institute and University of Geneva, Switzerland)  
P. Merchant and D.F. McMorrow (University College London, UK)  
B. Normand (Renmin University of China, China)  
K.W. Krämer (University of Bern, Switzerland)  
M. Boehm (ILL)

#### REFERENCES

- [1] P. Merchant *et al.*, Nat. Phys. 10 (2014) 373
- [2] S. Sachdev and B. Keimer, Physics Today 64 (2011) 29
- [3] T. Giamarchi *et al.*, Nat. Phys. 4 (2008) 198
- [4] Ch. Rüegg *et al.*, Phys. Rev. Lett. 93 (2004) 257201
- [5] Ch. Rüegg *et al.*, Phys. Rev. Lett. 100 (2008) 205701

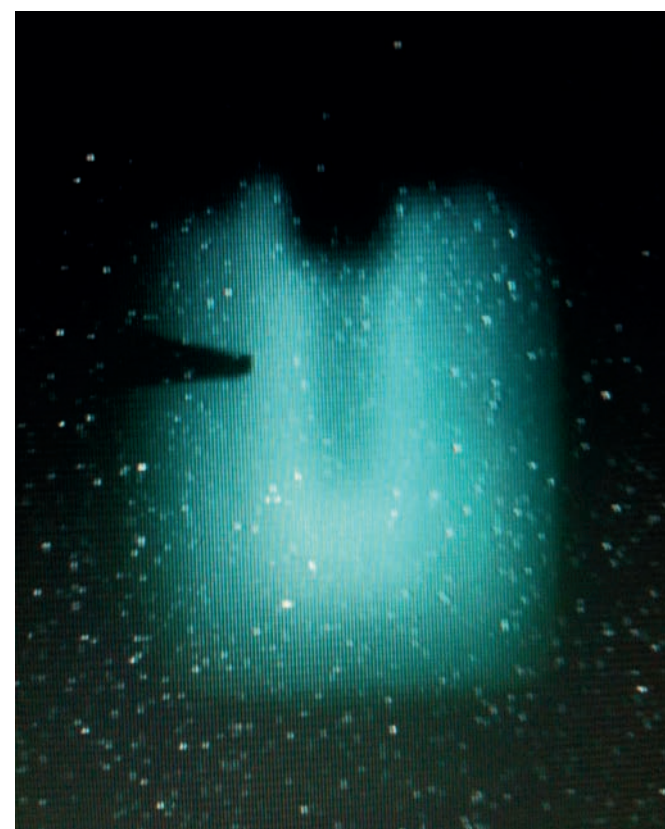
When ice is warmed, the water molecules forming its structure vibrate more and more vigorously until finally the forces between them are no longer strong enough to hold them together – the ice then melts and turns into liquid water. Quantum physics predicts that similar phenomena can be observed if the quantum mechanical fluctuations of the particles in a material can be altered. Such changes of state triggered by purely quantum effects – known as quantum phase transitions – play a role in many astonishing phenomena in solid-state systems, including high-temperature superconductivity and quantum magnets.

We have specifically controlled the magnetic ground state of the material  $\text{TlCuCl}_3$  by exposing it to a varying, external hydrostatic pressure at different temperatures [1]. By performing neutron-scattering measurements on IN14, we could observe what happens during a quantum phase transition, and compare the “quantum melting” of the magnetic structure with the classical “thermal melting” phase transition. For the first time fundamental theoretical predictions could be tested by fully quantitative comparisons with experimental data on the characteristic excitations and scaling at a quantum phase transition [2].

The compound  $\text{TlCuCl}_3$  is an inorganic material, where  $\text{Cu}^{2+}$  ions with spin  $S=1/2$  are structurally paired forming dimers with a strong antiferromagnetic exchange interaction. Previously its magnetic properties were studied extensively by neutron spectroscopy. At ambient pressure, its ground state is formed by quantum-disordered, non-magnetic singlets. An external magnetic field can then cause a quantum phase transition, which can be described by Bose-Einstein condensation of magnons [3]. Alternatively, application of hydrostatic pressure increases interactions between dimers reducing the amount of quantum fluctuations and controls a quantum phase transition to a state with long-range magnetic order above a critical pressure of just 1 kbar [4,5].

#### Figure 1

Neutron image of the ILL helium gas-pressure cell used by Ch. Rüegg and his team for the experiment on IN14. The shadow in the centre of the image shows the position of the  $\text{TlCuCl}_3$  single crystal sample. The tip on the left (cadmium mask) marks the centre of the neutron beam. In the pressure cell, helium gas is used to expose the sample to pressures up to 5 kbar. In  $\text{TlCuCl}_3$  the quantum critical point is reached at  $p_c = 1.07$  kbar [1,4,5].



For the present experiment, the ILL helium gas-pressure cell was used, which allows pressures up to 5 kbar with a base temperature of 1.5 K. **Figure 1** shows a neutron image of the sample in the pressure cell taken with a neutron camera directly on IN14. Inelastic background signal from the helium pressure medium and general absorption by the cell are experimental challenges, but the relatively large available sample volume enables clean, inelastic neutron-scattering experiments in combination with systematic and continuous control of pressure.

The evolution of the characteristic excitations at quantum phase transitions, as shown in **figure 2**, and quantum critical scaling were amongst the key questions addressed in the experiment. We were able to demonstrate a number of remarkable properties arising at the interface between quantum and classical physics [1]. Quantum and thermal fluctuations have remarkably similar effects in melting the magnetically ordered phase and in opening excitation gaps, but operate quite independently close to the quantum critical point in this material. In the quantum critical regime there is robust scaling of the energies and widths of critically damped excitations. This scaling crosses over to a classical critical form in a narrow region around the thermal phase transition line. The critically damped longitudinal, or Higgs, mode of the ordered phase is exquisitely sensitive to thermal fluctuations and becomes over-damped in the classical regime. We could observe for the first time that such a Higgs mode plays an important role in classical “thermal melting” phase transitions near quantum critical points.

Although IN14 was known as one of the most powerful three-axis spectrometers for cold neutrons, the experiment has reached the limits of what is feasible today. The general trend over the last years, here in the field of quantum magnetism, towards smaller sample sizes, low or even vanishing magnetic moments, e.g. at a quantum phase transition, and extreme sample environments like high-pressure cells, requires continuous improvements in instrumentation. Therefore the ILL, in collaboration with Charles University in the Czech Republic, decided to replace IN14 with the new high-flux spectrometer ThALES (Three Axis Low Energy Spectroscopy). The new instrument was completed in autumn 2014 and has successfully started its commissioning phase. ThALES will be open to the ILL’s user programme from the first proposal round in 2015.

In summary, we have conducted high-resolution neutron spectroscopy experiments on IN14 on the quantum dimer antiferromagnet  $\text{TlCuCl}_3$ . They allowed us to probe the spin excitations of all phases in and around a generic quantum phase transition by varying the pressure and temperature. Using the ability to independently control the two phase transitions that the material can undergo we obtained unique insights. We could disentangle the effects of quantum and classical physics and found that the thermal and the quantum ‘melting’ proceed in a very similar manner, but that the two mechanisms operate quite independently of one another.

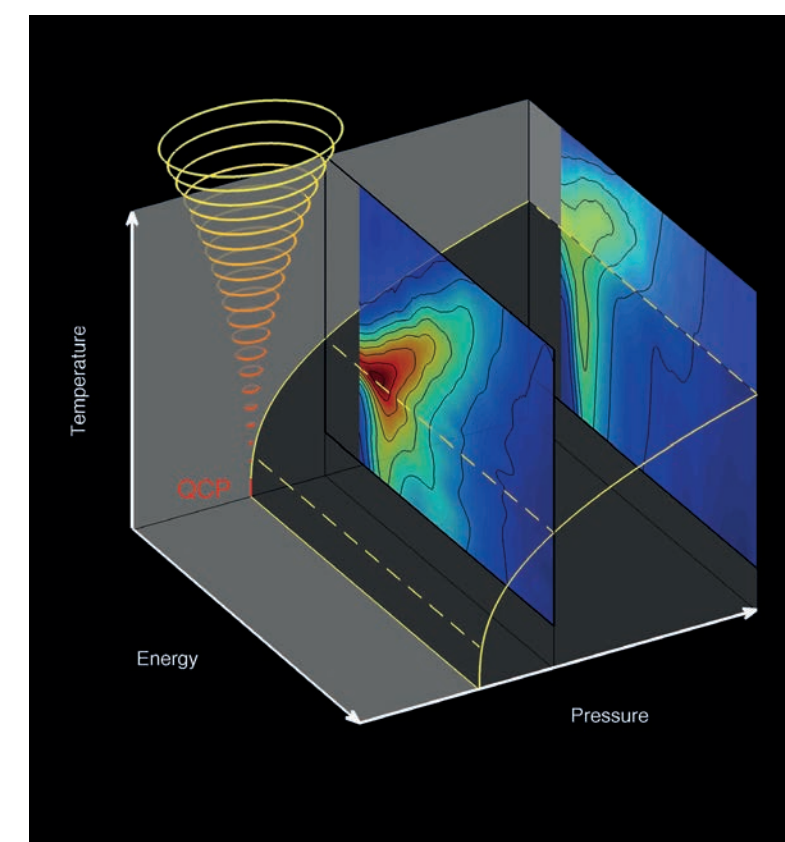


**Figure 2**

Spectroscopy with neutrons enables detailed experiments on the dynamics and fundamental scaling properties near quantum phase transitions. The figure shows schematically the pressure-temperature phase diagram of  $\text{TlCuCl}_3$  with the evolution of magnetic excitations as a function of temperature, measured at two distinct pressures. At zero temperature the quantum critical point (QCP) separates a phase with long-range antiferromagnetic order (at high pressures and low temperature, dark grey region) from a quantum-disordered phase without order (grey region). At finite temperatures around the QCP, a quantum critical regime evolves with combined effects of quantum thermal fluctuations (red to yellow spiral). The coloured panels show the evolution of the characteristic excitations measured on IN14 (transverse spin waves and a longitudinal ‘Higgs’ mode) when approaching the QCP from the ordered phase at  $p = 1.75$  kbar and  $3.6$  kbar  $> p_c = 1.07$  kbar. Data from [1].

# MAGNETISM

## Strong ferromagnetic fluctuations in a heavy-fermion antiferromagnet

Time-of-flight spectrometer IN5

The rich, low-temperature magnetic phase diagram of the long-studied heavy-fermion metal  $\text{CeB}_6$  [1] was always considered to be solely governed by antiferromagnetic (AFM) interactions between the dipolar and multipolar Ce moments. However, in a recent experimental study performed on this material using the IN5 time-of-flight spectrometer [2], we overturned this established perspective by uncovering an intense, ferromagnetic, low-energy collective mode that dominates the magnetic excitation spectrum of  $\text{CeB}_6$ . Our inelastic neutron-scattering data reveal that the intensity of this new excitation by far exceeds that of conventional spin-wave magnons, thus placing  $\text{CeB}_6$  much closer to a ferromagnetic instability than could be anticipated. These results call for a substantial revision of existing theories that have so far largely neglected the role of ferromagnetic interactions.

### AUTHORS

D.S. Inosov (TU Dresden, Germany)  
H. Jang, G. Friemel and B. Keimer (Max Planck Institute for Solid State Research, Stuttgart, Germany)  
A.V. Dukhnenko, N.Y. Shitsevalova and V.B. Filipov (Institute for Problems of Material Sciences, Kiev, Ukraine)  
J. Ollivier (ILL)

### REFERENCES

- [1] G. Friemel *et al.*, *Nature Commun.* 3 (2012) 830
- [2] H. Jang *et al.*, *Nature Mater.* 13 (2014) 682
- [3] S.V. Demishev *et al.*, *Phys. Rev. B* 80 (2009) 245106

Cerium hexaboride,  $\text{CeB}_6$ , represents the structurally simplest example of a compound exhibiting the so-called magnetically hidden order – an exotic magnetic phase that in contrast to conventional magnetic order is invisible to standard neutron diffraction. In the case of  $\text{CeB}_6$ , its elusive order parameter has been attributed to the antiferroquadrupolar (AFQ) arrangement of cerium-4f moments. In its ground state,  $\text{CeB}_6$  also develops a more usual antiferromagnetic (AFM) order with an onset temperature  $T_N = 2.3$  K. As a result, its essential low-temperature physics were always considered to be solely governed by AFM interactions between the dipolar and multipolar Ce moments. On the other hand, the presence of a pronounced electron spin resonance (ESR) in this compound [3] would require strong ferromagnetic correlations that up to now had escaped any direct observation and remained largely neglected in theoretical models. Such an apparent discord between the results of different experimental probes has motivated us to investigate the magnetic fluctuation spectrum of this model system in more detail.

To resolve this controversy, we have carried out a high-resolution ( $\Delta E \sim 80 \mu\text{eV}$ ) time-of-flight (TOF) neutron-scattering experiment on a large single crystal of  $\text{CeB}_6$  to obtain the complete momentum-resolved spectrum of magnetic excitations in the low-energy range over the whole volume of the Brillouin zone. The measurements were taken at two temperatures,  $T = 1.5$  K and  $2.6$  K, i.e. in the AFM and AFQ states respectively, using the cold-neutron time-of-flight spectrometer IN5.

**Figure 1** shows a constant-energy cut taken from our four-dimensional dataset along the  $(H H L)$  plane in momentum space at an energy transfer of  $0.25$  meV. It reveals the strongest scattering intensity in the vicinity of the  $(110)$   $\Gamma$ -point (ferromagnetic zone center), whose magnetic origin can be concluded from its pronounced temperature dependence. Hence, it must represent a previously unknown magnetic excitation centered at the ferromagnetic wave vector. In addition, the same figure shows notably weaker intensity spots near the AFM ordering vectors, such as  $S(\frac{1}{4} \frac{1}{4} \frac{1}{2})$ ,  $S'(\frac{3}{4} \frac{1}{2} \frac{1}{4})$ ,  $S''(\frac{3}{4} \frac{3}{4} \frac{1}{2})$  or equivalent. They originate from conventional spin-wave modes that appear to be dwarfed by the intensity of the ferromagnetic excitation. At a higher energy of  $0.5$  meV (not shown), we

??  
labelled a >  
but no  
reference  
for a

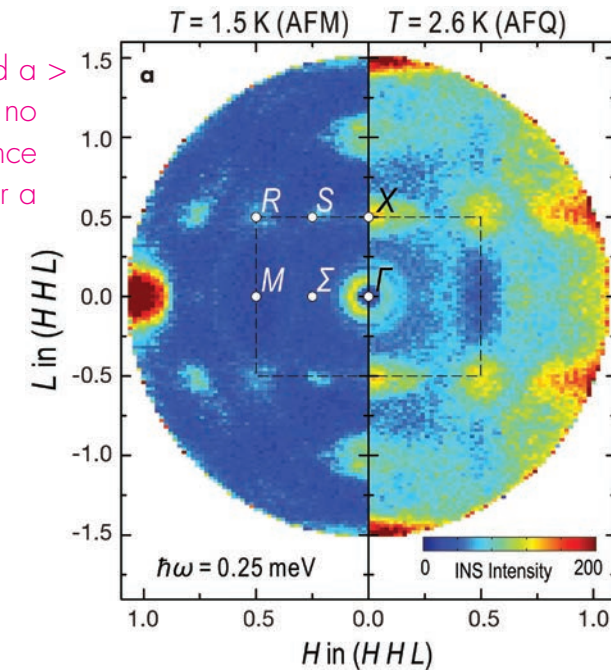


**Figure 1**

A constant-energy map in the  $(H H L)$  plane obtained from the TOF data at the energy of the ferromagnetic mode,  $\hbar\omega = 0.25$  meV. The data were symmetrised about the natural mirror planes of the reciprocal space. The left and right halves of the image were measured below and above the AFM transition, respectively.

also observed the previously reported magnetic resonant mode centered at the AFQ wave vector [1], which turned out to be approximately twice as weak in comparison to the ferromagnetic intensity.

The energy-momentum cut presented in **figure 2** also reveals the dispersion of the  $\Gamma$ -point mode in the AFM state (**left panel**) and its disappearance above the ordering temperature (**right panel**). It is characterised by a spin gap of  $\sim 0.2$  meV and disperses towards higher energy away from the zone center, reaching above  $0.5$  meV at the zone boundary. The mode is destroyed above  $T_N$ , giving rise to an intense quasi-elastic signal centered at zero energy. In total, we can distinguish three distinct types of low-energy magnetic excitations in  $\text{CeB}_6$ : a strong ferromagnetic soft mode at the zone center, a subsidiary maximum of intensity at the  $R$  point, and the spin-wave modes emanating from the AFM wave vectors. All these excitations hybridise to form a continuous dispersive magnon band in a narrow energy range between  $0.2$  and  $0.7$  meV. Absolute units normalisation performed by means of a vanadium standard, as described in [2], further allowed us to estimate the total integrated spectral weights peaked near the  $\Gamma$  and  $R$  points, which amount to  $0.06 \pm 0.02$  and  $0.03 \pm 0.01 \mu_B^2$  per formula unit, respectively.

In summary, the experiments presented here directly demonstrate the propensity of  $\text{CeB}_6$  to a ferromagnetic instability, evidenced by the intense exciton mode at the  $\Gamma$ -point. This resolves the long-standing controversy about the role of ferromagnetic correlations for the enigmatic low-temperature properties of this structurally simple material. In particular, our findings explain the appearance of sharp ESR lines observed in a broad range of magnetic fields and draw exciting new parallels between  $\text{CeB}_6$  and a number of other well-known Kondo-lattice systems, such as  $\text{YbRh}_2\text{Si}_2$  or  $\text{YbIr}_2\text{Si}_2$ , where the proximity to a ferromagnetic quantum critical point has been established. Further, they can have model character for a much broader class of Ce-based heavy-fermion systems, such as the novel clathrate compound  $\text{Ce}_3\text{Pd}_{20}\text{Si}_6$ , whose phase diagram is qualitatively identical to that of  $\text{CeB}_6$ , exhibiting a magnetically hidden AFQ phase side-by-side with AFM ordering.

The striking importance of ferromagnetic correlations, demonstrated in our experiments, should lead to a substantial revision of existing theories behind the magnetic ordering phenomena in  $\text{CeB}_6$ , which up until now relied exclusively on the AFM coupling between dipolar and multipolar moments of the Ce-4f electrons.

The complete high-resolution mapping of the energy-momentum space, which is possible thanks to recent advances in the cold-neutron TOF spectrometer instrumentation at the ILL, offers a strict testing ground for such new theoretical models. Future experiments addressing the magnetic-field and doping dependence of the newly found excitation will shed more light on its origin and relevance for the stabilisation of the hidden-order phases.

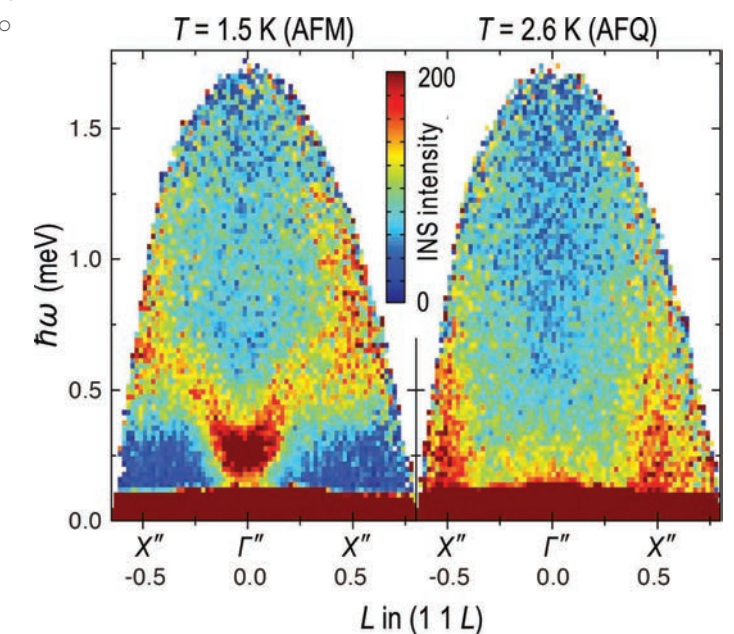


**Figure 2**

Unprocessed energy-momentum cuts along the  $(1 1 L)$  direction in momentum space, taken below and above the AFM transition. The intense feature in the left panel that disappears above  $T_N$  is a direct signature of ferromagnetic spin fluctuations.

# MAGNETISM

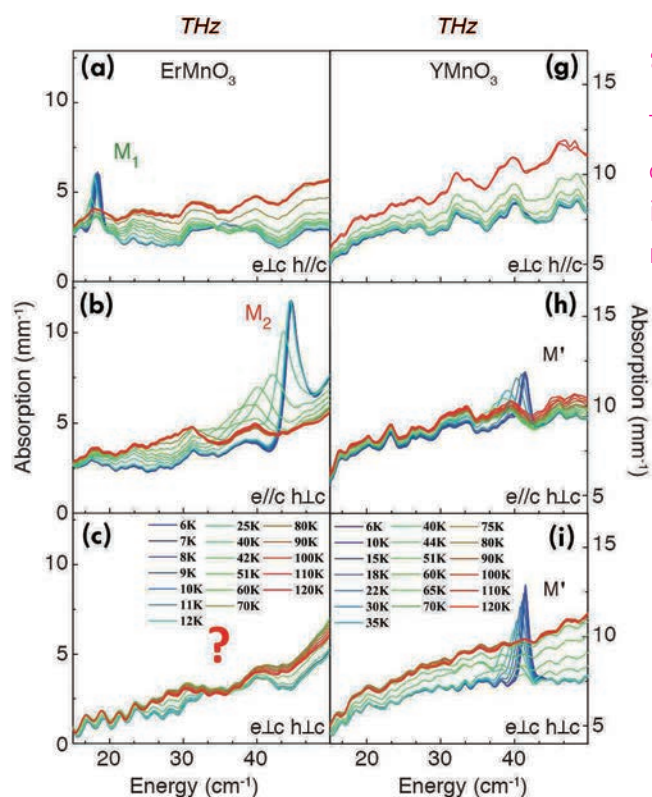
## Magneto- to electro-active transmutation of spin waves in the multiferroic $\text{ErMnO}_3$

*Time-of-flight spectrometer IN5 and three-axis spectrometer IN22 AILES beamline at SOLEIL*

Materials which show simultaneously both magnetism and ferroelectricity, for which the term multiferroics was coined, have recently received a great deal of attention. Indeed multiferroics open the way to the electric-field control of magnetic dipoles and, conversely, the magnetic-field control of electric dipoles in a number of future hybrid technologies (for instance, novel electronics based on the simultaneous manipulation of spins and charges). This electric/magnetic cross-manipulation, known as the magnetoelectric effect, can also be visible on elementary excitations, such as on magnons. In multiferroics, a new type of excitation was discovered in 2006, called the **electromagnon**, which is considered to be an electric-charge “dressing” of magnons [1]. This “dressing” enables the electric-field control of magnons and is therefore being considered for use in magnonics, a new type of information science using magnetic excitations to carry and process information. In this context, the search for new mechanisms triggering the electroactivity of magnons is a key issue.

**Figure 1**

THz absorption spectra of  $\text{ErMnO}_3$  (a-c) and  $\text{YMnO}_3$  (g-i) for three different orientations of the e and h fields of the THz wave with respect to the crystal c-axis, in the temperature range 6–120 K. The various excitation modes discussed in the text are shown.



?? query

THz does not appear as italic in text - does it need changed?

### AUTHORS

L. Chaix (ILL and Institut Néel, Grenoble, France)  
S. de Brion, R. Ballou, J. Debray, P. Lejay and V. Simonet (Institut Néel, Grenoble, France)  
S. Petit (Laboratoire Léon Brillouin, Gif-sur-Yvette, France)  
L.-P. Regnault and E. Ressouche (SPSMS-MDN, Grenoble, France)

### REFERENCES

- [1] A. Pimenov, A.A. Mukhin, V.Yu. Ivanov, V.D. Travkin, A.M. Balbashov and A. Loidl, Nat. Phys. 2 (2006) 97
- [2] L. Chaix, S. de Brion, S. Petit, R. Ballou, L.-P. Regnault, J. Ollivier, J.-B. Brubach, P. Roy, J. Debray, P. Lejay, A. Cano, E. Ressouche and V. Simonet, Phys. Rev. Lett. 112 (2014) 137201
- [3] S. Petit, F. Maussa, M. Hennion, S. Pailhès, L. Pinsard-Gaudart and A. Ivanov, Phys. Rev. Lett. 99 (2007) 266604

By combining two sophisticated techniques involving the use of large-scale facilities, we have found evidence of a new mechanism responsible for generating magnetoelectric excitations in the multiferroic compound  $\text{ErMnO}_3$  [2]. For our investigations, we used inelastic neutron scattering at the ILL and TeraHertz spectroscopy at the SOLEIL synchrotron on single crystals of  $\text{ErMnO}_3$ . Neutron scattering makes it possible to clearly identify the nature of the excitations (nuclear and magnetic) and reveal their full dispersion, while TeraHertz spectroscopy highlights the way the observed excitations at the zone centre are activated by the electric (e) and/or the magnetic (h) fields of the incoming THz wave. We applied both these techniques to study the energy spectrum of  $\text{ErMnO}_3$ , a hexagonal perovskite that is already ferroelectric above room temperature. The compound is characterised by a strong magnetic coupling between the two different magnetic species, the transition metal Mn and the rare earth Er. An antiferromagnetic order of the Mn magnetic moments occurs below 79 K, driving part of the Er magnetic moments

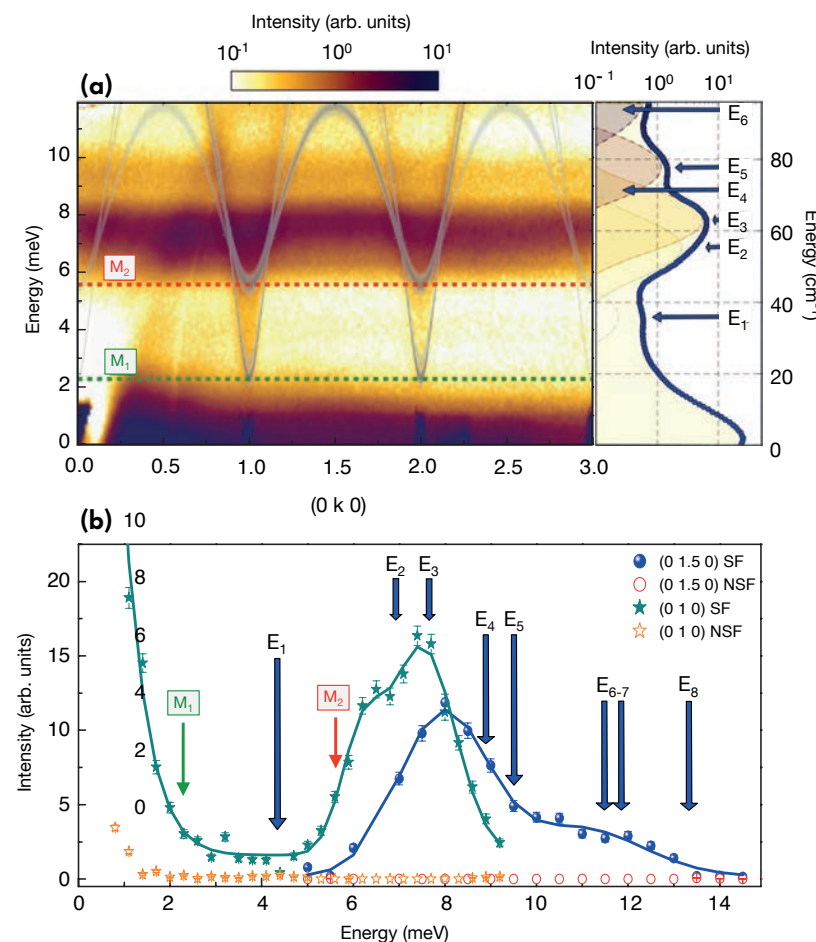


**Figure 2**

**Top:** IN5 inelastic neutron signal spectrum recorded at 1.5 K along (0 k 0). The calculated Mn spin-wave dispersions are reported as grey lines. Spectrum integration over the k range on the right highlights the crystal field non-dispersive excitations  $E_i$ . **Bottom:** IN22 spin-flip and non-spin-flip neutron-scattering signals recorded at 20 K at the (0 1 0) zone centre and (0 1.5 0) zone boundary. The  $M_i$  modes observed in THz spectroscopy and crystal field transitions  $E_1$  to  $E_8$  are shown.

??

figures labelled a) and b)

should captions be same rather than top and bottom?

to order. We also studied, for comparison, an isostructural compound  $\text{YMnO}_3$  with non-magnetic Y ions instead of Er.

The THz absorption spectra recorded on the AILES beamline at SOLEIL are shown in **figure 1** for  $\text{ErMnO}_3$  (a-c) and  $\text{YMnO}_3$  (g-i) for different orientations of the electric (e) and magnetic (h) THz wave components with respect to the six-fold c-axis of the hexagonal structure. A magnon, labelled  $M'$ , is identified in  $\text{YMnO}_3$  from its temperature dependence, its comparison with neutron work [3], and its h perpendicular to c (h $\perp$ c) excitation rule. In  $\text{ErMnO}_3$ , besides a standard magnon  $M_1$  identified at lower energy, a similar excitation to  $M'$  is observed for e parallel to c (e//c) and h $\perp$ c, but not for e $\perp$ c or h $\perp$ c. This unambiguously shows that this excitation  $M_2$  is actually excited by the THz electric-field component e//c.

To understand this result, we performed a characterisation of the  $\text{ErMnO}_3$  magnetic spectrum by inelastic neutron scattering on the IN5 time-of-flight spectrometer and on the IN22 three-axis spectrometer with polarised neutrons and polarisation analysis (see **figure 2**). This allowed us to determine the whole spin-wave spectrum associated with the Mn ions and the crystal field (CF) excitations associated with the Er ions [ $E_{1-8}$  on **figure 2**], which were also measured by far-infrared spectroscopy on the AILES beamline. These are non-dispersive ionic excitations due to the transition between degeneracy-lifted electronic levels under the influence of the surrounding charges. These measurements point to the magnonic nature of the

$M_2$  excitation and also its closeness to certain CF excitations. As the equivalent excitation  $M'$  behaves like a standard magnetoactive magnon in  $\text{YMnO}_3$ , this difference suggests that the electrical activity of the  $M_2$  excitation in  $\text{ErMnO}_3$  is related to the magnetic coupling between the magnetic rare earth and the Mn ions. It is known that a transition between CF levels of a rare-earth ion in ferroelectric compounds with no inversion centre can be electroactive. Therefore, by hybridisation, a magnetoactive CF excitation could in theory transfer its electroactivity to a magnon. From CF calculations and symmetry analysis, we were able to validate this scenario by identifying an electroactive CF transition excitation for e//c, sensitive to the Mn magnetic order and close enough to the  $M_2$  magnon to allow their hybridisation.

In conclusion, we have observed the complete loss of the magnetic character of a magnon in  $\text{ErMnO}_3$  and its transmutation into an electroactive excitation. We believe this magnetoactive dynamical process can be attributed to the hybridisation between a CF-level transition of the magnetic rare earth Er and a Mn magnon, a mechanism which may even be a general feature of other rare-earth-based multiferroics. This illustrates the richness of the emerging field of magnetoactive excitations and suggests new possibilities for manipulating these excitations, for instance through the action of magnetic and electric static fields.

[This work, supported by the French National Research Agency (ANR), was part of the ILL thesis work of Laura Chaix].

# MAGNETISM

## Unique magnetic phase in high-temperature superconductors doped with mobile holes

Three-axis spectrometer IN14

The many active degrees of freedom in transition metal oxides lead to intrinsic complexity with different electronic states being nearly degenerate. As a consequence, nanoscale phase separation can be observed in such different materials as the colossal magnetoresistance manganites and high-temperature superconducting (HTSC) cuprates [1]. A central challenging theme is how dopant disorder influences the details of the phase separation in otherwise electronically similar systems, e.g. fluctuating order [2]. We address this issue by investigating the electronic properties of an HTSC system with two essentially different mechanisms of charge-carrier doping, i.e. mobile oxygen ions and immobile Sr ions.

### AUTHORS

L. Udby and K. Lefmann (Niels Bohr Institute, University of Copenhagen, Denmark)  
 M. Böhm (ILL)  
 T.B.S. Jensen and N.H. Andersen (Technical University of Denmark, Kongens Lyngby, Denmark)  
 Ch. Niedermayer (PSI, Switzerland)  
 R. Toft-Petersen (HZB, Berlin, Germany)  
 B.O. Wells (University of Connecticut, USA)

### REFERENCES

- [1] E. Dagotto, Science 309 (2005) 257
- [2] S.A. Kivelson, I.P. Bindloss, E. Fradkin, V. Oganesyan, J.M. Tranquada, A. Kapitulnik, and C. Howald, Rev. Mod. Phys. 75 (2003) 1201
- [3] H. Takagi, T. Ido, S. Ishibashi, M. Uota, S. Uchida, and Y. Tokura, Phys. Rev. B 40 (1989) 2254
- [4] H.E. Mohottala, B.O. Wells, J.I. Budnick, W.A. Hines, C. Niedermayer, and F.C. Chou, Phys. Rev. B 78 (2008) 064504
- [4] L. Udby, J. Larsen, N.B. Christensen, M. Boehm, Ch. Niedermayer, H.E. Mohottala, T.B.S. Jensen, R. Toft-Petersen, F.C. Chou, N.H. Andersen, K. Lefmann and B.O. Wells, Phys. Rev. Lett. 111 (2013) 227001

It is well-established that at low temperatures, modulated antiferromagnetic order coexists with superconductivity in certain ranges of hole-doping in high- $T_c$  cuprates. When the hole-dopants are immobile, such as in the lanthanum cuprate  $\text{La}_{2-x}\text{Sr}_x\text{CuO}_4$ , it is also well established that both the superconducting and magnetic properties are strongly dependent on Sr content  $x$ , as shown on the left in the schematic phase diagram in **figure 1**. The maximum superconducting transition temperature is  $T_c = 38.5$  K and occurs at (optimal) Sr doping  $x \sim 0.15$  in oxygen stoichiometric samples [3].

However, when mobile hole-dopants such as intercalated oxygen are introduced into the  $\text{La}_{2-x}\text{Sr}_x\text{CuO}_4$  crystals by electrochemical methods, which thus become

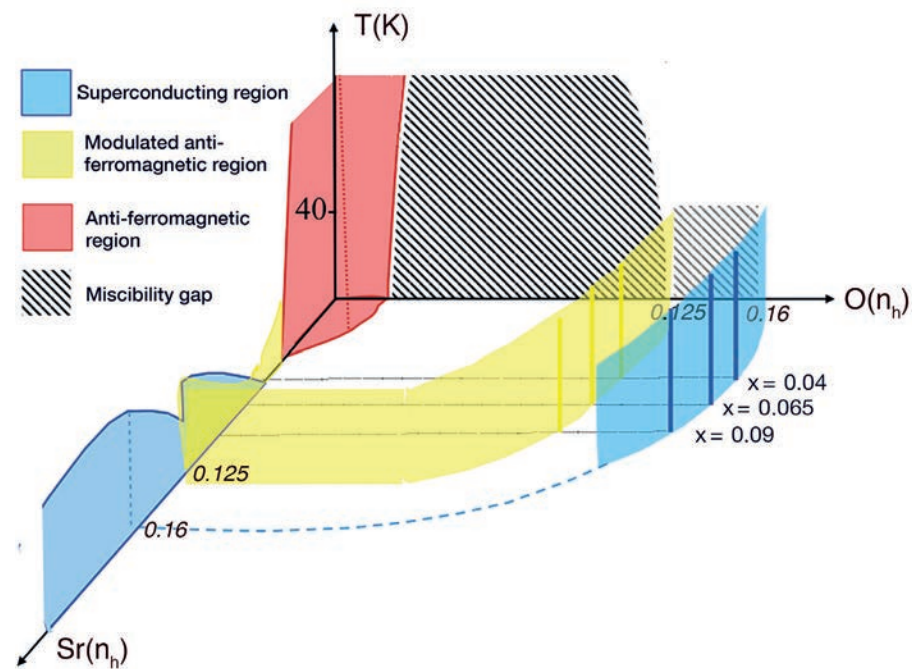


Figure 1

Schematic phase diagram showing electronic phases as a function of immobile Sr hole-dopants and mobile O hole-dopants. The horizontal lines labelled by  $x = 0.04, 0.065, 0.09$  respectively, indicate the Sr content of the Sr/O co-doped samples we have studied. Modified from [4].

$\text{La}_{2-x}\text{Sr}_x\text{CuO}_{4+y}$  we find that the superconducting transition temperature stabilises at  $T_c \sim 40$  K (onset value) [4]. Our neutron-scattering studies at the ILL have further revealed that the magnetic order too stabilises by intercalation of oxygen, which makes Sr/O co-doped samples very interesting as model systems for electronic phase separation.

We investigated the magnetic order of a range of Sr/O co-doped single crystals by elastic neutron scattering. The experiments were performed at the three-axis spectrometer IN14, due to the very low background and high energy resolution needed for these studies since the magnetic moment is small and only small samples were available.

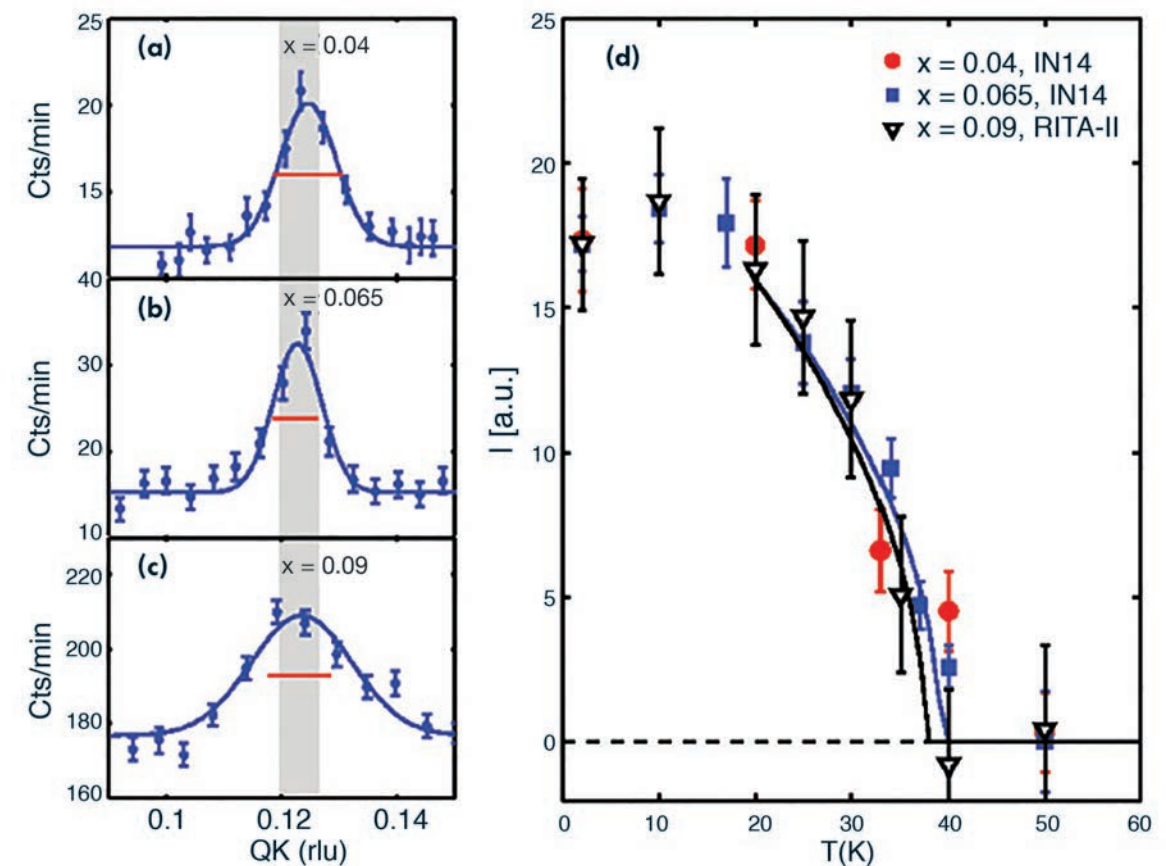
We found that, regardless of Sr content, in all samples the magnetic moment per Cu atom was the same with a value in the range  $0.12\text{--}0.17 \mu_B$  (exact value depending on interpretation model), and that it forms modulated antiferromagnetic order with period of  $\sim 8$  in large ( $> 300 \text{ \AA}$ ) domains which disappear above the Néel temperature  $T_N = 39(1)$  K. The periodicity of the magnetic order is found from the peak position of the modulated antiferromagnetic signal,  $QK = QH \sim 1/8$ , as shown in **figure 2a-c**. The Néel transition temperature  $T_N = 39(1)$  K is found from monitoring the intensity of this

peak upon heating, as shown in **figure 2d**. These characteristics of the magnetic order are similar to the so-called striped phase (also known as the  $1/8^{\text{th}}$  phase) which has previously been considered an anomaly, only occurring around Sr doping  $x \sim 1/8$  in the oxygen stoichiometric, lanthanum cuprate phase diagram. At this anomaly the magnetic phase competes with and suppresses the superconducting phase in oxygen stoichiometric samples. However, our studies show that the introduction of excess mobile oxygen facilitates co-existence rather than competition between electronically phase-separated volumes of the striped magnetic phase and a superconducting phase with the hallmarks of optimally doped oxygen-stoichiometric  $\text{La}_{2-x}\text{Sr}_x\text{CuO}_4$ .

It is our hope that further investigation of the oxygen mobility in these samples will add insight into the long sought-after mechanism behind the formation of Cooper-pairs in high temperature superconducting cuprates. Furthermore, it is highly interesting that the superconducting transition temperature coincides with the magnetic ordering temperature  $T_c \sim T_N \sim 40$  K, and we intend to investigate the significance of the transition temperatures for the electronic phase separation by theoretical modelling.

Figure 2

Elastic neutron-scattering data shows that the magnetic peak position **(a-c)** and its temperature dependence **(d)** is the same regardless of Sr doping  $x$  [from [5]].



??  
Cts (min) instead of / - match style throughout?

??  
also [ ] square brackets on fig d vertical legend

# MAGNETISM

## High-magnetic-field study on competing phases leading to the magnetisation plateau in the quantum spin system $\text{CuBrSr}_2\text{Nb}_3\text{O}_{10}$

High-intensity two-axis diffractometer D20

Quantum fluctuations developing in low dimensional  $S = 1/2$  magnetic systems have attracted strong interest in condensed matter physics. The layered square lattice  $S = 1/2$  system  $\text{CuBrSr}_2\text{Nb}_3\text{O}_{10}$  shows unconventional magnetic properties with a cycloidal spin ordering of  $\text{Cu}^{2+}$  ions and the existence of a  $1/3$  magnetisation plateau. As the formation of this plateau is not foreseen in existing theories on the antiferromagnetic square lattice  $J_1J_2$  model, field-dependent diffraction studies up to 10 T were conducted on D20. The results showed that the existence of the plateau is due to the competition between two antiferromagnetic phases and a ferromagnetic phase, and only coincidentally found at the value of  $1/3$ .

### AUTHORS

C. Ritter (ILL)

### REFERENCES

- [1] A. Tsirlin *et al.*, Phys. Rev. B 86 (2012) 064440
- [2] S.M. Yusuf *et al.*, Phys. Rev. B 84 (2011) 064407
- [3] Y. Tsujimoto *et al.*, J. Phys. Soc. Jpn. 76 (2007) 063711
- [4] C. Ritter *et al.*, Phys. Rev. B 88 (2013) 104401

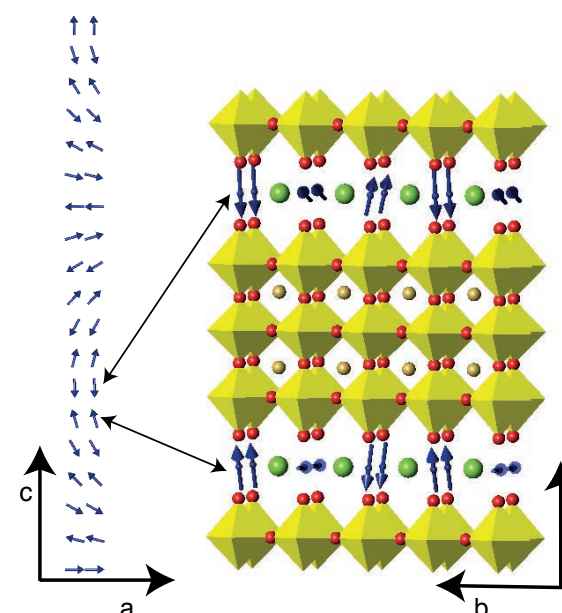
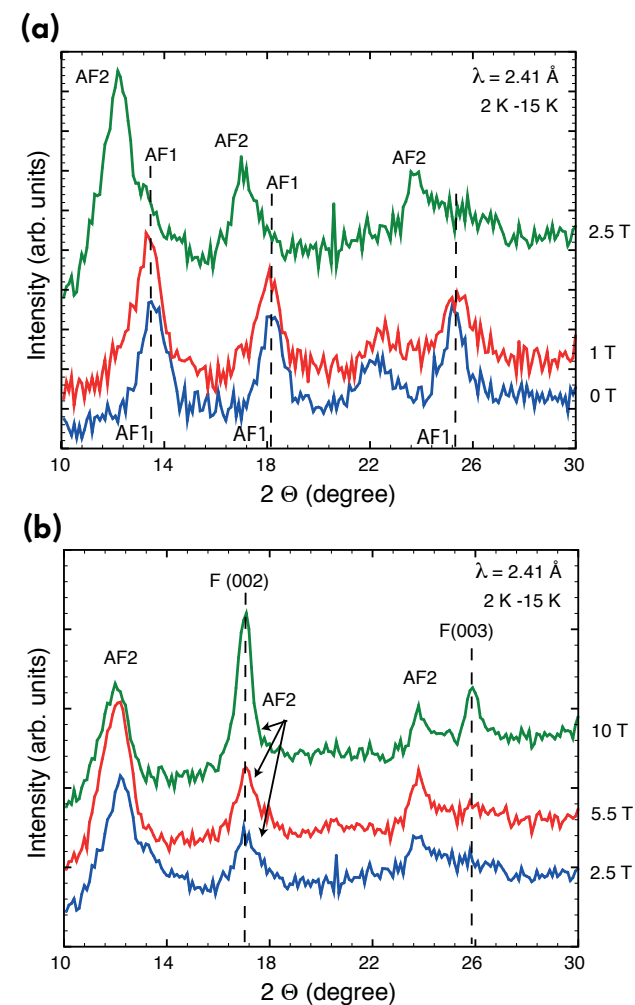
The crystal structure of the Dion-Jacobson series of compounds  $\text{CuX}_{n-1}\text{B}_n\text{O}_{3n-1}$  with X = Halide, A = La, Ca, Sr or Ba and B = Nb, Ta, Ti provides a geometric arrangement for the magnetic  $\text{Cu}^{2+}$  ions which was believed to represent a possible example of the frustrated two-dimensional (2D)  $S = 1/2$  square lattice  $J_1J_2$  model. For the  $n = 2$  compounds it has been shown that a slight orthorhombic distortion leads, however, to the existence of manifold different magnetic interactions going far beyond the simple  $J_1J_2$  model. The fourth nearest  $\text{Cu}^{2+}$  neighbour interaction turned out to be the strongest magnetic coupling, leading either to a spin gap ground state as found in  $\text{CuClLaNb}_2\text{O}_7$  or to the appearance of long-range magnetic order as in  $\text{CuBrLaNb}_2\text{O}_7$  and  $\text{CuClLaTa}_2\text{O}_7$  [1].

Members with  $n = 3$  should see an increased 2D character as the  $\text{CuX}$  layers are separated by a further non-magnetic perovskite block. Contrary to the situation in the  $n = 2$  compounds, high-resolution neutron diffraction data on  $\text{CuBrSr}_2\text{Nb}_3\text{O}_{10}$  did not detect any sign of a deviation from the tetragonal symmetry. Nevertheless high-intensity neutron data found long-range antiferromagnetic order (AF1) within the  $\text{CuBr}$  layers characterised by the magnetic propagation vector  $\kappa_1 = (0 \ 3/8 \ 1/2)$ . In order to explain this cycloidal magnetic structure, which is not foreseen in the  $J_1J_2$  model, a third magnetic interaction  $J_3$  was invoked [2]. Magnetisation data indicated the existence of a  $1/3$  magnetisation plateau in the magnetic field region between 2.4 and 8.2 T for this compound [3]. This finding was most surprising as the existence of a magnetisation plateau at one third of the saturation magnetisation is normally only predicted for triangle-based lattices, whereas square lattices should show plateaus at  $1/4$  or  $1/2$ . It was therefore decided to study the magnetic structure developed in this compound under magnetic field, installing for the first time a 10 T cryomagnets on the high-intensity powder diffractometer D20.

?? query  
(degree)  
appears as  
the symbol  
or word ??

Figure 1

Magnetic diffraction patterns (after subtraction of the 15 K, 0 T diffraction pattern as nuclear background) as a function of magnetic field at 2 K showing the evolution of the different magnetic phases.



Pressed pellets of  $\text{CuBrSr}_2\text{Nb}_3\text{O}_{10}$  powder were measured at six different field values between 0 and 10 T. The analysis was done on difference patterns where the non-magnetic background measured at 15 K and 0 T was subtracted from the low temperature data. It was found that the zero field AF1 type magnetic structure still persists at 1 T, then decreases and disappears at 4.5 T. It gets replaced by a new antiferromagnetic structure (AF2) with  $\kappa_2 = (0 \ 1/3 \ \sim 0.46)$  which at 2.5 T already represents the majority phase. **Figure 1** shows the evolution of the different magnetic diffraction patterns. Between 5.5 T and 10 T the AF2 phase decreases strongly while at the same time a ferromagnetic phase, which is first noticeable at 4.5 T, increases strongly.

It is not possible to explain the  $1/3$  magnetisation plateau by the existence of the purely antiferromagnetic AF2 structure with  $\kappa_2 = (0 \ 1/3 \ \sim 0.46)$ , see **figure 2**. The behaviour of the magnetisation can now, however, be explained by the field-dependent coexistence of the three magnetic phases AF1, AF2 and F. At low applied fields the AF1 phase persists but a ferromagnetic phase (or component) gets induced. Above about 2 T a region is entered where the AF2 phase not only rapidly replaces the AF1 phase but also retards the formation of the additional F phase. Finally in fields above about 5.5 T the AF2 phase starts in turn to disappear and to give way to an accelerated formation of the ferromagnetic phase. This leads in the magnetisation data to the situation where a first rise of the magnetisation at low fields gets slowed down at intermediate field values before it finally increases strongly at high fields. This means that the appearance of the plateau is only coincidentally centered at a magnetisation of  $1/3$  of the saturation magnetisation [4].

This experiment did not only give an explanation for the apparent existence of a  $1/3$  magnetisation plateau in the quantum spin system  $\text{CuBrSr}_2\text{Nb}_3\text{O}_{10}$  but proved as well the possibility of performing high-magnetic-field studies on the high-intensity powder diffractometer D20. Plans to adapt D20 for accepting the 15 T cryomagnets are underway.

Figure 2

AF2 structure with  $\kappa_2 = (0 \ 1/3 \ \sim 0.46)$ ; magnetic moments are confined in the  $ac$  plane forming a cycloidal spiral. Along the  $b$ -axis, the spins turn by  $120^\circ$  between neighbouring unit cells.

## MAGNETISM

## Longitudinal incommensurate static order and discrete dynamical modes in the chain-like antiferromagnet $\text{BaCo}_2\text{V}_2\text{O}_8$

Two-axis diffractometer D23  
and three-axis spectrometer IN12

One-dimensional antiferromagnetic low-spin systems are of particular interest for their exotic ground-state properties and excitations, resulting from enhanced quantum fluctuations.  $\text{BaCo}_2\text{V}_2\text{O}_8$  is a remarkable example of such a system, owing essentially to its anisotropic character and to its non-negligible inter-chain magnetic coupling with respect to the strong coupling within the chains. These ingredients are responsible for two interesting properties. First, an original incommensurate longitudinal static magnetic order is induced by the magnetic field, in which the direction of the magnetic moments is aligned with the field. Second, in a zero magnetic field, two interlaced series of discrete magnetic excitations (Zeeman ladders) are observed with fluctuations perpendicular (transverse) and parallel (longitudinal) to the direction of the static magnetic moments.

## AUTHORS

E. Canévet (IJF and ILL, Grenoble, France)  
B. Grenier (IJF and CEA, Grenoble, France)  
V. Simonet, B. Canals and P. Lejay (Institut Néel, Grenoble, France)  
S. Petit (ILL, CEA-Saclay, France)  
L.-P. Regnault and S. Raymond (CEA, Grenoble, France)  
M. Klanjšek (Jožef Stefan Institute and EN-FIST, Ljubljana, Slovenia)  
M. Horvatić and C. Berthier (LNCMI, Grenoble, France)

## REFERENCES

- [1] S. Kimura *et al.*, Phys. Rev. Lett. 100 (2008) 057202 and refs. therein  
[2] E. Canévet *et al.*, Phys. Rev. B 87 (2013) 054408  
[3] B. Grenier *et al.*, Phys. Rev. Lett. 114 (2015) 017201  
[4] P. Merchant *et al.*, Nature Phys. 10 (2014) 373

$\text{BaCo}_2\text{V}_2\text{O}_8$  consists of  $\text{Co}^{2+}$  chains twisted along the  $c$ -axis (see crystal structure in **figure 1**). The low-temperature magnetic state of the  $\text{Co}^{2+}$  ion is described by a highly anisotropic effective spin-1/2 (Ising-like  $\text{Co}^{2+}$  magnetic moments preferentially aligned along the  $c$ -axis), yielding strong quantum fluctuations. In a zero magnetic field, a Néel antiferromagnetic order occurs below 5.5 K due to weak inter-chain coupling. The application of a magnetic field  $H \parallel c$  induces a quantum phase transition at  $H_c \approx 3.9$  T [1].

Our single crystal neutron diffraction experiment performed on D23 [2], up to 12 T and down to 50 mK, allowed us to determine the full H-T phase diagram of  $\text{BaCo}_2\text{V}_2\text{O}_8$  (**figure 2c**), as well as the magnetic structures stabilised in a zero field and above  $H_c$ . Zero-field Néel order consists of antiferromagnetic chains of magnetic moments parallel to the chain direction (**figure 2a**). Above  $H_c$ , we observe a structure similar to that of the zero field, except that the moment amplitude, still parallel to  $c$ , is now modulated incommensurately with respect to the  $c$  lattice parameter (**figure 2b**).

Our measurements prove for the first time the longitudinal character of this incommensurate ordering. This is very different from what is observed in isotropic antiferromagnets, where the energy minimisation of the system under a magnetic field applied along the moment direction causes the antiferromagnetically coupled magnetic moments to flip perpendicularly to the magnetic field, thus adopting a canted configuration.

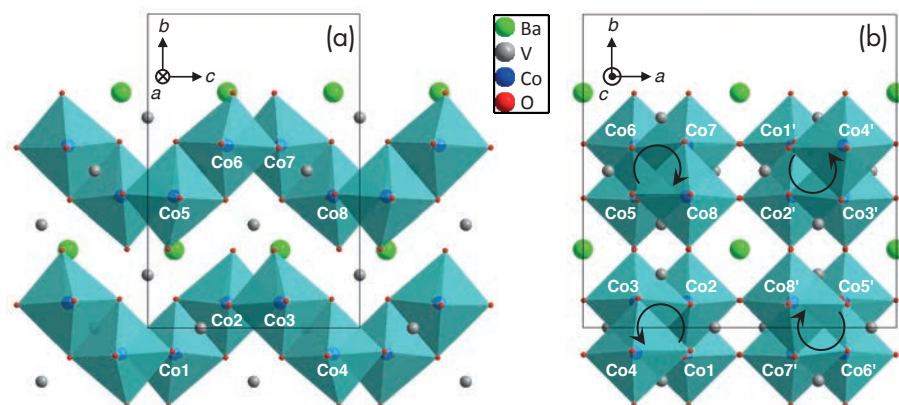
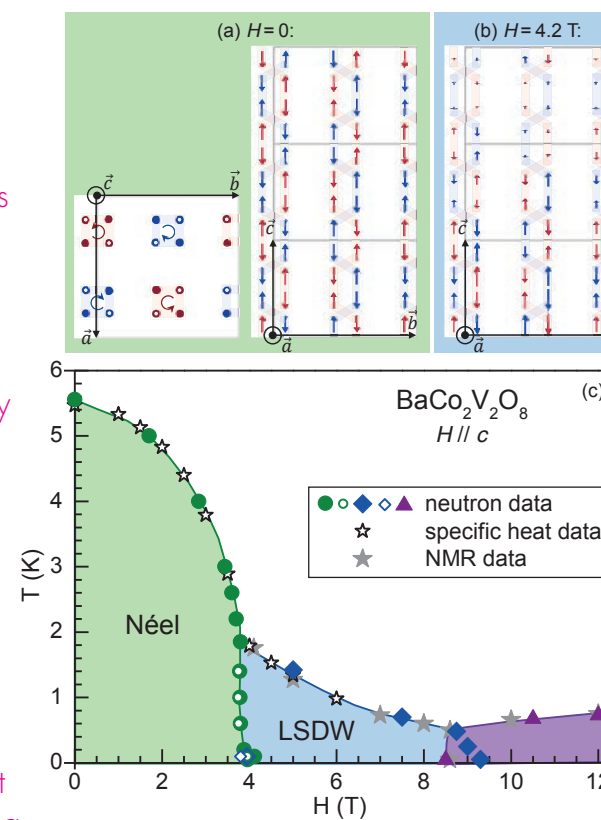


**Figure 1**  
Crystal structure of  $\text{BaCo}_2\text{V}_2\text{O}_8$  projected **a)** in the  $(b, c)$  plane, and **b)** in the  $(a, b)$  plane. The arrows in panel (b) indicate the sense of rotation of the screw chains on increasing  $z$  (thus evidencing the two different types of chains).

## Figure 2

Magnetic structure of  $\text{BaCo}_2\text{V}_2\text{O}_8$   
**a)** in the Néel phase at  $H = 0$  and  
**b)** in the longitudinal spin density wave (LSDW) phase at  $H = 4.2$  T. The blue and red colours correspond to the two different types of chains.  
**c)** H-T phase diagram obtained from the present neutron diffraction study, compared with specific heat and NMR results [3].



?? query

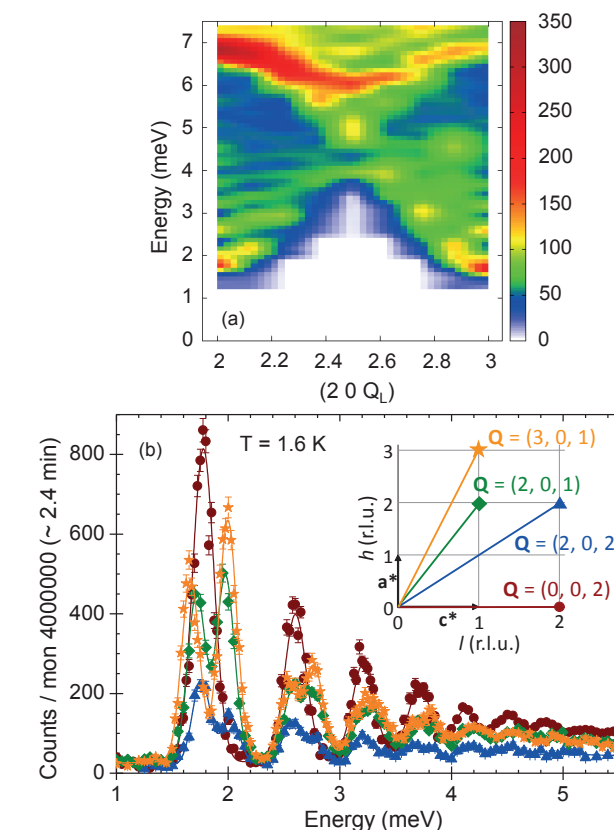
is this T (K) is the same as Temperature (K) - if it is there is an inconsistency with the graphs

?? query

H normal in captions but italic on fig a

## Figure 3

**a)** Inelastic scattering intensity map obtained from a series of  $Q$ -constant energy scans measured at  $T = 1.6$  K in zero field.  
**b)**  $Q$ -constant energy scans at various Bragg positions (shown in the inset), emphasising two series of interlaced sharp transverse and longitudinal modes. The latter arise and increase in intensity as the  $Q$  vector rotates from the  $c$ -axis towards the  $a$ -axis.



The new, longitudinal field-induced phase observed in  $\text{BaCo}_2\text{V}_2\text{O}_8$  is actually due to its Ising-like character; it is describable in terms of Tomonaga-Luttinger liquid physics [1, 2] in analogy with one-dimensional fermionic systems.

In  $\text{BaCo}_2\text{V}_2\text{O}_8$ , not only are the static properties unusual but so is its zero-field excitation spectrum, studied using inelastic neutron scattering on IN12 [3]. **Figure 3a** reveals remarkable features consisting of sharp, discrete spin excitations, topped by an intense optic-like mode at  $\delta \sim 7$  meV. These discrete modes are the direct result of the inter-chain coupling on the peculiar so-called spinon excitations of one-dimensional antiferromagnets. These spinons, similar to the free domain walls created in pairs, are spread in energy to form a continuum in the absence of inter-chain interactions. An Ising spin chain submitted to these interactions is susceptible to a molecular field from the neighbouring chains, confining the spinons in an attractive linear potential and provoking a discretisation of the spinon continuum. In addition to this discretisation, another remarkable observation is the presence of long-lived longitudinal as well as transverse modes. This was deduced from the distinct variation in intensity of both series of modes for different  $Q$  scattering vectors, using the neutron's sensitivity to spin fluctuations perpendicular to the  $Q$  vector (**figure 3b**).

The magnetic excitation spectrum evidenced in this work for the magnetically ordered phase of the spin-chain-like compound  $\text{BaCo}_2\text{V}_2\text{O}_8$  is in contrast to expectations for a classical three-dimensional antiferromagnetic phase; in this phase low-lying excitations consist of spin waves (magnons), which correspond to a precession of the ordered moment around its equilibrium direction with a transverse character. A distinctive feature of the present study is the evidence of long-lived longitudinal modes, which are rarely observed in quasi-one-dimensional magnetic systems. They vanish for strongly anisotropic Ising chain-like systems like, e.g.  $\text{CsCoCl}_3$ , and have only been seen as a damped excitation in Heisenberg chain-like  $\text{KCuF}_3$  with isotropic magnetic moments.

The observation, for the first time, of these quantised intense long-lived longitudinal excitations, in addition to the transverse ones, is ascribed to the moderate Ising anisotropy (coupling between the spin components parallel to the chain direction two times stronger than perpendicular to it) and to the sizeable inter-chain coupling in  $\text{BaCo}_2\text{V}_2\text{O}_8$  (about 10 times smaller than the intra-chain coupling). The observation of these longitudinal excitations is indeed a key issue in condensed matter studies and especially in magnetism, since it is related to the very active research being conducted into the Higgs amplitude mode arising at any phase transition with broken continuous symmetry [4].

# MAGNETISM

## Revealing the secrets of magnetic order in the new model compound $\text{SrTb}_2\text{O}_4$ by polarised and unpolarised neutron diffraction

Diffuse scattering spectrometer D7,  
two-axis diffractometer D23,  
three-axis spectrometers IN12 and IN3

Magnetic frustration, as a result of competition between interactions that cannot be satisfied simultaneously, remains a topic of considerable interest in condensed matter science. It can lead to intriguing quantum ground states such as spin ice and spin liquid, and provides an excellent testing ground for theories [1, 2]. Here we study a new frustrated member,  $\text{SrTb}_2\text{O}_4$ , of the family of  $\text{SrRE}_2\text{O}_4$  (RE = rare earth) compounds. By polarised and unpolarised neutron scattering, we solve an incommensurately modulated spin structure and observe an in-plane magnetic anisotropy, providing a critical step towards a complete understanding of the related magnetic interactions and frustrations.

### AUTHORS

H.-F. Li, K. Schmalzl and W. Schmidt (JCNS Outstation at ILL)  
C. Zhang and G. Roth (RWTH Aachen University, Germany)  
A. Senyshyn (FRM II and Technical University Munich, Germany)  
A. Wildes and M. Böhm (ILL)  
E. Ressouche (CEA-INAC and UJF, Grenoble, France)  
B. Hou (ESRF, France)  
P. Meuffels (PGI and JARA-FIT, Germany)  
Th. Brückel (JCNS, PGI and JARA-FIT, Germany)

### REFERENCES

- [1] H.T. Diep, *Frustrated Spin Systems*, World Scientific, Singapore (2004)
- [2] C. Lacroix *et al.*, *Introduction to Frustrated Magnetism*, Springer Series in Solid-State Sciences vol. 164, New York (2011)
- [3] H.-F. Li *et al.*, *Front. Phys.* 2 (2014) 42

The mechanism of spin interactions and the origin of magnetic frustrations in the new frustrated family of  $\text{SrRE}_2\text{O}_4$  (RE = rare earth) compounds still remain elusive. A detailed knowledge of the relevant structural and magnetic parameters is required and can be obtained by neutron scattering. In addition, the low antiferromagnetic (AFM) transition temperatures of these compounds make it technically challenging to obtain a complete understanding of the magnetic interactions and frustrations and the exploration of potential interesting properties.

We have used the D7, D23, IN12, and IN3 neutron-scattering instruments to study the magnetic structure and anisotropy of single crystal  $\text{SrTb}_2\text{O}_4$  in detail [3]. **Figure 1** shows the neutron polarisation analysis in the spin-flip (SF, i.e. Z-flipper on) and non-spin-flip (NSF, i.e. Z-flipper off) channels. We observe extra fourfold Bragg peaks around  $(\pm 1.6, \pm 1, 0)$  at 50 mK, which we attribute to a long-range magnetic transition. Our detailed polarisation analysis data complemented by a powder-diffraction study performed at SPODI (FRM II), reveal that the compound  $\text{SrTb}_2\text{O}_4$  displays an incommensurate AFM order (**figure 2**) with a transverse wave vector at  $(0.5924(1), 0.0059(1), 0)$ , albeit with partially-ordered moments,  $1.92(6) \mu_B$  at 0.5 K, stemming from only one of the two inequivalent Tb sites mainly by virtue of the different octahedral distortions on both sides (**figure 3b**).

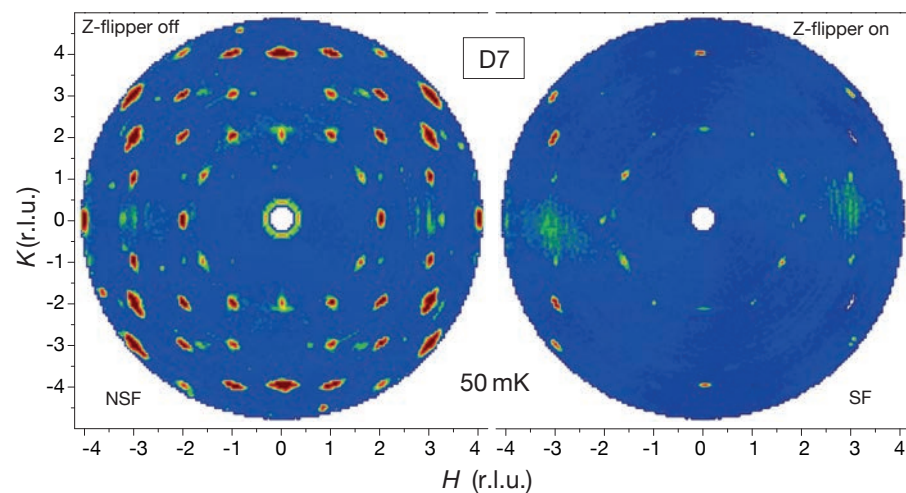


**Figure 1**  
Polarisation analysis data measured at 50 mK using D7.

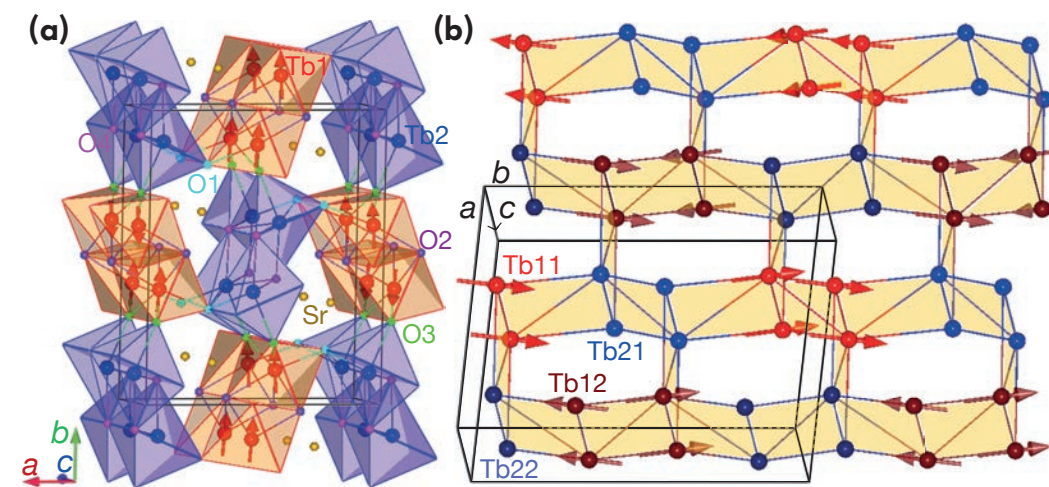


**Figure 2**  
(a) Crystal and magnetic structures as refined with the SPODI (FRM-II) data (0.5 K). (b) Arrangements of the  $\text{Tb}_6$  honeycombs. The arrows drawn through the Tb1 ions represent the Tb1 partially-ordered moments. The connected lines represent the crystallographic unit cell(s).

The temperature dependence of the intensity of the AFM  $(1.6, 1, 0)$  Bragg peak is shown in **figure 3a**, which was fitted with a power law, revealing that the noncollinear incommensurate AFM structure forms at  $T_N = 4.28(2)$  K, the highest magnetic transition temperature in the family. **Figures 3c** and **3d** show an in-plane (along the  $q_H$  and  $q_K$  directions) magnetic anisotropy, giving instrument resolution limited peaks.

To conclude, we have revealed that the AFM order of  $\text{SrTb}_2\text{O}_4$  is dominated mainly by dipole-dipole interactions and that the octahedral distortion, nearest-neighbour (NN) ferromagnetic (FM) arrangement, different next NN

FM and AFM configurations, and in-plane anisotropic spin correlations are vital to understanding the magnetic structure and associated multiple frustrations.

The discovery of the thus far highest AFM transition temperature shows  $\text{SrTb}_2\text{O}_4$  to be a particularly significant compound in the family for theoretical and further experimental studies. Inelastic neutron-scattering studies to determine the detailed crystal-field and magnetic-interaction parameters will be of great interest. The factors that influence the value of the AFM transition temperature will be further explored in combination with theoretical calculations.

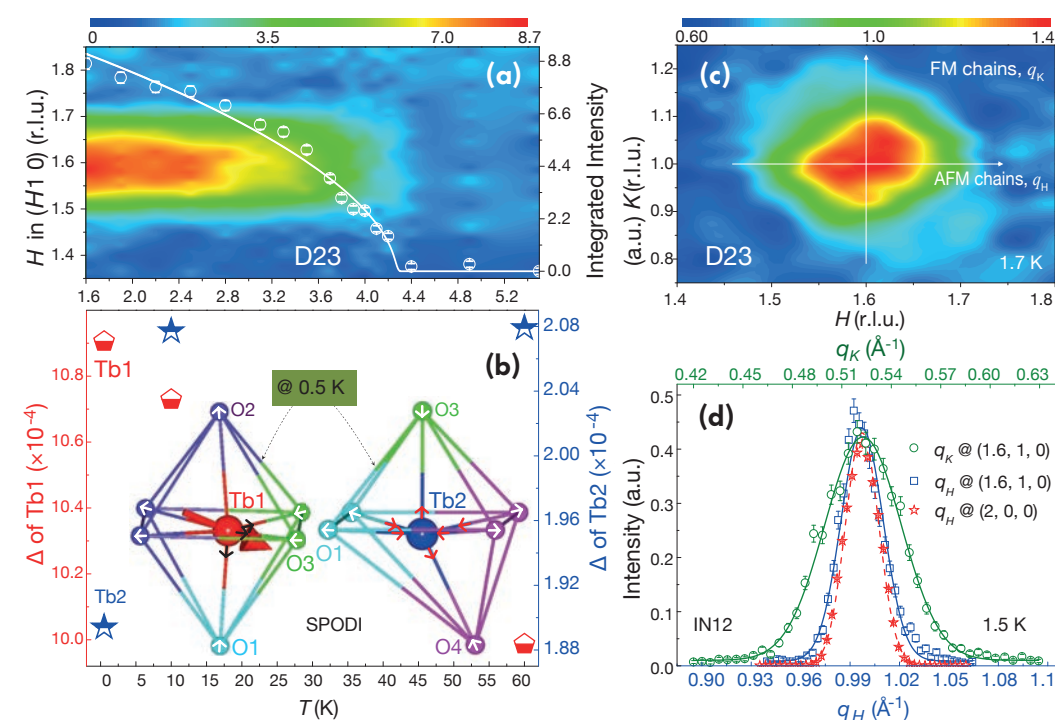


**Figure 3**  
(a) Temperature dependence of the AFM  $(1.6, 1, 0)$  peak and the corresponding integrated intensity (circles). The solid line is a fit with a power law. (b) Octahedral distortion  $\Delta$  of the Tb1 and Tb2 sites. The big arrow represents the Tb1 moment. The small arrows represent the deduced stress vectors of the related ions. (c) Q-map around the AFM  $(1.6, 1, 0)$  peak (1.7 K). The arrows point out directions of the in-plane AFM and FM chains, respectively. (d) Q-scans (void symbols) around the  $(1.6, 1, 0)$  and nuclear  $(2, 0, 0)$  peaks (1.5 K). For comparison, the  $q_H$  values around  $(2, 0, 0)$  are shifted.

# MAGNETISM

## A multifunctional molecular magnetic material under pressure

### High-intensity two-axis powder diffractometer DIB

The flexibility offered by molecular systems makes it possible to combine, in one and the same compound, different functional properties – ideally with some kind of interplay between them – and thus to produce multifunctional materials. Examples of the success of this approach are compounds featuring, for example, porosity and magnetism, superconductivity and magnetism, or electric and magnetic order (molecular multiferroics) [1]. The examples selected also show that magnetic ordering is one of the most sought-after functional properties, due to its potential use in a variety of applications. Here we describe a compound which displays magnetic ordering together with another interesting property – spin-crossover behaviour. Spin-crossover occurs in certain transition metal compounds where the electronic configurations can interconvert between high-spin and low-spin states under external stimuli [2]. This phenomenon is in itself a source of multifunctionality, as the change of spin state gives rise to drastic variations in magnetic, optical, dielectric and structural properties. Conveniently, this molecular bistability can be addressed by means of an external perturbation, such as temperature, magnetic field, light irradiation, chemical stimuli or pressure.

### AUTHORS

J.A. Rodríguez-Velamazán (ILL and CSIC – University of Zaragoza, Spain)  
O. Fabelo (ILL)  
C.M. Beavers (Advanced Light Source, Berkeley, USA)  
E. Natividad, M. Evangelisti and O. Roubeau (CSIC – University of Zaragoza, Spain)

### REFERENCES

- [1] a) D. Maspoch, D. Ruiz-Molina, K. Wurst, N. Domingo, M. Cavallini, F. Biscarini, J. Tejada, C. Rovira and J. Veciana, *Nat. Mater.* 2 (2003) 190; b) E. Coronado, C. Marif-Gastaldo, E. Navarro-Maratalla, A. Ribera, S.J. Blundell and P.J. Baker, *Nat. Chem.* 2 (2010) 1031; c) P. Jain, P.V. Ramachandran, R.J. Clark, H.D. Zhou, B.H. Toby, N.S. Dalal, H.V. Kroto and A.K. Cheetham, *J. Am. Chem. Soc.*, 131 (2009) 13625
- [2] Spin-Crossover in Transition Metal Compounds, Vols. III, in *Topics in Current Chemistry* (Eds. P. Gülich and H.A. Goodwin), Springer, Berlin (2004)
- [3] O. Roubeau, M. Evangelisti, E. Natividad, *Chem. Commun.* 48 (2012) 7604
- [4] J.A. Rodríguez-Velamazán, O. Fabelo, C.M. Beavers, E. Natividad, M. Evangelisti and O. Roubeau, *Chem. Eur. J.* 20 (2014) 7956

[Fe<sup>II</sup>(Metz)<sub>6</sub>][Fe<sup>III</sup>Br<sub>4</sub>]<sub>2</sub> (Metz = 1-methyltetrazole) is one of the rare systems combining spin-crossover and long-range magnetic ordering [3]. The spin-crossover phenomenon of the cationic sub-lattice [Fe<sup>II</sup>(Metz)<sub>6</sub>]<sup>2+</sup> (at ca. 165 K at room pressure) coexists in this material with an antiferromagnetic order of the anionic sub-lattice (Fe<sup>III</sup>Br<sub>4</sub>)<sup>-</sup> (below 2.4 K). A combined study involving neutron and X-ray diffraction, and bulk and single crystal magnetometry, has allowed us to determine the magnetic structure of this compound and has shown that pressure is a suitable external parameter for addressing the functional properties of the material, as it enhances the magnetic ordering and produces the switching of the spin state.

Powder neutron diffraction patterns collected at 1.5 and 4.5 K on DIB show an increase in intensity in some Bragg reflections at the lowest temperature, indicating the appearance of long-range magnetic order. The observed magnetic contribution can be indexed with a magnetic propagation vector  $k = (0, 0, 0)$ , indicating that the magnetic unit cell coincides with the nuclear one. The symmetry of the system allows four possible magnetic configurations, namely (i) ferromagnetic with moments along the *c*-axis, (ii) antiferromagnetic with moments along the *c*-axis, (iii) ferromagnetic with moments in the *ab* plane, and (iv) antiferromagnetic with moments in the *ab* plane. These configurations can be calculated and compared with the neutron data, showing that the last configuration (figure 1) is the only one compatible with our experiment. Single crystal magnetometry measurements fully agree with the *c*-axis being a hard axis of magnetisation and the *ab* plane an easy plane. Finally, the value of the magnetic moment obtained from the refinement of the neutron diffraction data is ca. 3.5 Bohr magnetons.

Once the magnetic structure at ambient pressure had been determined, we sought to investigate the effect of applied pressure on it, and on the properties of this compound in general. In fact, besides the well-established stabilisation of the low-spin state [2], pressure would probably affect

the magnetic ordering as well. As a first step, the crystal structure was determined at room temperature (RT) at a pressure of 2.3 GPa, using synchrotron radiation. The results clearly indicate a full pressure-induced spin-crossover of the cations, shown by a drastic contraction of the coordination sphere around Fe<sup>II</sup>. Magnetic susceptibility measurements with applied pressure confirmed this observation, showing how the spin-crossover centred at 165 K at ambient pressure is shifted to 325 K at 0.8 GPa. In other words, the spin-state of the Fe<sup>II</sup> ion is switched to low-spin at room temperature merely by applying ca. 1 GPa. Moreover, the application of pressure also produces a shift towards higher temperatures of the magnetic ordering temperature ( $T_N$ ) of the (Fe<sup>III</sup>Br<sub>4</sub>)<sup>-</sup> ions, following a linear dependence (figure 2). Powder neutron diffraction patterns collected at different temperatures between 1.5 and 10 K, and at applied pressures of 0.19 and 0.50 GPa, are compatible with the same magnetic structure model described previously for ambient pressure, but a significant magnetic moment can still be refined at 2.5 K (for example, ca. 2.9 Bohr magnetons at 0.50 GPa), which is a clear confirmation of the increase in  $T_N$ . This increase of  $T_N$  with applied pressure is probably an effect of structural modifications to the (Fe<sup>III</sup>Br<sub>4</sub>)<sup>-</sup> ions packing, as both the ferromagnetic exchange interaction along *c* and the antiferromagnetic dipolar interaction in the *ab* plane are expected to increase with reduced Fe<sup>III</sup>...Fe<sup>III</sup> distances.

In conclusion, we have determined the magnetic structure of [Fe<sup>II</sup>(Metz)<sub>6</sub>][Fe<sup>III</sup>Br<sub>4</sub>]<sub>2</sub>, a unique multifunctional material presenting magnetic order and spin-crossover. The effect of applied pressure on the magnetic order has been determined and correlated with aspects of the crystal structure determined at high pressure. The efficient spin-crossover induced by pressure at ambient temperature has also been demonstrated. Altogether our results highlight the great potential of combining properties based on a two-network molecular approach in order to produce original multifunctional materials.

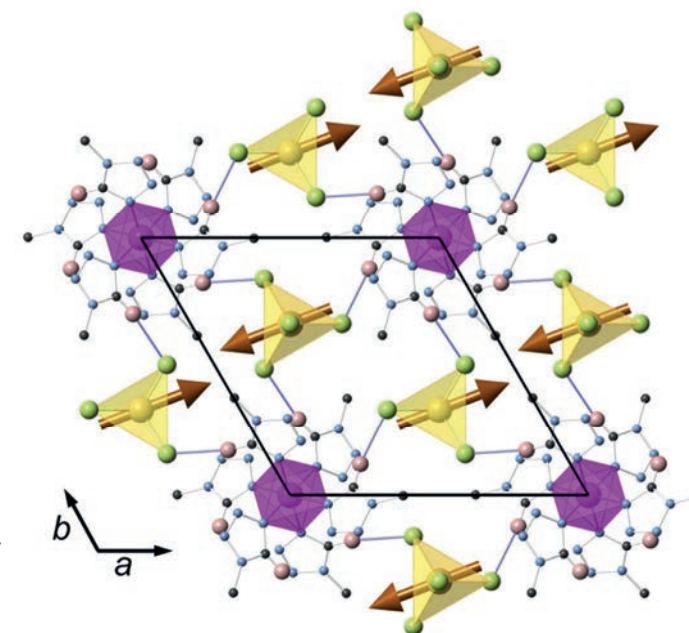


**Figure 1**

View of the magnetic structure of [Fe(Metz)<sub>6</sub>][FeBr<sub>4</sub>]<sub>2</sub> with the moments in the *ab* plane represented as brown arrows. Colour code: Fe<sup>II</sup> and [Fe(N)<sub>6</sub>] polyhedra, purple; Fe<sup>III</sup> and FeBr<sub>4</sub><sup>-</sup> anions, yellow; Br, light green; N, light blue; C, dark grey; H, pink; H...Br short contacts, blue sticks. The moments' orientation in the *ab* plane is arbitrary since powder neutron diffraction is not sensitive, in the present symmetry, to the absolute orientation angle of the magnetic moments contained in the *ab* plane.

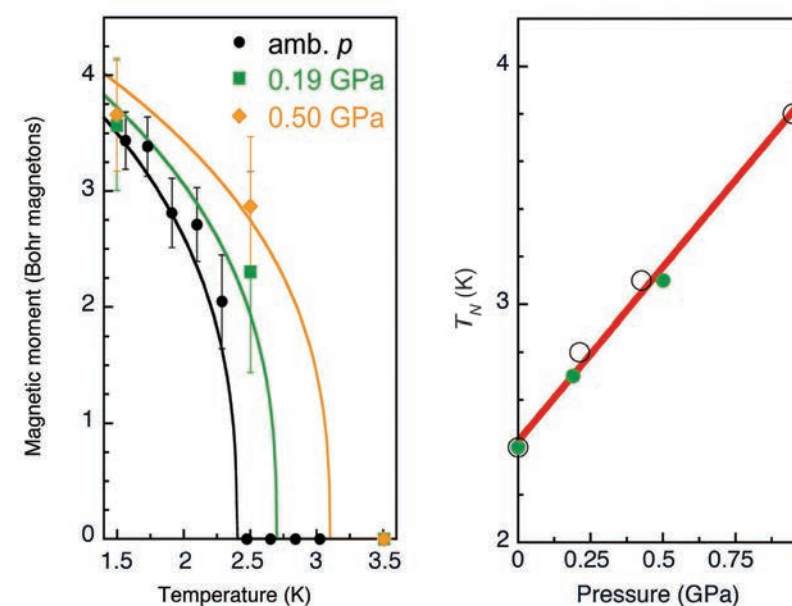


**Figure 2**

**Left:** Temperature dependence of the magnetic moment obtained from neutron diffraction at the indicated pressures. Solid lines are the power-law  $C\beta^t$  (where  $t = 1T-T_N/T_N$ ,  $C = 5$ ,  $\beta = 0.364$ , and  $T_N = 2.4$  K, 2.7 K and 3.1 K for the black, green and orange lines respectively), corresponding to a 3D Heisenberg ordering of  $S = 5/2$ .

**Right:** Pressure dependence of  $T_N$  as obtained from magnetic susceptibility (open black symbols) and neutron diffraction (full green symbols). The red line is a linear fit of data derived from both magnetic susceptibility and powder neutron diffraction.

# SOFT MATTER

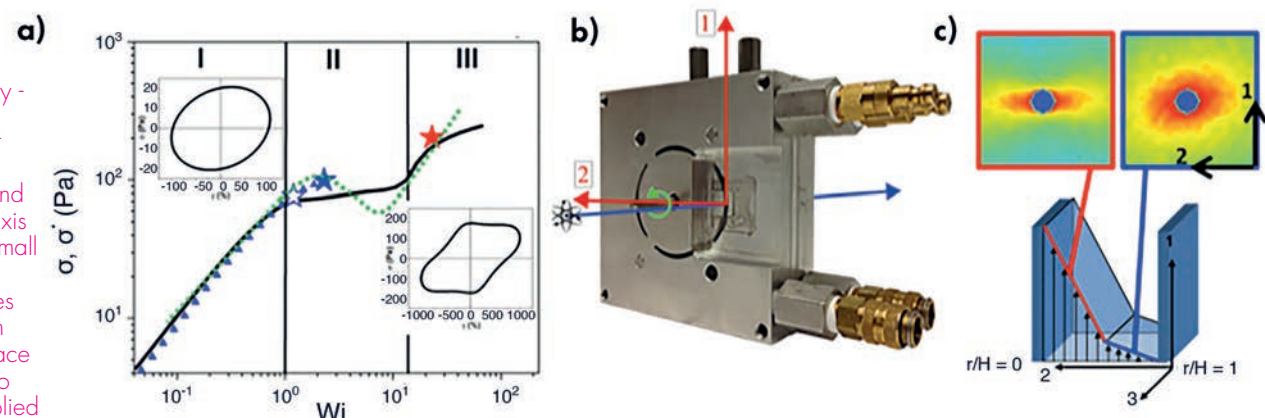
## Spatiotemporal stress and structure evolution in dynamically sheared polymer-like micellar solutions

Small-angle neutron-scattering diffractometer D22

One fundamental challenge in studying soft material under deformation is establishing a quantitative connection between the deformation field, local microstructure and macroscopic dynamic flow properties, i.e. the rheology. To address this, we present a new method coupling simultaneous small-angle neutron scattering (SANS) with nonlinear oscillatory shear deformation to study the dynamics of soft matter. This is demonstrated by investigating the structure-property relationship for a worm-like micellar solution (WLM) [1].

Figure 1

**a)** Shear stress as a function of dimensionless shear rate ( $Wi$ ) for WLM solution (black line). The green line shows the underlying constitutive equation and the stars denote conditions studied under LAOS. **b)** Flow-SANS 1-2 plane shear cell developed at the ILL in collaboration with NIST CNR and CNS University of Delaware. **c)** Schematic of the 1-2 plane of shear with corresponding 2D SANS scattering patterns of oriented and isotropic structure in the high and low shear bands [1].



### AUTHORS

A.K. Gurnon, C.R. López-Barrón and N.J. Wagner (Center for Neutron Science, University of Delaware, Newark, USA)  
A.P.R. Eberle (Center for Neutron Science, University of Delaware, Newark and NIST, Gaithersburg, USA)  
L. Porcar (ILL)

### REFERENCES

- [1] A.K. Gurnon, C.R. Lopez-Barron, A.P.R. Eberle, L. Porcar and N.J. Wagner, *Soft Matter* 10 (16) (2014) 2889
- [2] A.K. Gurnon, P.D. Godfrin, N.J. Wagner, A.P.R. Eberle, P. Butler and L. Porcar, *J. Vis. Exp.* (2014) e51068
- [3] **(a)** C.R. Lopez-Barron, A.K. Gurnon, A.P.R. Eberle, L. Porcar and N.J. Wagner, *Phys. Rev. E* (2014), 89 (4) 042301  
**(b)** A.K. Gurnon, C. Lopez-Barrón, M.J. Wasbrough, L. Porcar and N.J. Wagner, *ACS Macro Letters* (2014) 276  
**(c)** A.K. Gurnon and N.J. Wagner, *J. Rheol.* 56 (2) (2012) 333

A new, state-of-the-art flow SANS sample environment (**figure 1b**) developed in the ILL Large-Scale Structures group in collaboration with the Center for Neutron Science (CNS) and NIST Center for Neutron Research (CNR) enables simultaneous, quantitative measurements of the spatially resolved composition and microstructure alignment and orientation in the most influential velocity-velocity gradient [1-2] plane of shear [2]. From these structural measurements it is then possible to predict, through molecular-based theory and constitutive equation, the resulting shear stress properties measured macroscopically [3].

So-called shear-banding instabilities are present in many industrial processes and are macroscopically characterised by a stress plateau over a significant range of shear rates, meaning that material flow rates can increase by orders of magnitude with additional small amounts of energy (**figure 1a**). Microscopically, the solution presents inhomogeneous velocity fields: a distinct high shear band typically exhibits strong flow alignment while a low shear band has nearly isotropic microstructure (**figure 1c**). While theoretical and experimental research efforts have been successful in defining and predicting

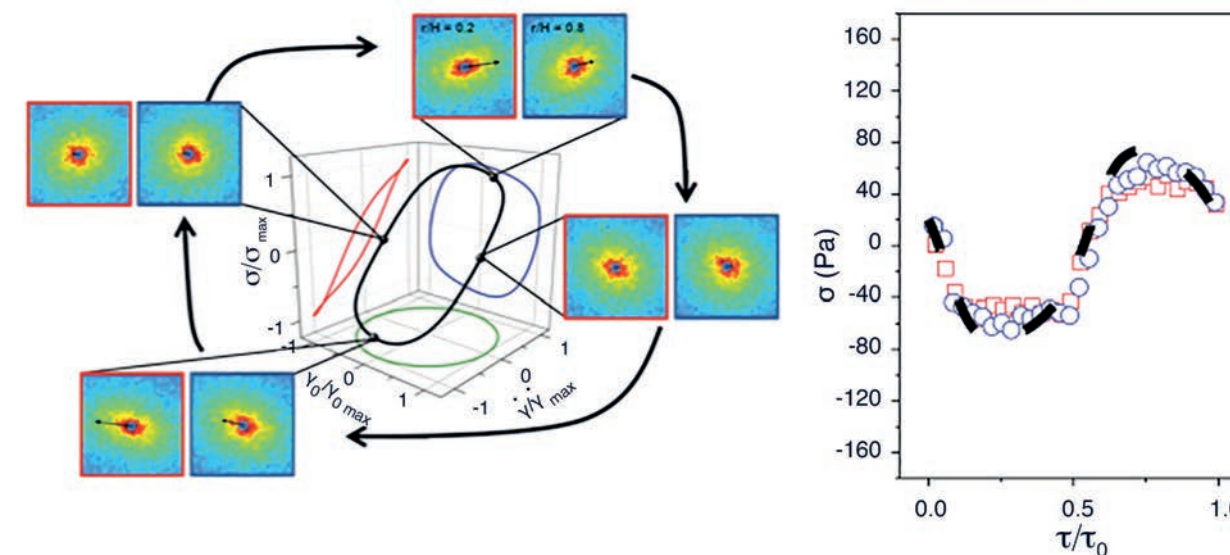


Figure 2

**Left:** Lissajous-Bowditch diagram for  $De = 0.23$  and  $Wi = 1.2$  where  $\omega = 0.56$  rad  $s^{-1}$  and  $\gamma_0 = 5$ . SANS scattering patterns inner ( $r/H = 0.2$ ) and outer ( $r/H = 0.8$ ) positions have red and blue borders, respectively. For the 2D SANS patterns the angle of the arrow reflects the average orientation angle  $\phi_0$  and the length of the arrow indicates the magnitude of alignment factor  $A_i$ . **Right:** Rheometry experiment stress reported (dashed line). Symbols use the stress-SANS rule.

the onset and microstructure of steady shear banding, the challenge now is to understand the dynamics of shear banding at a more fundamental level, including the spatiotemporal microstructure evolution that lies at the foundation of the mechanism. Nonlinear oscillatory shear is thus applied because of the method's ability to create and probe experimentally inaccessible metastable states using traditional steady shear methods. By changing the frequency at which strain is applied, we can tune the time it takes to reach the maximum shear rate or deformation and then control the viscoelastic states of the WLM otherwise known to exhibit shear banding during steady shear.

The worm-like micellar solution investigated in this work comprises 5.1 % w/w cetylpyridinium chloride and 1.1 % w/w sodium salicylate (1:1 molar ratio) in a 0.5 M NaCl and  $D_2O$  brine. The large amplitude oscillatory shear (LAOS) applied to the solution is defined by a frequency  $f = 0.089$  Hz and a strain amplitude of deformation of 500 %. These conditions correspond to the metastable state of shear banding (blue star on **figure 1**).

Time-resolved, small-angle neutron-scattering (TR-SANS) methods are used to capture 30 different measured microstructures over the course of a single oscillatory cycle during LAOS experiments at two positions in the gap (inner and outer positions  $r/H = 0.2$  and  $0.8$  where  $H$  is the gap size therefore  $r/H = 0$  &  $1$  correspond to the inner rotating wall and the outer fixed wall respectively, see **figure 1c**). The data are collected over multiple oscillation cycles such that statistically sufficient scattering events are recorded in each bin. The range

of scattering vectors probed by SANS is appropriate for defining the stress-SANS relationships between microstructure and shear and normal stresses under flow:  $\sigma \sim \sqrt{A_i} \sin(2\phi_0)$ . The nonlinear stress response shown in **figure 2a** corresponds with microstructures measured at the inner and outer positions, with slightly more alignment ( $A_i$ ) and flow orientation ( $\phi_0$ ), observed nearer to the inner wall as expected for a shear thinning fluid in Couette flow. The highest alignment indicating the greatest microstructural deformation corresponds to the largest stress response. We observe an isotropic scattering pattern that is indicative of an entangled PLM solution when the stress is at a minimum during the cycle.

**Figure 2b** shows quantitative agreement between shear stress measured by rheometry and the predicted shear stress at both positions in the gap, calculated using the  $\phi_0$  and  $A_i$  values gained from SANS measurements where the stress-SANS rule coefficient is independently defined from steady shear measurements. Thus, for this condition the validity of the stress-SANS rule relating segmental alignment to the polymeric stress tensor shows that the material behaviour is equivalent to that under steady shear conditions, as expected from theory. The three distinct material states (see **figure 1a**) have also been investigated and are reported in detail in [1]. We anticipate that this new combined method of LAOS rheometry and 1-2 flow-TR SANS will provide new opportunities to understand a broad range of nonlinear flow phenomena in shearing complex fluids. The authors encourage interested scientists to view reference [2] for further information.

query - emma

PLM

What does this stand for?

## SOFT MATTER

## How to weigh polymers packaged in viral capsids

## Small-angle diffractometer D22

Viruses are ubiquitous pathogens in all kingdoms of life; they are at the heart of a number of major public health issues and pose serious economic and veterinary concerns worldwide. The simplest viruses consist of an icosahedral protein shell, known as a capsid, which protects the genome encoded in one or more polynucleotide chains. Many of these viruses self-assemble in their host cells and capture the required segments of their genome with a remarkable selectivity. Whether such a level of selectivity is due to intricate molecular recognitions or to non-specific interactions between genome and capsid is a much-debated question. Accurate knowledge of the genome packaging process may give new insights into the viral life cycle and may eventually support the development of novel therapeutic strategies against viral infections.

## AUTHORS

G. Tresset, M. Tatou, C. Le Cœur, M. Zeghal, V. Bailleux and A. Lecchi (LPS, Orsay, France)  
K. Brach and M. Klekotko (Wrocław University of Technology, Wrocław, Poland)  
L. Porcar (ILL)

## REFERENCES

- [1] V.A. Belyi and M. Muthukumar, Proc. Natl. Acad. Sci. U.S.A. 103 (2006) 17174  
[2] R. Zandi and P. van der Schoot, Biophys. J. 96 (2009) 9  
[3] G. Tresset, M. Tatou, C. Le Cœur, M. Zeghal, V. Bailleux, A. Lecchi, K. Brach, M. Klekotko, and L. Porcar, Phys. Rev. Lett. 113 (2014) 128305

Cowpea chlorotic mottle virus (CCMV) is a non-enveloped, icosahedral, single-stranded RNA plant virus (**figure 1a**). It has a multipartite genome consisting of four RNA segments distributed in three indistinguishable particles: RNA 1 and 2 are packaged separately and have 3 171 and 2 774 nucleotides, respectively, while RNA 3 and 4 are packaged together and have 2 173 and 824 nucleotides, respectively. In other words, all particles package more or less the same mass of RNA. For the simplest viruses, such as CCMV, the packaging process can be regarded as charged chains interacting with a rigid shell through non-specific electrostatic interactions (see **figure 1c**).

One of the most intriguing results published in the literature revealed an experimental ratio of -1.6 between the total charge of the genome and the net charge on the capsid interior for a wide range of simple RNA viruses [1]. Furthermore, theoretical predictions based on free energy minimisation indicated a linear relationship between the total number of packaged monomers and the capsid interior area [2].

To date, no systematic and accurate measurements have been carried out to verify any linear relationship between the mass (or charge) of the packaged polymer and that of the capsid.

Poly(styrene sulfonic acid) (**figure 1b**) is a flexible, negatively charged homopolymer. It is an excellent model for assessing the selective capabilities of viral proteins in the absence of specific recognition. Upon mixing purified viral proteins in dimeric form with this polymer, capsids filled with the polymer are spontaneously formed (**figure 1d**) whose size distribution depends on the molecular weight of the polymer. We applied the contrast variation method in small-angle neutron scattering on a wide range of deuterated poly(styrene sulfonic acid) packaged in CCMV capsids. This non-destructive method made it possible to estimate both the mass of the packaged polymer and that of the surrounding capsid (**figure 1c**). Data were collected using the D22 diffractometer and the samples were exposed for up to three hours, depending on the distance to the detector.

The estimated mass ratio between packaged polymer and capsid is plotted on **figure 2** as a function of the polymer molecular weight. Remarkably, under fixed ionic

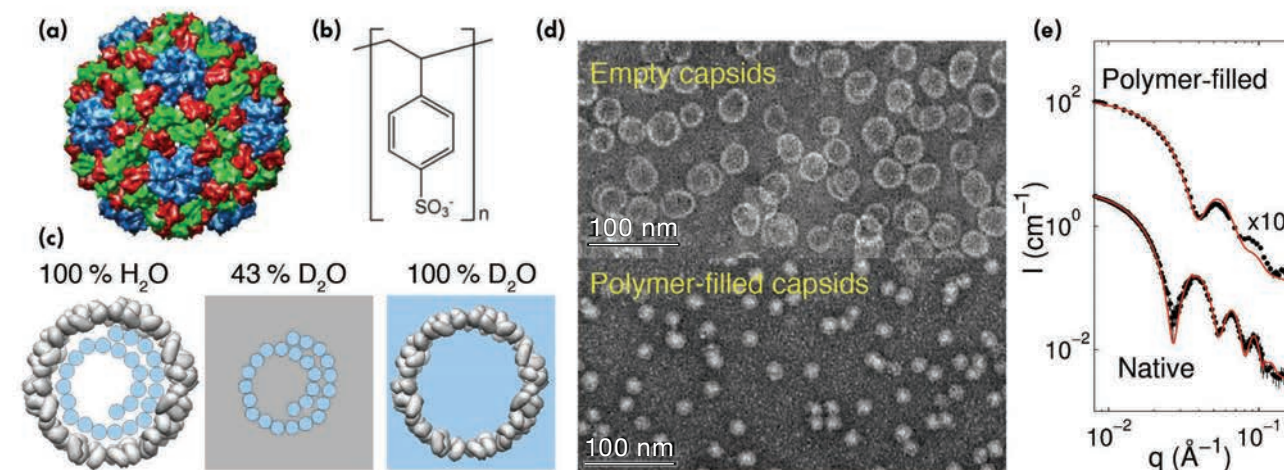
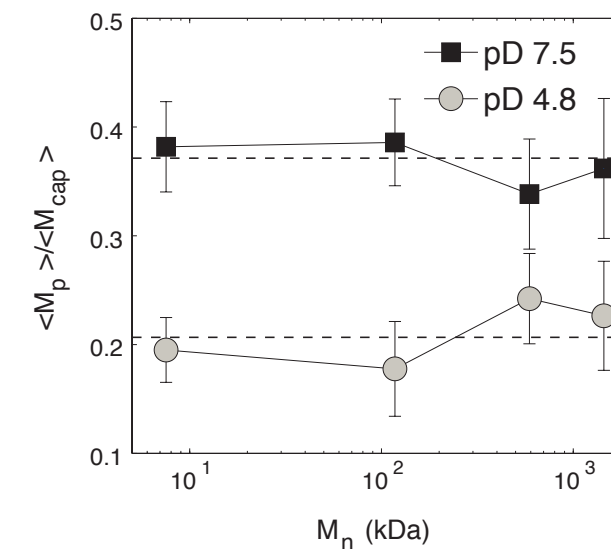


**Figure 1**  
(a) Crystal structure of CCMV. The icosahedral capsid has a diameter of 28 nm and is made of 180 copies of a single viral protein adopting three different conformations labelled in cyan, red and green.  
(b) Chemical structure of poly(styrene sulfonic acid) used in its deuterated form throughout this study.  
(c) Principle of the contrast variation method applied on polymer-filled capsids. In 100 % H<sub>2</sub>O, both capsid (gray) and polymer (cyan) contribute to the scattered intensity. In 43 % D<sub>2</sub>O, the capsid is contrast matched and only the polymer is visible, whereas in 100 % D<sub>2</sub>O, the intensity is solely due to the capsid and the polymer is contrast matched.  
(d) Electron microscopy images of empty (top) and polymer-filled (bottom) CCMV capsids. It can be noted that the latter are smaller than the former.  
(e) SANS patterns of capsids only (black dots) in native viruses and in polymer-filled capsids. Viral RNA and polymer were contrast matched with 43 % and 100 % D<sub>2</sub>O respectively. The data are fitted with a polydisperse shell model (red solid lines) and shifted for clarity. Clearly, polymer-filled capsids are less regular than native viruses and must therefore exhibit a few defects.

conditions – either physiological (pD 7.5) or acidic (pD 4.8) – the mass ratio remained unchanged within the uncertainties for polymer molecular weights spanning more than two orders of magnitude. In other words, the capsids packaged an amount of polymer proportional to their mass, either by uptaking a sufficient number of available chains or by selectively retaining the shortest chains that fitted the capsid interior. It should be noted that the invariance of the mass ratio implies that the charge ratio is also constant. The charge ratio was estimated to be -4.0 in physiological conditions and -2.3 in acidic conditions. These values deviate from the ratio of -1.6 found with RNA [1] because the excluded volume of the polymer is smaller than that of RNA and the protein self-energy varies with ionic conditions.

We have thus demonstrated that the strong selectivity displayed by viral proteins derived from an RNA plant virus for packaging polymers is mainly, but not exclusively, driven by electrostatic interactions, and that it can be explained within the framework of free energy minimisation. Our findings may therefore shed light on the non-specific origin of genome selectivity for a number of viral systems.

**Figure 2**  
Ratio of the mean mass of packaged polymer  $\langle M_p \rangle$  to the mean mass of capsid  $\langle M_{cap} \rangle$  as a function of polymer molecular weight  $M_n$  at pD 7.5 (squares) and pD 4.8 (discs). Dashed lines give the averages of the mass ratios in the least-squares sense.



## SOFT MATTER

## Molecular scale dynamics of large ring polymers

## Spin-echo spectrometer IN15

Ring polymers are unique among all polymer architectures, as rings are closed structures without ends. In dense melts their dynamics are expected to differ significantly from that of linear or branched polymers, where chain ends play the essential role in the versatile relaxation processes. Therefore, one of the remaining important questions in polymer science is: What happens when polymers have no ends at all? We present a novel, comprehensive study of the microscopic dynamics measured by neutron spin-echo spectroscopy.

## AUTHORS

S. Gooßen, A.R. Brás, M. Krutyeva, W. Pyckhout-Hintzen, A. Wischniewski and D. Richter (Jülich Centre for Neutron Science and Institute for Complex Systems, Forschungszentrum Jülich, Germany) M. Sharp and P. Falus (ILL)

## REFERENCES

- [1] P.G. De Gennes, J. Chem. Phys. 55 (1971) 572
- [2] G. Tsolou, N. Stratikis, C. Baig, P.S. Stephanou, and V.G. Mavrantzas, Macromolecules 43 (2010) 10692
- [3] J.D. Halverson, W.B. Lee, G.S. Grest, A.Y. Grosberg, and K. Kremer, J. Chem. Phys. 134 (2011) 204905
- [4] K. Hur, R.G. Winkler, and D.Y. Yoon, Macromolecules 39 (2006) 3975
- [5] S. Gooßen, A.R. Brás, M. Krutyeva, M. Sharp, P. Falus, W. Pyckhout-Hintzen, A. Wischniewski and D. Richter, Phys. Rev. Lett. 113 (2014) 168302

This is the first experimental investigation of microscopic dynamics of ring polymers by neutron spin-echo spectroscopy. Only recently has it become possible to synthesise a series of highly pure and monodisperse polyethylene oxide rings. This allows access to the microscopic dynamics of closed polymer structures and a strict test of a number of theoretical and simulation studies which have been carried out during the last decades.

For short linear chains the Rouse model successfully describes the segmental dynamics in terms of eigenmodes, whereas in the famous Reptation model the topological confinement in long, entangled polymer chains is represented by a virtual tube [1]. However, the creep motion out of the tube and secondary relaxation processes in this concept are strongly determined by the chain ends.

For pure entropy-driven Rouse dynamics, Mavrantzas *et al.* introduced a modified Rouse model for ring polymers [2], taking into account the different boundary conditions

query - emma

Reference [2] is actually Tsolou *et al.*, looking at references above.

due to the ring closure. It was found that this modified Rouse model did not yield a satisfying description of the dynamics for 10 kg/mol and 20 kg/mol rings, which relate to 5/10 times the entanglement molecular weight of the linear counterpart. Here, the longest wavelength modes are obviously suppressed. For the first active mode the amplitude pattern is characterised by four and eight nodes, respectively. Between these nodes loops can be formed as subunits of the ring. The loop size then corresponds to a segment mass of about 2 500 g/mol which is close to the entanglement molecular weight of polyethylene oxide (about 2 100 g/mol) and is independent of the ring size. This pattern, connected with the closed shape of the ring polymer, is a first indication of a lattice animal formation and the first experimental survey of a loop formation which was hypothesised in theoretical and simulation work.

While this approach describes very well the short-time dynamics in the dynamic structure factor measured by neutron spin-echo spectroscopy, it systematically underestimates the dynamics of the 20 kg/mol ring polymer at longer times (see dashed black lines in **figure 1**). We may interpret the result for the early time motion as a free Rouse relaxation of loops formed, for example, in a lattice animal structure. However, the data give clear evidence of a slower dynamical process, which dominates at longer times.

To model this slow process, we use the result of a recent simulation revealing a  $t^{1/4}$  evolution of the ring segmental mean-square displacement until the crossover to normal translational diffusion is reached [3]. Using this approach

we obtain an extremely good fit of the data (see coloured lines in **figure 1**) with only a single fit parameter, namely the spatial dimension of the slow process. This comes out at about 90 % of the radius of gyration of the ring polymer.

**Figure 2** schematically shows the results of our neutron spin-echo study in terms of the time-dependent mean-square displacement. The blue line displays the time-dependent loop relaxation at short times – it provides a steep increase related to the steep initial decay of the dynamic structure factor at high  $Q$ , and then it reaches a plateau displaying the spatial limit of the internal motions within the loop. The red line displays the slow dynamic process representing the dynamics of the loops. At short times this process contributes marginally but at intermediate times it takes over and dominates. This process is interpreted as loop migration along the contour of the lattice animal (see inset of **figure 2**).

Around the crossover time to pure centre of mass diffusion,  $\tau_{\text{cross}}$ , which was determined independently by pulsed-field gradient nuclear resonance spectroscopy, loop migration saturates and translational diffusion of the whole ring is observed. The sum of the Rouse-like loop relaxation and loop migration yields a slope of 0.32 at intermediate times (dashed black line). This is in very good agreement with simulation work yielding a slope of 0.35 [4].

Our experiments provide a first experimental verification of theoretical models that invoke lattice animals or crumpled globules, where the loop size would be an intrinsic ring property.

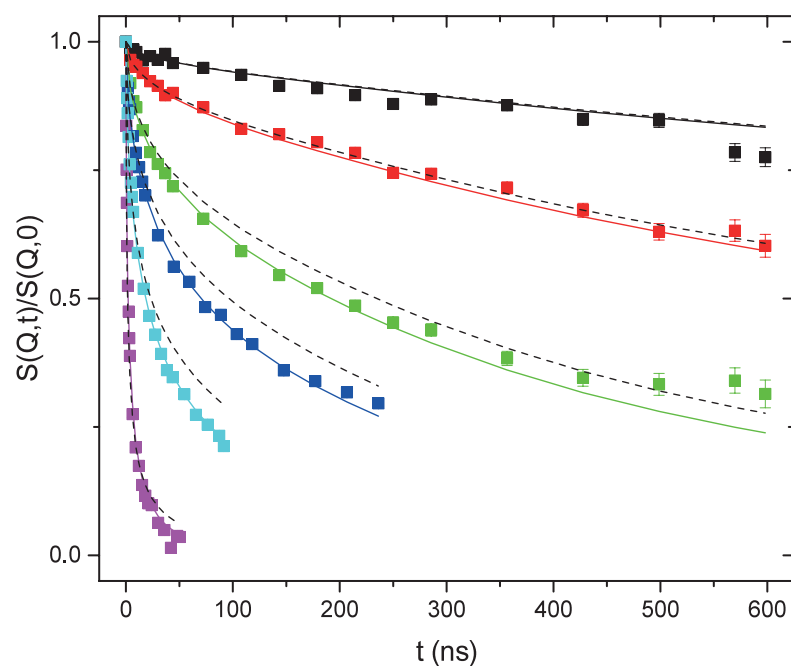


**Figure 1**

Neutron spin-echo data for a 20 kg/mol polyethylene oxide ring. Dashed black lines represent a fit to the data considering only internal loop dynamics (Rouse relaxation). Deviations to the data can be resolved solely by taking into account slower dynamics (loop migration), as can be seen by the coloured fit lines.

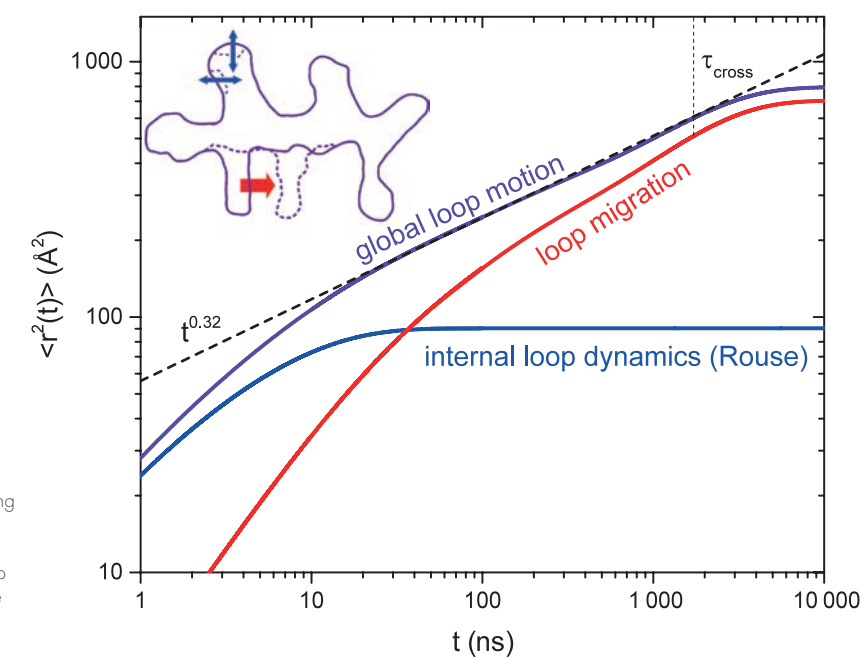


**Figure 2**

Schematic mean square displacement of a 20 kg/mol polyethylene oxide ring displaying the time dependence of the two individual dynamic processes and the sum of them (global loop motion). The inset illustrates these dynamic processes for a lattice animal with six loops.

# BIOLOGY AND HEALTH

## On the role of thylakoid lipids in the stacking of photosynthetic membranes

Small momentum-transfer diffractometer D16

A remarkable feature in the evolution of plant life, from single-celled cyanobacteria to higher plant forms, is the conservation of the lipid composition in thylakoid membranes, where photosynthesis takes place. In higher plants, these thylakoid membranes are found in highly specialised organelles called chloroplasts, thought to be inherited from ancestral cyanobacteria. Using neutron diffraction on reconstituted thylakoid lipid mixtures, we have observed that lipid extracts self-organise as regular stacks of bilayers or as hexagonal domains, depending on hydration level and lipid composition. Our analysis highlights the critical role of one particular glycolipid, DGDG, in the formation of regular membrane stacks in strong interactions. In developmental contexts or in response to environmental variations, lipid properties can contribute to the highly dynamic flexibility of plastid structures via the regulation of phase transitions from photosynthetic structures to non-photosynthetic ones.

### AUTHORS

B. Demé (ILL), C. Cataye, M.A. Block, E. Maréchal and J. Jouhet (CEA Grenoble, University, Grenoble Alpes, INRA, CNRS – all Grenoble, France)

### REFERENCES

- [1] B. Demé, C. Cataye, M.A. Block, E. Maréchal and J. Jouhet, *FASEB J.* 28 (2014) 3373
- [2] G. Lindblom, G. Oradd, L. Rilfors, and S. Morein (2002) *Biochemistry* 41 (2002) 11512

The lipid composition of photosynthetic membranes in plants and algae (thylakoid membranes or thylakoids) differs from that of all other cellular membranes; it is marked by a very low amount of phospholipids and a high fraction of glycolipids, in particular by a mono- and a di-galactosyldiacylglycerol (MGDG and DGDG). In all the photosynthetic membranes analysed to date, from cyanobacteria to algae, protists and plants, the complex lipid composition of the membranes has been well conserved.

We have shown, by producing bio-membranes made of natural thylakoid lipids [1], that the lipid composition can a) modulate the organisation of the membranes by tuning the transition from bilayer to non-bilayer structures, and b) contribute to membrane stacking by exerting cohesive forces between distant polar head groups. The results indicate that the MGDG/DGDG ratio plays a critical role in the stabilisation of lamellar structures and in the reversible formation of hexagonal (HII) domains. The transition and the coexistence of HII and  $L_{\alpha}$  domains can be modulated by fine-tuning the lipid profile (figure 1), or by hydration changes. This property could contribute to the highly dynamic flexibility of structures, as in the etioplast-to-chloroplast transition where cubic prolamellar bodies transform into lamellar stacks upon exposure to light.

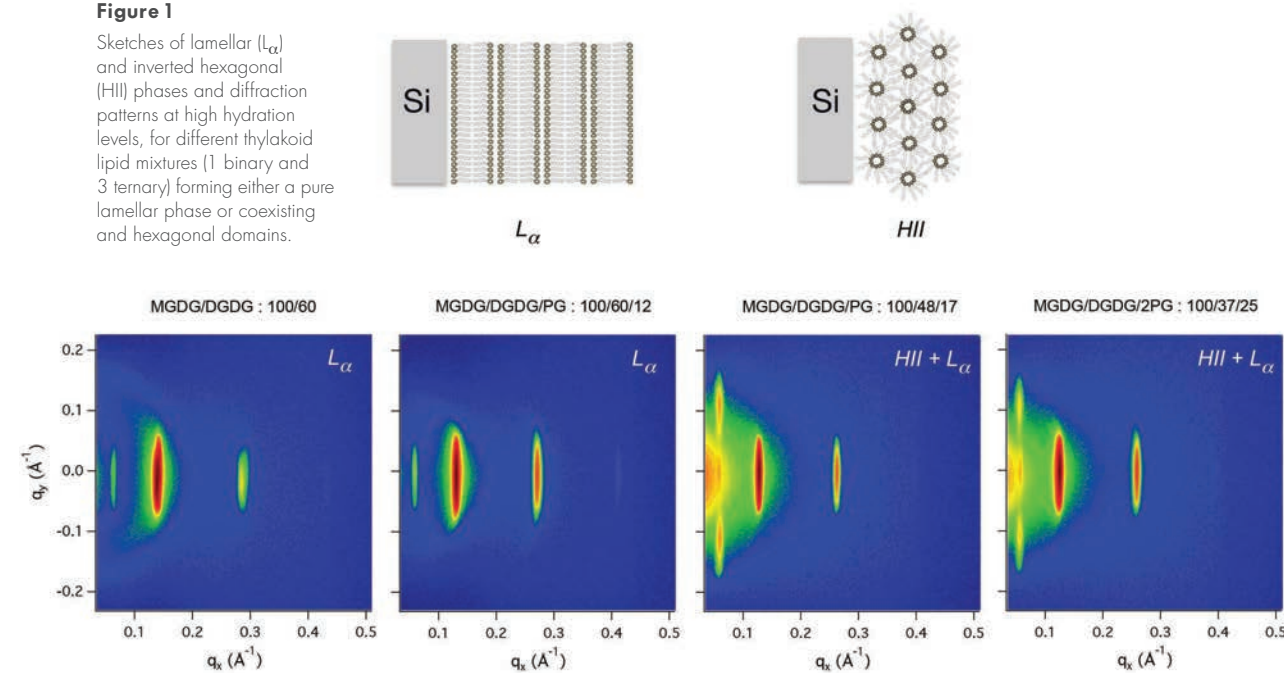
Furthermore, our analyses highlight the critical role of galactolipids, and most importantly of DGDG, as components contributing to membrane stacking via hydrogen bonds between galactose polar heads from adjacent bilayers. Their importance is emphasised by the fact that DGDG cohesive interactions indirectly neutralise the electrostatic contribution of charged lipids present in thylakoid membranes and allow the persistence of regularly stacked bilayers at high hydration levels, despite the negative charges harboured by a significant fraction of the constituent lipids. This remarkable property of chloroplast galactolipids might be a determinant in other membrane-ordered systems, such as that of the glycolipid-rich myelin sheath.

We recorded diffraction patterns at different levels of hydration for all the lipid mixtures in the study. We analysed the strength of the interaction between neighbouring membranes within a stack of bilayers, following the evolution of membrane-to-membrane distances as a function of the osmotic pressure applied to the bilayers via their hydration under controlled humidity conditions (figure 2).

For pure DGDG the decay of the pressure versus water layer thickness is exponential, as is commonly observed with

Figure 1

Sketches of lamellar ( $L_{\alpha}$ ) and inverted hexagonal (HII) phases and diffraction patterns at high hydration levels, for different thylakoid lipid mixtures (1 binary and 3 ternary) forming either a pure lamellar phase or coexisting and hexagonal domains.



phospholipids. It is known to be a regime dominated by hydration forces. At high hydration, the thickness of the water layers remains rather small (below 12 Å) for this uncharged glycolipid, compared with the more typical values of 25 Å observed for uncharged phospholipids. This is consistent with a higher cohesive interaction between DGDG membranes compared with phospholipids. The water layer thickness is compatible with hydrogen bonding between two DGDG di-galactose heads oriented parallel to the bilayer plane with a thickness of 8 Å. Other relevant lipid mixtures close to the natural thylakoids composition (ternary and quaternary mixtures) also present the typical exponential decay of the pressure-distance curves. However, at high hydration the increase in the water layer thickness vanishes and remains limited, as in the case of DGDG (less than 15 Å), despite electrostatic repulsions due to the presence of charged lipids. The effect of two negatively charged lipids (PG and SQDG) is clearly responsible for the increase in the thickness of the water layers due to additional electrostatic repulsions, but these negatively charged lipids do not significantly affect the swelling limit. This indicates that the attractive interaction between DGDG polar heads dominates these electrostatic repulsions between membranes.

The properties of individual thylakoid glycolipid classes previously reported as  $L_{\alpha}$  or HII forming lipids (or bilayer vs non-bilayer forming lipids), are subtly orchestrated in the matrix in which proteins are embedded in thylakoids. They contribute to the elaboration of the architecture of photosynthetic membranes and to their dynamics. The dissection of the roles of MGDG, DGDG and charged lipids helps the observation of chloroplast superstructures in various developmental, physiological, genomic and environmental contexts.

The results support the theory [2] that cells adjust their membrane lipid composition in response to perturbations, in order to maintain bilayer stability close to a phase limit, where a transformation to non-bilayer structures may occur. HII/ $L_{\alpha}$  coexistence in the natural membrane and the regulation of the MGDG/DGDG ratio explain a number of biological phenomena, such as the regulation of the lipid/protein ratio, the stabilisation of membrane proteins by increasing the membrane lateral pressure, and adaptation to environmental stress (frost, drought, salt deficiency).

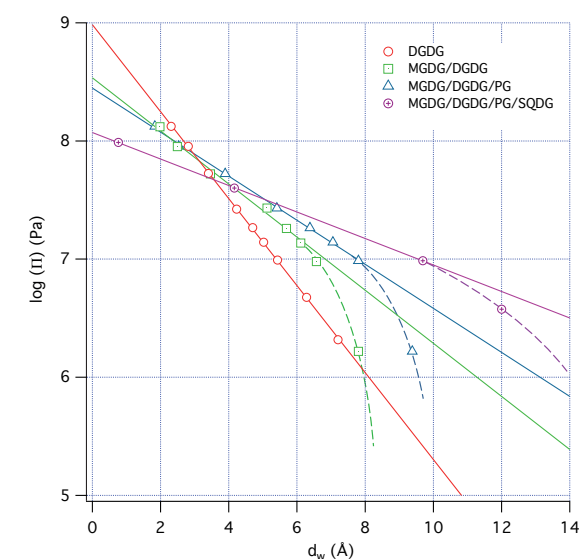


Figure 2

Pressure-distance curves obtained with four different lipid compositions: pure DGDG, a binary mixture (MGDG/DGDG : 100/60), a ternary mixture (MGDG/DGDG/PG : 100/48/17) and the thylakoid-like quaternary lipid mixture (MGDG/DGDG/PG : 100/48/17/17). The solid lines are linear fits to the data in the linear range of the decay.

# BIOLOGY AND HEALTH

## Neutron cryo-crystallography sheds light on heme peroxidases' reaction pathway

Quasi-Laue diffractometer LADI-III  
BioDiff instrument at FRM II

Knowledge of the structures of enzyme intermediates – including the positions of the hydrogen atoms – can be crucial for the comprehension of catalytic reaction pathways. Neutron cryo-crystallography provides a way to determine such structures, while also avoiding radiation damage issues that can occur using X-rays. This has been exemplified by our recent work. We successfully determined the structure of a transient intermediate using neutron cryo-crystallography that allowed a new catalytic mechanism to be proposed for the heme enzyme, cytochrome c peroxidase.

### AUTHORS

C.M. Casadei and M.P. Blakeley (ILL)

### REFERENCES

- [1] C.M. Casadei, A. Gumiero, C.L. Metcalfe, E.J. Murphy, J. Basran, M.G. Concilio, S.C.M. Teixeira, T.E. Schrader, A.J. Fielding, A. Ostermann, M.P. Blakeley, E.L. Raven and P.C.E. Moody, *Science* 345 (2014) 193

Enzymes are proteins that catalyse biochemical reactions in living organisms. An understanding of how enzymes work is crucial for the comprehension of metabolic pathways. In particular, knowledge of the structure of enzyme intermediates, namely structural forms along the catalytic pathway, are often essential for understanding enzymatic reaction mechanisms.

Heme peroxidases are a family of catalytic iron-containing proteins that are found in nearly all living organisms. These enzymes catalyse the  $H_2O_2$ -dependent oxidation of a substrate, thereby removing this potentially hazardous molecule from the cell. Heme peroxidases share a common reaction mechanism that involves the presence of two intermediate species known as Compound I and Compound II. Compound I contains an oxidised ferryl heme, plus either a porphyrin  $\pi$ -radical or a protein radical. Reduction of Compound I by one electron equivalent yields the closely related Compound II intermediate. Heme peroxidases have been the object of extensive studies in the last decades: of particular interest is the structural characterisation of the active site in the transient Compound I. The protonation state of the iron-bound oxygen ligand in Compound I has become a key question in the study of heme enzymes, due to its implications for the reaction mechanism. In particular, attention has been focused on whether the ferryl can be formulated as  $Fe(IV)=O$  or  $Fe(IV)-OH$ .

The methodologies that were traditionally employed to address this question appeared to be inadequate. Early approaches to the problem used resonance Raman methods to examine the iron-oxygen (Fe-O) bond as an indirect reporter on the oxygen protonation state.

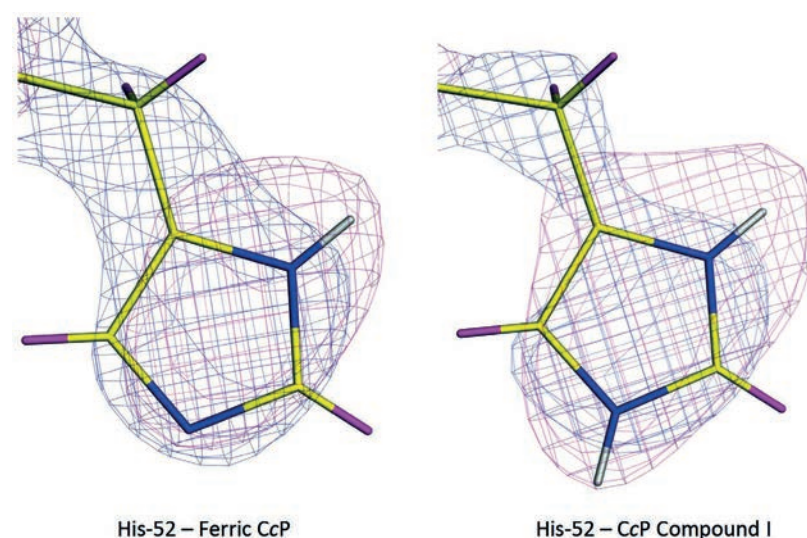


Figure 1

$2F_o-F_c$  neutron map (magenta) and X-ray map (blue) of the distal histidine in cytochrome c peroxidase in the resting state (left) and of transient Compound I (right).

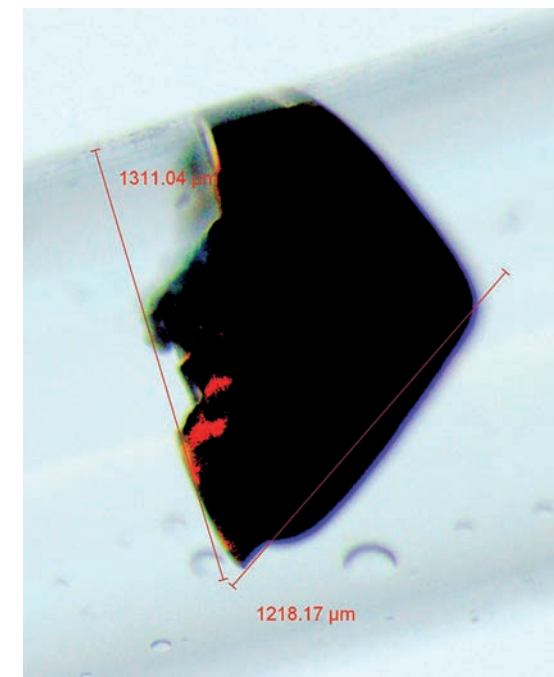


Figure 2

Cytochrome c peroxidase deuterium-exchanged single crystal used in the neutron crystallography experiment at LADI-III.

However the photolability of Compound I during laser excitation is well documented and results in ambiguous experimental findings. More recently, X-ray crystallography was employed with the purpose of inferring the ligand protonation state from the study of the iron-oxygen distance. However, the catalytic centre in these proteins is particularly sensitive to radiation damage effects and X-ray determined Fe-O distances are now considered unreliable.

For these reasons we adopted a different approach. Neutron crystallography allows the localisation of deuterium-substituted hydrogen atoms in medium resolution (2.5 Å or better) nuclear-scattering density maps. By contrast, hydrogen atoms are localised in X-ray maps only at ultra-high resolutions of 1.2 Å or beyond. The high X-ray dose required for ultra-high resolution data collection

cannot be employed in the study of heme enzymes due to their sensitivity to radiation damage.

Due to the lack of radiation damage effects and its ability to localise deuterium atoms, neutron crystallography is an excellent tool for the study of hydrogen-related biochemistry, such as the determination of the protonation state of key residues and ligands, the positions and orientations of water molecules in the active site and the study of hydrogen bond networks. Neutron crystallography data collection from cryo-trapped reaction intermediates is a unique tool for probing reaction mechanisms but presents a number of challenges, in particular the need to flash-cool the larger crystals required for neutron crystallography to the cryogenic temperature required for studying transient species.

We determined the neutron structure of the heme enzyme cytochrome c peroxidase (CcP) in the resting state, using the quasi-Laue diffractometer LADI-III, at the ILL. The data were collected at room temperature on a  $D_2O$ -soaked single crystal (figure 2). We have also determined the neutron structure of CcP Compound I at 100 K: a deuterium-exchanged CcP single crystal was reacted to form Compound I and subsequently cryo-cooled at 100 K. Monochromatic neutron data were collected at the BioDiff instrument at FRM II.

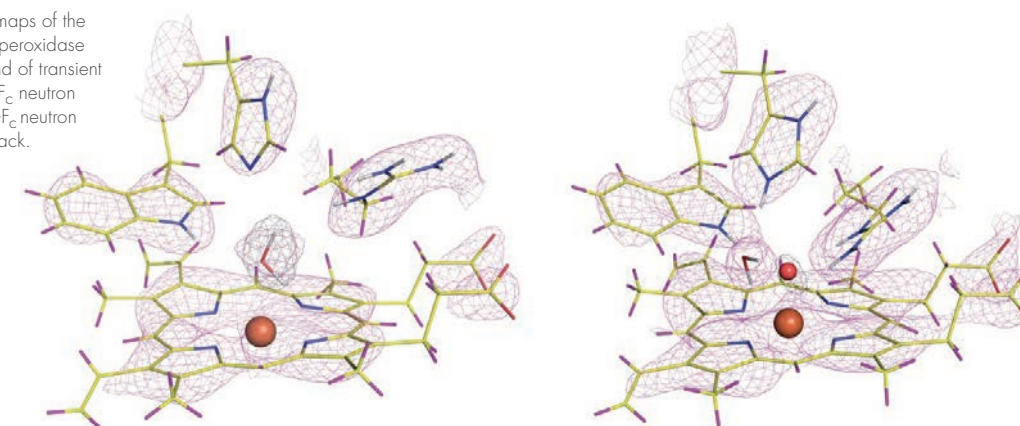
The structures showed that the distal histidine residue (His52) in the active site is neutral in the resting state but doubly protonated in Compound I, which was unexpected (figure 1). The iron axial ligand in Compound I is an oxygen atom, and it is non-protonated (figure 3). The oxygen forms hydrogen bonds to the side chains of tryptophan 51 and arginine 48. Our observations indicated that the widely assumed role of the distal histidine in Compound I formation needed to be reassessed and we proposed alternative possible mechanisms for O-O bond cleavage.

This work shows the feasibility of using neutron cryo-crystallography for clarifying enzymes reaction mechanisms. Our results provided a new picture of the reaction pathway in heme enzymes and were recently published in *Science* [1].

[This work is part of the ILL thesis work of Cecilia Casadei].

Figure 3

Neutron scattering density maps of the active site of cytochrome c peroxidase in the resting state (left) and of transient Compound I (right).  $2F_o-F_c$  neutron map shown in magenta.  $F_o-F_c$  neutron difference map shown in black.



# BIOLOGY AND HEALTH

## Structural insight into interactions between proteins and polymer brushes – towards a rational design of biocompatible surfaces

Vertical reflectometer D17

Protein adsorption to material surfaces causes problems in medical applications such as implanted biomedical devices, e.g. stents or catheters. A popular approach to prevent undesired protein adsorption is to decorate surfaces with hydrophilic polymer brushes, most commonly of poly[ethylene glycol] (PEG) [1]. However, the interaction of proteins with polymer brushes is not well understood. In particular, little is known about the mechanisms responsible for regularly observed “brush failure”, where protein adsorption occurs despite brush functionalisation [2]. We have designed PEG brushes of well-defined grafting layer chemistry, polymer length, and polymer grafting density, and structurally investigated different modes of undesired protein adsorption. Our results with different types of proteins highlight the importance of the brush parameters and the implications of PEG's often neglected antigenicity.

### AUTHORS

E. Schneck (ILL and MPI of Colloids and Interfaces, Potsdam, Germany)  
A. Schollier (ILL and University of Bruxelles, Belgium)  
I. Berts (ILL and Ludwig-Maximilians University of Munich, Germany)  
A. Halperin (University Joseph Fourier, Grenoble, France)  
M. Moulin, G. Fragneto and M. Haertlein (ILL)  
J. Daillant (Synchrotron Soleil, France)  
M. Sferazza (University of Bruxelles, Belgium)

### REFERENCES

- [1] D.L. Elbert and J.A. Hubbell, *Annu Rev Mater Sci* 26 (1996) 365
- [2] D. Belway and F.D. Rubens, *Expert Rev Med Devices* 3 (2006) 345
- [3] E. Schneck, A. Schollier, A. Halperin, M. Moulin, M. Haertlein, M. Sferazza and G. Fragneto, *Langmuir* 29 (2013) 14178
- [4] E. Schneck, I. Berts, A. Halperin, J. Daillant and G. Fragneto, *Biomaterials* 46 (2015) 95
- [5] T. Riedel *et al.*, *Langmuir* 29 (2013) 3388

PEG brushes were created from amphiphilic molecules with PEG portions of defined lengths. They were initially prepared as water-insoluble Langmuir monolayers at an air/water interface and then transferred at controlled lateral densities onto the hydrophobised surfaces of planar silicon blocks.

The experiments were carried out at the ILL on the vertical reflectometer D17. In the first step, the resulting polymer brushes at the silicon/water interface were characterised using neutron reflectometry (NR) with contrast variation. Contrast variation was enabled by liquid cells with a computer-controlled pumping system that allows the liquid to be replaced with mixtures of the light and heavy versions of water, H<sub>2</sub>O and D<sub>2</sub>O, respectively. The recorded neutron reflectivity curves contained detailed information on the structure of the polymer brushes, such as brush thickness and PEG volume fraction.

In the second step, the brushes were incubated in protein solutions and then again characterised by NR with various water contrasts. **Figure 1** shows a representative set of reflectivity curves from a PEG brush in H<sub>2</sub>O and D<sub>2</sub>O as well as in H<sub>2</sub>O/D<sub>2</sub>O mixtures termed 4MW and SMW, before (left) and after (right) incubation with proteins. The adsorption of proteins leads to a number of additional features (e.g. minima and maxima) in the reflectivity curves, from which detailed information on the density profiles of the adsorbed proteins was reconstructed with the help of a suitable reflectivity model (solid lines in **figure 1**).

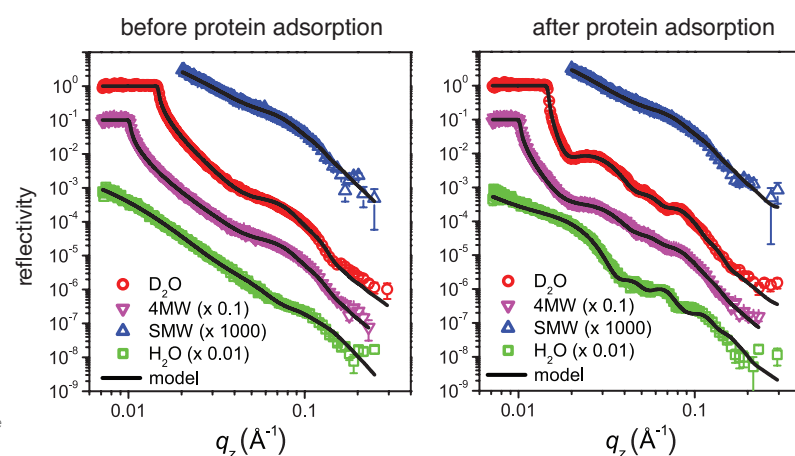
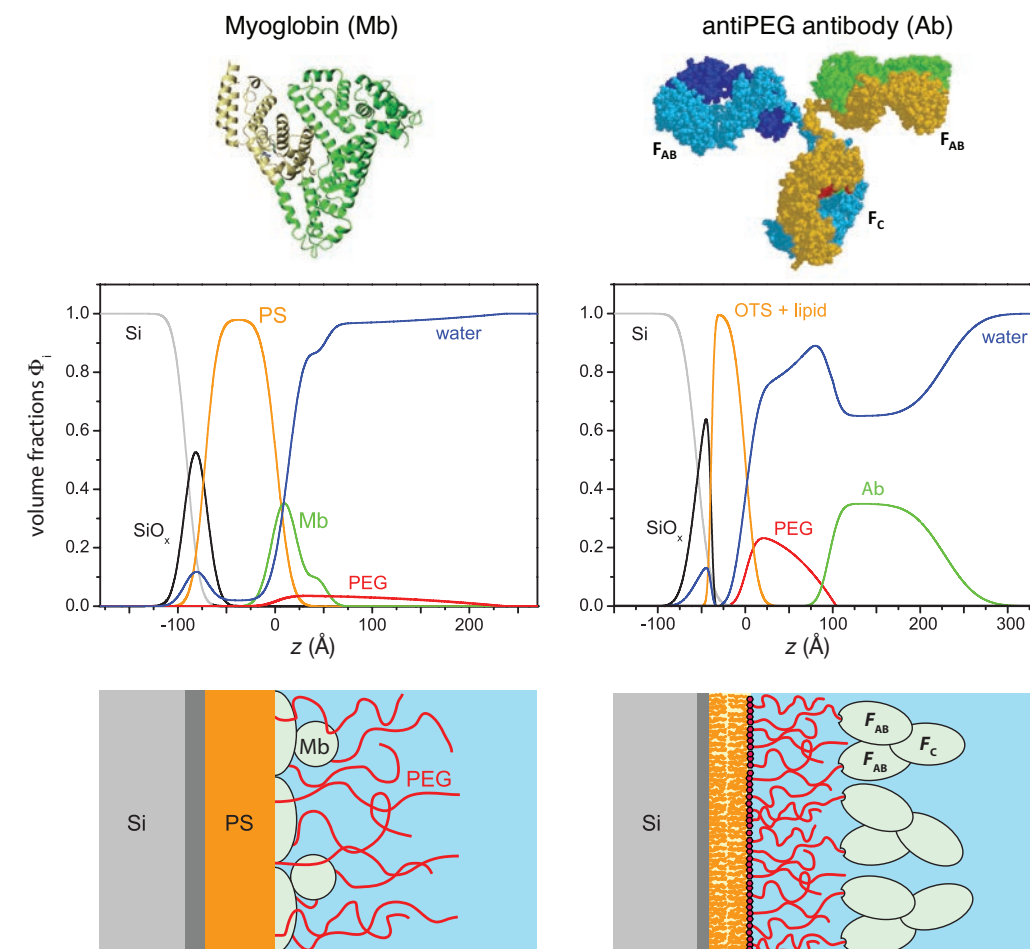


**Figure 1**

Reflectivity curves from a PEG brush in H<sub>2</sub>O and D<sub>2</sub>O as well as in H<sub>2</sub>O/D<sub>2</sub>O mixtures termed 4MW and SMW, before (left) and after (right) incubation with proteins. Solid lines indicate the reflectivity model used to reconstruct the protein density profiles.

**Figure 2**

**Top:** Structures of the proteins (left: myoglobin, right: anti-PEG antibody) with which the brushes were incubated.  
**Middle:** Density profiles of proteins, PEG, and other compounds in the vicinity of the silicon/water interface as reconstructed from the reflectivity curves (left: primary adsorption of Mb, right: ternary adsorption of Ab).  
**Bottom:** Cartoons illustrating the different protein adsorption modes corresponding to the density profiles in the panels above.



One series of experiments focused on the adsorption of small globular proteins, represented by myoglobin (Mb, see **figure 2 top left**), onto polymer brushes dependent on two brush parameters, namely the polymerisation degree  $N$  and the polymer grafting density  $\alpha$ . In this series the polymers were grafted onto a hydrophobic polystyrene (PS) layer and the sensitivity of NR was enhanced by the use of deuterated Mb. The reconstructed protein density profiles (**figure 2 middle left**) showed that Mb exhibits adsorption to the grafting surface (“primary adsorption”), which consists of two distinct protein layers (**figure 2 bottom left**). The amount of Mb adsorbed in the inner layer was independent of  $N$  but varied with  $\alpha$ , while for the outer layer it was correlated to the amount of grafted PEG and thus depended on both  $N$  and  $\alpha$  [3]. Such precise structural information provides a valuable basis for the rational design of protein-repellent surface functionalisation.

Another series of experiments focused on the implications of PEG's often neglected antigenicity. For this purpose, brushes grafted to hydrophilic phospholipid surfaces were incubated

with solutions of anti-PEG IgG antibody (Ab, see **figure 2 top right**), as is sometimes found in human blood. This time the reconstructed protein density profiles (**figure 2 middle right**) clearly demonstrated that the adsorption of Ab occurred onto the brush itself (“ternary adsorption”). Closer inspection revealed that the Abs form dense layers and assume an inverted “Y” configuration (**figure 2 bottom right**), suggesting strong and specific protein/polymer interactions involving the binding regions on the F<sub>AB</sub> segments [4]. In this configuration the Abs display their F<sub>C</sub> segment to the aqueous phase, potentially promoting foreign body reaction.

We are currently extending the approach described towards incubation of polymer brushes with blood serum as a biomedically relevant complex fluid. Recent literature has indicated that the adsorption of certain blood proteins is mediated by other molecular species present in blood [5].

[The deuterated recombinant myoglobin was prepared in the ILL Deuteration Lab in the Life Science group].

[This work was part of the ILL thesis work of Ida Berts].

# BIOLOGY AND HEALTH

## Neutrons help to reveal the structural basis of a gene-regulation mechanism in *Drosophila* flies

Small-angle scattering diffractometer D22

The information encoded in our genes is translated into proteins, which ultimately mediate biological functions in an organism. Messenger RNA (mRNA) plays an important role, as it is the molecular template used for translation. The number of genes in humans, mice and fruit flies is almost identical, at around 20 000, and thus cannot explain the differences in phenotype (i.e. appearance) between these organisms. Thus, for the evolved diversity of life not only the number of genes but also differences during the regulation of gene translation play a critical role. Upon transcription of the DNA, mRNA is produced as an initial step, which subsequently functions as the template for the synthesis of proteins in ribosomes. This synthesis is regulated by the binding of regulatory proteins to the mRNA, but the structural details of this specific recognition remain poorly understood to date.

### AUTHORS

F. Gabel (IBS and ILL, Grenoble)  
J. Hennig and M. Sattler (Technical University Munich and Helmholtz Centre Munich, Germany)

### REFERENCES

[1] J. Hennig, C. Militti, G.M. Popowicz, I. Wang, M. Sonntag, A. Geerlo, F. Gabel, F. Gebauer and M. Sattler, Nature (2014) doi: 10.1038/nature13693

In an international collaboration between scientists of the Helmholtz Zentrum and Technische Universität München, Germany, the Centre de Regulació Genòmica, Barcelona, Spain, and the Institut de Biologie Structurale and the Institut Laue-Langevin, Grenoble, the structure of a ternary protein-RNA complex involved in a gene-regulation mechanism in fruit flies (figure 1) has been solved [1]. Specifically, we studied the complex formed by two regulatory proteins Sxl (Sex-lethal) and Unr (Upstream-of-N-Ras), and mRNA in the fruit fly (figure 2). This complex is a key player in gene regulation, which assures the equilibrium of proteins expressed by the sex chromosome in female and male *Drosophila melanogaster* flies.

Flies, like mammals (including humans), need to adjust the respective protein concentrations that are expressed in female XX and male XY sex chromosomes, a mechanism known as dosage compensation. If this delicate balance is perturbed, severe changes of the phenotype can be observed or have even lethal effects. In humans, abnormal numbers of sex chromosomes are responsible for the Klinefelter syndrome (XXY chromosome in males) and the Turner syndrome (single X chromosome in females), which both lead to perturbation of X-chromosome-linked gene expression.



Figure 1

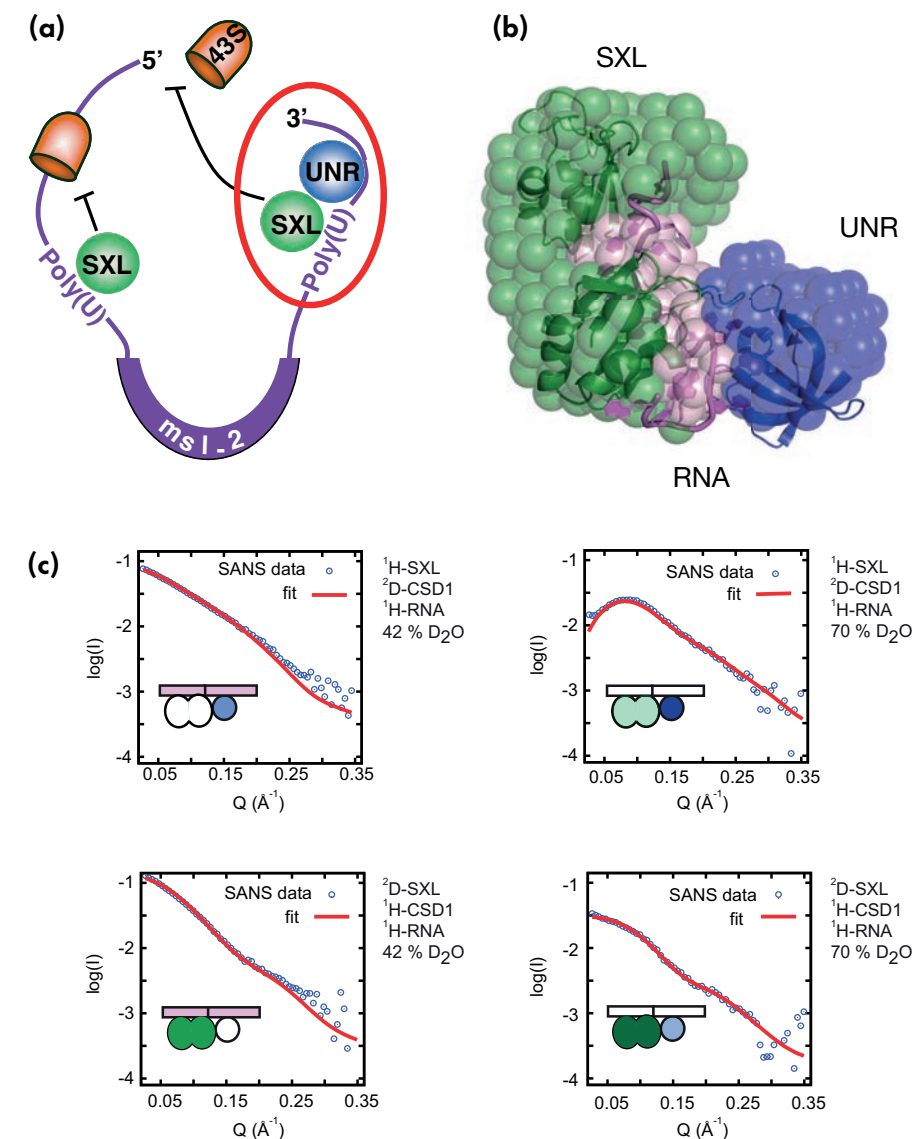
Coloured electron microscopy of the *Drosophila melanogaster* fruit fly (© Jürgen Berger, MPI for Developmental Biology, Tübingen).

In order to obtain a model of the three-dimensional structure of the complex, we used a combination of complementary techniques: nuclear magnetic resonance (NMR), crystallography and small-angle X-ray (SAXS) and small-angle neutron (SANS) scattering. The specific information contained in the neutron data was invaluable in demonstrating that the mRNA is sandwiched between the two protein partners. It also helped us to guide the refinement process based on structural restraints from NMR, and was vital in enabling the later determination of the high-resolution crystallographic structure. The three-dimensional structure now reveals how multiple proteins collaborate for the highly specific recognition of the mRNA.

Our results represent a paradigm for the regulation of various essential cellular processes at the mRNA level. The specific recognition of mRNA is achieved by the co-operation of several RNA-binding proteins, even though individually these proteins exhibit poor binding specificity and affinity, and are involved in distinct processes in the cell. By combining multiple proteins, the number and variety of biological processes that can be regulated by a relatively small number of regulatory RNA binding proteins is greatly expanded. We expect that this principle represents an essential and widespread mechanism of gene regulation in higher organisms, where mutation or misregulation of homologous proteins has been implicated in disease.

Figure 2

a) Schematic representation of the translational inhibition by the Sxl-Unr-RNA complex towards the 43S ribosomal subunit.  
b) SANS low-resolution envelopes of the three partners (determined by the program MONSA), superposed with the crystal structure of the complex.  
c) Fits of the crystal model at different contrast and deuteration conditions against experimental data recorded on D22 at the ILL.



# BIOLOGY AND HEALTH

## Diffusion and dynamics of $\gamma$ -globulin in crowded aqueous solutions

Backscattering spectrometer IN16B

The new backscattering spectrometer IN16B allows simultaneous access to both the global diffusion and internal molecular dynamics of proteins in aqueous solution, which opens up unprecedented opportunities to study the relation of protein function and dynamics under physiological conditions. In this spirit, the effect of macromolecular crowding on global and internal protein dynamics has been investigated.

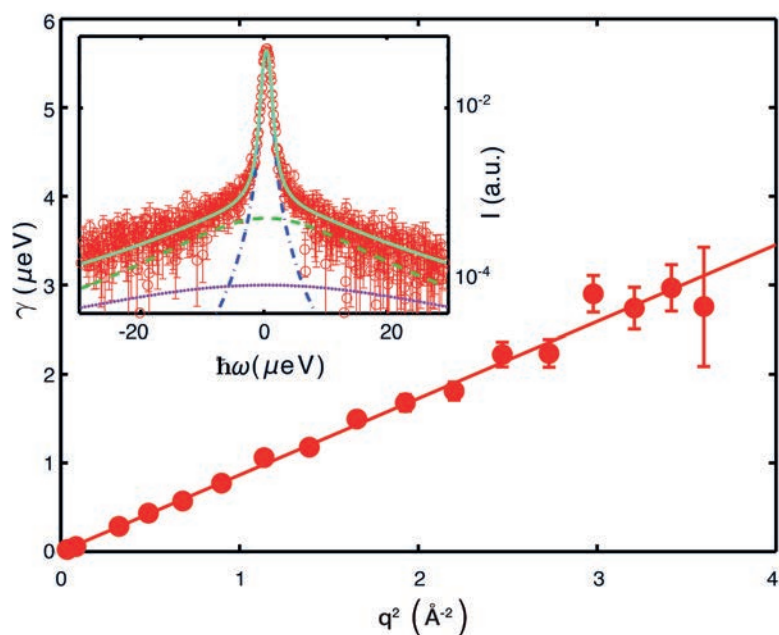


**Figure 1**

**Inset:** Example spectrum (symbols) recorded on  $\gamma$ -globulin in  $D_2O$  ( $c_p = 300$  mg/ml;  $T = 295$  K; detector at  $q = 0.81 \text{ \AA}^{-1}$ ). The lines depict the Lorentzians associated with the global protein motion [ $\gamma(\omega)$ ] (dash-dotted), the internal protein motions [ $\gamma + \Gamma(\omega)$ ] (dashed), and the  $D_2O$  solvent [ $\gamma(D_2O(\omega))$ ] (dotted), respectively. The solid line is the result of the complete fit.

**Main figure:** fitted  $\gamma$  (circles) for the full accessible  $q$ -range. The fit  $\gamma = Dq^2$  (line) indicates a simple Brownian diffusive behaviour.

### AUTHORS

F. Schreiber and F. Zhang (Tübingen University, Tübingen, Germany)  
M. Grimaldo (ILL and Tübingen University, Germany)  
F. Roosen-Runge and T. Seydel (ILL)

### REFERENCES

- [1] M. Grimaldo, F. Roosen-Runge, F. Zhang, T. Seydel and F. Schreiber, J. Phys. Chem. B 118 (2014) 7203
- [2] F. Roosen-Runge, M. Hennig, F. Zhang, R.M.J. Jacobs, M. Sztucki, H. Schober, T. Seydel and F. Schreiber, PNAS 108 (2011) 11815
- [3] M. Tokuyama and I. Oppenheim, Phys. Rev. E 50 (1994) R16
- [4] L. Stagg, S. Zhang, M.S. Cheung and P. Wittung-Stafshede, PNAS 104 (2007) 18976

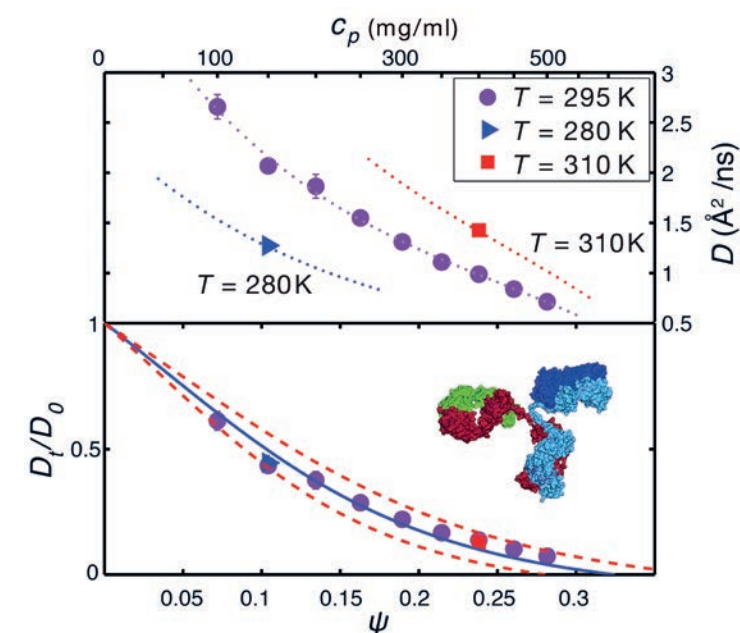
Dynamics in protein solutions is essential for both protein function and cellular processes. The hierarchical complexity of global protein diffusion, side-chain diffusion, and microscopic motions of chemical groups renders a complete understanding challenging.

We have studied solutions of  $\gamma$ -globulin, an important protein of the immune system, as a function of the protein concentration and sample temperature [1]. The very high flux of the new backscattering spectrometer IN16B allows for data with excellent signal-to-noise ratio (inset of **figure 1**), thus providing unprecedented access to processes at nanosecond time and nanometer length scales. Using model fitting, the translational and rotational diffusion of the proteins can be self-consistently separated from internal motions. In the model, global and internal motions are each represented by a Lorentzian, supplemented by a third fixed Lorentzian for the water ( $D_2O$ ) solvent.

For the global diffusion, we find the dependence  $\gamma = Dq^2$  of the Lorentzian linewidth  $\gamma$  at scattering vector  $q$  without imposing this functional relationship in the fits. Therefore, our fits corroborate the picture that the protein centre-of-mass follows a simple Brownian diffusion with an apparent

**Figure 2**

Apparent diffusion coefficient  $D$  (upper panel) and reduced translational short-time diffusion coefficient  $D_t/D_0$  (lower panel) versus protein volume fraction  $\psi$  recorded at  $T = 295$  K (circles),  $T = 280$  K (triangles), and  $T = 310$  K (squares). The solid line in the lower panel depicts the normalised translational short-time self-diffusion from colloid theory for hard spheres [3].



global diffusion coefficient  $D$  (main part of **figure 1**). Following a method established in [2], we separate the translational,  $D_t$ , and rotational,  $D_r$ , contributions to  $D$ . The resulting  $D_t$  as a function of the protein concentration for different temperatures  $T$  (top part of **figure 2**) shows a strong dependence of the translational protein diffusion on both temperature and protein concentration. When normalising the diffusion coefficients  $D_t$  by the diffusion in the limit of infinite dilution  $D_0$ , the resulting  $D_t/D_0$  at different temperatures superimpose on a single master curve (lower part of **figure 2**) as a function of the protein volume fraction  $\psi$ . This master curve agrees with the theoretical prediction for the self-diffusion of colloidal hard spheres [3]. Therefore, the global protein diffusion on the nanosecond time scale is consistent with predictions for effective spheres even though the branched molecular shape of the proteins differs considerably from a sphere [1,2].

Concerning the internal protein dynamics, the second Lorentzian provides information on both type and geometry of the internal molecular motions. The non-linear behaviour of the associated linewidth  $\Gamma(q)$  (inset **figure 3**) would suggest a jump-diffusive mechanism of the underlying internal relaxations. The amplitude of the second Lorentzian, the so-called elastic incoherent structure factor (EISF, **figure 3**), evidences that internal relaxations occur within a confinement with dimensions of the length of the protein side-chains. Crowding due to an increased protein concentration decreases the characteristic residence time of the jump-diffusion, while the geometrical confinement appears unaltered [1].

In summary, our study draws a conclusive picture of effects of macromolecular crowding on the macromolecular dynamics at nanosecond time scales. The diffusion of the entire protein follows predictions for colloids. Internal relaxations occur on the level of side-chains in a jump-diffusive mechanism, and are slowed down by surrounding macromolecules. The general consistency of the data analysis and interpretation is promising for future studies of environmental effects on molecular dynamics and comparisons with theory [4]. The advent of new neutron spectrometers therefore allows the study of current questions including, *inter alia*, the coupling of intracellular dynamics and protein function.

[This work is part of the ILL thesis work of Marco Grimaldo].

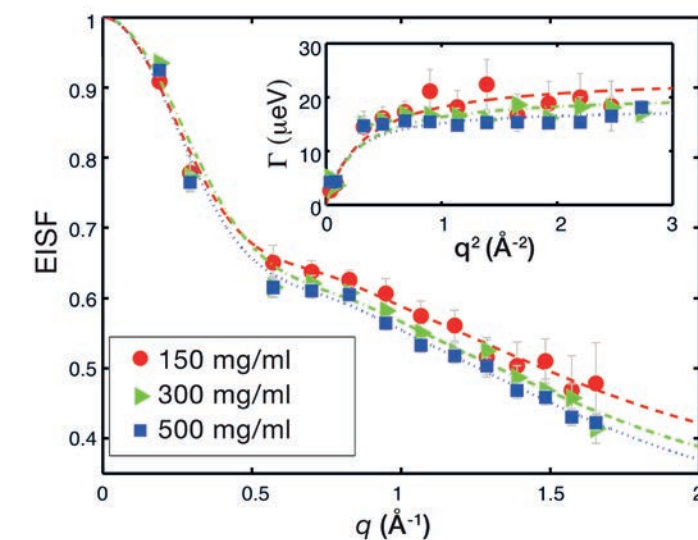


**Figure 3**

**Main figure:** elastic incoherent structure factor for different  $\gamma$ -globulin concentrations (symbols) and fits (lines).

**Inset:** Linewidth  $\Gamma$  for different protein concentrations (symbols) and fits of a jump-diffusion model for the internal relaxations (lines).

# NUCLEAR AND PARTICLE PHYSICS

## Quantum Cheshire Cat spotted at the ILL

### Interferometer S18

*“Well! I’ve often seen a cat without a grin,” thought Alice in Wonderland, “but a grin without a cat! It’s the most curious thing I ever saw in my life!”* Alice’s surprise stems from her experience that an object and its property cannot exist independently. It seems to be impossible to find a grin without a cat. However, the laws of quantum mechanics tell us that under very specific circumstances it is indeed possible to separate a particle from its property.

#### AUTHORS

T. Denkmayr, S. Sponar, H. Geppert, and Y. Hasegawa  
(Atominstiut, Vienna University of Technology, Austria)  
H. Lemmel (ILL and Vienna University of Technology, Austria)

#### REFERENCES

- [1] Y. Aharonov, S. Popescu, D. Rohrlich and P. Skrzypczyk, *New J. Phys.* 15 (2013) 113018  
[2] T. Denkmayr *et al.*, *Nat. Commun.* 5 (2014) 4492  
[3] Y. Aharonov, D.Z. Albert and L. Vaidman, *Phys. Rev. Lett.* 60 (1988) 1351

The idea of a Quantum Cheshire Cat was proposed theoretically in 2013 [1] and realised experimentally for the first time at the ILL shortly thereafter [2]. It is based on the well-known feline in Alice in Wonderland who suddenly vanishes, leaving his smile behind. In quantum physics, the term refers to an object whose properties can be separated from its physical location, with the result that the two can be measured at different places. While this is clearly not possible in our everyday experience, where objects are spatially linked to their properties, the laws of quantum mechanics allow it to be achieved.

We measured the Quantum Cheshire Cat effect for the first time using neutron interferometry, a perfect tool for investigating the foundations of quantum mechanics: when a neutron beam is divided in two using a crystal, individual neutrons do not have to decide which of the two paths to take. Instead, they can travel along both paths at the same time in a quantum superposition. Similarly, the property of a quantum Cheshire Cat in a Mach-Zehnder-type interferometer is that the cat is located in one beam path, whilst its grin is located in the other (an artist’s view of this behaviour is shown in figure 1).

**Figure 1**

Artist’s view of the Quantum Cheshire Cat – inside the interferometer, the Cat takes the upper beam path, while its grin travels along the lower beam path. (Figure courtesy of Leon Filter).

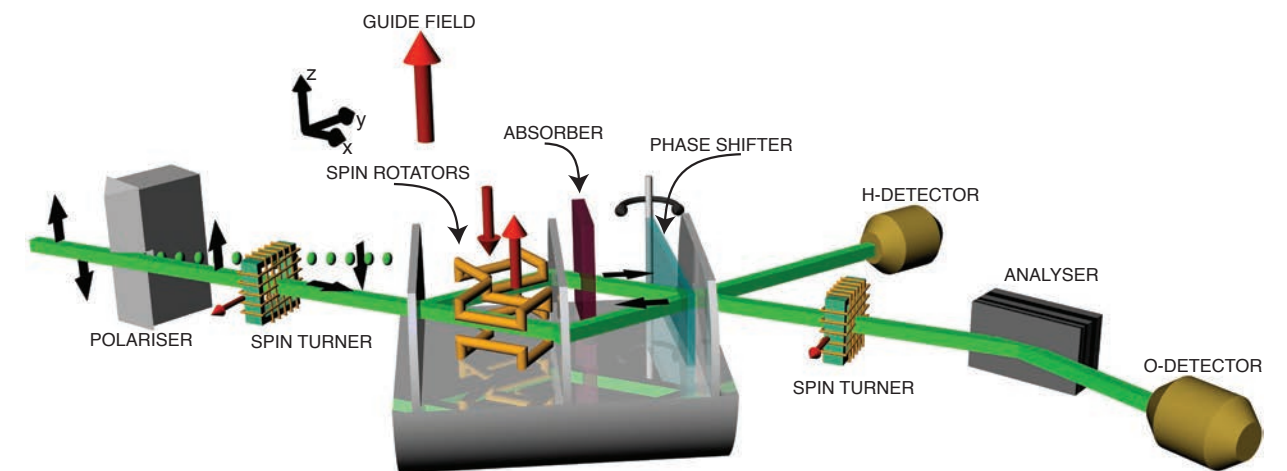
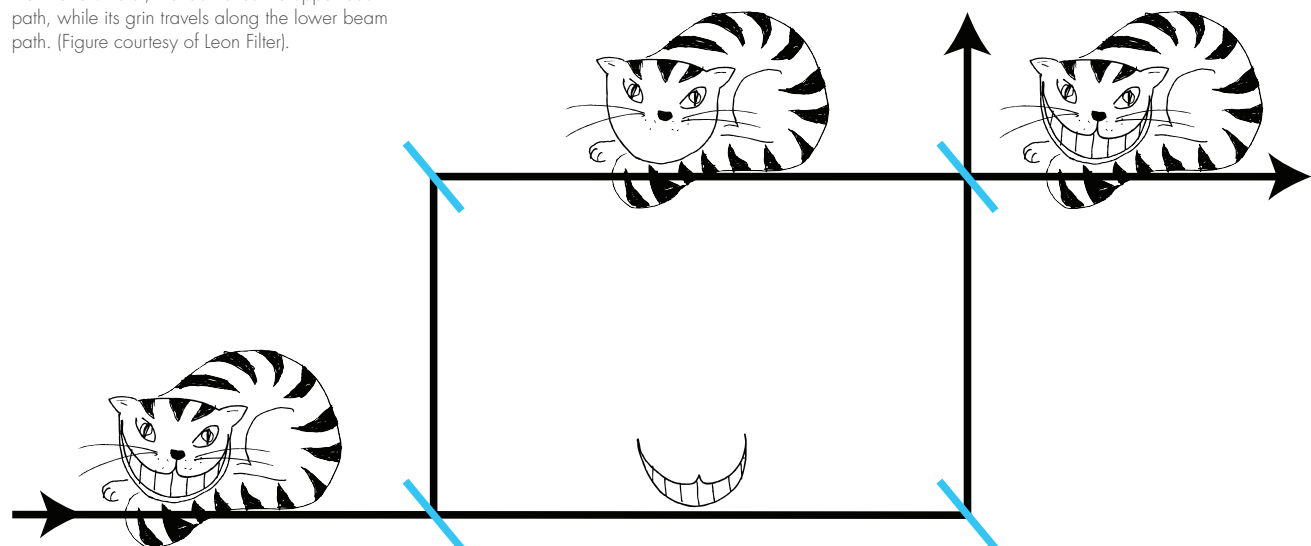


**Figure 2**

Schematic view of the experimental set-up for the observation of the quantum Cheshire Cat using single-neutron interferometry.

The only instrument available in the world to perform this kind of neutron interferometer experiment is the S18 instrument at the ILL. A schematic view of the experimental set-up is shown in figure 2 and the instrument set-up is shown in figure 3 (with the neutron interferometer in the centre).

Our aim was to get the neutrons to travel along a different path from their magnetic moment. In our experiment the neutron beam was split into two paths with different spin directions. The upper beam path had a spin parallel to the neutrons’ direction of flight, whilst the spin of the lower beam pointed in the opposite direction. In other words, the Cheshire Cat is a neutron and its grin is the neutron’s spin component along the z direction.

The neutron populations in the two paths of the interferometer were measured by inserting absorbers with high transmissivity into each path of the interferometer. In the lower beam path, the absorber had no effect; when compared to a reference measurement, no significant change could be detected. However, when placed in the upper beam path the very same absorber decreased the intensity. The measurement led us to conclude that the neutrons (the cat) took the upper beam path.

To test the location of the neutrons’ spin component (the grin), we applied small magnetic fields to the paths of the interferometer. When the field was applied to the lower beam path, the observed interference fringes changed (again in comparison to a reference measurement). In contrast, there was no effect on the measurement when the magnetic field was applied to the upper beam path; the interference fringes did not change. Obviously the neutrons’ spin component had taken the lower beam path.

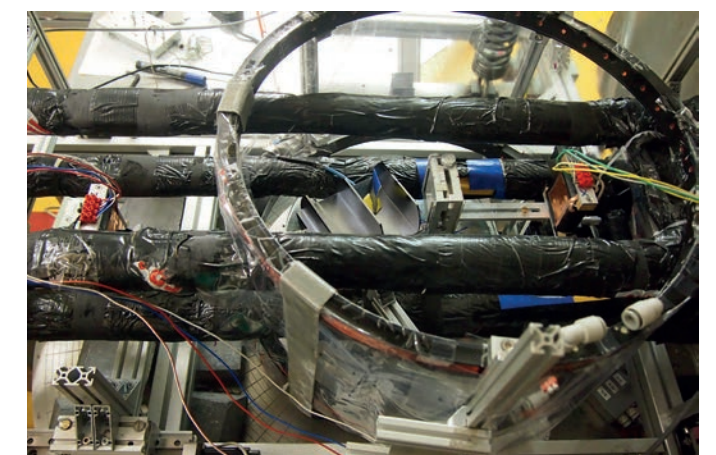
To summarise, we have shown experimentally that a weak interaction involving a coupling to the neutrons’ spatial wave function has no effect on average along the lower beam path, whereas a weak coupling involving the neutron spin wave function does have observational

consequences, on average only when the coupling takes place along this path. Consequently, any probe system that interacts with the Cheshire Cat system weakly enough will on average be affected as if the neutron and its spin are spatially separated.

Our experiment was the first realisation of this effect, which had previously only been proposed theoretically. The Cheshire Cat effect is completely general and can be applied to any quantum system. This quality could therefore make future applications of the effect possible in high-precision metrology and quantum information technology.

**Figure 3**

View of the experimental set-up at S18, with the neutron interferometer at the centre.



# NUCLEAR AND PARTICLE PHYSICS

## Neutrons constrain dark energy and dark matter scenarios

### Ultra-cold neutron facility PF2

Just five per cent! This is the proportion of the mass and energy in our universe whose particles we know and – more or less – understand. Although there have been many observations demonstrating its existence, the rest – “dark matter” and “dark energy” – remains a mystery. Many ideas about its content and nature exist, and numerous experiments worldwide, usually performed at huge particle accelerators, are trying to shed light on the unknown 95 %. But we do not always need a huge accelerator to search for new particle physics...

#### AUTHORS

T. Jenke, G. Cronenberg, A.N. Ivanov, T. Lins, H. Saul and H. Abele (Atominstut TU Wien, Vienna, Austria)  
 J. Burgdörfer, L.A. Chizhova and S. Rotter (Institute for Theoretical Physics, TU Wien, Vienna, Austria)  
 T. Lauer (FRM II, TU München, Garching, Germany)  
 U. Schmidt (Heidelberg University, Heidelberg, Germany)  
 P. Geltenbort (ILL)

#### REFERENCES

- [1] T. Jenke *et al.*, Phys. Rev. Lett. 112 (2014) 151105
- [2] T. Jenke *et al.*, Nature Physics 7 (2011) 468
- [3] P. Brax, G. Pignol, Phys. Rev.Lett. 107 (2011) 111301
- [4] A.N. Ivanov *et al.*, Phys. Rev. D 87(2013) 105013

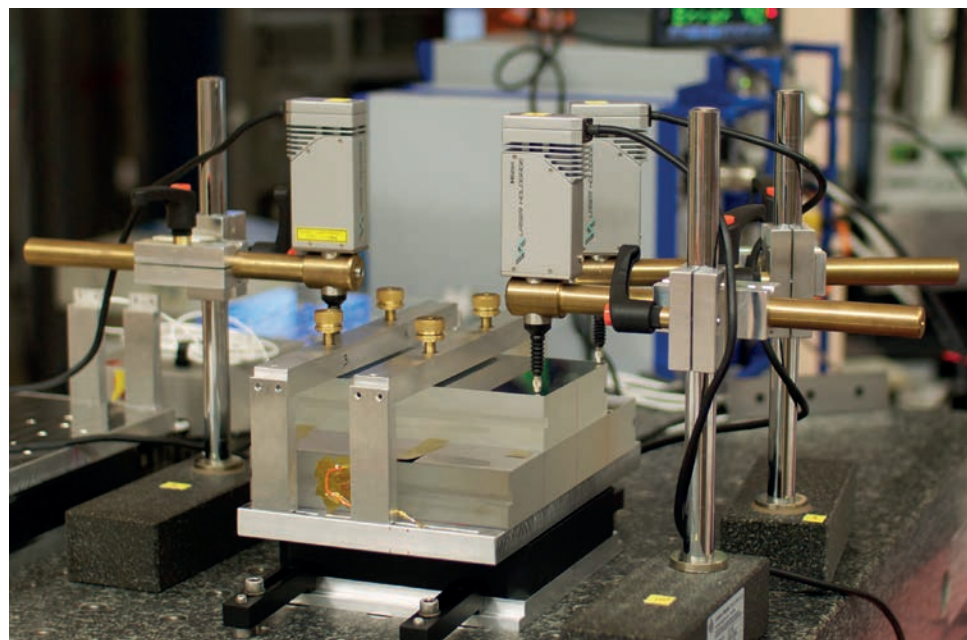
The qBounce collaboration led by researchers from Vienna University of Technology has recently published the results of extremely sensitive measurements of gravitational effects at very small distances. These experiments were performed at the ILL's ultra-cold neutron source PF2 and provide experimental limits for possible dark matter particles and/or fundamental forces related to dark energy which are a hundred thousand times more restrictive than previous estimates [1].

As in many other examples in science, the key to this order-of-magnitude improvement in sensitivity was provided by spectroscopy [2]. In the present case, the collaboration successfully applied Rabi spectroscopy to the very simple and clean quantum system of a neutron in the earth's gravitational field. This new method of gravity resonance spectroscopy translates the measurement of the energy eigenvalues of the studied quantum system into a frequency measurement. This is useful, because frequencies may be measured with incredibly high precision.

In our experiment, extremely slow, “ultra-cold” neutrons were sent into the space between two parallel horizontal mirrors serving as potential wells (**figure 1**). In contrast

**Figure 1**

The micron-precision adjustment of the neutron mirrors provides the key to the experiment. The picture shows this process. The two neutron mirrors are placed one above the other. The three linear laser gauges are then set in place and zeroed. The slit between the two mirrors is adjusted by mechanical spacers of ca. 30 microns in height. The system is fixed using four screws with an extremely fine thread, ensuring the laser gauge readings remain constant.



to the usual “particle in a box” example of quantum mechanics, the neutrons form bound quantum states in the linear gravity potential of the earth. The application of mechanical sinusoidal oscillations of the potential wells makes the neutrons jump up and down the energy levels of this “gravitational box”. Because the upper boundary condition has a well-defined rough surface, neutrons jumping up the energy ladder are likely to be scattered out of the system. In contrast, neutrons jumping down are likely to stay inside it and be detected. The transmission through the gravitational box was measured as a function of oscillation frequency and amplitude using a simple neutron counter.

By monitoring the oscillations very carefully, we observed sharp resonant dips in transmission, from which the corresponding transition frequencies were deduced. The resulting data for the transition frequencies turns out to match the predictions based on Newton's inverse-square law of gravity very closely; it can thus be considered accurate to a level of  $1 \times 10^{-14}$  eV at micron distances.

More specifically, transition frequencies in the order of a few hundred hertz are highly sensitive to all kinds of hypothetical non-Newtonian gravity effects at micron distances, because most of these extensions of Newtonian gravity evolve with different phase information.

The research focused on two particular scenarios. First, the transition frequencies measured were compared with predictions based on hypothetical chameleon fields. This particularly appealing realisation of a quintessence theory may explain the existence of dark energy without contradicting existing laboratory experiments or astronomical observations. This is explained by the screening mechanism of the chameleon field due to self-coupling – whenever the mass density of the environment is high (an experimentalist in the vicinity), the chameleon field vanishes (**figure 2**). As pointed out in [3,4], experiments with neutrons are not affected by this screening mechanism because the neutron is a fundamental particle. The resulting new experimental constraints are five orders of magnitude more restrictive than previous limits.

Second, a direct search for dark matter was performed. The underlying idea is that very light bosons might be detected through the macroscopic forces they mediate. These forces would result in deviations from Newton's inverse-square law at short distances. Here, the focus was on hypothetical particles that mediate a spin-dependent force, and on axions in particular.

For this purpose, the experiment was slightly modified. A homogenous magnetic guide field parallel to the direction of gravity was used to preserve the neutrons' spin direction. The neutron counter was equipped with a spin analyser. We then measured to determine whether transition frequencies depend on neutron spin direction – parallel or anti-parallel to gravity.



**Figure 2**

Artist's view of a chameleon that influences the bound quantum states of neutrons in the gravity field. The illustration was created by Leon Filter.

Only one day of beamtime was required to improve by a factor of thirty the previously established experimental limits using ultra-cold neutrons. This shows the enormous potential of the measurement technique; we believe that this technique can compete with the best limits over a wide range of the parameter space of axions.

In summary, the experiment described shows that gravity resonance spectroscopy could become a powerful new technique to probe new particle physics and to search for non-Newtonian gravity at short distances with neutrons. This would also include the search for hypothetical large extra dimensions and tests of the equivalence principle in the quantum regime.

# THEORY

## Acoustic excitations and elastic heterogeneities in disordered solids

A feature of glasses is their inhomogeneous mechanical response at the nano-scale, i.e. some regions are sensibly softer than others. These “elastic heterogeneities” should interfere with the vibrational excitations supported by the material which, in contrast to the case of perfect crystal, cannot be completely described in terms of phonons. We have addressed this issue by molecular dynamics simulations of a toy model, interpolating from the perfect crystal case, through increasingly defective phases, to fully developed glasses. By calculating appropriate dynamical structure factors, we have demonstrated a direct correlation between sound-waves features and the heterogeneous mechanical response at the nano-scale.

### AUTHORS

H. Mizuno (Alpes University and CNRS, Grenoble, France)  
S. Mossa (Alpes University, CNRS/INAC-SPRAM and CEA/INAC-SPRAM, Grenoble, France)  
J.-L. Barrat (Alpes University and ILL, Grenoble, France)

### REFERENCES

- [1] A. Mermet and E. Duval, *Phys. Rev. B* 58 (1998) 8159
- [2] A. Chumakov *et al.*, *Phys. Rev. Lett.* 112 (2014) 025502
- [3] L. Bocquet *et al.*, *J. Phys. Condens. Matter* 4 (1992) 2375
- [4] G. Monaco and V. Giordano, *Proc. Natl. Acad. Sci. USA* 106 (2009) 16907
- [5] H. Mizuno, S. Mossa, J.-L. Barrat, *Proc. Natl. Acad. Sci. USA* 111 (2014) 11949

Sound and heat propagate differently in crystals and amorphous solids, e.g. glasses. While the perfectly ordered crystal case is completely formalised in terms of phonons, some aspects of vibrational excitations in disordered solids still need to be clarified. Also, recently the inhomogeneous nature of the mechanical response at the nanoscale has been demonstrated in disordered solids. It is indeed possible to define “local” elastic constants, associated with coarse-grained nanometric volumes. These moduli have been found to vary in space, and to follow non-trivial distribution functions with average values corresponding to the macroscopic moduli but non-vanishing widths. These quantify the extent of the local mechanical heterogeneity of the material, at variance with the perfect crystal case, where the system responds to external stress conforming to the macroscopic moduli at all length scales. Although it is natural to speculate that vibrational excitations in disordered solids are scattered by these regions with anomalous mechanical responses [1], this hypothesis has never been demonstrated directly. In this work we have addressed exactly this point.

Recent experimental work has shown that comparing scattering experiments on glasses and the corresponding (poly-)crystalline polymorphs is extremely beneficial [2], helping to keep constant contact with the completely controlled crystalline reference case. We have followed this route and considered a smart toy model [3], constituted by a binary mixture of soft spheres with different diameters, of size ratio  $\lambda = \sigma_1/\sigma_2$ . Starting with a perfect fcc (face-centred cubic) crystal with  $\lambda = 1$ , defects are added in the form of size disorder, by simultaneously decreasing  $\sigma_1$  and increasing  $\sigma_2$  in a controlled way [3]. At a threshold value,  $\lambda^*$ , a transition to a series of amorphous structures occurs (figure 1).

We have systematically generated equilibrium system configurations spanning a wide range of  $\lambda$ , both above and below the amorphisation transition, encompassing the perfect crystal case, increasingly defective phases, and fully developed glasses. Next we have performed two independent calculations, in all cases. On one side, we have determined the probability distribution of the local moduli and extracted the corresponding standard deviations,  $\delta G$ . On the other, we directly calculated the relevant (transverse) dynamical structure factors,

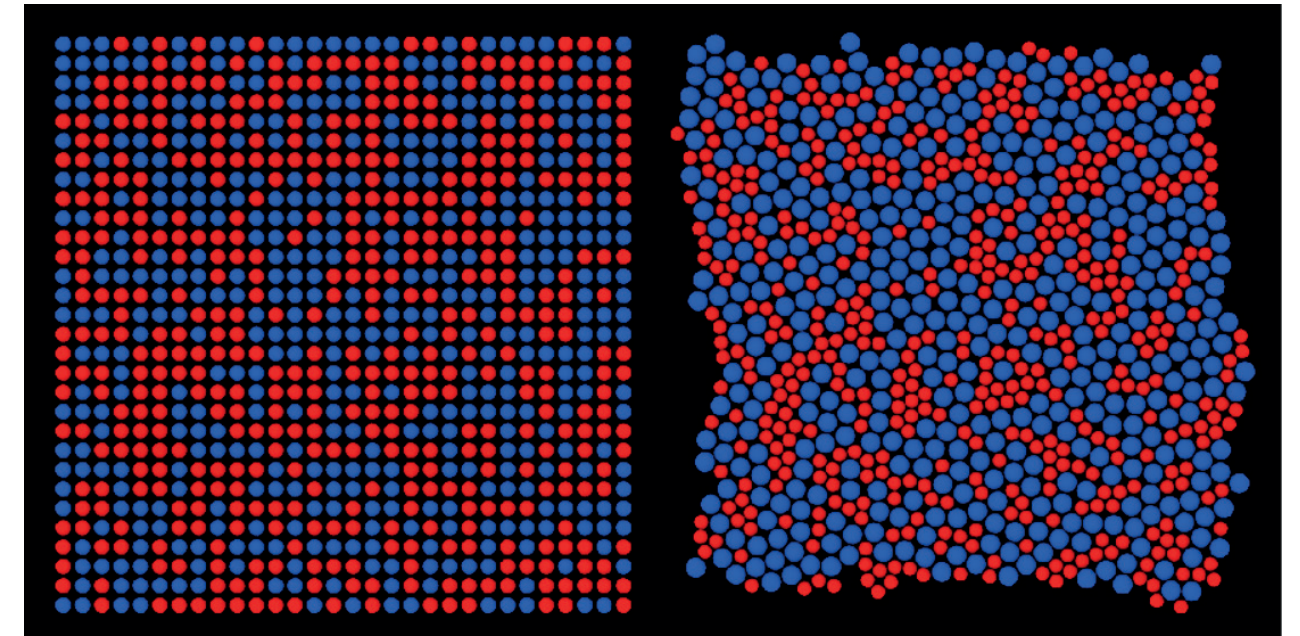


**Figure 1**

Two-dimensional representation of the simulated model (periodic boundary conditions are used). Starting from a perfect crystal (left) formed by a binary mixture of initially identical particles, the size of red particles is gradually decreased while the size of blue ones is increased. This is a well-defined method for introducing a controlled increasing amount of structural defects into the system. At a particular value of the ratio of the radii,  $\lambda$ , the system undergoes a transition to an amorphous phase (right). Configurations (positions and velocities) similar to those shown here are used to calculate directly the quantities of interest.

and characterised the vibrational excitations in terms of frequency-dependent sound velocity,  $c$ , and broadening,  $\Gamma$ , in analogy with experimental investigations [4]. From these data we also determined the so-called Ioffe-Regel frequency, quantifying the frequency limit above which the elastic continuum approximation for the acoustic excitations breaks down.

In figure 2 we show the most relevant results of our computer simulation *tour de force* [5], and plot both the broadening parameter  $\Gamma$  at two different frequencies and the Ioffe-Regel frequency  $\Omega^{\text{IR}}$ , as a function of the corresponding local elastic constants standard deviations  $\delta G$ . Remarkably, the different data all follow an exponential behaviour, with no adjustable parameters involved in these plots. These data are the first *direct* evidence that a strong correlation indeed exists among quantities relating to the nature of acoustic-like excitations and the heterogeneity of local elastic constants, in a wide range of different solid states of matter.

To conclude, we note that technology now provides the techniques to control materials' structure at the nano-scale, and some innovative applications try to degrade sound and thermal transport of nano-structured materials below the “glassy” limit. These needs clearly imply the most complete understanding of how this glassy limit behaves. We believe that our work is a significant contribution in this direction.

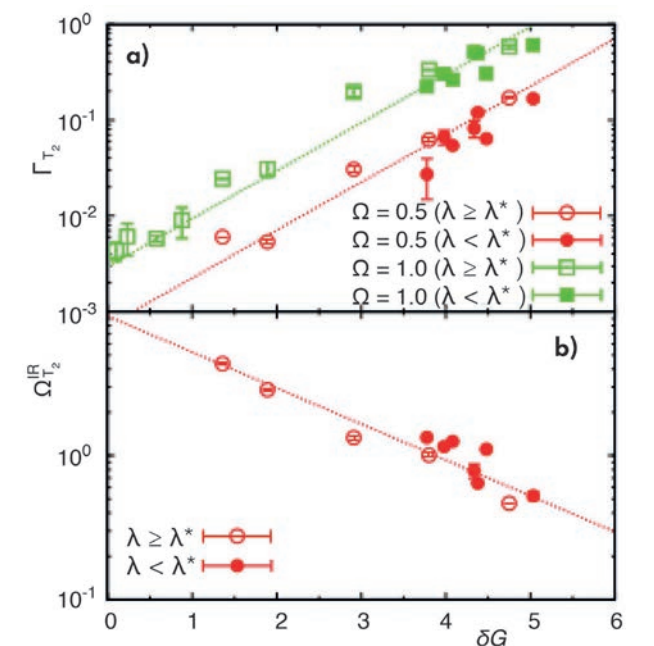


**Figure 2**

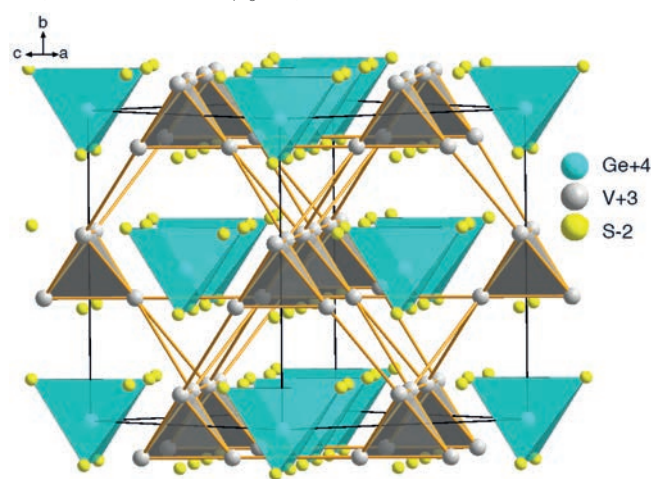
Direct correlation of features of acoustic-like excitations with local elastic heterogeneities [5]. Here we show the dependence on the extent of the elastic heterogeneities of the broadening,  $\Gamma$ , (top), and the Ioffe-Regel frequency,  $\Omega^{\text{IR}}$ , for the transverse acoustic excitations. Data are plotted versus the standard deviation  $\delta G$  of the distribution of the relevant local elastic modulus. In the top panel we plot values of  $\Gamma$  corresponding to two different frequencies,  $\Omega = 0.5$  and 1. Dashed lines are guides for the eye.

## THEORY

Orbital-ordering-driven  
multiferroicity in  $\text{GeV}_4\text{S}_8$ 

The amplitude of magnetoelectric coupling is usually directly related to the origin of ferroelectricity [1]. Whether it originates from a magnetic ordering (type II) or from more classical reasons (type I), such as Jahn-Teller distortion or presence of lone pairs, it will be large but associated with a small polarisation, or weak but associated with a larger polarisation. However, when ferroelectricity originates from an electronic instability, such as a charge order, it is possible to find together a large polarisation and a large magnetoelectric coupling [2]. In the present work we report that the  $\text{GeV}_4\text{S}_8$  compound exhibits an alternative order, namely an orbital order, responsible for simultaneous large polarisation and strong magnetoelectric coupling. This orbital ordering reorganises both the charge and the spin within the magnetic building blocks.

**Figure 1**  
Representation of the  $\text{GeV}_4\text{S}_8$  compound.



## AUTHORS

E. Cannuccia, K. Singh<sup>†</sup> and C. Simon (ILL)  
M.B. Lepetit (ILL and Néel Institute, CNRS, Grenoble, France)  
B. Corraze, E. Janod and L. Cario (IMN, Nantes University-CNRS,  
Nantes, France)  
<sup>†</sup> Present address: UGC-DAE, Consortium for Scientific Research, Indore,  
India.

## REFERENCES

- [1] S.W. Cheong and M. Mostovoy, *Nat. Mater.* 6 (2007) 13;  
K.F. Wangab, J.M. Liu, and Z.F. Ren, *Adv. Phys.* 58 (2009) 321;  
W. Eerenstein, N.D. Mathur, and J.F. Scott, *Nature (London)* 442  
(2006) 759; D. Khomskii, *Physics 2* (2009) 20
- [2] V.D. Brink and D.I. Khomskii, *J. Phys.: Condens. Matter* 20 (2008)  
434217
- [3] H. Ben Yaich, J.C. Jegaden, M. Patel, M. Sergent, A.K. Rastogi and  
R. Tournier, *J. Less-Common Met.* 102 (1984) 9
- [4] See for instance: V. Guiot, L. Cario, E. Janod, B. Corraze,  
V. Ta Phuoc, M. Rozenberg, P. Stolar, T. Cren, and D. Roditchev,  
*Nat. Commun.* 4, (2013) 1722
- [5] K. Singh, C. Simon, E. Cannuccia, M.-B. Lepetit, B. Corraze,  
E. Janod and L. Cario, *Phys. Rev. Lett.* 113, (2014) 137602
- [6] D. Bichler, V. Zinth, D. Johrendt, O. Heyer, M.K. Forthaus, T. Lorenz,  
and M.M. Abd-Elmeguid, *Phys. Rev. B* 77, (2008) 212102

The  $\text{AM}_4\text{Q}_8$  ( $A = \text{Ga}, \text{Ge}$ ;  $M = \text{V}, \text{Nb}, \text{Ta}$ ;  $Q = \text{S}, \text{Se}$ ) compounds present a lacunar spinel structure (figure 1) in which the metal atoms are located at the positions of a deformed pyrochlore structure. The magnetic building blocks are tetrahedral transition metal clusters  $M_4$ , containing one or two unpaired electrons [3]. In addition to the fascinating properties encountered in this family, such as the ability to control the Mott transition by electric pulses [4], the  $\text{GeV}_4\text{S}_8$  compound is a type I multiferroic system with a large polarisation (about  $0.75 \mu\text{C}/\text{cm}^2$ ) and a large magnetoelectric coupling [5]. The ferroelectric transition occurs at  $T_s = 32 \text{ K}$ , the system switching from cubic  $F\bar{4}3m$  to orthorhombic  $Imm2$  space groups. A commensurate antiferromagnetic order takes place at lower temperature,  $T_N = 17 \text{ K}$ , associated with a structural transition to the ferroelectric  $Pmn2_1$  space group, and a strong reduction of the polarisation amplitude. The application of a large enough magnetic field can, however, reverse the sign of the polarisation jump, which is direct evidence of the presence of strong magnetoelectric coupling [5]. The number of systems presenting such a large change in polarisation with the application of magnetic field is rather limited. Most of these compounds are of type II, with spiral spin order. A type I multiferroic, with commensurate spin order and a large magnetic field dependence of the polarisation, is a very rare compound.

A deeper examination of the structure below  $T_s$  [6] is instructive to address the origin of ferroelectricity. Indeed, the ferroelectric phase ( $Imm2$ ) shows a strong distortion of the tetrahedral clusters compared with the high temperature cubic phase ( $F\bar{4}3m$ ), with the appearance of two crystallographically different vanadium sites ( $V_1$  and  $V_2$ ) and a long and a short V-V distance. In order to better understand the origin of the ferroelectric ordering, we performed electronic structure calculations – using density functional theory (DFT) with the hybrid B3LYP functional – at the experimental geometries of both the ferroelectric phase and the closest non-polar structure. Our calculation

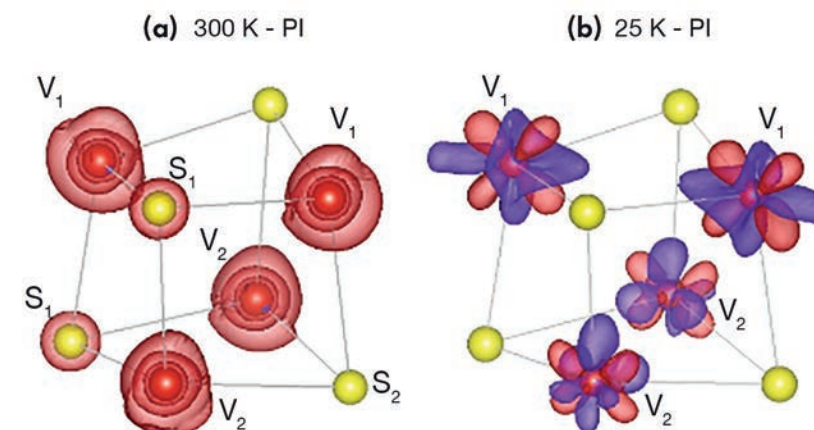


**Figure 2**

(a) Differential charge density between the non-polar structure (300 K) and the sum of atomic densities.  
(b) *Idem* for the ferroelectric structure (25 K). Purple: negative, red: positive.

of the  $Imm2$  structure reproduces the physical properties of the system (insulating state and a spin 1 per cluster). The comparison between the  $Imm2$  structure and the non-polar one tells us that the onset of the polarisation is related to a spatial rearrangement of the electronic density within the  $V_4S_4$  clusters (see figure 2 and figure 3), without any significant change in the atomic charges. Projection on the V atomic orbitals shows that this rearrangement is in fact an orbital ordering, the occupation of the  $d_{xz}$  orbital of the  $V_1$  atoms and of the  $d_{yz}$  orbital of  $V_2$  atoms being equal by symmetry in the non-polar phase and different in the polar one (see figure 3). It results in a lowering of the electronic density between the two  $V_1$  atoms, i.e. a weakening of the bond, associated with the elongation of the  $V_1 - V_1$  distance.

To better investigate the origin of the ferroelectricity, we made a calculation imposing on the electronic structure only the  $Imm2$  group symmetry operations, while the atomic positions were set as in the non-polar structure. This calculation reveals both an orbital order (despite the totally symmetric, non-polar atomic arrangement) and a weak polarisation of purely electronic origin ( $P = 1.3 \times 10^{-3} \mu\text{C}/\text{cm}^2$ ). This is a clear indication that the orbital ordering is not a consequence of the onset of the polarisation, but rather its cause. Indeed, if the onset of the polarisation was the consequence of the structural phase transition toward the polar  $Imm2$  group, this calculation would have yielded exactly the same results as when the non-polar group symmetry operations are imposed on the electronic structure. The non-polar electronic structure is thus unstable with respect to the orbital ordering, a fact that drives both the inset of the polarisation and the structural transition. The atomic displacements associated with the structural transition toward  $Imm2$  group thus only plays the role of a polarisation amplifier.

The remaining question to elucidate is the origin of this electronic instability. We thus performed an electronic structure calculation, including the whole treatment of the electronic correlation with the vanadium 3d shell (CASSCF method), on a  $V_4S_4$  cluster. The cluster was embedded in such a way as to reproduce on it the

main effects of the rest of the crystal. As with the DFT calculation on the whole crystal, this local but fully correlated calculation exhibit the orbital ordering. These results clearly show that

- the ferroelectricity is of local origin, located within the  $V_4S_4$  cluster,
- the orbital ordering is a true phenomenon and not a consequence of the improper treatment of the electronic correlation within the DFT scheme,
- it originates from the lifting of the cluster ground-state degeneracy as in a “regional” Jahn-Teller distortion,
- each  $V_4S_4$  cluster presents a dipolar moment of  $5.9 \times 10^{-3} \text{ D}$  responsible for the macroscopic polarisation.

In conclusion, the clustered lacunar spinel  $\text{GeV}_4\text{S}_8$  is a type I multiferroic compound with both a large polarisation and a large magnetoelectric coupling. These rare properties are due to the onset of an orbital order that reorganises the charge and spin within the vanadium tetrahedral clusters, but without charge transfers between atoms.

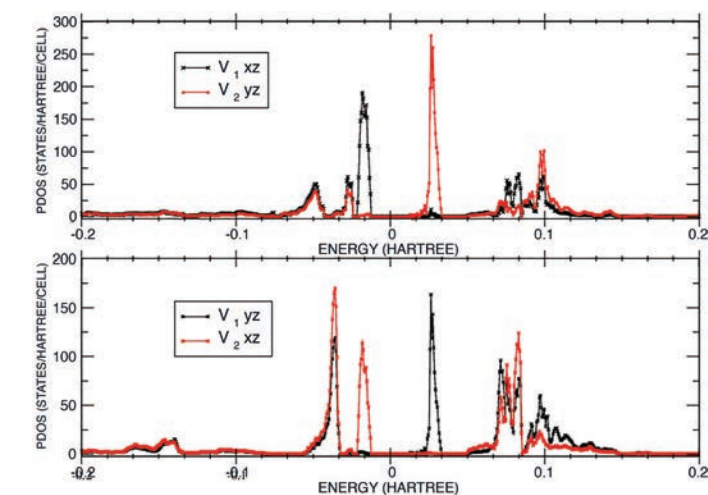


**Figure 3**

Non-polar structure calculation with only the  $Imm2$  symmetry operations imposed. Projected density of states on the  $d_{xz}$  [ $d_{yz}$ ] orbital of the  $aV_1$  atoms and the  $d_{yz}$  [ $d_{xz}$ ] orbital of the  $bV_2$  atoms that should be equal for symmetry reasons.

## THEORY

## Proton tunnelling in short hydrogen bonds

Hydrogen bonds are ubiquitous in nature, underpinning complex molecular architecture and reactions which involve proton transfer. Quantum tunnelling facilitates proton dynamics in hydrogen bonds described by a two-well potential. Short hydrogen bonds, which are more reactive, are usually described by an asymmetric single-well potential in which quantum tunnelling cannot occur. We provide experimental evidence of quantum tunnelling in one of the shortest known hydrogen bonds and an Ising model to reconcile this spectroscopic data with neutron diffraction data [1].

## AUTHORS

H.P. Trommsdorff and M.R. Johnson (ILL)  
I. Frantsuzov and A.J. Horsewill (University of Nottingham, UK)  
S.J. Ford (ILL and University of Durham, UK)  
I.R. Evans (University of Durham, UK)

## REFERENCES

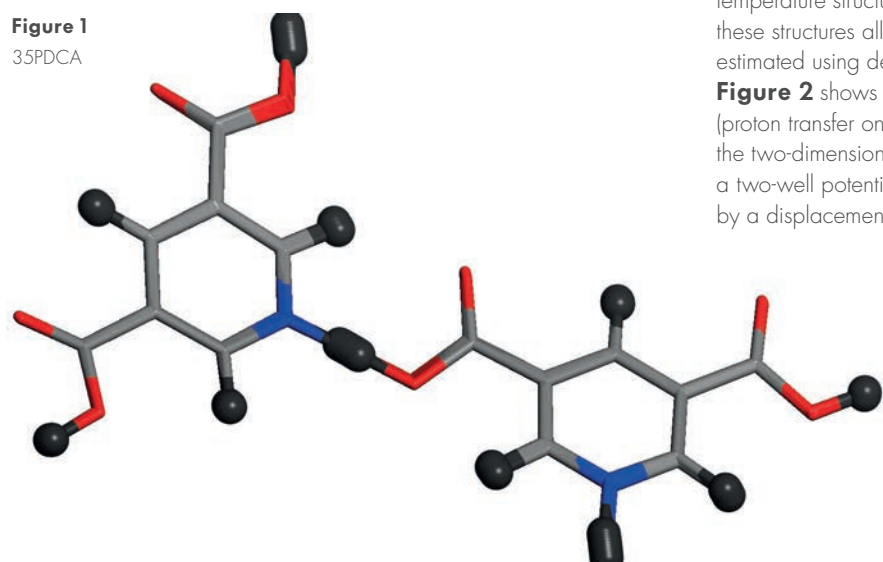
- [1] I. Frantsuzov, S.J. Ford, I.R. Evans, A.J. Horsewill, H.P. Trommsdorff and M.R. Johnson, *Phys. Rev. Lett.* 113 (2014) 018301  
[2] T.S. Moore and T.F. Winmill, *J. Chem. Soc.* 101 (1912) 1635  
[3] M. Neumann, D.F. Brougham, C.J. McGloin, M.R. Johnson, A.J. Horsewill and H.P. Trommsdorff, *J. Chem. Phys.* 109 (1998) 7300  
[4] S.J. Ford, O.J. Delamore, J.S.O. Evans, G.J. McIntyre, M.R. Johnson and I.R. Evans, *Chem. Eur. J.* 17 (2011) 14942

Hydrogen bonds have been studied for more than one hundred years [2]. Short hydrogen bonds are essential in enhancing catalytic rates, protons being almost centred and easily able to move from donor to acceptor atom. Proton tunnelling in longer hydrogen bonds has also been shown to enhance enzymatic rates through its non-classical dependence on the proton (H/D/T) mass – the kinetic isotope effect. In model systems, like benzoic acid, single crystal, nuclear magnetic resonance (NMR) and quasi-elastic neutron scattering directly reveal a non-zero proton transfer rate in the low temperature limit [3]. Quantum tunnelling in short hydrogen bonds has, however, never been demonstrated.

3,5-pyridinedicarboxylic acid (35PDCA) is an almost perfect model system in which to study proton transfer in a very short hydrogen bond (figure 1). The inter-molecular HB has an N...O distance of 2.54 Å and lies within the few percent of the shortest known N-H...O hydrogen bonds. The proton is almost centred and is clearly observed in neutron diffraction to migrate from the donor N at low temperature to the acceptor O at room temperature [4]. At 200 K the proton is, on average, centred. Since the proton migrates completely from donor to acceptor, the skeletal change accompanying proton transfer can be estimated from the difference between low and high temperature structures. Linear interpolation between these structures allows the potential energy surface to be estimated using density functional theory calculations.

Figure 2 shows that the one-dimensional (1D) potential (proton transfer only) is a single asymmetric well, but that the two-dimensional (2D) potential energy surface displays a two-well potential when proton transfer is accompanied by a displacement of the molecular skeleton.

Figure 1  
35PDCA



The proton transfer rate has been investigated on a single crystal of 35PDCA using NMR. The dependence of  $\tau_c^{-1}$  at low temperature in figure 3 demonstrates quantum tunnelling. At  $T < 77$  K,  $\tau_c^{-1}$  is virtually independent of temperature, levelling off at  $\tau_c^{-1} \approx 8 \times 10^7$  s<sup>-1</sup>, while below 91 K there is a clear deviation from the temperature dependence of a classical Arrhenius process. At higher temperature the apparent dynamical rate saturates above 110 K, whereas it could be expected to continue to increase given that various techniques (diffraction, nuclear quadrupole resonance (NQR), vibrational spectroscopy) report the crossover from donor to acceptor species at 200 K. Similarly, the temperature dependence of the spectral density amplitude shows a clear maximum at 105 K.

The apparent discrepancy between the temperature-dependent NMR and neutron diffraction data is addressed in terms of the NH...O and N...HO domains (populations  $p(N)$  and  $p(O)$  respectively), using a 1D Ising model in which the two hydrogen bond states are treated as positive and negative unit spins, i.e. proton transfer equates to inverting one spin. The ground state depends on the sign of the coupling term  $J$ : a 'ferro' ground state, pure NH...O or N...HO domains, is obtained for  $J < 0$ . An energy bias  $B < 0$  favours the NH...O ground state. The energy of this system of  $n$  spins is described by the equation

$$E = \sum_i^n (Js_i \cdot s_{i+1} + Bs_i)$$

which is solved numerically in a Monte Carlo simulation in order to analyse the domain and domain wall (DW) populations. Figure 4 shows the behaviour for an energy bias of  $B = -100$  K and a coupling of  $J = -20$  K, giving the energy cost ( $-2B/T - 4J$ ) of 280 K for transferring one proton at low temperature (0 K), in good agreement with calculations. The crossover temperature, corresponding to  $p(N) = 0.5$ , occurs at 200 K.

In order for the maximum in the spectral density amplitude, corresponding to the maximum of  $p(N)p(O)$ , to be shifted to a temperature lower than 200 K, we reason that neither the N...HO phase nor the domain walls contribute to the measured spin-lattice relaxation, their proton dynamics being, respectively, slower and faster than can be sampled by the experiment. The resulting product ( $p(N)p(DW)$ ),  $[p(N)p(O)]$  is a more sharply peaked function with a maximum just above 100 K, in good agreement with the experimental data.

The results presented here demonstrate that quantum tunnelling occurs in one of the shortest known hydrogen bonds and should therefore be considered as a mechanism for proton transfer in all hydrogen bonds.

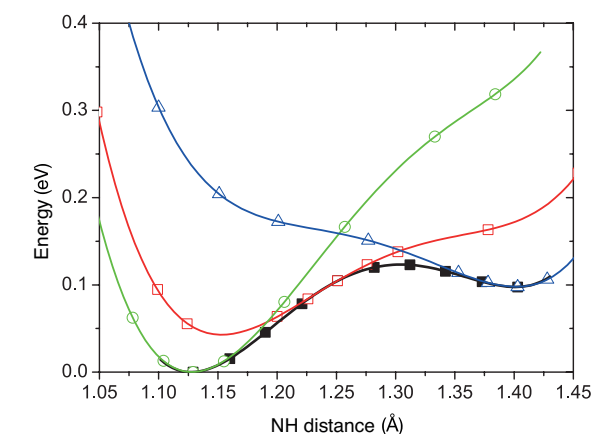


Figure 2

Two-well potential along the linear path (full squares). Single-well potentials obtained from 1D mapping (proton co-ordinate only) of the potential energy variation for the low temperature (open circles) and high temperature (open triangles) structures and one intermediate structure (open squares).

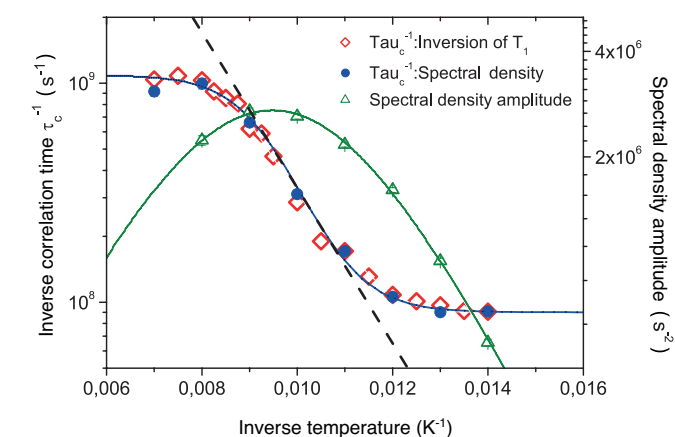


Figure 3 fig 3 x-axis - should figures have commas?

Left axis: Inverse temperature dependence of the proton transfer rate,  $\tau_c^{-1}$ . The dashed line shows the temperature dependence of the proton dynamics for a classical Arrhenius process.  
Right axis: Spectral density amplitude.

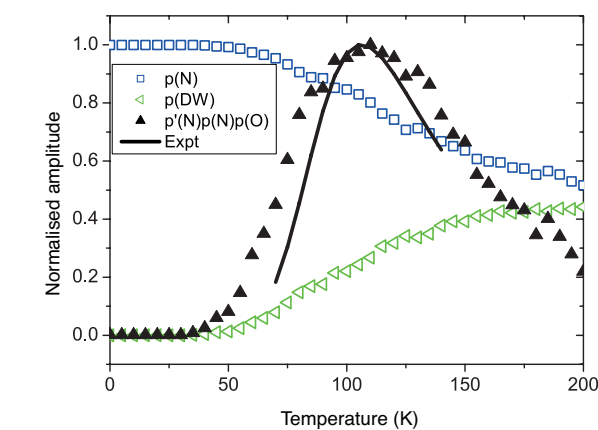


Figure 4

Normalised amplitudes from the Ising model showing the switch-over in NH...O and N...HO populations at 200 K and the corresponding products of populations ( $p(N)$ ,  $p(O)$ ) and domain walls (DW). Note that  $p'N = p(N)p(DW)$ .

fig 4 y-axis - should this have a measurement unit?

# MILLENNIUM PROGRAMME AND TECHNICAL DEVELOPMENTS



MILLENNIUM PROGRAMME	80
NEW EXPERIMENTAL TECHNOLOGIES	82
TECHNICAL DEVELOPMENTS	86

**A**s the world's leading facility in neutron technology and science, the ILL plays a crucial role in many technical developments. The Millennium Programme (MP) has had a major impact over the last 15 years on instruments and instrumentation in this respect. The MP is now coming to an end and the time has come to assess its results in terms of both scientific output and technological innovation.

In scientific terms, the MP has brought exciting new capabilities with a new set of instruments. The list is long, but we should at least mention D33, the small-angle diffractometer, with its new time-of-flight option and four side detectors which broaden the Q dynamic range by an order of magnitude. There is also IN16B, a backscattering spectrometer providing simultaneous increases in both energy range and flux by one order of magnitude. And LAGRANGE, the spectrometer with flux allowing samples of challengingly small size to be measured. LADI too has been reinvigorated, providing novel capabilities in protein structure determination. And ThALES, almost last, but not least, a new triple-axis cold neutron spectrometer under commissioning as I write, in an enhanced guide position and sporting a brand new monochromator.

But instruments need neutrons, and neutrons need guides. The MP has therefore also concentrated on a new constellation of guide and detector infrastructure, designed to streamline the delivery of neutrons up to and across each new instrument: innovative guide technology, new neutron-focusing optics and beam-shaping facilities, monochromators, optimised detectors and so on. In parallel with this, a campaign across all the services to standardise parts and equipment has brought major savings in terms of both finance and operator input (for guide alignment and instrument control software, for instance). The end result of course is data, ever more data – and the ILL has now modernised its data policy to ensure data management procedures that are second to none.

Our achievements under the Millennium Programme are now set to cross frontiers: the benefits will be transferred to other neutron facilities through agreements on the supply of high-tech instrumentation – detectors, monochromators and polarisation analysis devices. The Programme ends in 2015, but only to be transformed into the feasibility phase of Endurance, the new programme inspired by Millennium, to ensure the continuous renewal of the ILL's scientific resources. The Endurance programme will design and deliver nine new instruments between 2016 and 2021, and four others yet to be defined for a second phase.

***Our achievements under the Millennium Programme are now set to cross frontiers but only to be transformed into the feasibility phase of Endurance.***

The plans for Endurance will cover the whole range of instrumentation (diffractometers for very small samples and extreme-condition measurements, nuclear physics, time-of-flight spectrometers and reflectometers). It will benefit from the high levels of expertise available at the institute across the technical spectrum (guides, optics and detectors, electronics and software), and from the technical and scientific experience of our Instrument Responsibilities. We are confident that Endurance will ensure that the entire scientific programme at the ILL exploits to the full the ILL's undoubted advantage – the most intense neutron source in the world. Our Associates and Scientific Members can be assured that the ILL will remain the reference for neutron science and technology for the next ten years at least.

**Charles Simon**  
Associate Director

# MILLENNIUM PROGRAMME

## Millennium Programme 2014

In 2014, work on the Millennium Programme once again progressed at an impressive pace. All the existing instruments of the guide hall ILL22 were rebuilt and construction of the new instrument ThALES, which is located on a branch of the guide H5, was completed. D16 and SuperADAM were put back into user operation, while D22 and IN15 were made ready for commissioning. Work also began on the construction of a new reflectometer, D50, dedicated to industrial research, as well as that of the wide-angle spin-echo spectrometer WASP.

**AUTHOR**  
C. Simon (ILL)

The cold neutron triple-axis spectrometer ThALES, which was constructed in co-operation with the Charles University of Prague, is now in the commissioning phase. The first measurements have been very promising both in terms of flux (10 times higher than its predecessor) and background (similar to the previous instrument). Polarised options and various monochromators have still to be installed. **Figure 1** shows the new instrument.

The guide hall ILL22, which houses the full set of instruments of the guide H5, is now back in operation after being closed for an entire year while it underwent a complete refurbishment. The new structure of the guide H5 has made it possible to truly optimise the flux on each of the seven instruments (including ThALES, which is also fed by the same guide). The neutrons produced by the horizontal cold source benefit enormously from the new design. Gains in neutron flux at the sample range from 1.3 to 10, depending on the instrument. The diffractometer D16, which is already available again for user operation, will take full advantage of this factor-of-10 increase (**figure 2**). The collaborative research group (CRG) reflectometer SuperADAM, operated by Sweden, has been completely upgraded and received its first users in December (**figure 3**). The small-angle scattering spectrometer D22, with its new collimation, and the brand new version of the high-resolution spin-echo instrument IN15, with its new precession coils, are ready to be commissioned in April.

A new reflectometer D50, devoted to industrial use, will be ready for commissioning in September/October in partnership with the Grenoble-based nanoelectronics initiative "IRT NanoElec". The construction phase of the wide-angle spin-echo spectrometer WASP will continue in 2015, with commissioning scheduled for 2016. The cancellation by its consortium of the project to build the instrument CryoEDM has left a free position on the H5 guide for a cold neutron instrument.

The year 2014 was one of the most productive of the Millennium Programme so far, with the construction of seven instruments. This next one, 2015, promises to be very fruitful for the user programme, which will be able to take full advantage of the availability of six of the seven new Millennium Programme instruments.

**Figure 1**  
The secondary spectrometer of ThALES

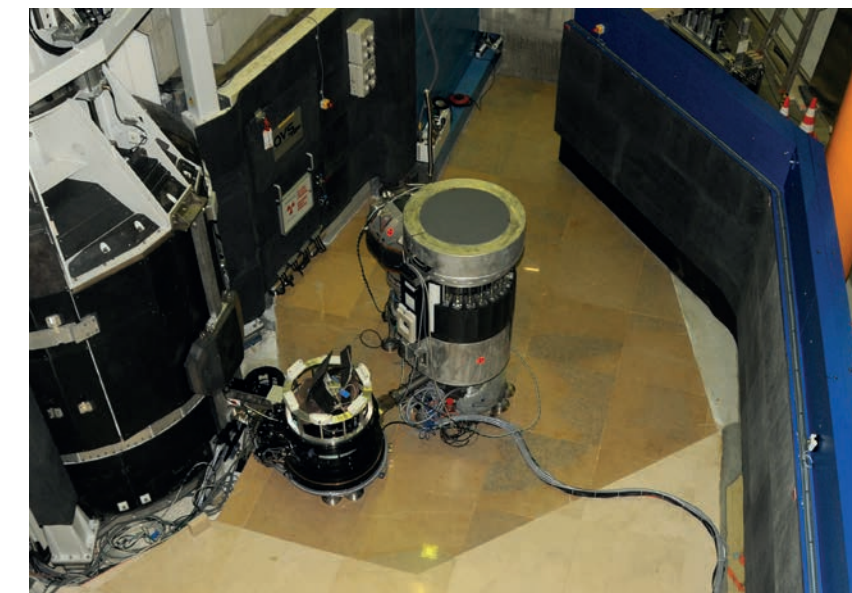


**Figure 2**  
The secondary spectrometer of D16

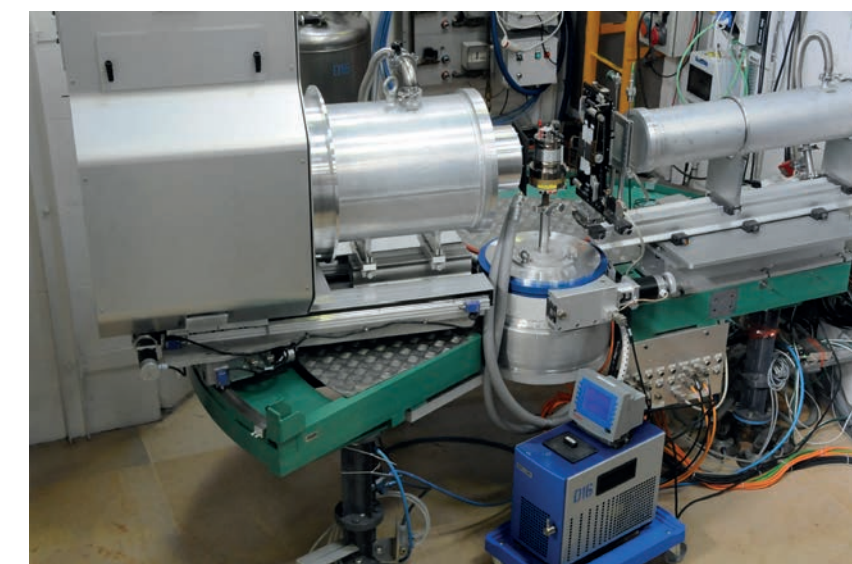


**Figure 3**  
The secondary spectrometer of SuperADAM



## NEW EXPERIMENTAL TECHNIQUES

### Novel multiple-beam very-small-angle neutron scattering (VSANS) using a conventional SANS instrument

This paper describes a novel technique to produce multiple neutron beams that focus on the sample and allow very-small-angle neutron scattering (VSANS) measurement to be made using a conventional small-angle neutron scattering (SANS) instrument. This extends the range of material length scales able to be studied by almost one order of magnitude to greater than  $1\ \mu\text{m}$  (and scattering vectors down to  $|q| = 10^{-4}\ \text{\AA}^{-1}$ ), with potential gains in intensity of up to two orders of magnitude. The technique uses an optical 'trick' allowed by the intrinsic properties of the neutron guide system, source and sample apertures with no additional optical devices or precise aperture array alignments. The technique naturally lends itself to the study of small samples or small sample areas and is a major advantage over the conventional multi-pinhole VSANS method.

#### AUTHORS

C.D. Dewhurst and I. Grillo (ILL)

#### REFERENCES

- [1] C.D. Dewhurst, *J. Appl. Cryst.* 47 (2014) 1180
- [2] C.D. Dewhurst, *Meas. Sci. Technol.* 19 (2008) 034007
- [3] H. Graetsch and K. Ibel, *Phys. Chem. Minerals* 24 (1997) 102

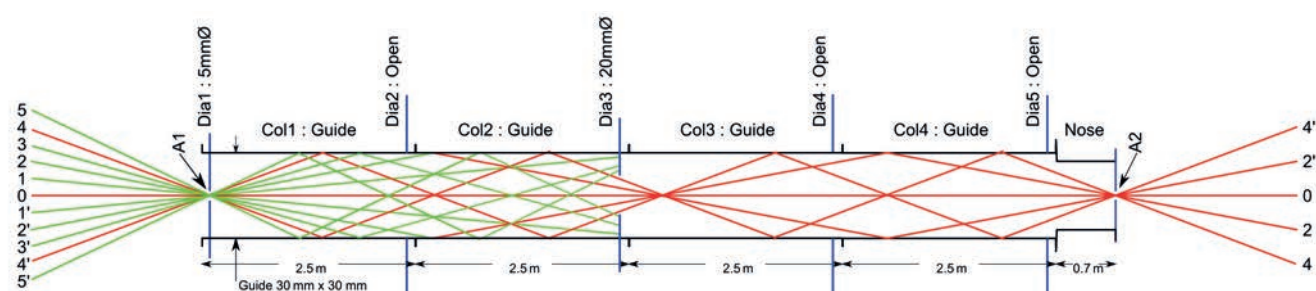
Small-angle neutron scattering (SANS) is a well-established and powerful technique used to study material or magnetic structures in the size range of about  $10\ \text{\AA}$  to  $1000\ \text{\AA}$ . The broad applicability of the technique stretches from the scientific fields of molecular biology and soft matter to fields of materials science, physics and magnetism. Access to the smallest scattering vectors,  $q$ , allows structural information to be obtained from 'large' material structures bridging the gap between scattering and surface only microscopy techniques.

Two main techniques, ultra-small-angle neutron scattering (USANS) and very-small-angle neutron scattering (VSANS), have been developed to resolve even smaller scattering angles. The VSANS technique produces multiple, finely collimated neutron beams defined by mask arrays of pinholes covering a large source neutron guide and defining multiple beams at the sample. A series of precisely positioned intermediate masks with converging geometry are placed between the source and sample masks to eliminate cross-talk and allow only beams that converge on a single spot on the neutron detector. A major drawback is that the technique requires large, spatially homogeneous samples. It also suffers from rather severe alignment problems associated with the cross-talk masks and must be aligned for each wavelength due to the effects of gravity.

**Figure 1** shows schematically the layout of the collimation section of the D33 SANS instrument. In regular operation, collimation distances of between  $12.8\ \text{m}$  and  $2.8\ \text{m}$  can be selected by the addition or removal of four  $2.5\ \text{m}$  sections of neutron guide [Col 1 to 4]. **Figure 1** shows a particular set-up with the final beam 'nose' of the instrument shortened to only  $0.7\ \text{m}$  in order to allow multiple neutron beams out of the collimator at relatively high angles. With the detector now positioned at a distance much larger than the shortest collimation length, the beam profile can be magnified onto the detector and is essentially unusable for performing regular SANS measurements. If the first

**Figure 1**

Schematic diagram of the collimation and aperture system of the D33 SANS instrument. The particular configuration depicted allows 25 finely collimated beams in two dimensions containing the  $0^{\text{th}}$ ,  $2^{\text{nd}}$  and  $4^{\text{th}}$  order neutron trajectories (red).



diaphragm, Dia 1, is now reduced to the smallest pinhole ( $A1 = 5\ \text{mm}$  on D33), and a suitably small sample aperture ( $A2 = 2\ \text{mm}$ ) is chosen, then the magnified beam profile is resolved into a quasi-regular array of well-separated beam spots shown in **figure 2** and depicted by the ray tracing in **figure 1**. The angular divergence of the beams,  $\Delta\theta$ , remains determined by the source, the sample apertures  $A1$  and  $A2$  and their separation.

**Figure 2a** shows the beam spot pattern measured on D33 for a neutron wavelength of  $14\ \text{\AA}$ , with all the neutron guides in the collimation [Col 1 to 4] in the 'in' position and for source and sample diaphragms,  $A1 = 5\ \text{mm}$   $\varnothing$  and  $A2 = 2\ \text{mm}$   $\varnothing$ , a short beam nose of  $0.7\ \text{m}$  and with the  $64\ \text{cm} \times 64\ \text{cm}$  ( $256 \times 128$  pixel) multi detector positioned at  $15\ \text{m}$  from the sample aperture. The variation in intensity over the spot pattern comes from the reflectivity and number of reflections for beams of a given angle back to the neutron source, while the regularity of the spot pattern indicates a good alignment of the D33 guide system through the instrument. **Figure 1** shows that reducing Dia 3 to  $20\ \text{mm}$   $\varnothing$  blocks beams 1, 3 and 5. In two dimensions this gives 25 regularly spaced beams on the detector, as shown in **figure 2b**. The intensity of the 25 beams is measured here to be about 10 times that of the central beam.

Inserting a sample of opal into the instrument configured to provide 25 finely collimated beams results in the two-dimensional (2D) scattering pattern shown in **figure 3a**. The regular arrangement of the lattice of silica spheres in the opal sample gives rise to diffraction and a Bragg peak at  $q = 3.76 \times 10^{-3}\ \text{\AA}^{-1}$ , seen as a Debye-Scherrer ring of scattering intensity due to the sampling of a large number of randomly oriented, individual micro crystallites [3]. Using multiple beams the resulting data on the area neutron

detector consists of multiple diffraction images which extend and overlap those produced by neighbouring beams. It is desirable to extract the one-dimensional (1D) scattering function of intensity (cross-section) vs.  $q$  from the overlapping 2D scattering patterns. The most simple method is to neglect the contamination due to the overlap between neighbouring patterns or assume that it is small such that each pattern can effectively be numerically cut-and-pasted together to create a single 2D scattering function of limited dynamic range but resembling that of conventional SANS data. The second method involves finding the 1D function that when expanded to 2D and weighted for the intensities and positions of the multiple beams satisfies the measured 2D data. The problem is essentially that of a great many simultaneous equations, the same number as the detector pixel data (e.g.  $256 \times 128 = 32\ 768$ ), and a number (e.g. 200 in this case) of parameters to solve for. The results of these two methods are shown in **figure 3b** and are described in detail in [1].

The rather novel and simple manner in which to extract more than a few hundred individual, finely collimated beams can be applied to most conventional SANS instruments with little or no modification or additional instrument components. The high degree of collimation allows scattering measurements to be made in the VSANS range down to  $q$  values approaching  $10^{-4}\ \text{\AA}^{-1}$ , thereby decreasing the accessible lowest  $q$  values by nearly one order of magnitude. The approach described is rather simple, with no intermediate masks and only two pinholes to define the beams. The technique is particularly suited to operation in time-of-flight (TOF) mode, and as such may be applicable as an instrument concept suitable for the next generation of neutron sources such as the European Spallation Source (ESS).

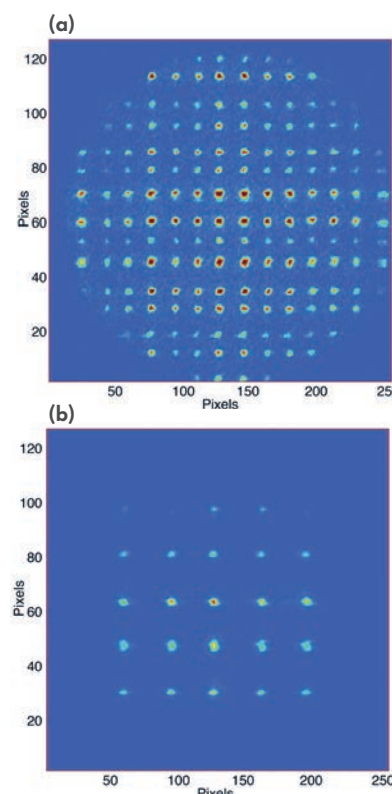


**Figure 2**

Measured multiple beam spot patterns for **a)** all beams allowed through the D33 collimation. **b)** 25 beams extracted from the D33 collimation for the instrument configuration depicted in figure 1.

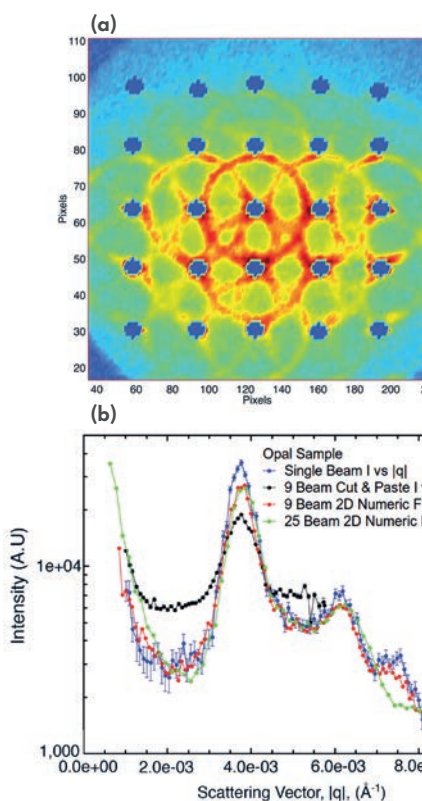


**Figure 3**

**a)** Scattering data from an opal sample measured using 25 beams on D33, showing clearly the first-order Debye-Scherrer Bragg ring at  $|q| = 3.76 \times 10^{-3}\ \text{\AA}^{-1}$ . **b)** One-dimensional scattering function measured using a single beam and extracted from the two-dimensional 9-beam and 25-beam data.

??

y-axis - should A.U be in CAPS

## NEW EXPERIMENTAL TECHNIQUES

### Single-axis acoustic levitator for structure measurements of liquids and aqueous solutions

A single-axis acoustic levitator device is now available at ILL for the user community. This apparatus permits the levitation of a solid or liquid sample by acoustic waves enabling non-contact positioning and manipulation. It also avoids sample contamination or parasite effects driven by the sample container interactions.

#### AUTHORS

V. Cristiglio and I. Grillo (ILL)  
A. Novikov and L. Hennet (CNRS-CEMHTI, Orléans, France)

#### REFERENCES

- [1] S. Krishnan, J.J. Felten, J.E. Rix, J.K.R. Weber, P.C. Nordine, M.A. Beno, S. Ansell and D.L. Price, *Rev. Sci. Instrum.* 68 (1997) 3512
- [2] C. Landron, X. Launay, J.C. Rifflet, P. Echegut, Y. Auger, M. Ruffier, J.-P. Coutures, M. Lemonier, M. Gailhanou, M. Bessiere, D. Bazin and H. Dexpert, *Nucl. Instrum. Methods Phys. Res. B* 124 (1997) 627
- [3] R.J.K. Weber, C.A. Rey, J. Neufeind and C.J. Benmore, *Rev. Sci. Instrum.* 80 (2009) 083904
- [4] K.J. Fontell, *Colloid Interface Sci.* 44 (1973) 318

Acoustic levitation can be combined with various analysis techniques for the study of the temperature-dependent structure and the kinetic of liquids at low melting point, in order to study soft matter systems, including protein aggregation in solution and biological samples.

It is known that at low temperatures, heterogeneous nucleation by the container limits the ability to supercool liquids below their equilibrium melting point or to make supersaturated solutions. In the past, various container-free sample handling techniques have been developed to overcome these problems. Of these, the acoustic levitation has the large advantage that liquid droplets of pure solvents, suspensions or solutions can be levitated very easily, held up by the force exerted on the sample inside a stationary ultrasonic field to compensate for gravity [1-3].

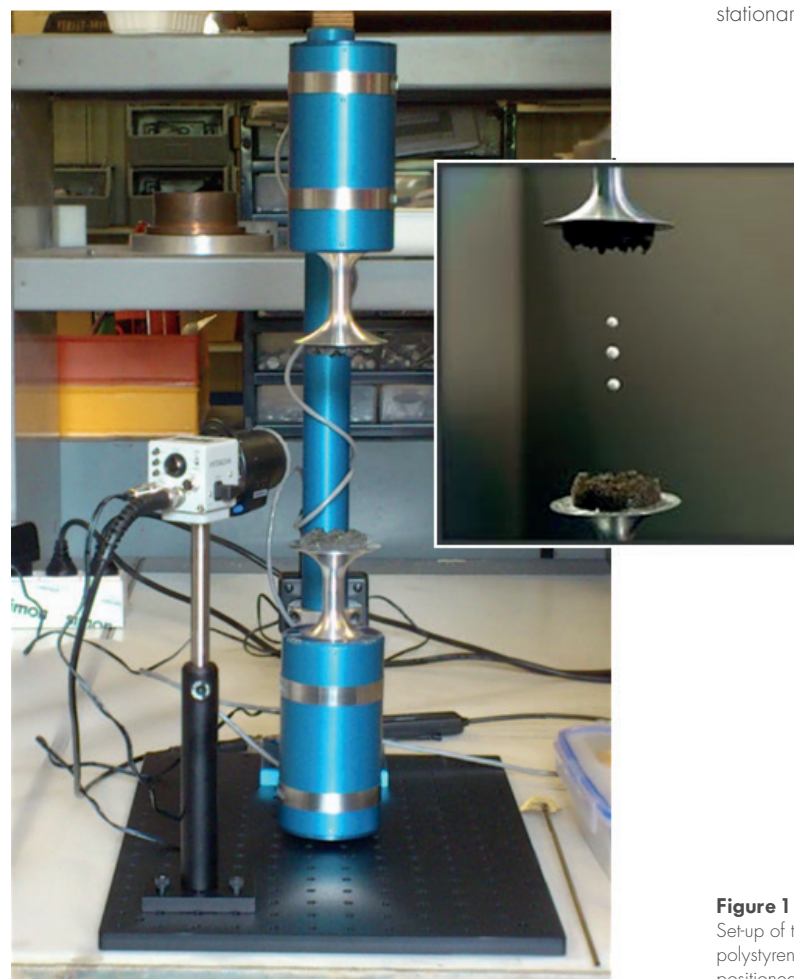


**Figure 1**  
Set-up of the acoustic levitation device. In the inset three polystyrene balls, trapped in the acoustic field, are positioned in the different interference nodes.

The single-axis acoustic levitator device available at the ILL is shown in **figure 1** (see [3] for a full description of it). Two opposed transducers operated at a frequency of 22 kHz generate a sound field and a single droplet is held in a node of a standing acoustic wave.

We can control the sample position by electronically adjusting the relative acoustic phases, enabling the levitated object to be moved along the axis of the levitator. Solids and liquids samples with size range of 1-3 mm are introduced from a small syringe and can be cooled or warmed with a gas stream and a heating coil to cover a temperature range of about -40 °C to +100 °C.

To help the sample positioning and to record images and video we use a high-speed imaging camera. The device is relatively compact and can be easily integrated into most of the ILL diffractometers and small-angle neutron-scattering (SANS) machines. Further developments will allow operation in a variety of gaseous atmospheres and controlled humidity conditions.

The acoustic levitator was originally designed to study the evaporation rate of pure solvent droplets suspended in a dry gas, but was later extended to studies of solution droplets. Evaporation of the solvent during levitation gradually decreases the volume of the droplet and therefore increases the corresponding concentration of the solute. This allows us to study volume-free phenomena like aggregation and crystallisation *in situ*, and to quickly find suitable crystallising conditions.

At large-scale facilities, until recently it was used only at synchrotron sources for the purpose of studying soft matter systems, including protein aggregation in solution, and other materials science applications.

Despite the small quantities of product that it is possible to suspend (just a few tens of nanolitres in volume), the high performances of neutron instruments make it possible to monitor fast container-less reactions *in situ*, providing detailed molecular and structural information.

Preliminary kinetics tests have been carried out on the SANS instrument D33. A 1 mm diameter diaphragm was placed in front of the levitating droplet and one minute measurements were repeated over a half-hour period. **Figure 2** shows the evolution over time of the scattered intensity of a 1 vol % solution of AOT, a double-chain anionic surfactant [4]. The acoustic wave induces the transition from micelles to a swollen lamellar phase, which then dehydrates with time, as evidence with the shift of the Bragg peak position to a higher  $q$ .

It is anticipated that future experiments at the ILL will use the acoustic levitation set-up to examine the drying of pharmaceutical formulations of proteins, in order to understand more about the behaviour of a protein during the drying process, its stability or instability and particle morphology. These studies could generate enormous interest in many research institutes and industrial research laboratories that develop new technologies for biological agents to market protein-based therapeutics.

The main difficulty in this domain is maintaining the safety and efficacy of the protein solutions throughout the drug product development process and during its storage. With the single droplet drying methodology, we can investigate the drying behaviour and kinetics of proteins formulations by looking at the nanoscale changes.

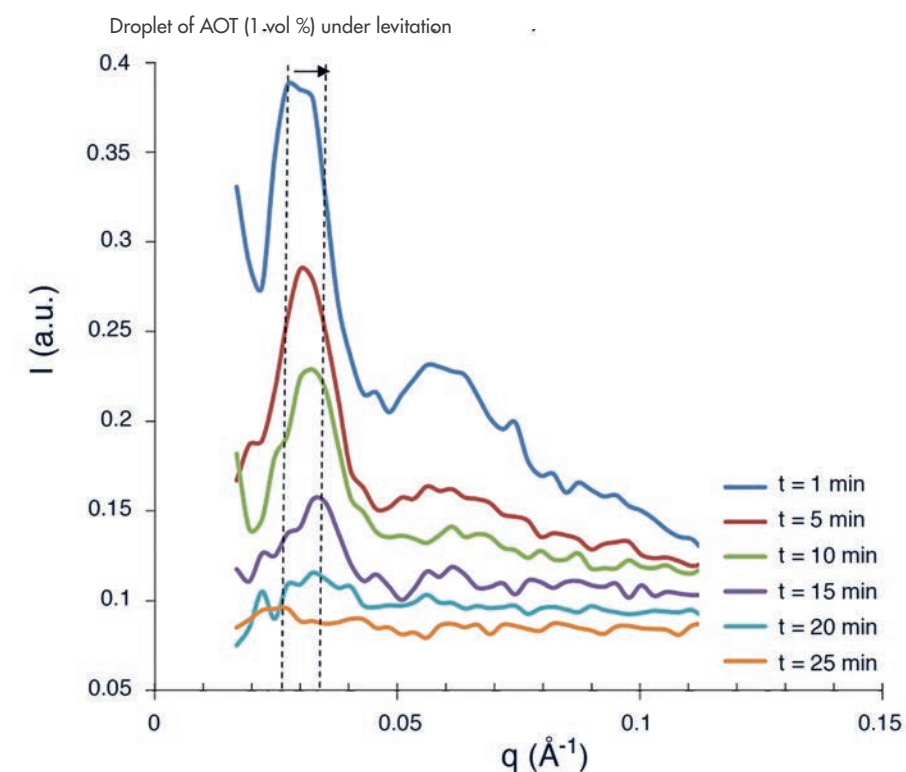


**Figure 2**  
Fast kinetics measurements of 1 vol % solution of a double-chain anionic surfactant AOT carried out on the SANS instrument D33.

## TECHNICAL DEVELOPMENTS

### Electronic renewal of the D11 detector

The D11 detector readout electronics was changed during the 2013-14 long shutdown as part of a larger electronics-renewal programme. The basic building block of the new system is the MCC-v2 module which contains a new FPGA<sup>1</sup> and a new signal processing. The MCC-v2 can be programmed and combined in different structures in order to realise different functions. On the instrument D11, all the functionality can be included in one single module. On other instruments, such as D4, D16 and D20, multiple modules are used.

#### AUTHORS

P. Van Esch, P. Lindner, M. Platz and R. Schweins (ILL)

The D11 detector is a bi-dimensional, multiwire, proportional gas chamber detector (MWPC), in which a neutron is detected by nuclear reaction with a <sup>3</sup>He nucleus, giving rise to a "charge cloud" in the detector. This event in the MWPC gives rise to tiny electrical signals on a few "X-wires" and a few "Y-wires". Every X-wire and every Y-wire has a dedicated amplifier, and the amplified and discriminated logic signals of all the wires are sent to the MCC-v2 module. In that module, the different X-wire signals are clustered together in an X-wire event cluster, corresponding to a neutron impact. In the same way, a Y-wire event cluster is formed. The data within an X-wire cluster allow for an estimation of the centre of gravity of the X position, while the data within the Y-wire cluster allow for an estimation of the centre of gravity of the Y position of a given neutron event. A coincidence algorithm groups together the X and the Y positions into a two-dimensional position, which is an estimate of the centre of gravity of the impact charge cloud.

This centre of gravity calculation allows us to have a finer-grained two-dimensional image than the physical two-dimensional grid defined by the wires of the MWPC. In this case we opted for a factor of two improvement in definition. As such, the original 128 x 128 image can be turned into a 256 x 256 image. However, this does not mean that the image resolution has improved by a factor of two. The image resolution is a function of the physics of the detector (especially the size and the asymmetry of the charge cloud of the <sup>3</sup>He reaction). The higher definition allows one to exploit fully the physical limits of the detector, without limiting *a priori* the resolution of the wire step of the detector.

This improvement of the detector in terms of a finer-grained two-dimensional picture is illustrated by the measurement of a concentrated solution of large microgel particles with added linear polymer in toluene (**figure 1**).

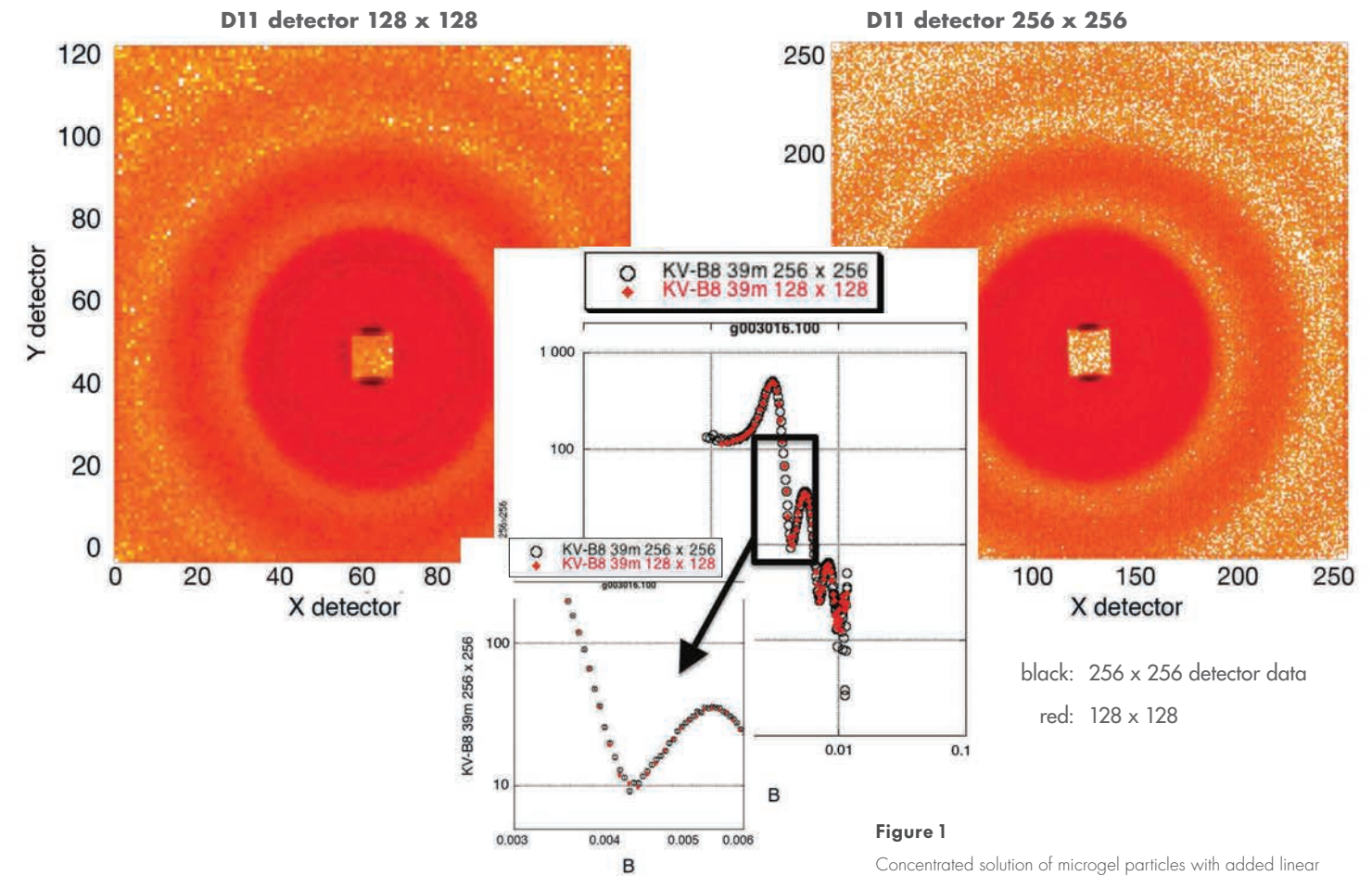


**Figure 1**

Concentrated solution of microgel particles with added linear polymer in toluene (D11 TEST-2369, E. Bartsch *et al.*, University of Freiburg).

The small-angle scattering of this system is a superposition of the pronounced structure factor due to the high microgel concentration (peak at low momentum transfer  $Q$ ) and the form factor of the spherical particles (subsequent minima towards higher  $Q$ ).

The left-hand side of **figure 1** shows the detector image for 128 x 128 data; the right hand picture shows the result in the new 256 x 256 data acquisition mode. After radial averaging the increased number of data points (black symbols) allows for a refined analysis of the scattering curve (middle), especially for such systems with distinctive peaks and minima.

The deadtime of the detector after the modification of its electronics has been determined at different wavelengths from the non-linearity of the observed countrates for very high neutron flux by two methods, i.e. (i) the measurement of the non-attenuated direct beam as a function of sample aperture and (ii) the measurement of the water transmission without attenuator for different thicknesses of the water sample and for different areas of illumination. The results are 316 ns for method (i) and 379 ns for method (ii), giving a mean deadtime of 330 ns. In addition, the physical spatial resolution with the new electronics has been determined by illuminating the detector through a cadmium mask with small slit-like apertures. The mean spatial resolution has been found to be 6.8 mm.

<sup>1</sup> Field Programmable Gate Array: a type of programmable digital circuit

## TECHNICAL DEVELOPMENTS

### In situ crystal alignment at low temperature

We present novel devices for aligning single crystals in cryostats. Remotely driven at cryogenic temperatures, these systems aim at simplifying users' operations and reducing beamtime losses.

#### AUTHORS

J. Allibon, E. Bourgeat-Lami, L.C. Chapon, Ph. Decarpentrie, A. Filhol, J.-P. Gonzales, J. Halbwachs, E. Lelièvre-Berna, J. Ollivier, B. Ouladdiaf and G. Pastrello (ILL)

#### REFERENCES

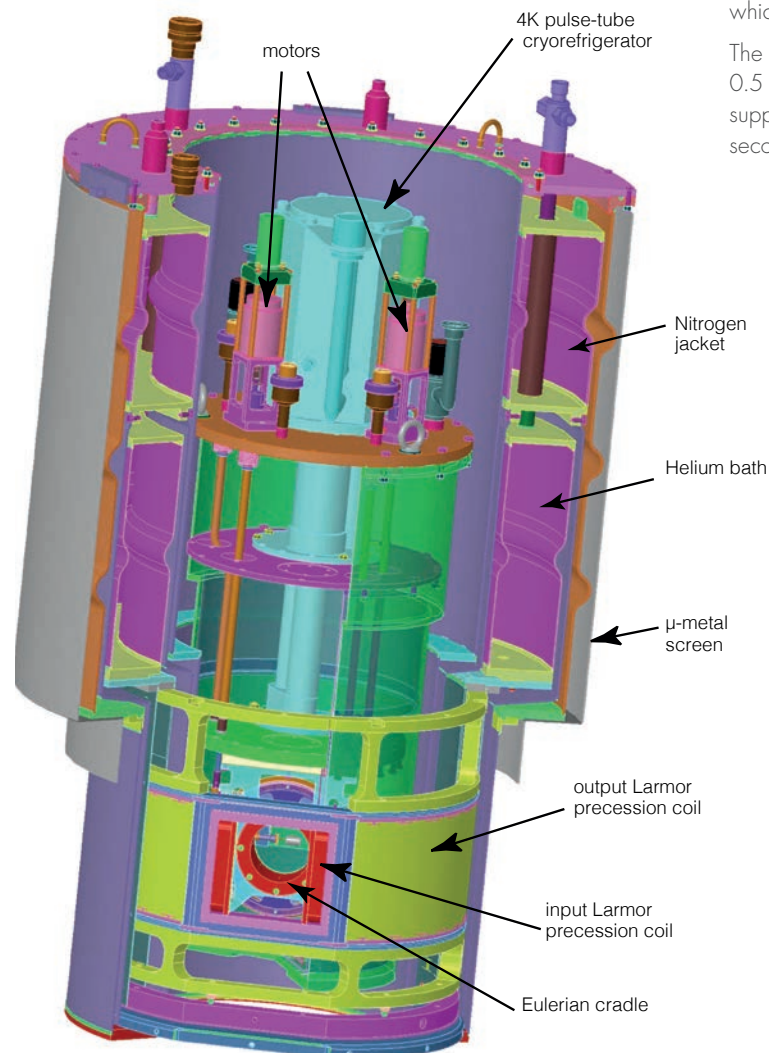
- [1] P.J. Brown, *Physica B* 297 (2001) 198
- [2] P.J. Brown, J.B. Forsyth, E. Lelièvre-Berna and F. Tasset, *J. Phys. Condens. Matter* 14 (2002) 1957
- [3] E. Lelièvre-Berna, E. Bourgeat-Lami, Y. Gibert *et al.*, *Physica B* 356 (2005) 131
- [4] M. Berneron, A. Filhol, J.-J. Vernier and M. Thomas, *Revue Phys. Appl.* 19 (1984) 795

#### CRYOCRADLE: SPHERICAL NEUTRON POLARIMETRY AT A GLANCE

To carry out elastic Spherical Neutron Polarimetry experiments, access to Bragg peaks in different scattering planes is required to elucidate complex magnetic structures from a few specifically chosen Bragg reflections [1], and to determine magnetisation distributions from many reflections [2]. With the aim of drastically enhancing reciprocal space coverage, we decided to build a cryostat containing a fully non-magnetic Eulerian cradle called *Cryocradle* and which can be installed inside Cryopad (**figure 1**).

The prototype consists of two circles mounted inside a 0.5 W at 4.2 K pulse-tube cryo-refrigerator. The first circle supports the sample and fixes the angular position  $\chi$ . The second circle controls the  $\phi$  axis of the sample by means

**Figure 1**  
Schematic overview of the *Cryocradle* inside the zero-field chamber of Cryopad.



of a gear. Both circles are motorised using tangential axes, with the motors and encoders outside the zero-field sample chamber of Cryopad [3].

The whole cradle is made from hardened BeCu to reduce the cool-down time, with the tangential axes mounted on flexible arms to compensate for thermal expansion. These flexible supports prevent the displacement of the axes and minimise hysteresis. The friction is reduced with a DLC (diamond-like carbon) coating and using BN (boron nitride) powder as a lubricant.

The *Cryocradle* was commissioned on the polarised neutron diffractometer D3 in July 2013. We measured the polarisation matrix of 27 Bragg peaks of the langsite  $\text{BaNbFe}_3\text{Si}_2\text{O}_{14}$  at 3.2 K in five days. We verified that positioning a Bragg reflection can be achieved reproducibly with an absolute angular resolution of  $0.1^\circ$  from 3 to 300 K.

#### GONIOSTICK: CRYSTAL ALIGNMENT IN CRYOSTATS

The alignment of single crystals on instruments cannot always be realised by tilting the sample environment. On some time-of-flight spectrometers the inclination of the equipment is very restricted. This is also the case with focusing optics installed inside the environment. The alignment of lattice planes with a magnetic field or the incident neutron polarisation can only be performed inside a cryostat or cryomagnet. Moreover the precession of a tilted cryostat creates a non-homogeneous background.

For these reasons we decided to build a new eucentric system called *Goniosstick*, based on the idea developed at the ILL by Berneron *et al.* in the 80s [4]. Basically this is a special stick for top-loading cryostats, with two motors or micrometer screws mounted at the top and driving a compact goniometer inside the sample space.

The inclination of the sample is actuated by the translation of two rods protruding from the top flange of the stick. At the lower end of these rods there is a groove which acts as a push rod on right-angled levers positioned on orthogonal axes. The combined displacement of these levers provokes the inclination of the sample around a pivot (point located on the main vertical axis of the stick). The sample holder is identical to those used on ILL single crystal diffractometers and allows the centring of the crystal on the pivot.

As shown in **figure 3**, the *Goniosstick* hosts a Cernox sensor in the exchange gas of the cryostat to ensure a reliable determination of the sample temperature. The stick fits inside a  $\varnothing 49$  mm top-loading cryostat and allows remote sample inclination of  $\pm 7^\circ$ .

The *Goniosstick* was commissioned on the time-of-flight spectrometer IN5 in July 2014. The measured backlash of  $0.14^\circ$  is easily compensated by finishing movements in the same direction. In this way, we measured a precision of  $0.02^\circ$  between 20 and 300 K.



**Figure 2**  
Photograph of the *Cryocradle* mounted inside the 3 K pulse-tube cryostat. (© Ecliptique – Laurent Thion).



**Figure 3**  
Photo of the *Goniosstick* with the sample holder inclined by both levers. (© Ecliptique – Laurent Thion).

# EXPERIMENTAL AND USER PROGRAMME



USER PROGRAMME	92
USER AND BEAMTIME STATISTICS	94
INSTRUMENT LIST	98

**T**he ILL User Support team is dedicated to helping all visiting researchers to make the most of its facilities. If you are coming to the ILL to carry out experiments, the User Office is here to give you the organisational and administrative support you need to successfully perform your experiments.

Neutron beams and instrument facilities are free of charge for proposers of accepted experiments. Scientists affiliated to the institute's member countries will also, in general, be assisted with necessary travel and daily subsistence for a limited period. The User Support team makes all arrangements for accommodation and will process claims for expenses after users have completed their experiments.

For further information about the institute's facilities, applications for beamtime, user support and the experimental programme, please visit our website:

**<http://www.ill.eu/users>**

---

*Neutron beams and  
instrument facilities  
are free of charge  
for proposers of  
accepted experiments*

---

# USER PROGRAMME

## THE ILL USER CLUB

All administrative tools and information for our scientific visitors are grouped together and directly accessible on the web, courtesy of our user-friendly, online User Club. Club members can log on using their own personal identification<sup>1</sup> to gain direct access to all the information they need. Users with particular responsibilities have privileged access to other tools, according to their role. The ILL User Club includes the electronic proposal and experimental reports submission procedures, as well as electronic peer review of proposals. Additional electronic services have also been put in place: acknowledgement of proposals, subcommittee results, invitation letters, user satisfaction forms and so on.

## PROPOSAL SUBMISSION

There are different ways of submitting a proposal to the ILL:

- Standard submission – twice a year – via the Electronic Proposal Submission system (EPS)
- Long-Term Proposals (LTPs) – once a year – via the Electronic Proposal Submission system (EPS)
- Easy access system (EASY) – throughout the year – via our User/Visitors' Club website
- Director's Discretion Time (DDT) – throughout the year – via the Head of Science Division
- Special access for proprietary research and industrial users

## Submission of a standard research proposal

Applications for beamtime should be submitted electronically, via our Electronic Proposal Submission system (EPS) available on the User Club website. Proposals can be submitted to the ILL twice a year, usually in February and in September. The web system is activated two months before each deadline. Submitted proposals are divided amongst the different colleges (**see box below**) according to their main subject area.

### THE ILL SCIENTIFIC LIFE IS ORGANISED INTO 10 COLLEGES:

<b>College 1</b>	Applied Metallurgy, Instrumentation and Techniques
<b>College 2</b>	Theory
<b>College 3</b>	Nuclear and Particle Physics
<b>College 4</b>	Magnetic Excitations
<b>College 5A</b>	Crystallography
<b>College 5B</b>	Magnetic Structures
<b>College 6</b>	Structure and Dynamics of Liquids and Glasses
<b>College 7</b>	Spectroscopy in Solid State Physics and Chemistry
<b>College 8</b>	Structure and Dynamics of Biological Systems
<b>College 9</b>	Structure and Dynamics of Soft Condensed Matter

Proposals are judged by a Peer Review Committee of the subcommittees of the ILL Scientific Council. Subcommittee members are specialists in relevant areas of each College. Two proposal review rounds are normally held each year, approximately eight weeks after the deadline for submission of applications. Before each meeting, the subcommittee receives a report from the appropriate College on the technical feasibility and safety of a proposed experiment. The subcommittee evaluates the proposals for scientific merit and recommends that the ILL Management award beamtime to the highest-priority proposals.

There are normally four reactor cycles a year, each of which lasts 50 days. Accepted proposals submitted by February will receive beamtime in the second half of the year and those submitted by September, in the first half of the following year. More detailed information on application for beamtime and deadlines is given on our website, at <http://www.ill.eu/users/applying-for-beamtime/>.

## Easy access system

The easy access system (EASY) grants diffraction beamtime to scientists from ILL member countries who need a rapid structural characterisation of samples and data analysis. Access is open all year long and allows applicants to bypass the ILL's standard proposal round and consequent peer review process.

The system offers applicants one neutron day per cycle, on two instruments (D2B and D16), in which to perform very short experiments at room temperature. The users are not invited to the ILL but send their samples to one of two designated ILL scientists who are responsible for the measurements and sample radiological control. The ILL ships back the sample once the measurement is finished. Interested parties can apply for EASY beamtime through the User/Visitors' Club. More information is available at [http://club.ill.eu/cvDocs/EASY\\_Guidelines.pdf](http://club.ill.eu/cvDocs/EASY_Guidelines.pdf).

## Long-Term Proposals

Users from ILL member countries can also apply for extended periods of beamtime by submitting a Long-Term Proposal (LTP). The purpose of this process is to facilitate the development of instrumentation, techniques or software – that could be beneficial to the ILL community as a whole – through the award of beamtime over several cycles. The total amount of beamtime that may be allocated to LTPs on any particular instrument is capped at 10 %, and beamtime is not awarded to LTPs to perform science beyond essential testing.

LTPs can be submitted once a year at the autumn proposal round, using the specific LTP application form. The primary criterion for acceptance of an LTP is the excellence of the science that it will ultimately enable. The length of LTP projects is expected to be three years typically, with continuation approved at the end of each year, based on an annual report; a final report is also required at the end of the project. More details are given at <http://www.ill.eu/users/applying-for-beamtime/>

## Submission of a proposal to the Director's Discretion Time

This option allows a researcher to obtain beamtime quickly, without going through the peer-review procedure. Director's Discretion Time (DDT) is normally used for 'hot' topics, new ideas, feasibility tests and to encourage new users. Applications for DDT can be submitted to the Head of the Science Division, Professor Helmut Schober, at any time.

## Experimental reports

Users are asked to complete an experimental report on the outcome of their experiments. The submission of an experimental report is compulsory for every user who is granted ILL beamtime. Failure to do so may lead to the rejection of any subsequent continuation proposals.

All ILL experimental reports are archived electronically and searchable via the web server as PDF files (under <http://club.ill.eu/cv/>).

## COLLABORATIVE RESEARCH GROUP INSTRUMENTS

The ILL provides a framework in which Collaborative Research Groups (CRGs) can build and manage instruments at the ILL to carry out their own research programmes. CRGs represent a particularly successful form of long-term international scientific collaboration. They are composed of scientists from one or two research disciplines, are often multinational and involve carrying out a joint research programme centred around a specific instrument. CRGs enjoy exclusive access to these instruments for at least half of the beamtime available. The CRGs provide their own scientific and technical support, and cover the general operating costs of these instruments. If there is demand from the user community and the resources are available, the beamtime reserved for the ILL can be made accessible to users via the subcommittees.

There are currently three different categories of CRG instruments.

- In the **CRG-A** category, external groups lease an instrument owned by the ILL. They have 50 % of the beamtime at their disposal and for the remaining 50 % they support the ILL's scientific user programme.
- In the **CRG-B** category, groups own their instrument and retain 70 % of the available beamtime, supporting the ILL programme for the other 30 %.
- Finally, in the **CRG-C** category instruments are used full time for specific research programmes by the external group, which has exclusive use of the beam.

## Support laboratories

The opportunities we offer to our users extend beyond the privilege of access to the world's leading suite of neutron instruments. The ILL – in collaboration with the European Synchrotron Radiation Facility (ESRF) and other institutes – is actively responding to the needs of scientists unfamiliar with neutron techniques and in need of training and support facilities. New support facilities have been already set up on the ILL site. For more information see the chapter "More than simply neutrons" (*p.106*).

## ACCESS FOR INDUSTRIAL USERS

The ILL's instruments are used by a wide range of industries besides academic research, from pharmaceutical and chemical companies to materials and process engineering, energy and environment sectors. Neutron techniques are of particular interest in the industrial context as they provide unique and essential information at the atomic and molecular level.

The Business Development Office (BDO) is the single point of contact for industry looking to use the ILL's neutron-scattering instruments. The Business Development Office matches the needs of industrial customers, directs them towards the best technique and scientists, and takes care of the administrative procedures. It provides industrial customers with fast, proprietary access and confidentiality under specific contract to any of the world-leading scientific instruments of the ILL. The BDO may also set up dedicated research and development partnerships for technological research with consortia including academic and industrial partners.

Contact: Jérôme Beaucour, [beaucour@ill.eu](mailto:beaucour@ill.eu).

<sup>1</sup> If you have not yet registered with the User (formerly Visitors') Club and you wish to join it, you can register directly at <https://userclub.ill.eu/cvng/>

# USER AND BEAMTIME STATISTICS

## THE ILL USER COMMUNITY

The ILL welcomed 980 users in 2014, including 256 from France, 195 from Germany and 167 from the UK (figure 1). Many of our visitors were received more than once (giving a total of 1 263 user visits).

We value feedback from our users as an indicator of how well our facility is fulfilling their needs and to initiate action when this is not the case (see figure 2). The *User Satisfaction Form* is a means of finding out what our users think of the facility. Users who have just finished an experiment at the ILL are asked to share their views on different topics by completing the questionnaire through the User Club. User comments are made available to managers for their information and action when appropriate. Overall, about 56 % of all users invited to the ILL in 2014 sent us their feedback form.

**Figure 1**  
National affiliation of ILL users in 2014.

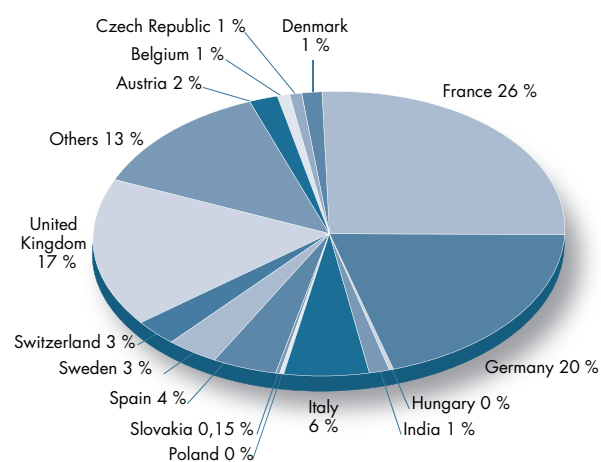
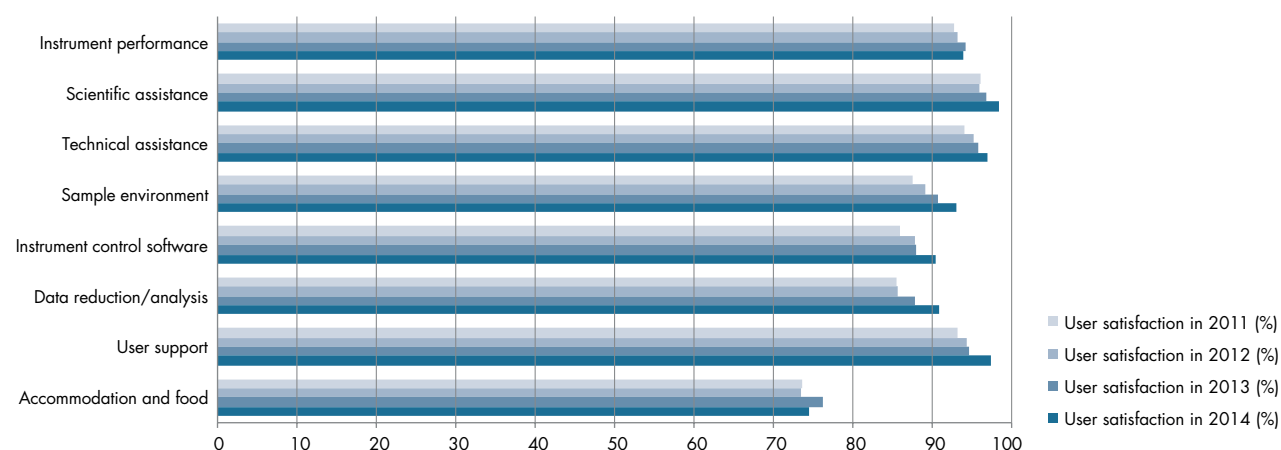


**Figure 2**  
User satisfaction survey results for 2014, compared with those obtained in previous years.



## INSTRUMENTS

The instrumental facilities at the ILL are shown in the schematic diagram on page 98. The list of instruments as of December 2014 is summarised below. Besides the 29 ILL instruments there are 9 Collaborative Research Group (CRG) instruments (marked with an asterisk \*):

- powder diffractometers: D1B\*, D2B, D20, SALSA
- liquids diffractometer: D4
- polarised neutron diffractometers: D3, D23\*
- single crystal diffractometers: D9, D10
- large-scale structures diffractometers: D19, LADI,
- small-angle scattering diffractometers: D11, D22, D33
- low momentum-transfer diffractometer: D16
- reflectometers: SuperADAM\*, D17, FIGARO
- diffuse scattering and polarisation analysis spectrometer: D7
- three-axis spectrometers: IN1-LAGRANGE, IN8, IN12\*, IN20, IN22\*
- time-of-flight spectrometers: BRISP\*, IN4, IN5, IN6,
- backscattering and spin-echo spectrometers: IN11, IN13\*, IN15, IN16B
- nuclear physics instruments: PN1, PN3
- fundamental physics instruments: PF1, PF2, S18\*

LADI and IN15 have special status, since they are joint ventures of the ILL with other laboratories: in the case of LADI, with the European Molecular Biology Laboratory (EMBL), and for IN15, with Forschungszentrum (FZ) Jülich and Helmholtz-Zentrum Berlin (HZB). Cryo-EDM\* is not listed above because as a CRG-C instrument (see p.93) it is not available as a 'user' instrument. Details of the instruments can be found on our website at <http://www.ill.eu/instruments-support/instruments-groups/>.

## BEAMTIME ALLOCATION AND UTILISATION FOR 2014

During 2014 the reactor operated for about 2.5 cycles, representing 117 days of neutrons (see § Reactor Operation, p.102). The reactor power was maintained at the low level of 30 MW during the first half of the qualification cycle.

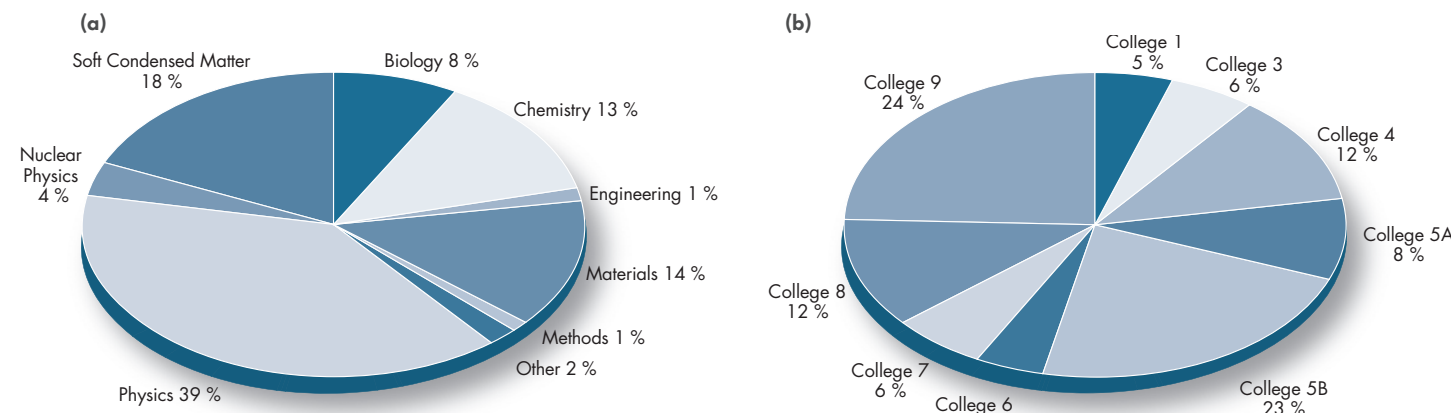
This allowed a series of radioprotection tests and validation exercises to be carried out in order to obtain authorisation from the French Nuclear Authorities to restart the reactor on full power on 28 August. During the qualification cycle very few user experiments were scheduled.

Overall, the subcommittees of the Scientific Council examined 738 proposals requesting 4 708 days in 2014. Of these 469 proposals received beamtime, requiring the allocation of 2 457 days of beamtime on the different instruments. A total of 495 experiments were scheduled. The distribution of accepted proposals amongst the different research areas and colleges is given in figure 3.

In 2014, the member countries of the ILL were as follows: France, Germany, UK, Austria, Belgium, the Czech Republic, Denmark, Hungary, Italy, Poland, Slovakia, Spain, Sweden, Switzerland and India.

Table 1 gives the beamtime distribution amongst the different member countries (request and allocation in 2014). In calculating the statistics of beamtime per country, the attribution is based on the location of the laboratory of the proposers, not their individual nationality. For a proposal involving laboratories from more than one member country, the total number of days is divided amongst the collaborating countries and weighted by the number of people from each. Local contacts are not counted as proposers except when they are members of the research team. The beamtime requested by and allocated to scientists from the ILL, ESRF or EMBL is allocated to the member countries according to

**Figure 3**  
Beamtime allocation in 2014: distribution amongst the different research areas (a) and colleges (b).



	Request days	Request %	Allocation days	Allocation %	Allocation days	Allocation %
<b>Member countries only</b>			Before national balance		After national balance	
AT	161.16	3.42	126.13	5.03	80.60	3.28
BE	19.89	0.42	12.70	0.51	12.68	0.52
CH	279.29	5.93	161.28	6.43	161.20	6.56
CZ	48.63	1.03	31.87	1.27	31.85	1.30
DE	1 186.59	25.21	625.56	24.94	624.56	25.42
DK	81.87	1.74	52.74	2.10	52.71	2.15
ES	214.73	4.56	111.77	4.46	111.70	4.55
FR	1 085.89	23.07	552.88	22.04	551.88	22.46
GB	1 021.16	21.69	594.88	23.72	593.87	24.17
HU	29.30	0.62	8.28	0.33	8.27	0.34
IN	140.86	2.99	31.61	1.26	31.58	1.29
IT	255.87	5.44	103.99	4.15	103.88	4.23
PL	39.57	0.84	6.43	0.26	6.42	0.26
SE	138.19	2.94	84.87	3.38	84.80	3.45
SK	2.05	0.04	1.29	0.05	1.29	0.05
<b>Total</b>	<b>4 707.51</b>	<b>100.00</b>	<b>2 507.99</b>	<b>100.00</b>	<b>2 457.28</b>	<b>100.00</b>

**Table 1**  
Distribution amongst the Associate and Scientific Member countries of beamtime requested and allocated in 2014 during the subcommittees of the Scientific Council.

Proposals from purely non-member countries and from purely ILL or ESRF proposals do not appear in this table, therefore the total request and allocation is different in table 2.

# USER AND BEAMTIME STATISTICS

a weighting system based on the fractional membership of the country of the institute concerned. When a proposal involves collaboration with a non-member country, the allocated time is attributed entirely to the collaborating member country (or countries), and weighted by the number of people from each member country. Proposals in which all proposers are from non-member countries therefore do not appear in this table. This explains why the total number of allocated days differs from that in **table 2**.

A more complete view of beamtime use is given in **table 2**. Requests for and allocation of beamtime, as well as the number of scheduled experiments, refer to standard submissions to the subcommittee meetings. The effective number of days given to our users also takes into account Director's Discretion Time and CRG time for CRG instruments.

## INSTRUMENT PERFORMANCE

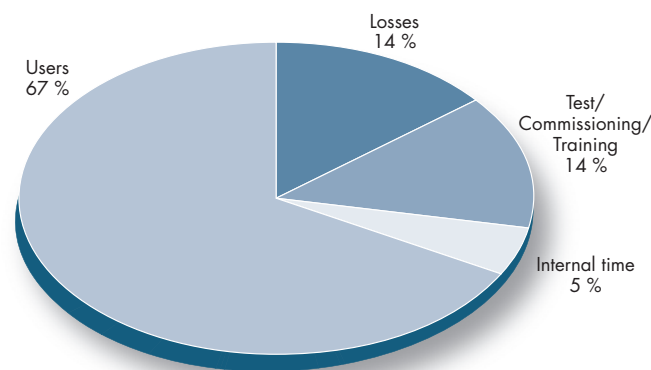
**Table 2** also gives a summary of instrument performance for 2014. For each cycle a record is kept of any time lost from the total available beamtime and the reasons for the lost time analysed, for all the instruments. The table gives a global summary for the year.

Overall 2 557 days were made available to our users in 2014 on ILL and CRG instruments, which represents about 66 % of the total days of operation. A total of 161 days were used by ILL scientists to carry out their own scientific research. About 14 % of the total beamtime available on the ILL instruments was allowed for tests, calibrations, scheduling flexibility, recuperation from minor breakdowns and student training.

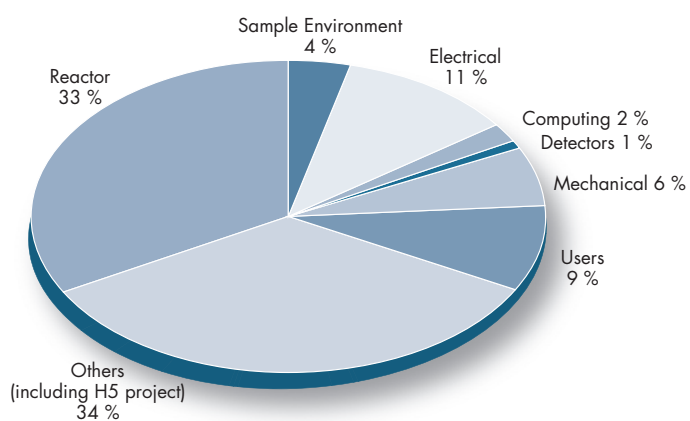
Beam days given to science in 2014 amounted to 2 718 (used for users and internal research).

In 2014, 558 out of 3 833 days were lost as a result of various malfunctions, which represents about 14 % of the total available beamtime. The breakdown by reason for beamtime losses is shown in **figure 4b**. Most instruments could not schedule experiments during the qualification cycle, and these days are counted as lost beamtime.

**Figure 4**  
**(a)** Use of ILL beamtime



**(b)** Reason for beamtime losses.



Detailed comments on the larger beamtime losses (more than 25 days) are as follows:

- The instrument BRISP was not operative in 2014 because of its delayed remounting.
- PF1B lost 35 days because one user experiment was not ready on time.
- All instruments of the guide hall ILL22 (IN15, D16, D22, SuperADAM) were dismantled and then rebuilt during the one-year long shutdown, because of the renovation of the H5 guide. This had an impact on their user programme.

Instrument	Days requested	Days allocated*	Number of scheduled experiments	Available days	Days used for users**	Days lost	Days for commissioning /test/training	Days for internal research
BRISP	105	25	2	0	0	0	0	0
D1B	52	48	22	117	85.64	8.36	23	0
D10	124	90	15	113	92.5	0.5	10	10
D11	151	79	43	117	64.04	28.06	24.9	0
D16	140	66	11	37	24	7	3	3
D17	102	79	22	117	79.69	10.01	27.3	0
D19	125	86	14	117	80.92	7.08	29	0
D2B	141	80	38	117	88	5.33	9	14.67
D20	164	80	32	117	79.5	14.42	10.5	12.58
D22	125	15	7	48	0	28.06	24.9	0
D23	96	35	5	117	96	4	17	0
D3	94	89	11	117	84	24	4	5
D33	163	79	33	117	70.28	3.72	40	3
D4	111	32	8	50	32.67	9.58	3.5	4
D7	159	80	13	117	74.7	5.8	18.5	18
D9	61	61	9	117	57	6.79	9.41	43.8
FIGARO	143	84	23	117	86.18	9.67	19.64	1.51
IN1	149	41	9	67	34	18.3	9.7	5
IN11	117	75	8	117	78	9.5	27.5	2
IN12	160	46	8	117	80	7	17	13
IN13	87	31	5	117	86.88	5.12	25	0
IN15	95	21	3	28	0	18	10	0
IN16B	158	62	21	117	68.55	12.45	32	4
IN20	123	87	11	117	76	34	7	0
IN22	101	37	6	115	99	7	9	0
IN4	153	93	25	117	85.75	12.54	17	1.71
IN5	168	57	13	117	99	4	10	4
IN6	88	80	20	113	85	1	24	3
IN8	88	75	12	117	77	14	20	6
LADI	163	90	11	117	83	17	15	2
PF1B	200	125	1	117	59	42	16	0
PF2/5	158	112	3	117	109	2	6	0
PN1	184	135	8	117	92	17	8	0
PN3 - GAMS 6	90	28	1	99	32	56	11	0
SALSA	88	79	16	117	91.5	6	14.5	5
SUPERADAM	133	30	6	117	31	81	5	0
S18	81	0	0	117	94.8	22.2	0	0
<b>Total</b>	<b>4 640</b>	<b>2 412</b>	<b>495</b>	<b>3 829</b>	<b>2 556.6</b>	<b>558.49</b>	<b>557.35</b>	<b>161.27</b>
Percentage of the total available beamtime					66.00 %	14.00 %	14.00 %	4.00 %

**Table 2**

Beamtime request/allocation (via standard subcommittees and Director Discretion Time – DDT together) by instrument and instrument performance. CRG instruments are in blue.

\* 'Days allocated' refers to only those days reviewed by the subcommittees (i.e., excluding CRG days and DDT)

\*\* 'Days used' refers to the total number of days given to users (i.e., including CRG days for CRGs and DDT)

PF2 consists of different set-ups where several experiments are running simultaneously. The values given are averages for these positions.

D4 and IN1 share the same beam port and cannot be run simultaneously.

# INSTRUMENT LIST

??

should this be IN1 - lagrange

## INSTRUMENT LIST – DECEMBER 2014

ILL INSTRUMENTS		
D2B	powder diffractometer	operational
D3	single crystal diffractometer	operational
D4 (50 % with IN1) ??	liquids diffractometer	operational
D7	diffuse-scattering spectrometer	operational
D9	single crystal diffractometer	operational
D10	single crystal diffractometer	operational
D11	small-angle scattering diffractometer	operational
D16	small momentum-transfer diffractometer	operational
D17	reflectometer	operational
D19	single crystal diffractometer	operational
D20	powder diffractometer	operational
D22	small-angle scattering diffractometer	operational
D33	small-angle scattering diffractometer	operational
FIGARO	horizontal reflectometer	operational
INI-LAGRANGE (50 % with D4)	three-axis spectrometer	operational
IN4	time-of-flight spectrometer	operational
IN5	time-of-flight spectrometer	operational
IN6	time-of-flight spectrometer	operational
IN8	three-axis spectrometer	operational
IN11	spin-echo spectrometer	operational
IN16B	backscattering spectrometer	operational
IN20	three-axis spectrometer	operational
PF1	neutron beam for fundamental physics	operational
PF2	ultracold neutron source for fundamental physics	operational
PN1	fission product mass-spectrometer	operational
PN3 - GAMS	gamma-ray spectrometer	operational
SALSA	strain analyser for engineering application	operational
VIVALDI	thermal neutron Laue diffractometer	on hold

CRG INSTRUMENTS		
BRISP	Brillouin spectrometer	CRG-B operational
CRYO EDM	installation for the search for the neutron electric dipole moment	CRG-C operational
D1B	powder diffractometer	CRG-A operational
D23	single crystal diffractometer	CRG-B operational
GRANIT	gravitation state measurement	CRG operational
IN12	three-axis spectrometer	CRG-B operational
IN13	backscattering spectrometer	CRG-A operational
IN22	three-axis spectrometer	CRG-B operational
SuperADAM	reflectometer	CRG-B operational
S18	interferometer	CRG-B operational

JOINTLY FUNDED INSTRUMENTS		
LADI (50 %)	Laue diffractometer	operated with EMBL
IN15	spin-echo spectrometer	operated with FZ Jülich and HZB Berlin
GRANIT	gravitation state measurement	operated with LPSC (UJF, CNRS)

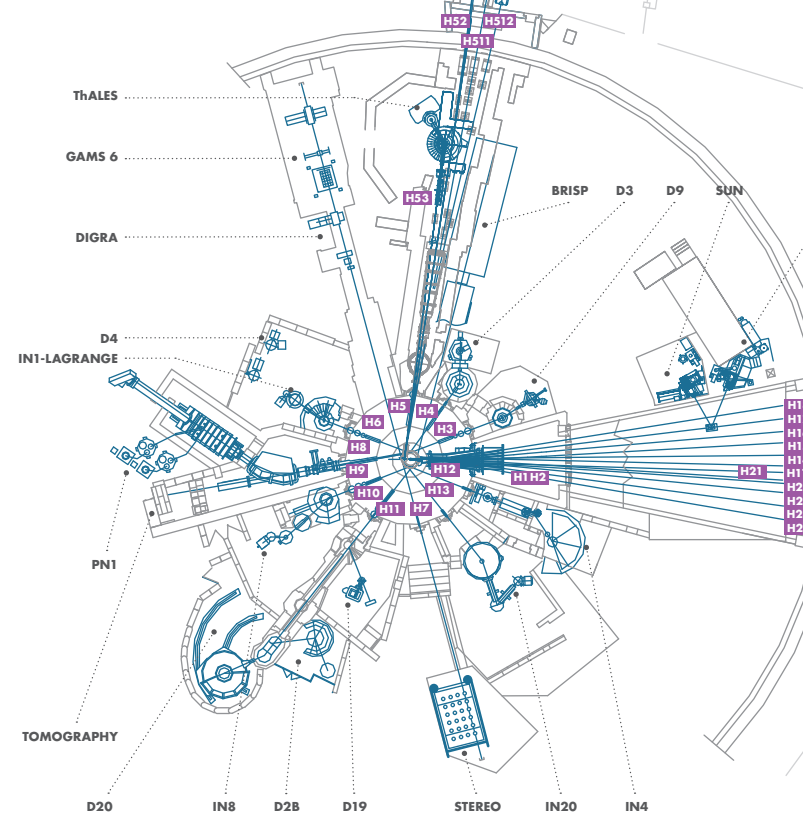
TEST AND CHARACTERISATION BEAMS	
CT1, CT2	detector test facilities
CYCLOPS	Laue diffractometer
TOMOGRAPHY	neutrography
OrientExpress	Laue diffractometer
T3	neutron optics test facility
T13A, C	monochromator test facility
T17	cold neutron test facility

## INSTRUMENT LAYOUT – JANUARY 2015

### NEUTRON GUIDE HALL/ILL 22

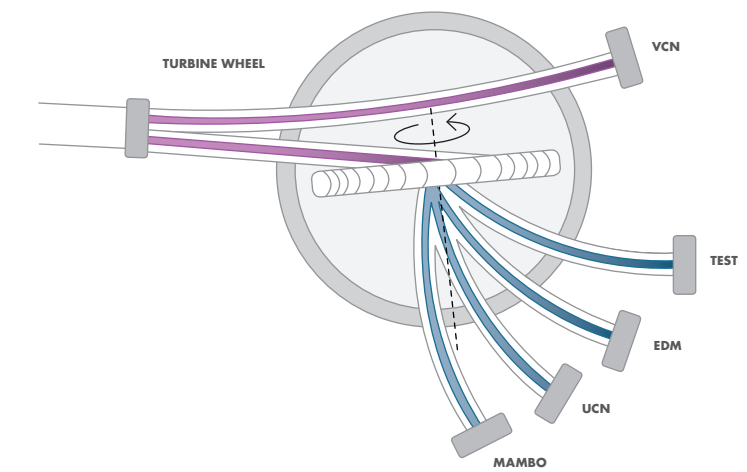


### REACTOR HALL/INCLINED GUIDE H4

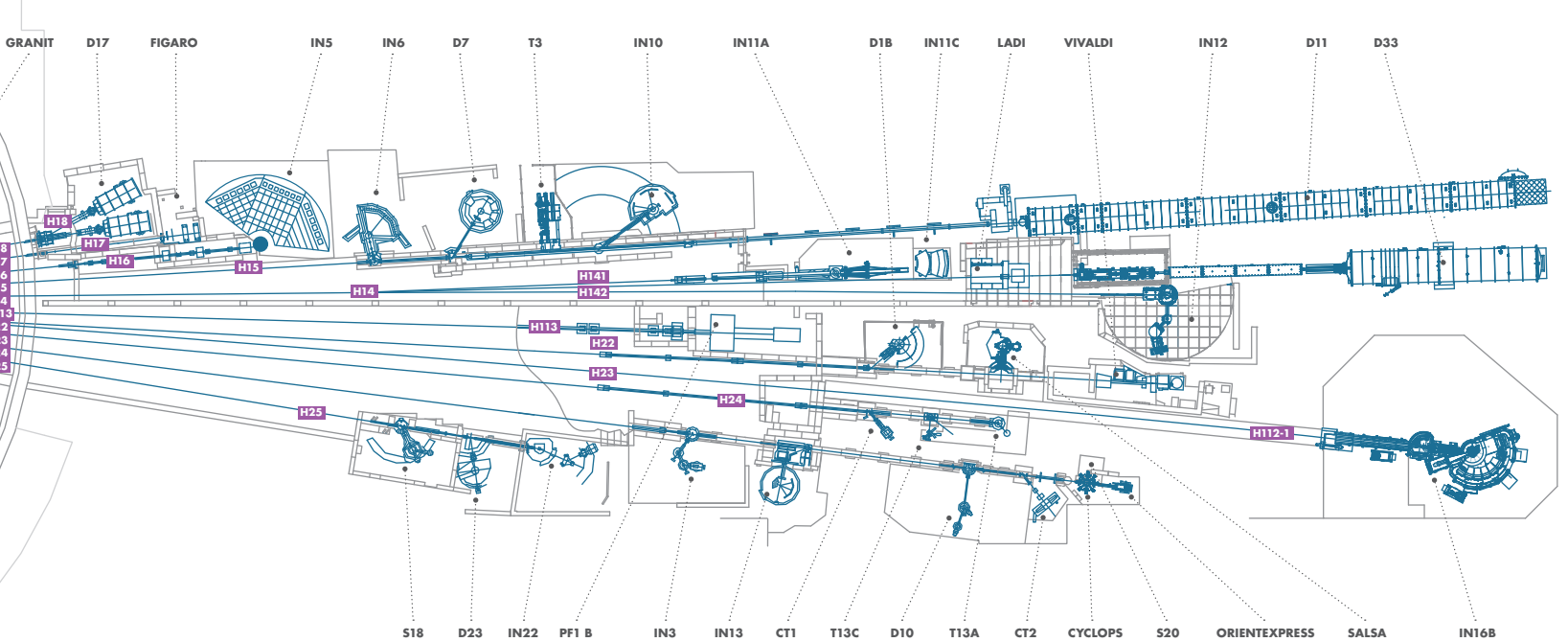


### REACTOR HALL ILL 5/EXPERIMENTAL LEVEL (C)

### REACTOR OPERATIONAL LEVEL (D)



### NEUTRON GUIDE HALL/ILL 7 - VERCORS SIDE (WEST)



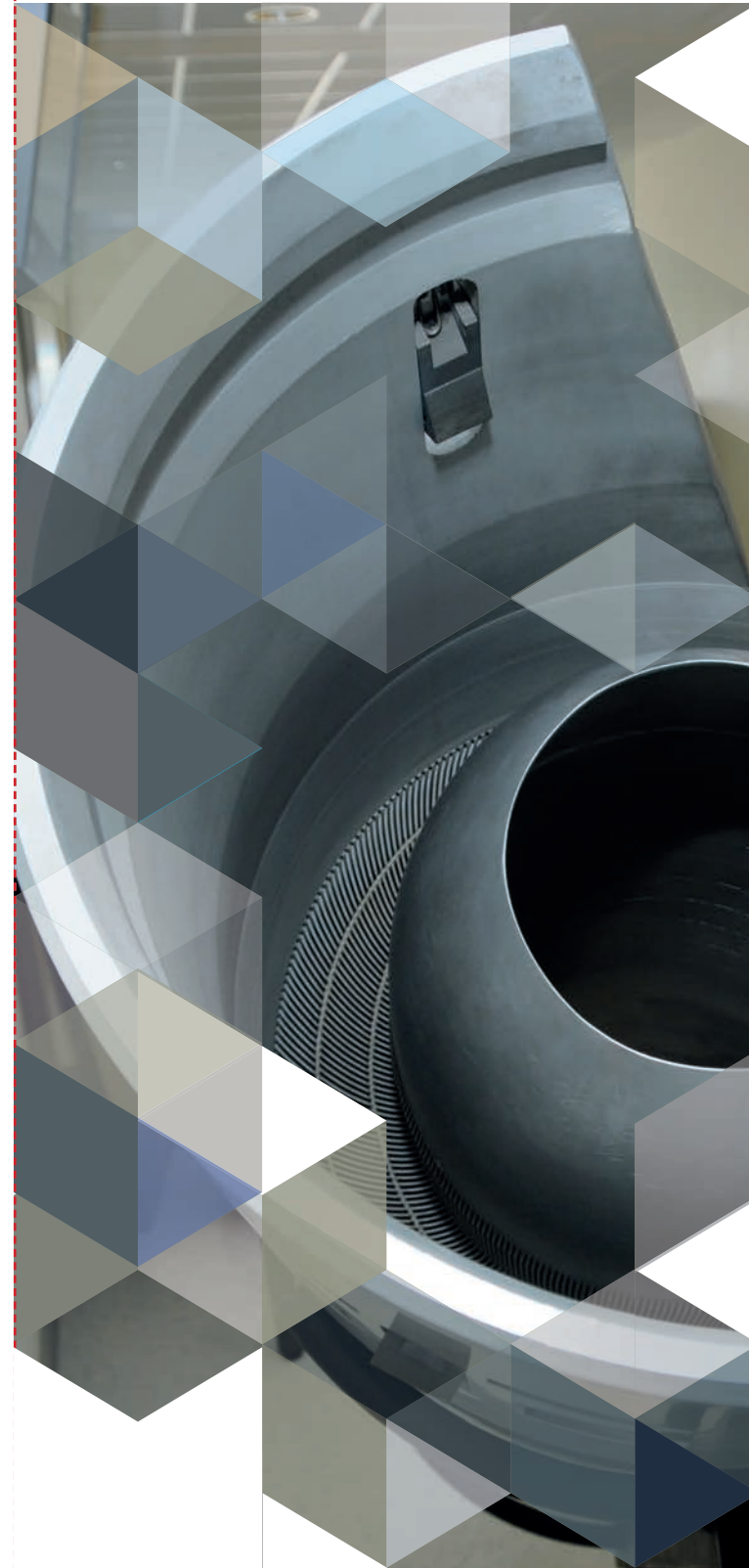
### NEUTRON GUIDE HALL/ILL 7 - CHARTREUSE SIDE (EAST)



# INSTRUMENT LAYOUT 2015

© R. Cubitt

# REACTOR OPERATION



REACTOR OPERATION IN 2014	102
THE FUKUSHIMA REINFORCEMENT WORK	104

The ILL High-Flux Reactor (HFR) produces the most intense neutron flux in the world:  $1.5 \times 10^{15}$  neutrons per second per  $\text{cm}^2$ , with a thermal power of 58.3 MW. The reactor operates 50-day cycles, with each cycle of operation followed by a shutdown period during which the fuel element is changed and a number of checks are carried out. Occasional longer shutdowns allow for equipment maintenance. There are normally four reactor cycles per year, supplying 200 days of neutron flux for scientific use.

Following the nuclear disaster at Fukushima, Japan, the French nuclear safety authority (ASN) decided to launch additional safety assessments on all French nuclear bases (INBs), including the ILL. The impact of this additional safety review on the institute and its budget in the years leading up to it, will continue to be felt into the future.

Studies performed by the reactor division teams have analysed the behaviour of the ILL reactor under extreme conditions: the earthquake scenarios envisaged would cause major damage to a town like Grenoble, leading to the failure of all the dams on the river Drac and leaving the centre of town under 10 metres of water. The studies demonstrated the robustness of the reactor against the maximum, physically expectable earthquake combined with the loss of the four dams upstream on the river Drac. Their results implied the need for the reinforcement of elements traversing the reactor containment and the construction of a new emergency reactor control room for the crisis management teams from which all the emergency safety circuits can be controlled. The civil works for the building which will house the emergency control room have already been completed. The whole work is scheduled to be carried out over five years (from 2012 to 2016), with no major disruption to the ILL User Programme.

---

*Following the nuclear disaster at Fukushima, Japan, the French nuclear safety authority (ASN) decided to launch additional safety assessments on all French nuclear bases (INBs), including the ILL.*

---

# REACTOR OPERATION

## Reactor operation in 2014

### AUTHORS

H. Guyon and J. Tribolet (ILL)

Three reactor cycles were completed in 2014 and a total of 117 days of scientific activity were provided (see table below).

Cycle n°	Start of cycle	End of cycle	Number of days scheduled	Number of days of operation	Number of unscheduled shutdowns
171	08.07.14	26.08.14	18	18	0
172	28.08.14	18.10.14	50	48	1 (7 to 10.09)
173	03.11.14	22.12.14	49	49	0
<b>Total</b>			<b>117</b>	<b>115</b>	<b>1</b>

During the second cycle, the reactor had to be shut down briefly in order to start up the 2<sup>nd</sup> turbine on the cold source cryogenic system.

### THE KEY REACTOR COMPONENTS PROGRAMME

In order to guarantee the safety and reliability of the reactor for the coming years of operation, the Reactor Division has continued to pursue its "Key Reactor Components" programme, the aim of which is to upgrade or replace some of the reactor's most important components. The programme started in 2005 and will continue until 2017, the date of the next ten-year safety review of our installations.

The main operations still to be completed under this programme concern:

- the replacement of beam tubes
- the upgrade of the out-of-pile part of the horizontal cold source, including its instrumentation and control system
- the manufacture of hafnium safety rods
- the procurement of replacement cells for the cold sources.

### WORK RELATING TO THE POST-FUKUSHIMA ADDITIONAL SAFETY ASSESSMENT

The investigations carried out in 2011 and presented to the safety authority's groups of experts in November of the same year successfully demonstrated that:

- the ILL has significant safety margins available with respect to the design-basis earthquake
- the loss of a single safety function would never lead to a so-called "cliff-edge effect", i.e. a sudden or very rapid deterioration of the facility's safety conditions
- the combined loss of both reactivity and containment would never lead to a cliff-edge effect
- there are always at least two major barriers in place to prevent and mitigate the accidents feared, and
- fusion in water would never lead to a cliff-edge effect.

To comply with the requirements resulting from the post-Fukushima Additional Safety Assessment, the ILL must ensure that it is equipped with a "hard core" of safety components by:

- completing the installation of the emergency core reflood system and the seismic depressurisation circuit, and
- installing a groundwater circuit, implementing an emergency system for 'dropping' irradiated fuel elements onto the bottom of the transfer canal and constructing a new emergency reactor control room, known as PCS3.

The programme of work has been defined. Work is progressing according to schedule and to date 80 % of the operations have been completed.

### WORK CARRIED OUT DURING THE LONG 2013/2014 SHUTDOWN

The long shutdown from 9 August 2013 to 8 July 2014 was accompanied by a particularly ambitious programme of work, including work on the Key Reactor Components programme and work required by the safety authority in light of the post-Fukushima safety assessment, as well as numerous maintenance operations. To avoid a second long shutdown before 2016, we also took this opportunity to complete preparatory work for future, post-Fukushima projects.

A detailed list of the main work carried out in 2013 was provided in the 2013 Annual Report (<http://www.ill.eu/quick-links/publications/annual-report/>).

### MAIN WORK CARRIED OUT IN 2014

#### Maintenance operations:

- Encapsulation in concrete shells of the ion-exchange resins produced over the last 20 years of reactor operation; this work involved the use of the MERCURE mobile encapsulation unit of the company SOCODEL.
- Modifications to the filters on the cooling water intake from the river Drac.
- All the periodic maintenance, test and inspection programmes.
- Cleaning of the heat exchangers.

#### Work on the Key Reactor Components:

- Replacement of the joints of the flange that holds the coupling sleeve of the beam tube H13 in place (not originally planned).
- Installation of beam tube H13.
- Reassembly of the internal components of the beam tube H5 up to the safety valve.
- Completion of the heavy water exchange programme with Canada within a very tight time frame.
- Replacement of the emergency low-voltage master distribution panels ASO, 1, 2 and 3.
- Reinforcement of the handling gantry.

#### Work following the post-Fukushima safety assessment:

- Laying of all the measurement and power cables of the "hard core" components.
- Installation of the two seismic depressurisation circuits.
- Installation of the two groundwater circuits.
- Fitting-out of the emergency reactor control room to be able to manage all types of emergencies.
- Construction of the seismic electronics room.

### RADIOACTIVE WASTE AND EFFLUENTS

In compliance with the regulatory limits applicable to our installation, reactor operations and maintenance work in 2014 generated the following levels of waste and effluents:

Evacuation of radioactive waste	Quantity
Decay bins (60 l)*	0
5 m <sup>3</sup> pre-concreted crates (low and intermediate-level waste)	0
5 m <sup>3</sup> crates (low and intermediate-level waste)	6
200 l drums of "incinerable" (laboratory) waste	72
120 l HDPE drums (laboratory waste)	15
30 l cylinders (liquid)	3

\*Waste stored in decay bins is still too active and must be held in interim storage for several years before meeting ANDRA's specifications for processing as intermediate-level waste.

Gaseous effluents	Released in 2014 (TBq)
Tritium	8.3
Noble gases	0.81
Carbon-14	0.076
Iodine	0.00000088
Aerosols	0.00000015

Liquid effluents	Released in 2014 (TBq)
Tritium	0.18
Carbon-14	0.00022
Iodine	0.00000071
Other activation products	0.000051

The seismic depressurisation circuit on the outside of the reactor containment.



# REACTOR OPERATION

## The Fukushima reinforcement work

After the Fukushima accident, the French authorities asked the ILL to re-evaluate the risks to be addressed in preparation for a natural disaster. This request was made to all French nuclear operators.

All the ILL teams responded promptly, and three quarters of the work subsequently planned was performed in 2013 and 2014. The operations remaining will be completed by 2016.

Ten years ago the ILL had already carried out a major programme of reinforcement to protect the facilities from a severe earthquake (Richter 5.7). After Fukushima, however, the severity of the earthquake to be taken into account was raised to the 7.3 level. In addition, the authorities required us to protect the facilities against the possibility of an earthquake combined with severe tsunami-level flooding.

The earthquake scenario we had to prepare for was that of a quake such as would occur only every 20 000 years. The hypothesis was that this would subsequently result in the breach of the four dams upstream of the ILL on the river Drac, and as a consequence a wave ten metres high would sweep across the town. The water would reach the institute in less than one hour, and the reactor must remain under control in these extreme conditions.

### AUTHORS

B. Desbrière (ILL)

The reinforcement work focused on three priorities:

#### 1. Ensure efficient cooling

As soon as the reactor shuts down the core must be cooled by natural convection, as long as there is enough water in the reactor pool. To guarantee the water level, the emergency core reflood circuit (CRU) has been reinforced and automated, and a new groundwater supply (the CEN) added. This means that, even in the event of an earthquake and dam burst, the water supply to the reactor pool will be sufficient to ensure that the fuel element remains under water and that the cooling process continues efficiently.

#### 2. Ensure confinement

The hypothesis here is that, despite the cooling measures above to prevent a core meltdown (CRU and CEN), the fuel element could fail to cool and would melt in the reactor hall. We are currently installing a new seismic depressurisation circuit (CDS) to limit the effects of a meltdown to acceptable proportions. This circuit will ensure that the reactor hall (containing any radioactivity released by the melting core) remains at a slightly lower pressure than its surroundings. There should thus be no risk of any uncontrolled or unfiltered releases into the environment.

#### 3. Ensure good crisis management

To manage a major crisis on the site, the ILL has had to build a new emergency control room (PCS3). The PCS3 has now been built. It is designed to be able to house all the equipment and personnel required to manage a crisis. It is also sufficiently robust to protect them from all the envisaged external hazards: earthquake and flood, of course, but also clouds of toxic pollution from the chemical complex to the south and even outside explosions.

### THE COST OF THE PROGRAMME

The safety authorities' requirements forced us into breaking new ground, as no other nuclear installation in France had had to reinforce its facilities against the combined risk of earthquake and tidal wave.

A first estimate of 12 M€ was prepared for the Steering Committee of December 2011. The ILL's Associates (France, Germany and the UK) decided on this basis to release a supplementary 12 M€ over four years for the reinforcement programme. As the studies progressed, and as the safety authorities made new and more demanding requirements, the cost of the programme began to rise sharply. In December 2014 it settled at 20.9 M€.

The ILL has done what is necessary to finance the increase of about 9 M€ in the costs, by making savings on the operating budgets of 2013, 2014 and 2015 and by postponing some expenditure to later years.

The overall cost of the Fukushima programme – 21 M€ – amounts to 1.5 % of the ILL's annual budget every year for the next 15 years. It is a lot of money of course, but it will ensure that the reactor facilities continue to function in the safest conditions possible until 2030... at least!



The new emergency reactor control room.

Just some of the 100 km of cabling.



# MORE THAN SIMPLY NEUTRONS



THE EPN-CAMPUS	108
SCIENTIFIC SUPPORT LABORATORIES	110

In order to maintain their ranking on the international scene, European research institutes must optimise their resources and develop synergies at every level.

The ILL is firmly committed not only to building high-performance instruments but also to offering the best scientific environment to the user community. We have established successful collaborations with neighbouring institutes over the years. After the successful Partnership for Structural Biology, we have now launched a Partnership for Soft Condensed Matter.

In parallel, the ILL and the ESRF have been working on plans to transform our joint site into a research campus – the “European Photon and Neutron science campus”, or EPN-campus for short – with a truly international reputation. We have also launched an ambitious project to extend the facilities already offered by our international site. The new scientific and technological installations will be complemented with other more general improvements, such as a new Science Building, a new site entrance, a despatch and reception platform, a bigger restaurant and internal roadways.

In addition, the ILL has teamed up with the other institutes located on the *Polygone Scientifique* science park (where our institute is located) for the GIANT partnership, a project which aims to develop our neighbourhood into a world-class science and technology park.

---

*The ILL is firmly committed not only to building high-performance instruments but also to offering the best scientific environment to the user community.*

---

# THE EPN-CAMPUS

The year 2014 saw the start of a new era for the EPN (European Photon and Neutron) science campus.

Several new buildings on the campus, which were funded in part or in full by the local and regional authorities within the framework of a so-called CPER (*Contrat de Projets Etat-Région*) contract, were officially opened on 21 February. The opening ceremonies were attended by the then French Minister for Higher Education and Research, Geneviève Fioraso, the President of the Rhône-Alpes region, Jean-Jack Queyranne, the President of Grenoble Alpes Metropole, Marc Baietto, and the deputy Mayor of Grenoble, Jérôme Safar, in their capacity as representatives of the funding agencies and faithful supporters of these projects.

The most emblematic of the inaugurated buildings is the 5 000 m<sup>2</sup> Science Building, which was brought into operation in 2014. The building is home to the Large-Scale Structures group scientists and their ESRF colleagues, and includes facilities shared between them – the chemistry laboratory, the soft condensed matter laboratory and the scientific library. It also serves as the contact point for industrial users.

For its part, the Institut de Biologie Structurale (IBS) celebrated the completion of its new building: 5 600 m<sup>2</sup> of laboratories, platforms and offices dedicated to structural biology. UNESCO declared 2014 the *International Year of Crystallography*. It is therefore fitting that the IBS now has at its disposal a unique environment for exploring the molecular architectures of living organisms and their dynamics, in order to further our understanding of the main cellular functions.

Furthermore, 22 April saw the opening of the new EPN site entrance. The new entrance building handles 2 000 entries a day – by ILL, ESRF, EMBL and IBS staff and our scientific visitors.

It is also no coincidence that the ILL and the EPN-campus are now well served by the new tramline, which runs seven days a week, 20 hours a day, making access to the campus a lot easier for our visitors. It will take about 10 minutes now to go from the ILL to Grenoble railway station and 15 minutes to the town centre.

The inauguration of the new buildings of the EPN science campus (©: F. Fouladoux).



The new EPN science campus entrance.

## ILL AND THE INTERNATIONAL YEAR OF CRYSTALLOGRAPHY

On October 18 the ILL and its campus colleagues participated in France's *Fête de la science*, our most important public relations event of the year and a major opportunity to reach out to the people of Grenoble.

Thanks to the brand-new site entrance – highly visible and easy to access – we were able to install a marquee on the site in which we held a variety of practical demonstrations, computer games and mock-ups. Visitors were given a 90-minute guided tour of the buildings and discovered the reality of international, large-scale structure research. Those visiting the ILL were taken into the large experimental hall to see the new instruments built under the Millennium Programme.

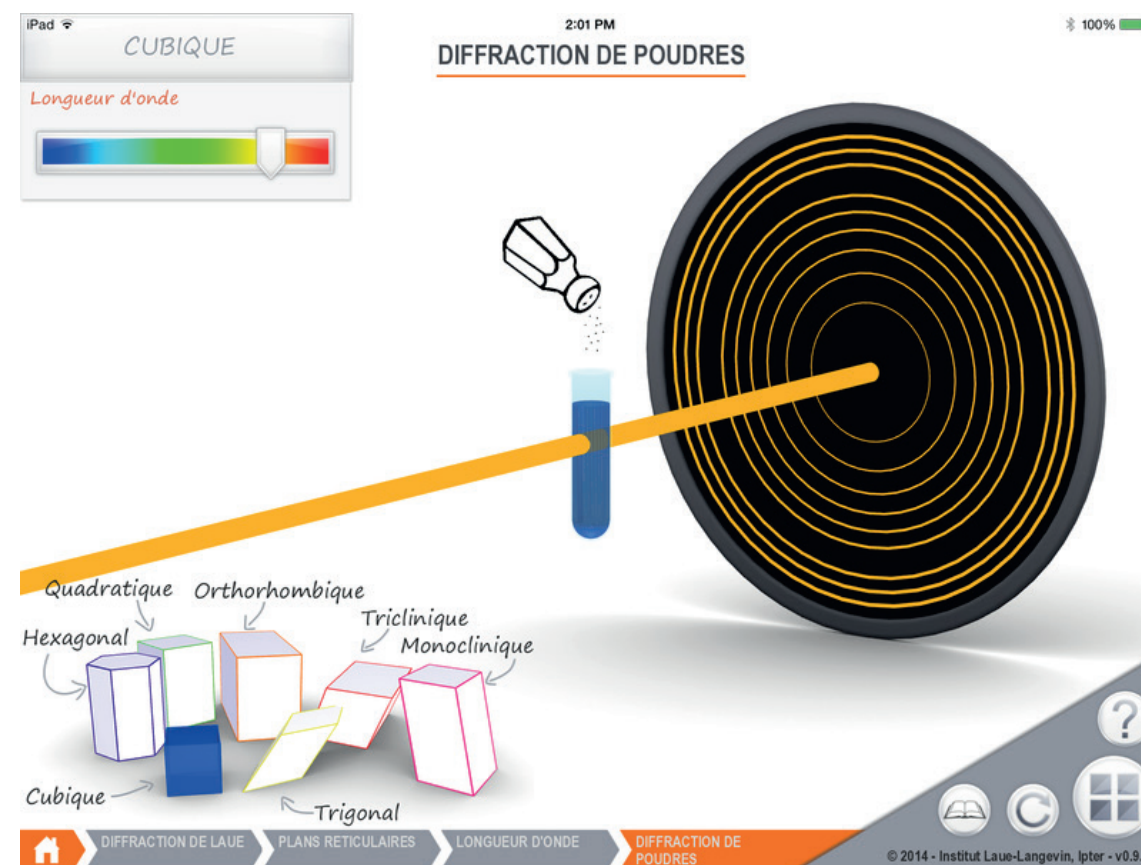
As part of the *International Year of Crystallography*, the guided tour and marquee displays focused on how crystallography in all its forms – neutron, electron and X-ray – helps us delve into the mysteries of matter. The EPN science campus is incontestably a prime location for crystallographers from all over the world.

The ILL also made a significant contribution to the 2014 centenary celebrations. We participated in the travelling international crystallography exhibition conceived and



Visitors in the EPN marquee during the French science festival.

carried out in Grenoble, and we organised conferences and other events for the general public, combining art with science to get our messages across. We also produced a variety of learning applications, such as a resources website and *vDiffraction*, an educational web application ([www.ill.eu/vDiffraction](http://www.ill.eu/vDiffraction)). *vDiffraction* is a serious learning game for science students and teachers, helping them to carry out a virtual experiment and see in practice how scientists determine the symmetry of a crystal. We have produced *vDiffraction* in French and in English, making it accessible to a wider audience.



A screen shot of the learning application *vDiffraction*.

## SCIENTIFIC SUPPORT LABORATORIES

### PARTNERSHIP FOR SOFT CONDENSED MATTER (PSCM)

The year 2014 saw the relocation of the soft matter laboratories to the 2<sup>nd</sup> floor of the Science Building, along with the Soft Matter Science and Support group.

In these laboratories, scientists can prepare experiments with highly complex, self-assembled and soft matter systems in fields related to nanotechnologies, life sciences, the environment as well as renewable energy. A number of research institutes have requested to join the initiative and we are happy to welcome the groups of S. Köster (Göttingen, Germany), J. Cabral (London, UK) and K. Huber (Paderbon, Germany) as our first collaborative partners.

The second PSCM workshop on Enhanced User Support and Partnership Projects for Soft Matter Science was held on 18-19 June 2014, with the participation of 20 invited speakers representing the European Soft Matter user community of the ESRF and the ILL. Participants were selected from among those who had already expressed interest in submitting a proposal for Partnership Agreement and those who had already started the application process. The aim of the workshop was to promote constructive discussion between representatives of the PSCM and the European Soft Matter user community, now that PSCM is officially established and the Science Building is operational.

External ILL users have benefitted from the new laboratories since the reactor restart in July this year and have greatly appreciated the progress made with the move to the new building.

Users wishing to use the facility in conjunction with neutron measurements should indicate this when submitting their request for beamtime.

Further details can be found at <http://www.epn-campus.eu/pscm/>

### PARTNERSHIP FOR STRUCTURAL BIOLOGY

The Partnership for Structural Biology (PSB) contains a powerful set of technology platforms that are contributed by the various partner institutes (ILL, ESRF, EMBL, IBS, and the unit for host-pathogen interactions). These platforms include advanced capabilities that complement the powerful neutron-scattering facilities available to ILL users: synchrotron X-rays, electron microscopy, Nuclear Magnetic Resonance (NMR), high-throughput methods (soluble expression and crystallisation), and a range of biophysical techniques such as isothermal calorimetry and surface plasmon resonance. A joint small-angle neutron and X-ray scattering (SANS/SAXS) platform has been developed and there is also strong connectivity and collaboration between the ILL and ESRF crystallography groups involved in structural biology and related industrial efforts. The aim of the PSB is to enhance the interdisciplinary capabilities of each of the facilities co-located on the site.

Further details are provided on its website <http://www.psb-grenoble.eu/>. The Carl-Ivar Brändén building (CIBB) is the principal site for the PSB and its partner organisations.

### DEUTERATION LABORATORY

The ILL's Life Science Group is located within the CIBB and contains the Deuteration Laboratory platform (D-LAB). The group is involved in a wide variety of externally funded programmes that exploit the capabilities of the PSB as well as promoting interdisciplinary structural biology (see <http://www.ill.eu/PSBLS>). The group also has a number of programmes for method development relating to sample preparation and data collection using crystallography, SANS, fibre diffraction and dynamics; it is therefore of central importance to all the ILL instrument groups involved in biology research.

### CHEMISTRY LABORATORIES

With the end of the long shutdown in 2014, the Chemistry Laboratories restarted operation in the new facilities of the Science Building under significantly improved conditions. The Chemistry Laboratories are run by the Soft Matter Science and Support Group and, together with the adjacent PSCM laboratories, they offer ILL users various possibilities for advanced sample preparation. The Main Chemistry Laboratory provides bench space, fume cupboards and basic laboratory equipment, e.g. glassware, balances, hot plates, micro-pipettes. A special laboratory for the handling of corrosive substances has been installed and a selection of ovens, vacuum ovens and high temperature furnaces are available now in a separate furnace room. For the handling of air-sensitive solid samples, ILL users can find a glovebox with an argon atmosphere in which traces of oxygen and water are kept below 0.1 ppm. Lab space for the preparation of bio-orientated samples is provided, together with the option to perform SDS-page or NanoDrop measurements. For convenient sample preparation at a sub-ambient temperature, a cold room with bench space is available.

Access for users to the Chemistry and PSCM laboratories can be requested by the main proposer via the ILL User Club.

Further details on the Chemistry Laboratories can be found at <http://www.ill.eu/instruments-support/labs-facilities/chemistry-laboratories/home/>

### MATERIALS SCIENCE SUPPORT LABORATORY

The joint ILL-ESRF Materials Science Support Laboratory (MSSL) provides a range of support to our users, from advice with experiment proposals, through sample preparation to advanced sample metrology. In particular, the Laboratory works with users to optimise the experimental methodology before the start of an experiment. This takes the form of standardised specimen mounting, digitisation of samples, definition of measurement macros and liaising with the instrument responsible. It is recommended that users arrive at the ILL a day or two prior to the start of an experiment to enable these off-line preparations to be performed.

More information may be found on the MSSL's website <http://www.ill.eu/sites/mssl/>

### C-LAB

The Computation Lab (C-Lab) offers support to ILL users for atomistic simulations using classical and *ab initio* methods. Typical applications for simulations are structure, phonons and (some) magnetism in crystals, and structure and dynamics in (partially) disordered systems ranging from liquids and glasses to macro/bio-molecular systems. As samples become more complex, simulations can provide key, complementary information that will help to interpret experimental data and understand how systems behave. Scientists and thesis students at the ILL benefit from the software, hardware and expertise of the C-Lab, while users can benefit via their local contacts. In order to improve access to simulations for users, they are able to request simulation support for their neutron-scattering experiments on the first page of the ILL proposal forms by ticking the appropriate box. Between autumn 2007 and spring 2014, 437 proposals were submitted to the C-Lab.



Yuri Gerelli, Ralf Schweins and David Hess in the light scattering lab of the PSCM.



Estelle Mossou, Trevor Forsyth and Valerie Laux-Lesourd in the Deuteration Laboratories.



Anne Martel doing electrophysiology measurements in the PSCM.

# WORKSHOPS AND EVENTS

## ILL WORKSHOPS AND SCHOOLS IN 2014

### 13-16 JANUARY

PSB school on SAXS-SANS techniques

### 10-13 FEBRUARY

14<sup>th</sup> REIMEI Workshop on Spin Currents and Related Phenomena

### 19-21 FEBRUARY

NIBB 2014 "Neutrons in Biology and Biotechnology"

### 23 FEBRUARY – 26 MARCH

HERCULES 2014 – Higher Education Research Course for Users of Large Experimental Systems

### 17 MARCH

CRISP – Workshop on Imaging with Neutrons

### 24-27 MARCH

Third International Workshop SKIN 2014

### 3 APRIL

CARAC 2014 - La science rencontre l'industrie autour des Plateformes de Caractérisation grenobloises

### 8 APRIL

Clip session of the ILL PhD students

### 9-10 MAY

MDANSE school 2014 - Molecular Dynamics to Analyse Neutron-Scattering Experiments

### 11-16 MAY

GENS 2014/WINS 2014 (L'Escandille, Autrans, France)

### 16-23 MAY

Bombannes 2014 – 12<sup>th</sup> European School on "Scattering Methods Applied to Soft Condensed Matter" ("Les Bruyères", Carcans-Maubuisson, France)

### 2 JULY

First Science Building clip session

### 7-11 JULY

SCES 2014 University Campus in Saint Martin d'Hères near Grenoble

Short reports on the ILL workshops can be found on the ILL News for Reactor Users December 2014 issue –

<http://www.ill.eu/top-links/publications/ill-news/>

Workshops websites can be found at

<http://www.ill.eu/news-events/past-events/>

## ILL CHRONICLE 2014

### 3-4 FEBRUARY

Visit of the EPN campus by a delegation from Lund

### 21 FEBRUARY

CPER Opening ceremony

### 18-21 MARCH

Meetings of the ILL Scientific Council and its Subcommittee

### 24-25 MARCH

Visit of a delegation from the Petersburg Nuclear Physics Institute

### 2 APRIL

STFC/ILL/ESRF Directors' meeting

### 13-14 MAY

Meeting of the Subcommittee on Administrative Questions (SAQ)

### 2-4 JUNE

CRISP 3<sup>rd</sup> Annual Meeting (at the ILL and ESRF)

### 6 JUNE

Visit of Professor Daniel Filâtre, rector of Grenoble academy and chancellor of the universities

### 26-27 JUNE

Meeting of the Steering Committee

### 19 SEPTEMBER

Visit of Professor Carla Andreani, from the National Research Council (CNR), Italy

### 25 SEPTEMBER

Visit of Robert Dautrey

### 6-7 OCTOBER

Visit of a Belarus delegation and signature of a letter of intentions for cooperation between the ILL and the National Academy of Sciences of Belarus

### 10 OCTOBER

Visit of Mrs. Hermione Gough (UK Embassy, Ministerial Counsellor for Europe and Global Issues) and Mrs. Sara Gills (UK Embassy, Science and Innovation Officer)

### 14-15 OCTOBER

Meeting of the Subcommittee on Administrative Questions (SAQ)

### 12-14 NOVEMBER

Meetings of the ILL Scientific Council and its Subcommittee

### 25-26 NOVEMBER

Meeting of the Steering Committee

# A YEAR IN PHOTOS

## Visits and events

1



2



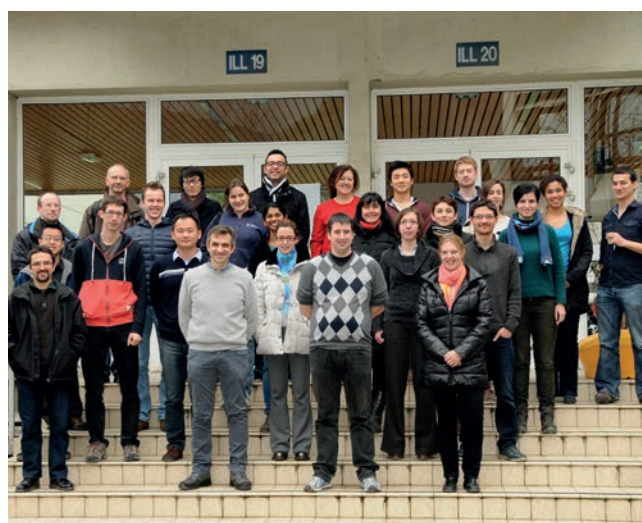
3



4



5



1. Colin Carlile accompanying a delegation from Lund during a visit of the EPN campus on 3-4 February.
2. Several new buildings on the EPN campus, which were funded in part or in full by the local and regional authorities in the framework of a so-called CPER contract, were officially opened on 21 February, in the presence of the former French Minister for Higher Education and Research, Geneviève Fioraso.
3. Visit of Mrs. Sara Gill and Mrs. Hermione Gough (UK Embassy in Paris, first two from the left) and Pascale Berruyer (CEA Grenoble, first on the right) are given a tour of ILL facilities by Bill Stirling (ILL Director) and Giovanna Cicognani (Head of Communication and Scientific Support) on 10 October.
4. Robert Dautrey (ancient science director of CEA who contributed to the construction of the ILL reactor) visits the ILL on 25 September.
5. Participants to the PSB school on SAXS-SANS techniques on 13-16 January.

6



7



8



6. Clip session of the ILL PhD students on 8 April.
7. The ILL summer trainees with Anita Schober (first on the right, Human Resources service).
8. Charles Simon (Associate Director) welcoming a visiting group during the EPN science campus open day on 18 October.

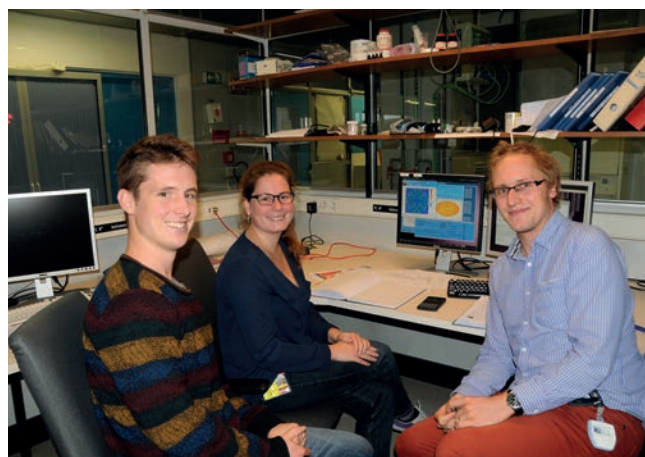
# A YEAR IN PHOTOS

## Happy users

1



2



3



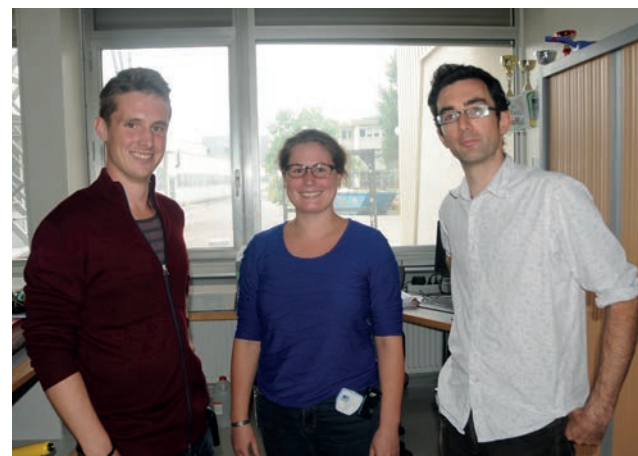
4



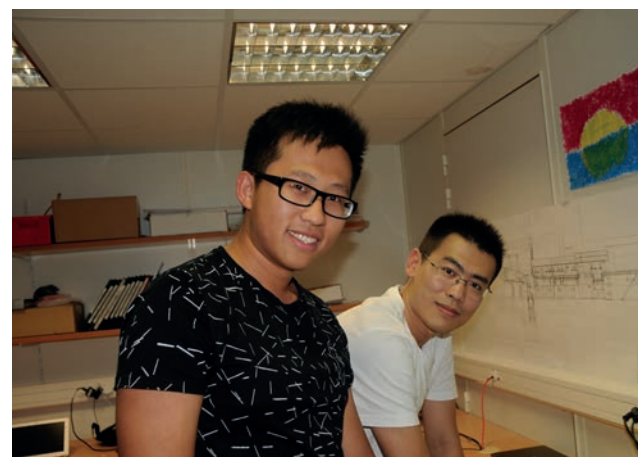
5



6



7



8



9



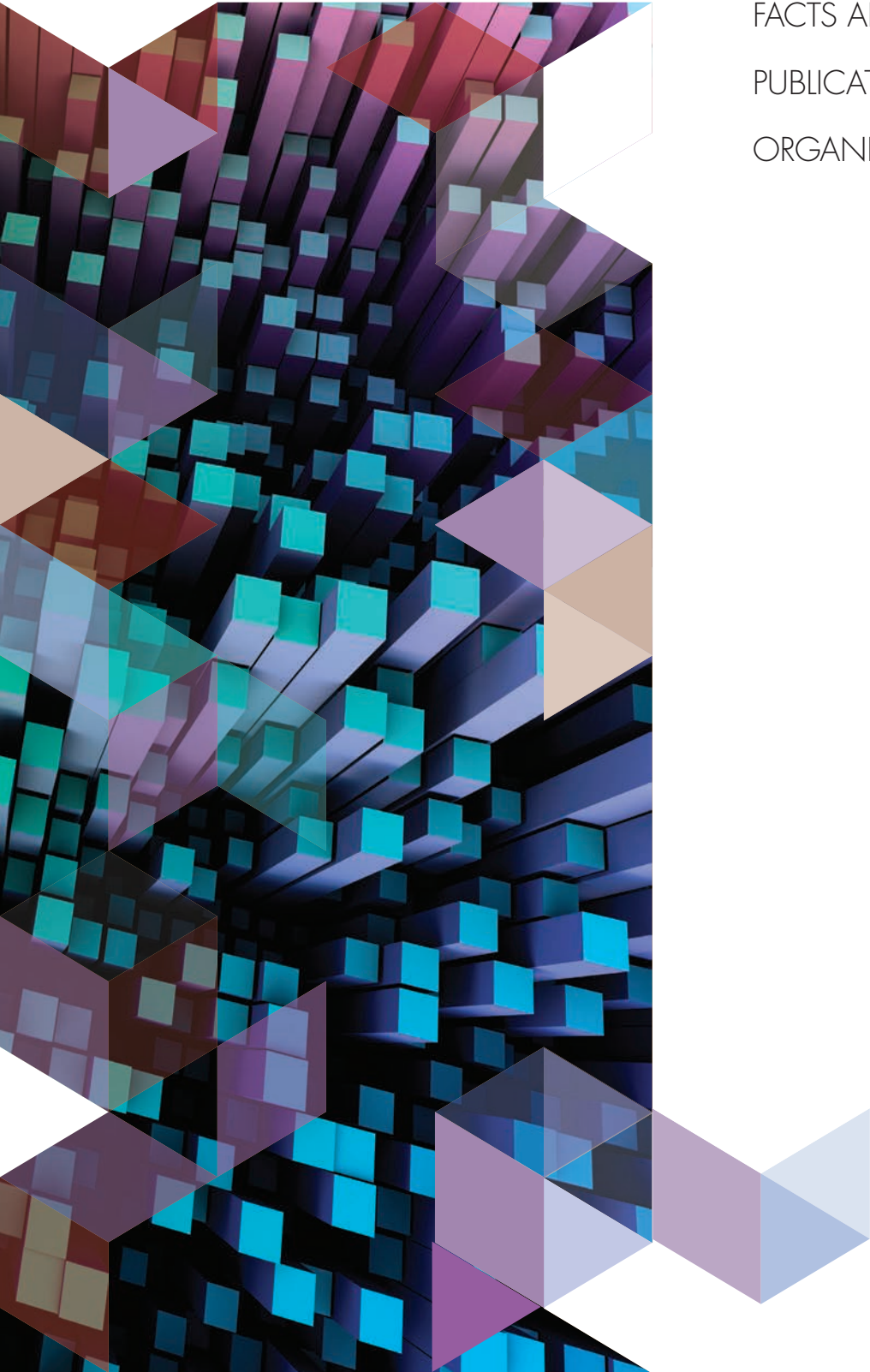
10



1. From left: Tobias Denkmayr, Stephan Sponar, Hartmut Lemmel and Hermann Geppert (Atominstiut, Vienna) chasing the "Cheshire Cat" on S18 (see article on page 68).
2. From left: Erik Christensen (Copenhagen University) and Sonja Holm (Copenhagen University and PSI) with Gøran Nilsen on D7.
3. Marité Cárdenas (Malmö University, Copenhagen) and Vivien Jagalski (Copenhagen University) investigating Terpenoids' effect on biological membranes.
4. From left: Eron Cemal (ILL), Toby Willis (University of London, UK), Peter Fouquet (ILL) and Jon Goff (University of London, UK) on IN11.
5. From left: Katarzyna Zielinska, Huihui Sun and Ali Zarbakhsh (University of London). In the back, Giovanna Fragneto (ILL).

6. From left: Dreier Erik Christensen (ILL) with Sonja Holm (Niels Bohr Institute) and Tom Fennel (PSI) during their experiment on IN8.
7. From left: Zhiming Lu and Ruiheng Li (Manchester University, UK) during their last experiment on FIGARO.
8. A very happy Paul Freeman (EPFL, Lausanne).
9. Franck Cecillon and Franck Rey (Instrument Control Service) replacing the acquisition card for a test experiment on IN10.
10. Bob Cubitt (ILL) and Giovanni Bruno (University of Postdam and BAM, Berlin) during the SKIN workshop poster session.

# FACTS AND FIGURES



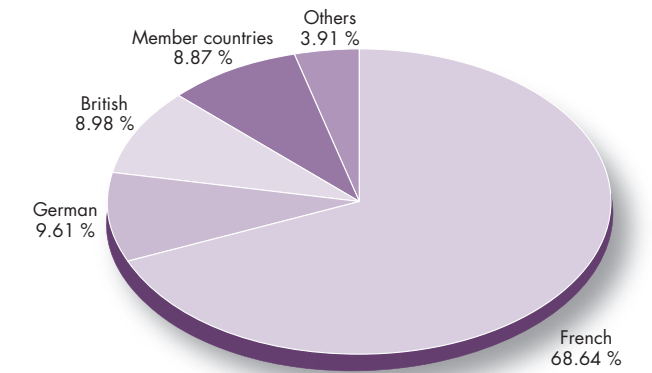
FACTS AND FIGURES	119
PUBLICATIONS IN 2014	121
ORGANISATION CHART	122

## STAFF ON 31/12/2014

473.5 people including 66 experimentalists in the scientific sector and 36 thesis students.

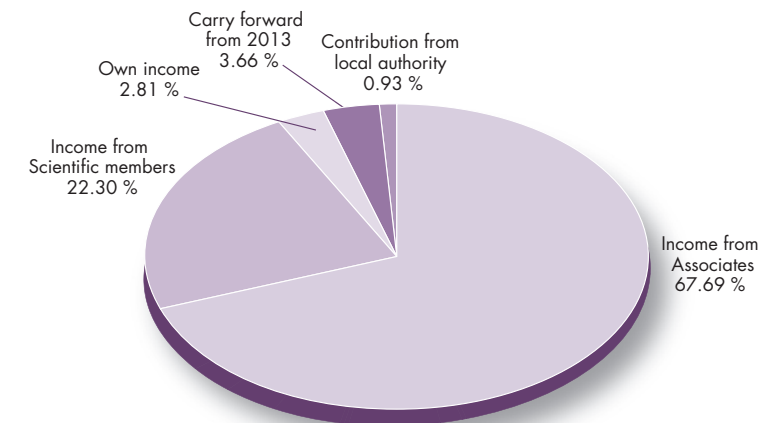
325 French, 45.5 German, 42.5 British, 42 scientific participating countries and 18.5 others.

Country		%
French	325.0	68.64 %
German	45.5	9.61 %
British	42.5	8.98 %
Member countries	42.0	8.87 %
Others	18.5	3.91 %
<b>Total</b>	<b>473.5</b>	<b>100 %</b>

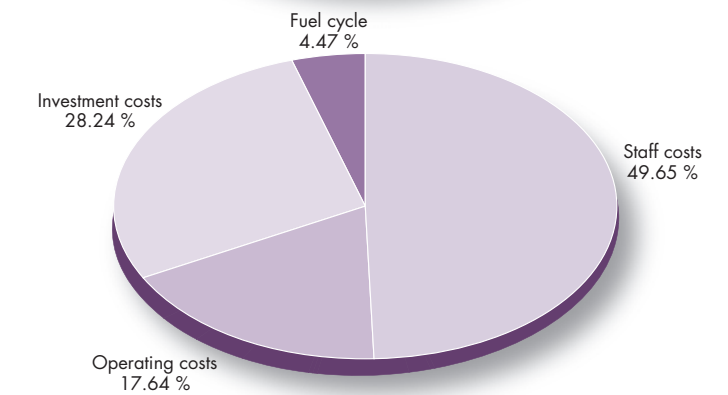


## REVISED BUDGET 2014: 90.908 M€ (excluding taxes)

Income	M€	%
Income from Associates (incl. Fukushima & Millennium Programme & add. nuclear tax)	61.535	67.69 %
Income from Scientific members	20.270	22.30 %
Own income	2.550	2.81 %
Carry forward from 2013	3.330	3.66 %
Contribution from local authority	0.848	0.93 %
Cashflow	2.375	2.61 %
<b>Total</b>	<b>90.908</b>	<b>100.00 %</b>

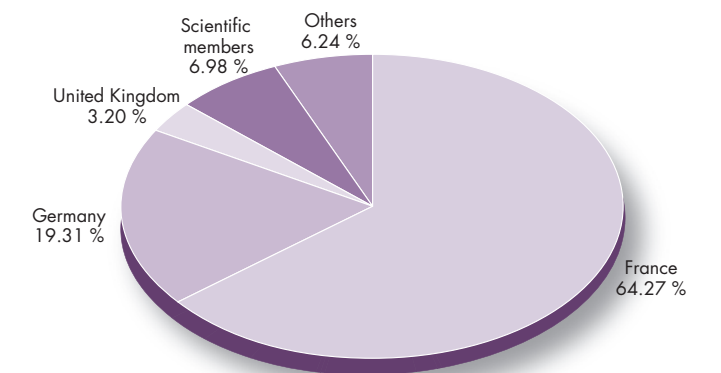


Expenditure	M€	%
Staff costs	45.140	49.65 %
Operating costs	16.040	17.64 %
Investment costs	25.668	28.24 %
Fuel cycle	4.060	4.47 %
<b>Total</b>	<b>90.908</b>	<b>100.00 %</b>



## PURCHASING STATISTICS (Figures 2014 to end September 2014)

	M€	%
France	12.247	64.27 %
Germany	3.684	19.31 %
United Kingdom	0.608	3.20 %
Scientific members	1.330	6.98 %
Others	1.192	6.24 %
<b>Total</b>	<b>19.061</b>	<b>100.00 %</b>



France captif market	6.083
<b>Total captif / non captif</b>	<b>25.144</b>

# FACTS AND FIGURES

## NAME

Institut Max von Laue-Paul Langevin (ILL).

## FOUNDED

17 January 1967.

Intergovernmental Convention between France, Germany and United Kingdom (19/07/1974).

## ASSOCIATES

### France

Commissariat à l'Énergie Atomique et aux Énergies Alternatives (CEA).

Centre National de la Recherche Scientifique (CNRS).

### Germany

Forschungszentrum Jülich (FZJ).

### United Kingdom

Science & Technology Facilities Council (STFC).

## COUNTRIES WITH SCIENTIFIC MEMBERSHIP

### Spain

MINECO Ministerio de Economía y Competitividad.

### Switzerland

Staatssekretariat für Bildung und Forschung (SBF).

### Italy

Consiglio Nazionale delle Ricerche (CNR).

### CENI (Central European Neutron Initiative)

Consortium composed of:

- Austria: Österreichische Akademie der Wissenschaften.
- Czech Republic: Charles University of Prague.
- Hungary: Research Institute for Solid State Physics and Optics (RISP) / Budapest on behalf of the Hungarian Academy of Sciences (MTA).
- Slovakia: Comenius University Bratislava.

### TRANSNI

(Belgian-Danish-Swedish Transnational Neutron Initiative Consortium)

- Belgium: Belgian Federal Science Policy Office (BELSPOL).
- Sweden: Swedish Research Council (SRC).
- Denmark: Danish Agency for Science, Technology and Innovation (DASTI).
- Poland: ILLP Consortium of Polish Scientific and Research Institutions.

### India

Bhabha Atomic Research Centre (BARC). Interim scientific membership 01/01/2011 - 31/12/2014.

## SUPERVISORY AND ADVISORY BODIES

- Steering Committee, which meets twice a year.
- Subcommittee on Administrative Questions, which meets twice a year.
- Audit Commission, which meets once a year, and statutory auditor.
- Scientific Council with 9 Subcommittees, which meets twice a year.

## REACTOR

58 MW, operating about 2.5 cycles in 2014 (117 days).

## EXPERIMENTAL PROGRAMME

- 495 experiments (allocated by subcommittees) on 28 ILL-funded and 9 CRG instruments.
- 980 visitors from 36 countries.

## Publications in 2014

In 2014, the ILL received notice of 587 publications by ILL staff and users.

They are listed on the ILL website:  
[www.ill.eu/science-technology/scientific-publications/list-of-publications/](http://www.ill.eu/science-technology/scientific-publications/list-of-publications/)

## THE DISTRIBUTION BY SUBJECT IS AS FOLLOWS

Applied Physics, Instrumentation and Techniques	42
Biology	65
Crystallography	87
Liquids and Glasses	23
Magnetic Excitations	37
Magnetic Structures	77
Materials Science and Engineering	46
Nuclear and Particle Physics	48
Theory	17
Soft Matter	100
Spectroscopy in Solid State Physics and Chemistry	41
Other	4

## ILL PHD STUDENTSHIPS

PhD students at ILL in 2014*	45
PhD theses completed in 2014	16

\* Receiving a grant from ILL.

# ORGANISATION CHART IN 2014



## REVIEW PANELS

(Chairs)

**APPLIED METALLURGY, INSTRUMENTATION AND TECHNIQUES**  
**D.J. Hughes** (WMG, Warwick University, UK)

**NUCLEAR AND PARTICLE PHYSICS**  
**W. Heil** (University of Mainz, Germany)

**MAGNETIC EXCITATIONS**  
**T.G. Perring** (ISIS, UK)

**CRYSTALLOGRAPHY**  
**R. Walton** (Warwick University, UK)

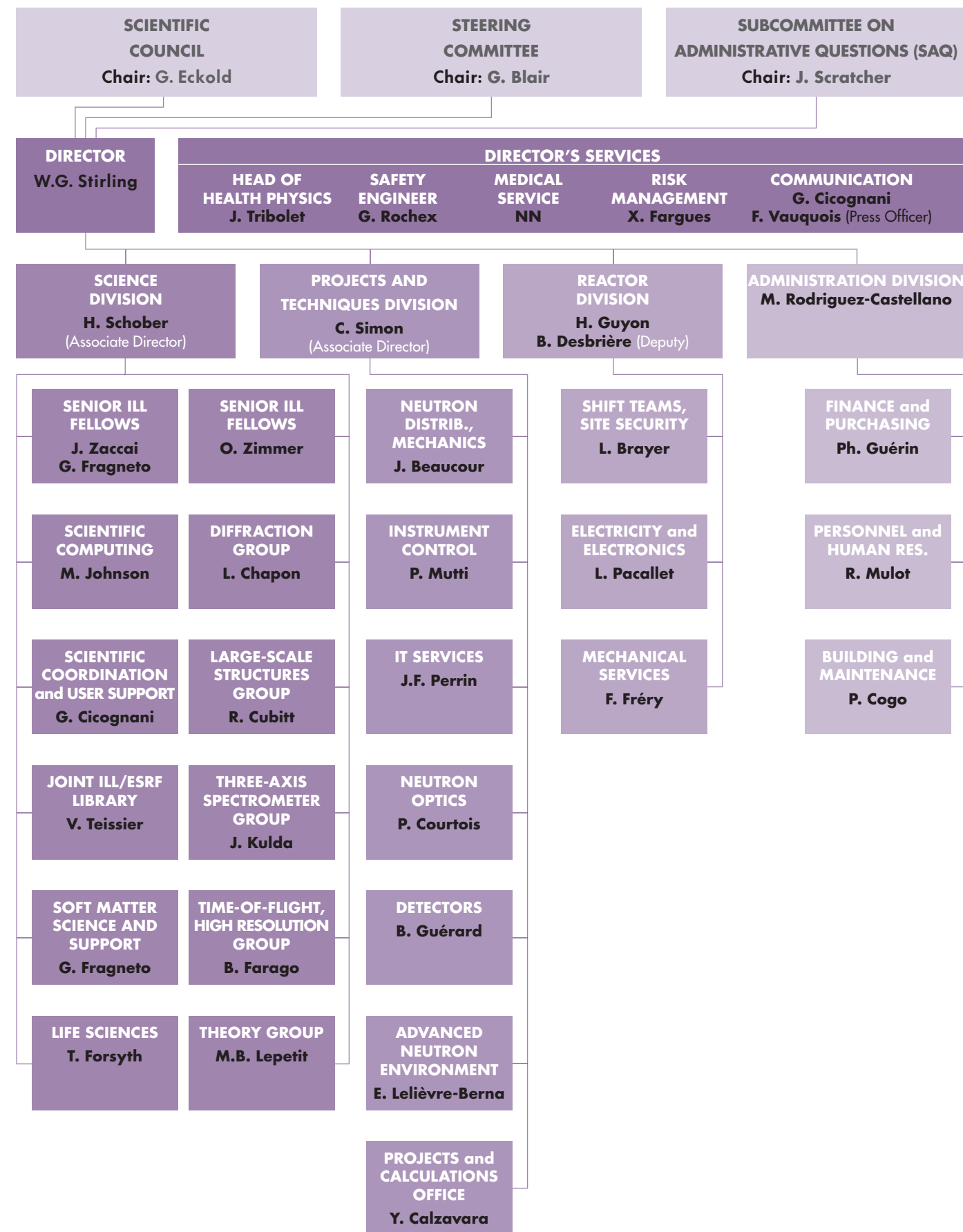
**MAGNETISM**  
**R.K. Kremer** (MPI Stuttgart, Germany)

**STRUCTURE AND DYNAMICS OF LIQUIDS AND GLASSES**  
**N. Clarke** (Sheffield University, UK)

**SPECTROSCOPY IN SOLID STATE PHYSICS AND CHEMISTRY**  
**D. Djurado** (CEA Grenoble, France)

**STRUCTURE AND DYNAMICS OF BIOLOGICAL SYSTEMS**  
**A.D. Podjarny** (University of Strasbourg, France)

**STRUCTURE AND DYNAMICS OF SOFT CONDENSED MATTER**  
**O. Sandre** (CNRS Pessac, France)







71, avenue des Martyrs  
38000 Grenoble  
France  
[www.ill.eu](http://www.ill.eu)



This report has been printed using FSC certified paper [www.fsc.org](http://www.fsc.org)